Atmospheric Environment 93 (2014) 3–100

Contents lists available at ScienceDirect

Atmospheric Environment

journal homepage: www.elsevier.com/locate/atmosenv

A global assessment of precipitation chemistry and deposition of sulfur, nitrogen, sea salt, base cations, organic acids, acidity and pH, and phosphorus

Robert Vet [a,*], Richard S. Artz [b], Silvina Carou [a], Mike Shaw [a], Chul-Un Ro [a], Wenche Aas [c], Alex Baker [d], Van C. Bowersox [e], Frank Dentener [f], Corinne Galy-Lacaux [g], Amy Hou [a], Jacobus J. Pienaar [h], Robert Gillett [i], M. Cristina Forti [j], Sergey Gromov [k], Hiroshi Hara [l], Tamara Khodzher [m], Natalie M. Mahowald [n], Slobodan Nickovic [o], P.S.P. Rao [p], Neville W. Reid [q]

[a] Atmospheric Science and Technology Directorate, Environment Canada, Toronto, Ontario, Canada
[b] Air Resources Laboratory, National Oceanic and Atmospheric Administration (NOAA), College Park, MD, USA
[c] Norwegian Institute for Air Research (NILU), Kjeller, Norway
[d] School of Environmental Sciences, University of East Anglia, Norwich, UK
[e] QA/SAC Americas, World Meteorological Organization Global Atmosphere Watch, Champaign, IL, US
[f] European Commission, Joint Research Centre, Institute for Environment and Sustainability, Ispra, Italy
[g] Laboratoire d'Aérologie, Observatoire Midi Pyrénées, Toulouse, France
[h] Faculty of Natural Sciences, North-West University, Potchefstroom, South Africa
[i] CSIRO Marine and Atmospheric Research, Aspendale, Victoria, Australia
[j] Instituto Nacional de Pesquisas Espaciais, Ministério da Ciência, Tecnologia e Inovação, São José dos Campos, São Paulo, Brazil
[k] Institute of Global Climate and Ecology, Roshydromet and RAS, Moscow, Russian Federation
[l] Department of Agriculture, Tokyo University of Agriculture and Technology, Tokyo, Japan
[m] Limnological Institute, Siberian Branch of the Russian Academy of Sciences, Irkutsk, Russian Federation
[n] Earth and Atmospheric Sciences, Cornell University, Ithaca, NY, USA
[o] Atmospheric Research and Environment Branch (AREB), World Meteorological Organization, Geneva, Switzerland
[p] Indian Institute of Tropical Meteorology, Pune, India
[q] Retired from Ontario Ministry of the Environment, Toronto, Ontario, Canada

HIGHLIGHTS

- Assessed the global distribution of precipitation composition and deposition of major ions.
- Produced a global data set of quality assured wet deposition monitoring data for 2000–2002 and 2005–2007.
- Generated global wet deposition maps of major ions combining measurement and modeling results.
- Established that sulfur and nitrogen wet deposition is highest in parts of Asia, Europe and eastern North America.
- Determined that major gaps in wet and dry deposition monitoring exist globally.

ARTICLE INFO

Article history:
Received 9 May 2013
Received in revised form
9 October 2013
Accepted 26 October 2013
Available online 12 December 2013

Keywords:
Precipitation chemistry

ABSTRACT

A global assessment of precipitation chemistry and deposition has been carried out under the direction of the World Meteorological Organization (WMO) Global Atmosphere Watch (GAW) Scientific Advisory Group for Precipitation Chemistry (SAG-PC). The assessment addressed three questions: (1) what do measurements and model estimates of precipitation chemistry and wet, dry and total deposition of sulfur, nitrogen, sea salt, base cations, organic acids, acidity, and phosphorus show globally and regionally? (2) has the wet deposition of major ions changed since 2000 (and, where information and data are available, since 1990) and (3) what are the major gaps and uncertainties in our knowledge? To that end, regionally-representative measurements for two 3-year-averaging periods, 2000–2002 and

* Corresponding author. Tel.: +1 416 739 4853.
E-mail address: Robert.Vet@ec.gc.ca (R. Vet).

1352-2310 Crown Copyright © 2013 Published by Elsevier Ltd. Open access under CC BY-NC-ND license.
http://dx.doi.org/10.1016/j.atmosenv.2013.10.060

Deposition
Emissions
Major ions
Global Atmosphere Watch
Assessment
pH

2005–2007, were compiled worldwide. Data from the 2000–2002 averaging period were combined with 2001 ensemble-mean modeling results from 21 global chemical transport models produced in Phase 1 of the Coordinated Model Studies Activities of the Task Force on Hemispheric Transport of Air Pollution (TF HTAP). The measurement data and modeling results were used to generate global and regional maps of major ion concentrations in precipitation and deposition. A major product of the assessment is a database of quality assured ion concentration and wet deposition data gathered from regional and national monitoring networks. The database is available for download from the World Data Centre for Precipitation Chemistry (http://wdcpc.org/). The assessment concludes that global concentrations and deposition of sulfur and nitrogen are reasonably well characterized with levels generally highest near emission sources and more than an order of magnitude lower in areas largely free of anthropogenic influences. In many parts of the world, wet deposition of reduced nitrogen exceeds that of oxidized nitrogen and is increasing. Sulfur and nitrogen concentrations and deposition in North America and Europe have declined significantly in line with emission reduction policies. Major regions of the world, including South America, the more remote areas of North America, much of Asia, Africa, Oceania, polar regions, and all of the oceans, are inadequately sampled for all of the major ions in wet and dry deposition, and particularly so for phosphorus, organic forms of nitrogen, and weak acids including carbonates and organic acids. Measurement-based inferential estimates of dry deposition are limited to sulfur and some nitrogen in only a few regions of the world and methods are highly uncertain. The assessment concludes with recommendations to address major gaps and uncertainties in global ion concentration and deposition measurements.

Crown Copyright © 2013 Published by Elsevier Ltd. Open access under CC BY-NC-ND license.

1. Introduction

The World Meteorological Organization (WMO) states that observations of the chemical composition and physical characteristics of the atmosphere on global and regional scales are required to provide the scientific community with the means to predict future atmospheric states, and to contribute to scientific assessments in order to inform environmental policy (WMO/GAW, 2007). Under the auspices of the WMO Global Atmosphere Watch, and using data from inside and outside the WMO system, this assessment was produced as an important contribution to precipitation chemistry science. It was meant to provide the science and policy communities with the best available information on atmospheric deposition of major ions. It is based on the complementary merging of precipitation chemistry measurements, measurement-inferred dry deposition estimates, and global modeling results.

The assessment contributes to global understanding of many major contemporary environmental issues, e.g., air pollution, atmospheric chemistry, acidification and eutrophication of ecosystems, and climate change. These issues are of increasing importance as growing populations strive to ensure food and energy security while encouraging economic growth. Recent reviews demonstrate this point. For example, in order to evaluate anthropogenic nitrogen (N) inputs to the global N cycle, Galloway et al. (2004) constructed global N budgets for the past 150 years and projected the global N budget for 2050. They concluded that global and regional N budgets have been increasingly influenced by anthropogenic activities and estimated that global atmospheric nitrogen emissions (NO_x and NH_3) increased from 23 Tg N a^{-1} in 1860 to 93 Tg N a^{-1} in the early 1990s to 189 Tg N a^{-1} in 2050. Dentener et al. (2006) noted that 11% of the world's natural vegetation now receives N deposition in excess of the "critical load" threshold of 1000 mg N m^{-2} a^{-1}. Most affected are the United States, western Europe, eastern Europe, South Asia, East Asia, Southeast Asia, and Japan. Howarth (2008) reviewed sources and trends of global and regional coastal N pollution noting that atmospheric and riverine fluxes have increased by 10–15-fold or more and that over half of the synthetic N fertilizer ever produced has been used in the past 15 years. Examining evidence for N deposition effects on terrestrial plants, Bobbink et al. (2010) evaluated the N deposition thresholds for protecting plant diversity across ecosystems ranging from Arctic and boreal systems to tropical forests. Doney (2010) concluded that climate change, rising atmospheric carbon dioxide concentrations, excess nutrient inputs, and pollution in its many forms are fundamentally altering the chemistry of near-shore coastal waters and the open oceans. This is occurring on a global scale and, in some cases, at rates greatly exceeding those in the historical and recent geological record. The results challenge the science community to provide more definitive assessments of the implications for ocean life and marine resources. Monks et al. (2009) addressed air quality issues by examining both anthropogenic and natural emissions. They discussed recent findings in an effort to quantify the impact of long-range transport on regional air quality and to discuss the resulting challenges for air quality and climate change policies. Fowler et al. (2009) focused on the exchange of trace gases and aerosols between the atmosphere and the earth's surface. They reported evidence that trace atmospheric constituents are changing the earth's climate (IPCC, 2007), global biodiversity (Powledge, 2006) and the biogeochemical cycling of major nutrients including nitrogen, carbon, and sulfur. They also identified important current and emerging policy needs and the need for appropriate data to address research questions in the coming decade. Laj et al. (2009) noted that the key to the design of effective climate and air quality policies requires knowing and understanding past and present atmospheric composition and changes therein. The authors recommend state-of-the-art atmospheric modeling and the establishment of long-term global and regional atmospheric observations to understand and quantify current conditions. Finally, regional assessments have been generated in Canada (Environment Canada, 2005), Europe (Lövblad et al., 2004; Tørseth et al., 2012), East Asia (EANET, 2006, 2011), the United States (NAPAP, 2005, 2011) and North America (IJC, 2012). These assessments were initiated to inform policy and regulatory applications and support the need for robust data collection of ion deposition data globally and the use of these data by the modeling community.

In 1995, the first global precipitation chemistry assessment was released as a World Meteorological Organization publication (Whelpdale and Kaiser, 1996). The assessment provided a critical review of worldwide acidic atmospheric deposition. The report examined the magnitude, geographical distribution, and temporal changes of acidic deposition in all regions of the globe for which data were available. Although data in many regions were limited, the report provided a scientifically sound analysis of the acidic deposition phenomenon and contributed to its understanding. This

first assessment formed the basis for additional national and international initiatives designed to understand and reduce the adverse effects of acidic deposition.

The first assessment concluded that, although most of the physical and chemical processes that control acidic deposition were well understood, emission and deposition were only measured and quantified adequately in Europe and North America. It was clear that on a global scale anthropogenic emissions of SO_2 and NO_x equaled or exceeded natural emissions and that measured wet and estimated dry deposition were generally of comparable magnitude in many regions. In most regions, sulfate was the dominant contributor to acidic deposition, although nitrate was also important in many areas. Organic acids were found to be important contributors in the southern hemisphere, but overall were poorly quantified. Sulfur deposition had significantly declined in North America and Europe due to emission reductions in the early 1990s. In sensitive areas of the developing world, deposition levels equaled or exceeded those that had caused damage in the industrialized world. Finally, the assessment concluded that the global database was inadequate to evaluate the extent, severity, and impact of acidic deposition in all parts of the world.

This second assessment presents a global overview of worldwide deposition by using quality assured measurements to complement and validate the best available global models. The assessment benefits from a more extensive yet still severely incomplete global database. To the extent possible, data quality was assessed and screened against guidelines established by WMO/GAW (2004), a key contribution toward harmonizing global wet deposition network measurements. This assessment focuses on regionally-representative chemical concentrations and deposition measurements; thus, urban data or data otherwise representative of very limited areas are not included. Unlike the first assessment, this assessment combines measurements with the ensemble-mean modeling results of 21 Eulerian (fixed grid) global models used to simulate chemical fate and transport in the atmosphere (Dentener et al., 2006). This approach improves geographical coverage where measurements of acceptable quality are sparse or lacking, thereby providing a more complete global picture.

Precipitation chemistry and deposition measurements were obtained from regional and national monitoring networks and were carefully screened to ensure the highest quality possible. Model results were contributed by the Task Force on Hemispheric Transport of Atmospheric Pollutants (TF HTAP) under the United Nations Economic Commission for Europe (UNECE) Convention on Long-Range Transboundary Air Pollution (CLRTAP) and are presented in detail in HTAP (2010), available electronically at www.htap.org. Measurement-model comparison results are presented to show the suitability and value of combining the models with high quality monitoring data for obtaining a global overview of precipitation chemistry and deposition. However, this assessment is not intended to be a comprehensive model evaluation.

Using the combined measurement-modeling approach, wet, dry and total deposition are assessed at the global scale for the period 2000–2007. Here, wet deposition is defined as the flux of a chemical compound to the earth's surface by precipitation (in whatever form falls into the collector), dry deposition as the flux of trace gases and particles via turbulent exchange and gravitational settling followed by interaction with exposed surfaces (NAPAP and Irving, 1990), and 'total' deposition as the sum of the two. Measurements of dry deposition are much sparser than wet deposition, and dry deposition estimates are limited and complicated by the fact that different methodologies are employed in different parts of the world. The term 'total deposition' has been defined here as the sum of wet plus inferred dry deposition of known compounds. This has been done with full recognition that all of the relevant chemical compounds may not be included. Largely due to the scarcity of data, this assessment does not attempt to address deposition from fog, clouds, and dust storms, despite their potential localized importance, particularly in mountainous and marine areas (e.g., Fowler, et al., 1993). This assessment also does not address the wet and dry deposition of organic nitrogen due to the lack of network measurements. Cape et al. (2011) noted that while organic nitrogen may account for about 30% of total airborne nitrogen, it is chemically complex with a composition that has not yet been fully described and that varies in time and space.

This assessment addresses three key questions:

1. What do measurements and model estimates of precipitation chemistry and wet, dry and total deposition of sulfur, nitrogen, sea salt, base cations, organic acids, acidity (pH), and phosphorus show globally and regionally?
2. How has wet and dry deposition of major ions changed since 2000 and, where information and data are available, since 1990 as a result of changing precursor anthropogenic emissions?
3. What are the major gaps and uncertainties in our knowledge?

The assessment presents results for the following regions: North America, South America, Europe (west of the Ural Mountains), Africa, Asia (east of the Ural Mountains plus southern and southwestern Asia), Oceania, and the oceans. In the process of answering the key science questions, additional issues were raised for consideration within each of the regions:

- What is the contribution of sea salt to precipitation chemistry?
- What is the relative importance of wet versus dry deposition?

The assessment begins with a description of the data and modeling sources and methods used to generate the maps, results and conclusions. This is followed by a discussion of each of the major ions listed in the first key science question above, describing their emissions (or emissions of their precursors as appropriate), their relative contributions to precipitation chemistry and deposition, and their spatial and temporal patterns on global and regional scales. In regions where measurements are especially sparse (South America, Africa, Oceania, the polar regions and the oceans), model simulations were used as the basis for discussion. In other regions where sufficient measurements were available (East Asia, North America and Europe) both measurement and model results are presented. In each case, uncertainties and knowledge gaps are also discussed with a view to improving the capacity to conduct future assessments. Throughout the assessment, dry deposition was included wherever possible.

Fig. 1.1 shows the spatial variability of the ion composition of precipitation around the globe for the period 2005–2007. Each vertical bar on the map shows the ion composition at a single site deemed representative of most sites in the surrounding area. The length of each bar, scaled by a constant plus a linear scaling factor, indicates the total ion concentration averaged over the 3-year period 2005–2007 (as annotated by the number in the center of the bar in $\mu eq\ L^{-1}$). Major ions are shown in different colors, making it clear where anthropogenic or sea salt influences are important – as well as making obvious the areas of the world where there are no measurements. It is believed that the uncharacterized "other" anions shown in white are associated with weak organic acids (primarily formic and acetic acid) that are typically not measured and are unstable in unpreserved samples. Only sites in west central Africa provided organic acid and bicarbonate measurement data; these values are shown on this map.

This assessment has relied upon national and regional monitoring methods and networks. It has culminated in the

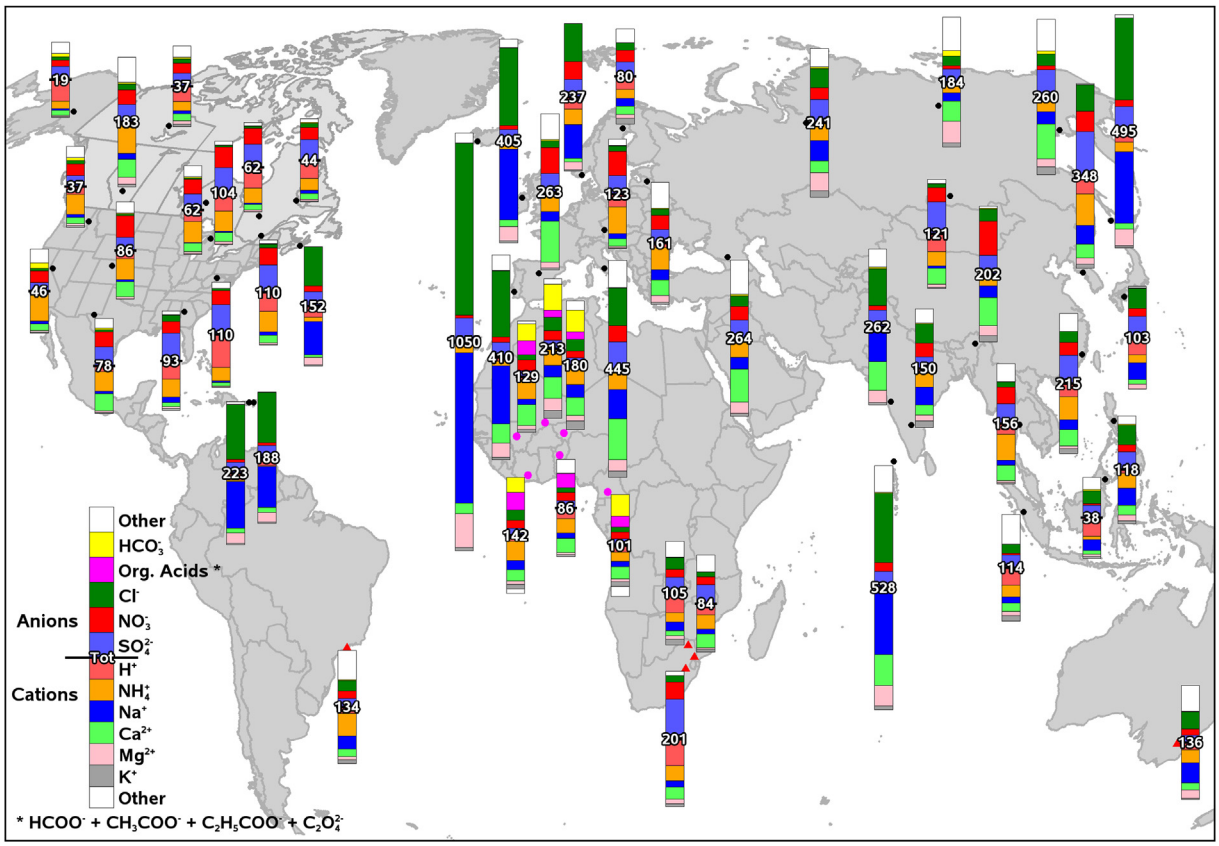

Fig. 1.1. Contribution of individual ions in precipitation to total ion composition (the number at the centre of each bar in μeq L^{-1}) at selected regionally-representative sites. A (constant plus linear) scaling factor was used to establish the length of the vertical bars. The white sections in the bars represent the calculated differences between the total anions and total cations typically assumed to be non-measured carbonates. Sites represented by black circles show the 3-year average ion composition (2005–2007) with no measured organic acid and bicarbonate data; pink circles show the 2005–2007 values that include measured organic acid and bicarbonate data; red triangles show data from outside of the 2005–2007 period. (Data can be obtained from the GAW World Data Centre for Precipitation Chemistry (http://wdcpc.org/).

development of a dataset of high quality precipitation chemistry measurements as determined by regional experts. The dataset is publicly available at the GAW World Data Centre for Precipitation Chemistry (http://wdcpc.org/).

2. Measurements, models and maps

As mentioned in the Introduction, the objective of this assessment is to characterize the chemical composition of precipitation and deposition (wet, dry, total) for sulfur, nitrogen, acidity, sea salt, mineral base cations, organic acids and phosphorus on global and regional scales. For these chemical species, with the exception of organic acids and phosphorus, measurement data were collected, screened and analyzed for two 3-year average time periods: 2000–2002 and 2005–2007. The 2000–2002 period was chosen to represent the early part of the decade; the 2005–2007 period to represent more recent conditions. Differences between the two periods were calculated to assess changes in deposition due to changing emissions. A global analysis of the changes since 1990 is beyond the scope of the present effort; however, it was possible to incorporate findings generated by regional assessments in North America and Europe. The 3-year averaging periods were selected to smooth the effects of interannual meteorological variability on the deposition data. Note, however, that one and two years of data were accepted at selected sites having fewer than three years of data (see Section 2.1). Organic acids and phosphorus deposition were assessed differently because so few data sets were available, making it necessary to accept data from the mid-1990s to 2007 to provide a global perspective.

This assessment involved the creation and analysis of global (and regional) deposition maps using measurement data collected during the two 3-year averaging periods. The maps are limited spatially by the low density and, in some cases, complete lack of measurement data in many parts of the world. To compensate for such large data gaps, the 2000–2002 measurement data were superimposed on the TF HTAP ensemble-mean modeling maps for the meteorological year 2001 that were derived from a number of global chemical transport models (see below for a discussion of the modeling approach). Thus, the wet deposition maps in this assessment consist of measurement-only and measurement-plus-model maps for 2000–2002 and measurement-only maps for 2005–2007. Maps of dry deposition and total deposition are model-based only – except for measurement-based total deposition presented for North America, Africa and Australia – due to the lack of measurement data. The text below provides a description of the sources and methods used to collect, analyze, map and interpret the measurement and modeling results.

2.1. Wet deposition measurement data

Major ion precipitation chemistry and wet deposition measurement data were collected from international, national and subnational long-term precipitation chemistry monitoring networks and research studies. With the assessment's focus on global and regional deposition, data from only regionally-representative sites

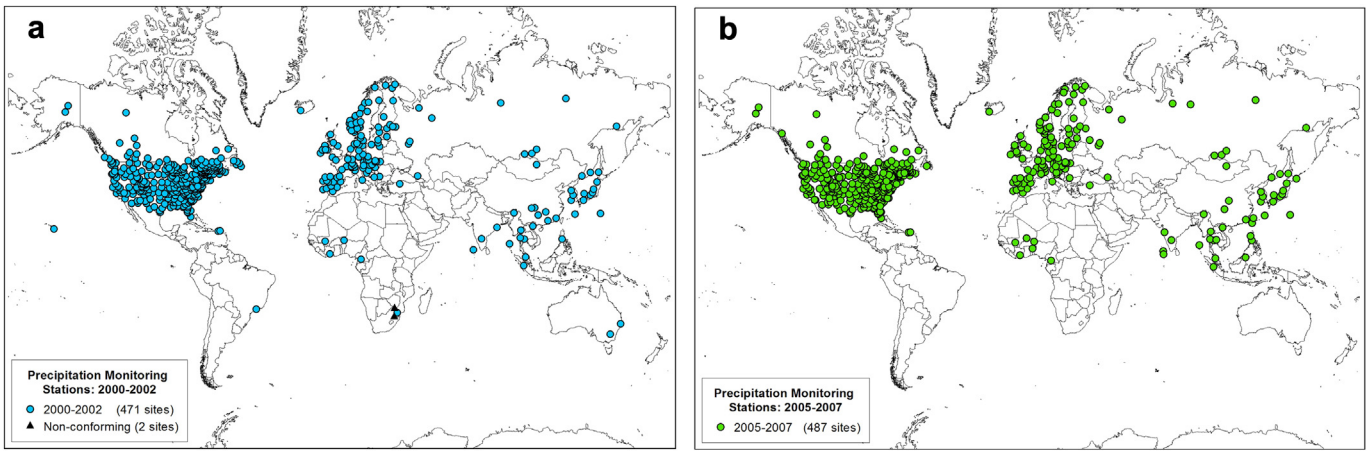

Fig. 2.1. Global maps of precipitation monitoring stations for (a) 2000–2002 and (b) 2005–2007. Non-conforming sites (triangles) apply to sites/data outside the standard 3-yr period.

were accepted; data from urban, suburban and industrial sites were excluded. Fig. 2.1 shows the wet deposition measurement sites and networks/programs from which the major ion data were collected, screened and accepted. As mentioned earlier, because of the paucity of measurements, phosphorus and organic acid data were gathered separately from networks and published long-term studies. Data from Global Atmosphere Watch (GAW) stations were obtained from the regional measurement programs to which they contributed, such as the European Monitoring and Evaluation Programme (EMEP) and the Acid Deposition Monitoring Network in East Asia (EANET), and from national networks such as the Canadian Air and Precipitation Monitoring Network (CAPMoN) and the United States National Atmospheric Deposition Program (NADP). The sources of major ion wet and dry deposition data (including those not associated with major regional or national networks), the respective numbers of sites and the web-based links or citations, are listed in Table S1 (Addendum). A total of 533 wet deposition sites were included.

Wet deposition, a key component of this assessment, is estimated as the product of an ion or species concentration in precipitation times the precipitation depth (WMO/GAW, 2004). The ion and species concentrations measured by these networks include sulfate, nitrate, chloride, pH, sodium, potassium, calcium, magnesium, and ammonium. Organic acids and phosphorus were measured at a small subset of monitoring stations. Precipitation depth was also measured. A number of other networks were approached for data and chose not to contribute; thus, the data used here set represents the best available at the time of writing. As

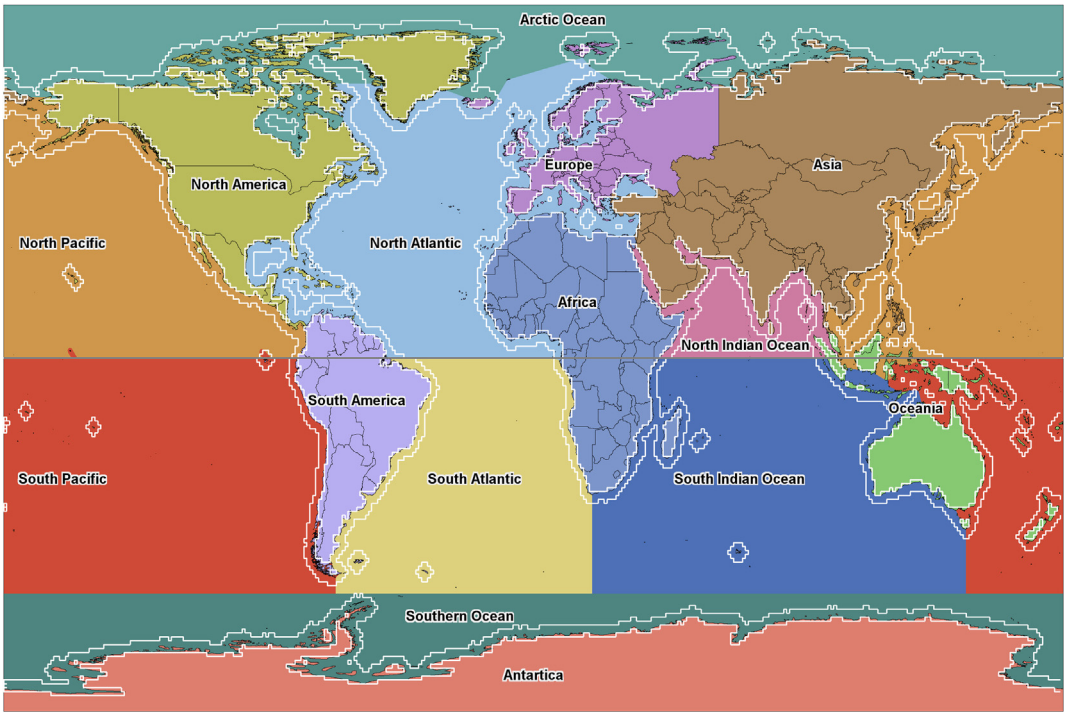

Fig. 2.2. Defined areas of the continents, oceans and coastal zones used to calculate the area-integrated emission and deposition mass budgets from the ensemble mean modeling results. White lines delineate the coastal zones.

a reference for later discussion of precipitation depth and its influence on wet deposition, global precipitation maps of precipitation depth are included as Fig. S2a,b of the Addendum. It was beyond the scope of this study to attempt to assess the precipitation measurements by precipitation type (e.g., snow or rain), or to establish whether the precipitation at a location was from convective rainstorms, monsoons, tropical storms, or long periods of low intensity precipitation.

All precipitation chemistry and wet deposition annual data in this assessment were carefully screened. Screening was initially carried out by each network/program and was followed by a secondary screening by Environment Canada's National Atmospheric Chemistry Database and Analysis facility in Toronto, Canada. This facility then carried out most of the data analyses, archiving and mapping of the final data. The outcome is a final database of quality assured, regionally-representative data. Data screening included the assessment of site representativeness, sampling protocols, laboratory methods, data completeness, and the assignment of a quality rating. Details of the screening and quality rating procedures are shown in Table 1 and are described briefly in the text that follows.

Measurement sites were screened to ensure that only regionally-representative sites were used; sampling protocols and laboratory methods were screened to ensure that the protocols and methods were consistent with the standard protocols defined by the World Meteorological Organization in WMO/GAW (2004) (including good performance in external laboratory intercomparison studies where possible); data were screened for completeness through a quantitative comparison of the annual data against the data completeness criteria identified in Table 1; data quality was assessed and every 3-year average measurement value accepted in the final data set was assigned a Data Quality Rating. Three Data Quality Ratings were used and are shown on all measurement-based maps: *Satisfactory*, *Conditional*, and *Non-Conforming Time Period*. *Satisfactory* data were considered to meet acceptable standards of measurement quality while *Conditional* data were considered to have higher uncertainties. *Non-Conforming* data applied to time periods outside of the standard 2000–2002 and/or 2005–2007 3-year averaging periods and were included only in Africa, where very limited wet deposition data were available.

The use of 1- and 2-year averages at sites without 3-year averages was less than ideal but allowed large data gaps in the global deposition patterns to be filled in. In the 2005–2007 period, 411 sites had 3-year averages of non-sea salt sulfur (nssS) wet deposition, 59 had 2-year averages and 14 had 1 year averages; for N wet deposition, the numbers were 408, 61 and 15 sites, respectively. The uncertainties of the 2- and 1-year averages were estimated through a sensitivity analysis based on sites with 3 years of annual nssS and N data. These data were used to evaluate all possible 1- and 2-year averages against the 3-year averages. The distributional statistics of the 1233 (for nssS) and 1224 (for N) possible combinations of 2- and 1-year averages relative to the actual 3-year averages were computed. For nssS, 80% of the 2-year averages were between −12% and +10% of the 3-year averages and 80% of the 1-year averages were between −22% and +20% of the 3-year averages (medians = −0.4% and −1.7%, respectively). For N, the results were more uncertain with 80% of the 2-year averages between −18% and +17% and 80% of the 1-year averages being between −21% and 20% of the 3-year averages (medians = +0.1% and −0.4%, respectively). In general, while larger outliers were possible, most 2-year and 1-year averages used in this assessment were likely within ±10% and ±20%, respectively, of the expected 3-year averages. These results are also shown in Fig. S1 of the Addendum.

The data files of annual and 3-year average wet deposition data are available and can be downloaded from the WMO/GAW Precipitation Chemistry Data Centre (http://wdcpc.org/).

2.2. Dry deposition

Direct measurements of dry deposition are difficult to make in monitoring networks because of the requirements for highly sophisticated methods and instrumentation (Wesely and Hicks, 2000). The few monitoring networks that contributed dry deposition estimates for this assessment, i.e., the Canadian Air and Precipitation Network (CAPMoN), IDAF (International Global Atmospheric Chemistry (**I**GAC)/Deposition of Biogeochemically Important Trace Species (**D**EBITS)/**Af**rica), and the Clean Air Status and Trends Network (CASTNET), did so using the so-called "inferential" technique, which involves making measurements of ambient air concentrations of gases and/or particles and multiplying the concentration values by dry deposition velocities estimated using modeling techniques (Wesely and Hicks, 2000; Zhang et al., 2005, 2009; Shen et al., 2009; Delon et al., 2010; Adon et al., 2013). Such estimates are available for only a limited number of regionally-representative long term monitoring sites worldwide (approximately 100) – in Africa, Australia and North America. Addendum Table S1 lists the number of sites, names of networks/programs and web links/references for the inferential flux data. Despite the presence of large uncertainties (Wesely and Hicks, 2000), inferential dry deposition estimates remain the best

Table 1
Criteria for assigning data quality ratings to 3-year average wet deposition data.

Data quality rating	Measurement methods			Data completeness		
	Wet-only or bulk sampling	Standard Gauge data availability	Sample collection period	Annual %PCL	Annual %TP	3-year average
Satisfactory	Wet-only	Yes	<1 Day	>90%	>70%	2 or 3 of the annual values are "Satisfactory"
Satisfactory	Wet-only	Yes	<1 Week	>90%	>70%	2 or 3 of the annual values are "Satisfactory"
Satisfactory	Wet-only or daily bulk	No	<1 Week	>90%	>70%	2 or 3 of the annual values are "Satisfactory"
Satisfactory	Wet-only or daily bulk or longer bulk proven-comparable to wet-only	Yes or no	<2 Weeks	>70%–89%	>50%–70%	2 or 3 of the annual values are "Satisfactory"
Conditional	Bulk	Yes or no	<2 Weeks	>70%	>70%	2 or 3 of the annual values are "Satisfactory"
Conditional	Wet-only daily bulk or proven-comparable bulk	Yes or no	<2 Weeks	Cannot be computed due to insufficient information	Cannot be computed due to insufficient information	All situations other than "Satisfactory"
Conditional	Bulk	No	<4 Weeks	Cannot be computed due to insufficient information	Cannot be computed due to insufficient information	All situations other than "Satisfactory"

available for assessing long term dry deposition on global and regional scales.

In North America, the U.S. CASTNET and Canadian CAPMoN inferential estimates of dry deposition velocities and fluxes differ markedly due to differences in their dry deposition velocity models (Schwede et al., 2011). Dry deposition velocities in the U.S. were modeled using the Multi Layer Model (Schwede et al., 2011) and were based on on-site meteorological measurements, while dry deposition velocities in Canada are modeled using the Routine Deposition Model and are based on model interpolated meteorological fields from the Canadian global weather forecast model (Zhang et al., 2001, 2003; Schwede et al., 2011).

Three-year average (2000–2002 and 2005–2007) dry deposition estimates of S and N in kg ha^{-1} a^{-1} were calculated from the two networks' annual S (i.e., S–SO_2 plus S–SO_4^{2-}) and N (i.e., N–HNO_3 plus N–NO_3^-) dry deposition estimates, respectively. Schwede et al. (2011) present an analysis of the sources of uncertainty and incomparability between the two inferential models and Mitchell et al. (2011) have evaluated the effects of the model differences based on watershed mass budgets. Detailed discussion of the uncertainties is given in both the sulfur and nitrogen sections that follow. Of particular importance is the fact that the dry deposition estimates of N from both networks do *not* include several major N species (most notably: NH_3, NO, NO_2, and PAN) and are therefore incomplete. The implications of the missing species are discussed in detail in the nitrogen chapter.

In Africa, inferential dry deposition estimates of S and N species were obtained from the DEBITS program, which used monthly measurements of gaseous SO_2, NO_2, NH_3, and HNO_3 concentrations using passive samplers (Adon et al., 2010; Martins et al., 2007) and monthly p-SO_4^{2-}, p-NH_4^+ and p-NO_3^- concentrations from aerosol filters (Kleynhans et al., 2008). Monthly-average dry deposition velocities of gaseous species were simulated using the Soil Vegetation Atmosphere (SVAT) big-leaf model ISBA (Noilhan and Mahfouf, 1996; Delon et al., 2010) coupled with Zhang et al., 2003 parameterizations (Adon et al., 2013). The meteorological forcing used in the model was developed within ALMIP (AMMA Land surface Model Intercomparison Project), from a data set based on merging the ECMWF (European Centre of Medium Range Weather Forecast) atmospheric state variables and the TRMM-3B42 3-hourly data for precipitation (Boone et al., 2009). Dry deposition velocities for particles were obtained from Zhang et al. (2009).

In Australia, SO_2 mixing ratios were measured at two sites (Tarah Rata and Burrup Peninsula) during two annual periods using passive samplers in duplicate (Ferm, 1991; Ayers et al., 1998). Dry deposition estimates of SO_2–S were estimated using a dry deposition velocity taken from an inferential model for Malaysian conditions (Manins, 1994) and used previously to estimate dry deposition in Indonesia (Gillett et al., 2000).

2.3. Total deposition

The term "total deposition" is used hereafter to describe the sum of wet plus dry deposition. The TF HTAP ensemble-mean modeled patterns of total deposition are shown throughout the article. However, measurement-based total deposition estimates (i.e., wet plus inferential dry deposition) are presented only for North America, Africa and Australia as these are the only continents with inferential dry deposition estimates. An alternative measurement-based method for estimating total deposition is the measurement of throughfall, which has been used to estimate total deposition of S in Europe by the CLRTAP ICP (Convention on Long-range Transboundary Air Pollution International Co-operative Programme) Forests network. These estimates are presented in Section 3.6.3.

2.4. Global modeling, mapping and mass budget calculations

Model-based deposition maps were created to complement the measurement data by filling in the large spatial gaps between and outside of measurement points. The model-based maps apply to the year 2001 and represent the ensemble-mean outputs of a set of global chemical transport models that contributed to Phase 1 of the Coordinated Model Studies Activities of the UNECE CLRTAP Task Force on Hemispheric Transport of Air Pollution (TF HTAP). Details of the TF HTAP modeling studies can be found at http://iek8wikis.iek.fz-juelich.de/HTAPWiki/ and in HTAP (2010), which can be downloaded at www.htap.org. The ensemble mean model values were created by re-gridding the individual model outputs (with grid sizes ranging from $1^\circ \times 1^\circ$ to $5^\circ \times 4^\circ$) to a common grid size ($1^\circ \times 1^\circ$) and then calculating the average of all available model values at each grid point. Some models were not included if their integrated global fluxes for a particular ion were markedly different from the median of all model fluxes for that ion, since this may have pointed to a model bug or unit problem in the output rather than model uncertainty. The limit for acceptance was the median $\pm$ 1.5$\times$ interquartile range.

The final number of models used to calculate the ensemble-mean deposition values for each chemical compound varied, namely, 19 (of a possible 23) were used for sulfur, 16 (of a possible 22) for oxidized nitrogen, 7 (of a possible 9) for reduced nitrogen, 16 (of a possible 24) for precipitation amount, and 8 (of a possible 13) for sea salt. The list of models (and associated names of modelers) used in each set of calculations is shown in Addendum Table S2. Based on the TF HTAP modeling activity, ensemble-mean maps were created for S and N emissions, wet deposition, dry deposition, total deposition, precipitation-weighted mean concentrations, sea salt deposition and precipitation depth. The model-based precipitation-weighted mean concentrations were derived by dividing the gridded ensemble-mean wet deposition by the ensemble-mean precipitation depth.

The TF HTAP global models were used in this assessment for two reasons: (1) to fill in gaps where no measurement data existed and (2) to demonstrate the usefulness of the measurement data for model evaluation. It is acknowledged that regional models exist for certain areas of the world (e.g., Europe, North America, Asia) but, in general, there has been little effort made to make them available to the science community in a well-described and accessible manner similar to the TF HTAP exercise. A one-to-one comparison of global and regional model performance – especially a cross-model intercomparison – has not been done to our knowledge. However, this is a prime of objective of the forthcoming TF HTAP Phase 2 Intercomparison in which global and regional models will perform simulations using shared data sets and, for the regional models, boundary conditions from a known set of global models. Thus, for this global assessment, the TF HTAP modeling exercise was deemed the best source of global modeling results. No regional models were used. Maps of the 2001 ensemble-mean modeling results combined with the 2000–2002 three-year average measurement data are shown throughout the body of the assessment.

The combined measurement-model maps provide the opportunity to fill in the very large spatial data gaps using the modeled estimates of deposition. The 2000–2002 3-year average measurement values were chosen for use with the 2001 modeling results to average out the variability encountered when comparing highly variable point measurement data with much less variable grid-box-average modeled values. Each map is accompanied by a measurement-versus-modeled scatterplot to show the complementarity of the measurement and ensemble-mean modeling results. In these scatterplots, multiple measurement values within given $1^\circ \times 1^\circ$ modeled grid cells appear as grid-cell-average values

rather than single-site values. Globally, only 40 grid cells contained multiple sites. Readers interested in detailed quantitative measures of measurement-model comparability will find them in Table S3 of the Addendum.

Ensemble-mean maps of S and N emissions for 2001 (for individual species and the sum of species) were created to provide a basis for linking measured and modeled deposition estimates to emissions. In the TF HTAP modeling exercise, each modeler was asked to use his/her 'best' emission inventory. Many, but not all of the global inventories of anthropogenic emissions were related back to one EDGAR inventory (e.g., EDGARv3.2) or to inventories prescribed for the Photocomp Exercise (Stevenson et al., 2006; Dentener et al., 2006), with the resultant variability shown in Fig. 3.5 of the TF HTAP Report Part A (HTAP, 2010) (see www.htap.org for download). The ensemble mean emissions were chosen for use in this assessment to be consistent with the ensemble-mean deposition maps and to provide mass consistency between global emissions and deposition when calculating global mass balances of sulfur and nitrogen (Sections 3.5 and 4.5).

The large and variable grid sizes of the multiple emission inventories (from $1^\circ \times 1^\circ$ to $5^\circ \times 4^\circ$) induced a notable uncertainty in the sulfur and nitrogen ensemble-mean emission results. This was due to continental emissions in coastal grid squares being artificially smeared over oceanic areas (and, vice versa, sea salt emissions being smeared over continental grid squares). As a result, the ensemble-mean emission and deposition values of S and N were artificially biased high in grid squares over coastal waters, and artificially low over coastal lands. A sensitivity analysis indicated that this effect extended roughly two degrees offshore (two degrees inland for sea salt).

Based on the ensemble-mean emission and deposition model results, continental and oceanic area-integrated emission and deposition mass budgets were calculated. Because of uncertainties in attributing $1^\circ \times 1^\circ$ model deposition values in coastal grid cells to either land or ocean, the continental and oceanic mass totals were attributed to four different zones: non-coastal continental, coastal continental, non-coastal oceanic and coastal oceanic, where the two coastal zones included all coastal land grids plus their two adjacent oceanic grids. Fig. 2.2 illustrates the zones used in the area-integrated mass budget calculations.

3. Sulfur

Due to the paucity of precipitation chemistry measurements around the world, publications of sulfur (S) precipitation composition and deposition on a global scale have necessarily been based on chemical transport model predictions – with the exception of the World Meteorological Organization's Global Acid Deposition Assessment (Whelpdale and Kaiser, 1996) described in the Introduction. Global patterns of sulfate (SO_4^{2-}) deposition estimated by chemical transport models over the last decade (Rodhe et al., 2002; Bouwman et al., 2002; Dentener et al., 2006; HTAP, 2010) indicate high deposition of SO_4^{2-} in East Asia (specifically in southeastern China), northeastern India and Bangladesh, central Europe, and northeastern North America. These studies also indicate good agreement between model estimates and measurements in Europe and North America, although less so in parts of Asia. Intercontinental contributions are estimated to be small (HTAP, 2010). Dentener et al. (2006) estimated that 36–51% of all SO_x is deposited over the oceans and that 50–80% of the fraction of deposition on land falls on natural (nonagricultural) vegetation. Bouwman et al. (2002) indicated that 7–17% of the global area of natural ecosystems is at risk of acidification from S and N (i.e., deposition exceeds the ecosystem critical load). Global modeling results are consistent with model predictions for individual regions, including East Asia (Han et al., 2006; Guttikunda et al., 2001; Wang et al., 2008), and North America (IJC, 2008; Environment Canada, 2005; NAPAP, 2005).

Sulfate deposition has long been implicated in aquatic and terrestrial ecosystem effects and in the exceedance of ecosystem critical loads in Canada and the U.S. (Environment Canada, 2005; IJC, 2010). Regional-scale S concentrations in precipitation and wet deposition from measurement data have been published for a number of areas worldwide and for various time periods. In North America, SO_4^{2-} deposition has been shown to be highest in the Great Lakes area of Canada and the U.S. (Environment Canada, 2005; NAPAP, 2005; Sickles and Shadwick, 2007; Lehmann et al., 2005; Baumgardner et al., 2002; Nilles and Conley, 2001; IJC, 2008). The most recent maps (IJC, 2012) show that the area once receiving more than 20 kg S ha^{-1} a^{-1} of wet deposited SO_4^{2-} as S has disappeared. Using long-term measurement data from national networks and mass balance calculations, Vet and Ro (2008) analyzed the contribution of long range transboundary transport of S emissions between the U.S. and Canada on wet S deposition in eastern North America. Results showed that in 1990–1994 and 1996–2000, eastern Canada emitted, on average, 8–9% of eastern North American S emissions but received 28–29% of eastern North American nssS wet deposition, while the eastern U.S. emitted 91–92% of the S but received only 71–72% of the nssS wet deposition.

Regional-scale results have been supplemented by studies of particular aspects of deposition including deposition through fog and cloud events, and at specific locations including high elevation areas (e.g., Clow et al., 2002; Hidy, 2003; Ingersoll et al., 2008; Kvale and Pryor, 2006; Kelly et al., 2002; Martin et al., 2000; Willey et al., 2006; Peters et al., 2002; Anderson et al., 2006; Sickles and Grimm, 2003; Hutchings et al., 2009; Aleksic et al., 2009; Dukett et al., 2011). Almost all of these studies showed significant declines in SO_4^{2-} deposition since the late 1980s and 1990s. In Mexico, high concentrations of SO_4^{2-} in precipitation have also been observed. Short-term studies show much higher concentrations in Mexico City (Baez et al., 2007) than in the Mayan Riviera (Bravo et al., 2000).

In South America, the majority of past studies on precipitation chemistry and deposition have focused on urban centers or industrial zones. Given the paucity of regionally-representative long-term data, S concentrations and deposition observations from this region were extracted from the literature and are summarized later in this chapter.

In Europe, regional-scale spatial and temporal analyses of ion concentrations in precipitation and wet deposition are regularly presented by the European Monitoring and Evaluation Programme (EMEP). The EMEP assessment report from 2004 (Lövblad et al., 2004) presented an analysis of the first 25 years of measurement data, and a review that includes data from 1972 up to 2009 has been recently published by Tørseth et al. (2012). EMEP annual status reports can be downloaded from http://www.emep.int/. There have been large reductions in ambient concentrations and deposition of S species during the last few decades. Reductions were of the order of 70–90% since the year 1980, and correspond well with reported emission changes (Tørseth et al., 2012; EMEP/CEIP, 2012). Consequently the European area estimated to be at risk of acidification from S and N deposition has been substantially reduced, with the most sensitive areas located in Northern Europe and Scandinavia (WGE, 2011). The area at risk of acidification was about 10% in 2000, and under current legislation it is projected to be reduced to 4% in 2020. Sulfate continues to be the most important acidifying anion in acidified surface waters (WGE, 2011).

Model predictions for the period 1990–2004 were presented in the review of the CLRTAP Gothenburg Protocol (Fagerli et al., 2006), and showed that in 1990 many areas in Europe had S deposition as high as 30 kg nssS ha^{-1} a^{-1}, while in 2004 only parts of eastern

Europe received S deposition above 10 kg nssS ha^{-1} a^{-1}. Furthermore, the area receiving highest S deposition has shifted from Central-East European countries such as Germany, Poland, Czech Republic and Slovakia to eastern European countries such as Bulgaria, Romania, Serbia, Bosnia and Herzegovina (Fagerli et al., 2006). In addition to monitoring under EMEP, special studies have been conducted in many of the countries in Europe, generally of a short-term nature and designed to increase understanding of the sources and impacts of concentrations in precipitation and deposition. Given the focus of this assessment on regionally-representative long-term trends, these studies are not discussed here.

In Asia, the Acid Deposition Monitoring Network in East Asia (EANET) periodically presents "State of acid deposition" reports. In 2006, EANET reported considerable variation of annual nssSO_4^{2-} concentrations across East Asia over the period 2000–2004, ranging from <1 to 9.7 mg S L^{-1} at rural and remote sites with the highest concentrations observed in China (EANET, 2006). Spatial patterns of SO_4^{2-} concentrations in precipitation observed at a large mix of sites in India (Siva Soumya et al., 2009) over the period 1978 to 2006 showed very scattered concentrations in relation to distance from the seacoast ranging from 0.33 to 3.67 mg S L^{-1} due to the influence from local emissions. Other recent long-term trend studies in the region include Zhang et al. (2012), who analyzed precipitation samples collected between 1989 and 2006 from the Lijiang region, southwestern China for all major ions. The study showed significantly increasing S concentrations, mostly contributed by soil/dust sources remarkably correlated with the increasing number of tourists. The presence of sulfate in mineral dust is attributed to emissions of soil evaporate minerals (calcium, magnesium or sodium sulfate) and to the coating and interaction of dust particles with sulfate and/or its precursors (SO_2 and H_2SO_4) originating from anthropogenic emissions (Rodriguez et al., 2011).

Wet deposition over the period 2005–2009 was reported to be highest in China (>64 kg S ha^{-1} a^{-1}) and lowest at sites in Phillipines, Mongolia and Russian Federation (<0.5 kg S ha^{-1} a^{-1}) (EANET, 2011). In East Asia, SO_2 emissions are still the major contributor to acidic deposition (EANET, 2011). Apart from regional assessments by EANET and others, smaller scale and short term sampling campaigns were conducted in individual Asian countries; however, these are too local for the scope of this assessment. Critical load assessments in China (Zhao et al., 2009) and Asia (Hicks et al., 2008) consistently show a risk of soil acidification from S deposition in eastern and southern China and parts of Southeast Asia, but there is no evidence of impacts outside of China.

In Africa, publications of regionally-representative and ecosystem-specific S concentrations and wet deposition report measurements collected at IDAF (IGAC/DEBITS/Africa program) sites in the following countries: Niger and Mali (Galy-Lacaux et al., 2009; Laouali et al., 2012), Republic of Côte d'Ivoire (Yoboué et al., 2005), Benin, Cameroon (Sigha-Nkamdjou et al., 2003), and South Africa (Mphepya et al., 2004, 2006). Sulfate was the predominant ion at sites in South Africa (0.23–0.94 mg S L^{-1}), but not at sites north of the equator (0.08–0.11 mg S L^{-1}).

Recent publications of S concentrations in precipitation in Oceania are limited. Two in particular report extremely different annual volume weighted ranges of nssSO_2^{4-} in rainwater at sites in the Indian Ocean (Baboukas et al., 2004) and in New South Wales and Malaysia (Ayers et al., 2002). Concentration ranges of nssSO_4^{2-} (as S) were 0.049–0.73 mg S L^{-1} in the Indian Ocean (1991–1999), 0.30–0.54 mg S L^{-1} in Malaysia (1993–1997) and 0.053–0.12 mg S L^{-1} in New South Wales (1993–1994).

Long-term observations in the Arctic show that SO_4^{2-} concentrations in precipitation are relatively low (below 0.5 mg S L^{-1}), with considerable spatial variation depending on the location of emission sources, and a decreasing trend in recent years (AMAP, 2006; Hole et al., 2009). Concentrations are generally higher in the winter, but deposition may be highly episodic (AMAP, 2006). Measurements of precipitation chemistry in cold regions with snow cover and low precipitation are difficult to obtain because of the interference of blowing snow at high wind speeds. A unique attempt to exclude blowing snow from precipitation sampling was made by Toom-Sauntry and Barrie (2002) in their 3-year study at Alert, Canada.

In the sections that follow, sulfur (S) concentrations and wet, dry and total deposition estimates are described at the global scale and in each region based on the 3-year average 2000–2002 and 2005–2007 measurement data and the complementary 2001 TF HTAP ensemble mean modeling results. For clarity, the following nomenclature is used for the S species and the various emission and deposition values: *S emissions* refers to the sum of SO_2 emissions plus non-sea-salt SO_4^{2-} (i.e., particle-SO_4^{2-} and/or H_2SO4) and DMS (dimethyl sulfide) emissions (over the oceans only), expressed as S; *measured S concentrations in precipitation* and *S wet deposition* refer to all oxidized S species measured as the sulfate ion in precipitation including dissolved inorganic SO_4^{2-} and dissolved SO_2 converted to SO_4^{2-}; *sea salt S (ssS)* refers to S from sea salt and *non-sea-salt S (nssS)* refers to all S not including sea salt S (where measured nssS is estimated using the methods specified in WMO/GAW, 2004); *model-based S wet deposition* refers to the sum of modeled wet nssSO_4^{2-}-S + wet SO_2–S deposition; *model-based S concentrations in precipitation* are derived values calculated as the model-based gridded nssS wet deposition values divided by their associated gridded precipitation depth values (i.e., the precipitation-weighted mean concentrations were not modeled directly); *measurement-based inferential dry deposition* refers to the sum of gaseous SO_2–S and aerosol SO_4^{2-}–S dry deposition estimates unless specified otherwise; *model-based dry deposition* refers to the sum of gaseous SO_2–S and aerosol nssSO_4^{2-}-S dry deposition estimates; *total deposition of S* (both measured and modeled) refers to the sum of wet plus dry deposition of S as defined above. Addendum Table S3 summarizes all comparability statistics associated with the combined measurement and model-based maps shown below.

3.1. Global and regional emissions of S

The TF HTAP global pattern of S emissions for the year 2001 is shown in Fig. 3.1 as context for the assessment of precipitation chemistry and deposition. The figure contains the gridded ensemble-mean emission values derived from the TF HTAP S models, 19 of which included SO_2–S emissions, 16 of which included DMS-S emissions (ocean and minor continental sources), and 11 that included nssSO_4^{2-}-S. SO_2–S and SO_4^{2-}–S emission sources included power generation, industry, transport (including shipping), biofuel use, large biomass burning and agricultural fires, and natural sources including volcanoes and terrestrial and oceanic DMS-S. Sea salt S emissions were not included. Global emissions of SO_2–S were considerably higher than SO_4^{2-}–S and DMS-S emissions (with relative percentages of 73%, 7% and 20%) except over the non-shipping portions of the oceans where DMS-S accounted for 85–100% of S emissions (this decreased in the major shipping channels to 40%).

Globally, the 2001 gridded S emission values (1° × 1°) in 2001 (Fig. 3.1) were highest (40–162.3 kg S ha^{-1} a^{-1}) in parts of Europe (global maximum = 162.3 kg S ha^{-1} a^{-1} in the Ionian Sea and European maximum = 83.4 kg S ha^{-1} a^{-1} in the Czech Republic), eastern China (max = 105.6 kg S ha^{-1} a^{-1}) and the eastern U.S. (max = 52.8 kg S ha^{-1} a^{-1}). Areas with emissions in the 10–40 kg S ha^{-1} a^{-1} range existed on all continents except Australia and Antarctica, although they occurred in only a few small areas of

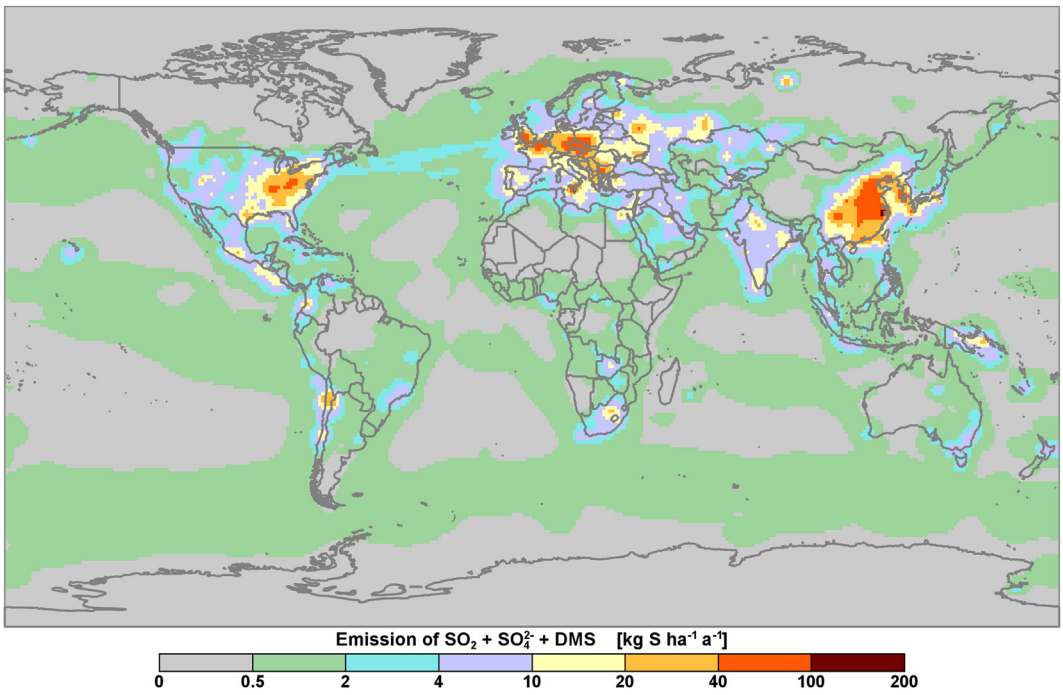

Fig. 3.1. 2001 ensemble-mean, 1° × 1°, global S emissions including SO_2–S, nssSO_4^{2-}–S and DMS-S in kg S ha^{-1} a^{-1}.

South America and Africa. Low emissions of <0.5 kg S ha^{-1} a^{-1} occurred over most of South America, northern Canada, northern Asia, Africa, Oceania, Antarctica and the oceans.

Area-integrated S emissions for the globe, continents, oceans and coastal-zones are presented for 2001 in Table 2. Note that Table 2 also contains area-integrated total deposition values that are discussed later. The area-integrated emissions and deposition represent only nssS and were calculated as the sum of all grid square ensemble-mean emission and deposition values within the continents, oceans and coastal zones defined by Fig. 2.2.

Global S emissions in 2001 were estimated at 91.0 (±7.3) Tg S a^{-1} where 7.3 represents the one sigma standard deviation of the emissions from all models in the ensemble. Of this, 55.4% (or 50.4 Tg S a^{-1}) came from continental sources, 21.1% (19.2 Tg S a^{-1}) from oceanic sources and 23.5% (21.4 Tg S a^{-1}) from coastal zone sources. As mentioned in Section 2, coastal zone sources included land-based emissions as well as ocean shipping and biogenic (DMS-S) emissions. Total ocean shipping and biogenic emissions accounted for roughly 3% and 6%, of the global S emissions, respectively. Non-coastal + coastal Asia accounted for

Table 2
2001 area-integrated estimates of S emissions and total S deposition in Tg S (and as a % of the global total) for continents, oceans and coastal zones. Values were calculated as the sum of the ensemble-mean grid square emissions and total deposition estimates within individual continents, oceans and coastal zones as defined by Fig. 2.2. Note that total Coastal emissions (and deposition) are equivalent for the Continents and Oceans. Thus, Global Total emissions and deposition equal the sum of the Non-coastal Continents, Non-coastal Oceans and one of the Coastal Continents or Oceans.

Region	Sulfur emissions in Tg S (% of Global S emissions)		Sulfur total deposition in Tg S (% of Global S total)	
	Non-coastal	Coastal	Non-coastal	Coastal
Continents				
Africa	3.4 (3.7)	1.3 (1.5)	3.4 (4.0)	1.2 (1.4)
Antarctica	0.0 (0.0)	0.1 (0.1)	0.1 (0.1)	0.1 (0.1)
Asia	21.5 (23.6)	7.9 (8.7)	17.9 (21.1)	7.2 (8.6)
Europe	11.6 (12.8)	4.8 (5.3)	8.2 (9.6)	3.9 (4.6)
North America	9.9 (10.9)	3.2 (3.5)	7.4 (8.7)	3.1 (3.6)
Oceania	1.0 (1.1)	2.8 (3.0)	0.9 (1.1)	2.3 (2.7)
South America	3.0 (3.3)	1.3 (1.4)	2.3 (2.8)	0.9 (1.1)
Σ Continents	**50.4 (55.4)**	**21.4 (23.5)**	**40.2 (47.4)**	**18.7 (22.1)**
Oceans				
North Atlantic	3.2 (3.6)	8.1 (8.8)	5.2 (6.2)	7.0 (8.3)
South Atlantic	2.0 (2.2)	0.5 (0.5)	2.1 (2.4)	0.4 (0.5)
North Pacific	4.7 (5.2)	7.7 (8.5)	8.4 (10.0)	6.7 (7.9)
South Pacific	4.6 (5.0)	2.3 (2.5)	4.6 (5.5)	1.6 (1.9)
North Indian Ocean	0.7 (0.8)	1.7 (1.9)	1.5 (1.7)	1.6 (1.9)
South Indian Ocean	3.0 (3.3)	0.9 (1.0)	3.2 (3.7)	0.8 (1.0)
Arctic Ocean	0.1 (0.1)	0.1 (0.2)	0.3 (0.3)	0.5 (0.5)
Southern Ocean	0.9 (0.9)	0.1 (0.1)	0.6 (0.7)	0.1 (0.1)
Σ Oceans	**19.2 (21.1)**	**21.4 (23.5)**	**25.9 (30.5)**	**18.7 (22.1)**
TOTAL	**69.6 (76.5)**	**21.4 (23.5)**	**66.1 (77.9)**	**18.7 (22.1)**

32.3% of the global emissions, Europe 18.1% and North America 14.4%. For the non-coastal oceans, the North Pacific and South Pacific emissions were highest at 5.2% and 5.0% of the global emissions, respectively, and the Arctic Ocean emissions were lowest at only 0.1% of the global total. The 2001 ensemble-mean global S emission estimate of 91.0 Tg S in Table 2 is consistent with the 2000 estimate of 90.2 Tg S in Dentener et al. (2006) in which the regional anthropogenic emissions were generated by IIASA and spatially distributed using the EDGAR 3.2 database. It must be acknowledged, however, that the ensemble variability of global emissions in our case was relatively high, with a standard deviation of ±7.3 Tg S.

3.2. Global S in precipitation and wet deposition

Measurement-based 3-year-average patterns of precipitation-weighted mean concentrations of S (as measured by SO_4^{2-}–S concentrations in precipitation samples and including ssS) are shown in Fig. 3.2a and b for the periods 2000–2002 and 2005–2007, respectively. It is clear that large areas of the globe have had (and continue to have) little or no measurement coverage. To fill the large measurement gaps in southern Africa, measurement data from South Africa were included for the non-conforming period 1986–2000. The screened-in data set shown in Fig. 3.2a consisted of 437 Satisfactory, 30 Conditional and 4 Non-Conforming-Period data points and the data set in Fig. 3.2b consisted of 470, 14 and 0 data points, respectively.

Globally, the highest 3-year-average annual precipitation-weighted mean concentrations of S ranged from 1.20 to 3.24 mg S L^{-1} in the 2000–2002 period and from 1.20 to 4.58 mg S L^{-1} in the 2005–2007 period. During both periods, the maximum values of 3.24 and 4.58 mg S L^{-1}, respectively, were measured at the Chongqing-Jinyunshan and Xi'an-Jiwozi EANET sites in eastern China. The other sites with concentrations $\geq$ 1.2 mg S L^{-1} were located in Asia (China, Russian Federation, the Republic of Korea, Japan) and Europe (Serbia, Spain). The lowest concentrations globally in the two periods were in the range of 0.02–0.06 mg S L^{-1} and were all in the U.S.. Not unexpectedly, the spatial patterns of concentration closely mimic the global pattern of S emissions (Fig. 3.1) with high values occurring in high emission areas and low values in low emission areas (with allowances for the added influences of long range transport and precipitation patterns).

The measurement-based 3-year average patterns of S wet deposition for 2000–2002 and 2005–2007 are shown in Fig. 3.3a and b, respectively, and for nssS in Fig. 3.3 c and d, respectively. As with the precipitation-weighted mean concentrations, the wet deposition patterns closely reflect the pattern of S emissions with the added influences of long range transport and precipitation. In 2000–2002 and 2005–2007, the highest 3-year average S wet deposition values were measured in Asia (China, Japan, India, Taiwan), Europe (Croatia and Ireland) and North America (U.S.), ranging from 12.00 to 34.90 kg S ha^{-1} a^{-1} and 12.00–49.82 kg S ha^{-1} a^{-1}, respectively. The highest global values of 34.90 and 49.82 kg S ha^{-1} a^{-1} for the two periods were measured at the Integrated Monitoring Programme on Acidification of Chinese Terrestrial Systems (IMPACTS) Tie Shan Ping site in eastern China in 2000–2002 and the EANET Chongquing-Jinyunshan site in eastern China in 2005–2007. Although this assessment does not consider urban deposition, it is interesting to note that the highest wet deposition value measured globally during our two periods was 76.16 kg S ha^{-1} a^{-1} at the urban EANET Xi'an-Weishuiyuan site in eastern China in 2000–2002.

The lowest 3-year average S wet deposition values measured globally were 0.05 kg S ha^{-1} a^{-1} in 2000–2002 at the Joshua Tree National Park NADP site and 0.08 kg S ha^{-1} a^{-1} in 2005–2007 at the NADP Smith Valley site, both located in western U.S.. Global maxima were 698 and 623 times higher than the global minima during the two periods. Sea salt sulfur (ssS) was an important contributor to wet deposition in the coastal and island areas of the world and is responsible for the difference between Fig. 3.3c and d (nssS) and Fig. 3.3a and b (nssS + ssS). Based on the WMO calculation method for calculating nssS at sites within 100 km of saltwater coastline (WMO/GAW, 2004), the global percentage contribution of ssS to S wet deposition for the 2005–2007 period (Fig. 3.4) varied globally from a low of 0.9% in the U.S. to a high of 86% in Ireland.

Anthropogenic S emissions changed markedly in North America, Europe and Asia from 2000 to 2007. Major reductions in S emissions occurred in Canada, the U.S., and Europe while major increases occurred in China, India and other parts of east and south Asia (IJC, 2010; EMEP/CEIP, 2012; EANET, 2011; HTAP, 2010). The effect of these emission changes on nssS wet deposition is shown in Fig. 3.5a which plots the global map of % changes between the 2000–2002 and 2005–2007 3-year average annual nssS wet deposition values, and in Fig. 3.5b which plots the data in continent-by-continent box-and-whisker plots. In all cases, the % changes were calculated as $100 \times [D_{2005-2007} - D_{2000-2002}]/[D_{2000-2002}]$ where D is the 3-year average value. For context, Fig. 3.5b also shows the % changes in the 3-year average nssS concentrations and precipitation depth given

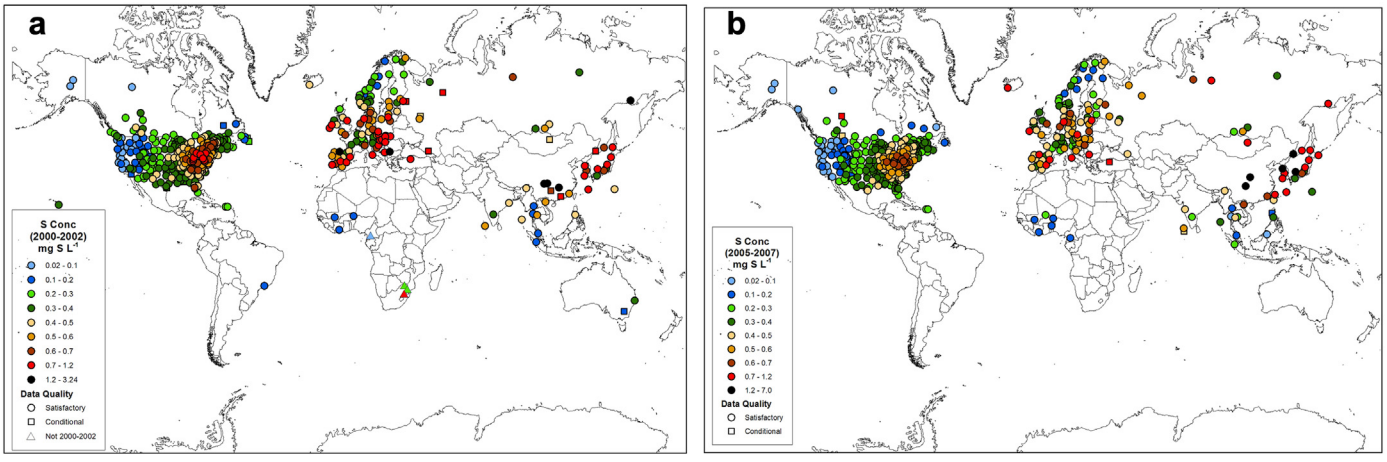

Fig. 3.2. Measured 3-year annual average precipitation-weighted mean concentrations of S in precipitation for (a) 2000–2002 and (b) 2005–2007.

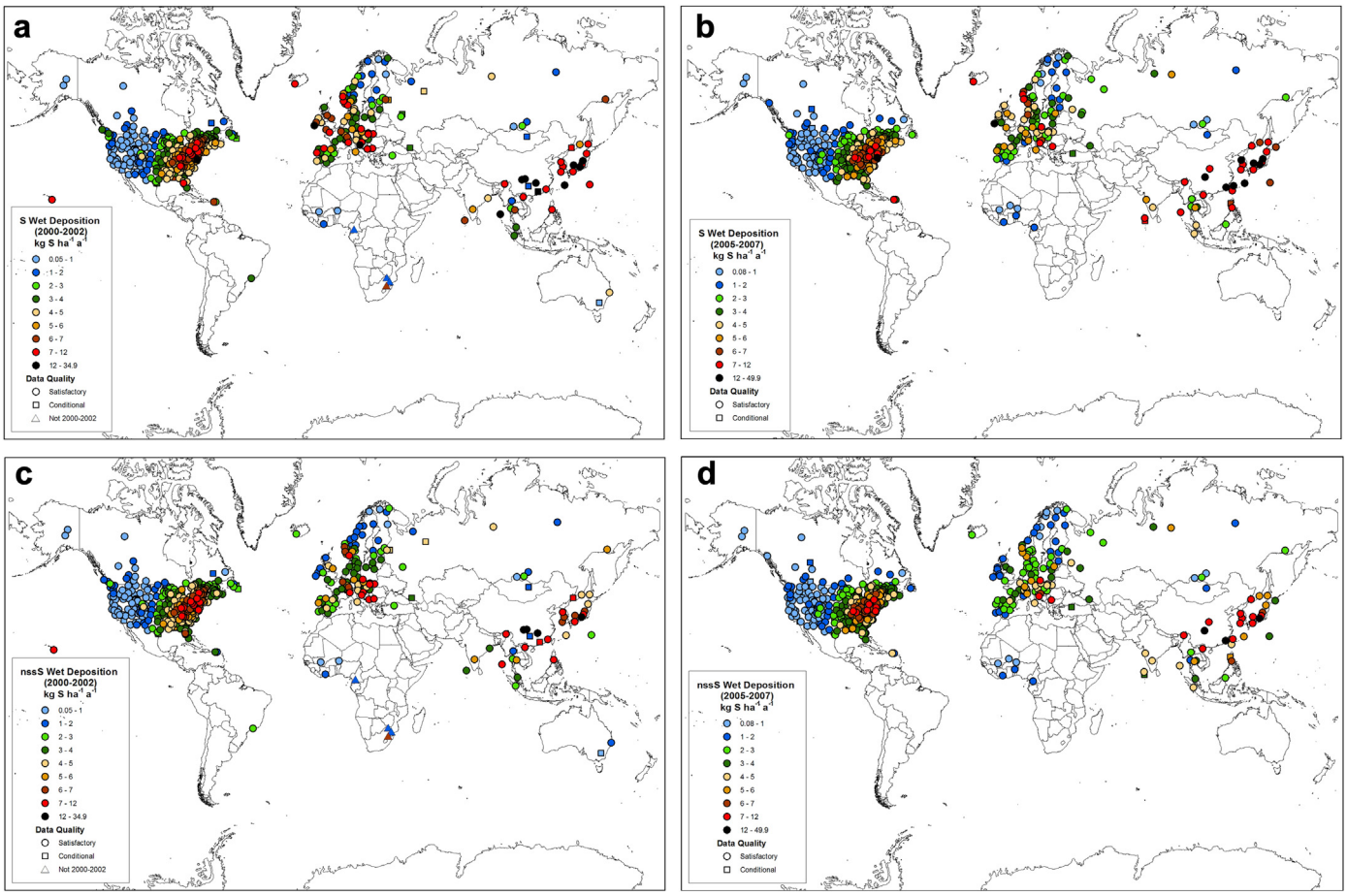

Fig. 3.3. Measured 3-year annual average wet deposition of: (a) S for 2000–2002, (b) S for 2005–2007, (c) nssS for 2000–2002, and (d) nssS for 2005–2007.

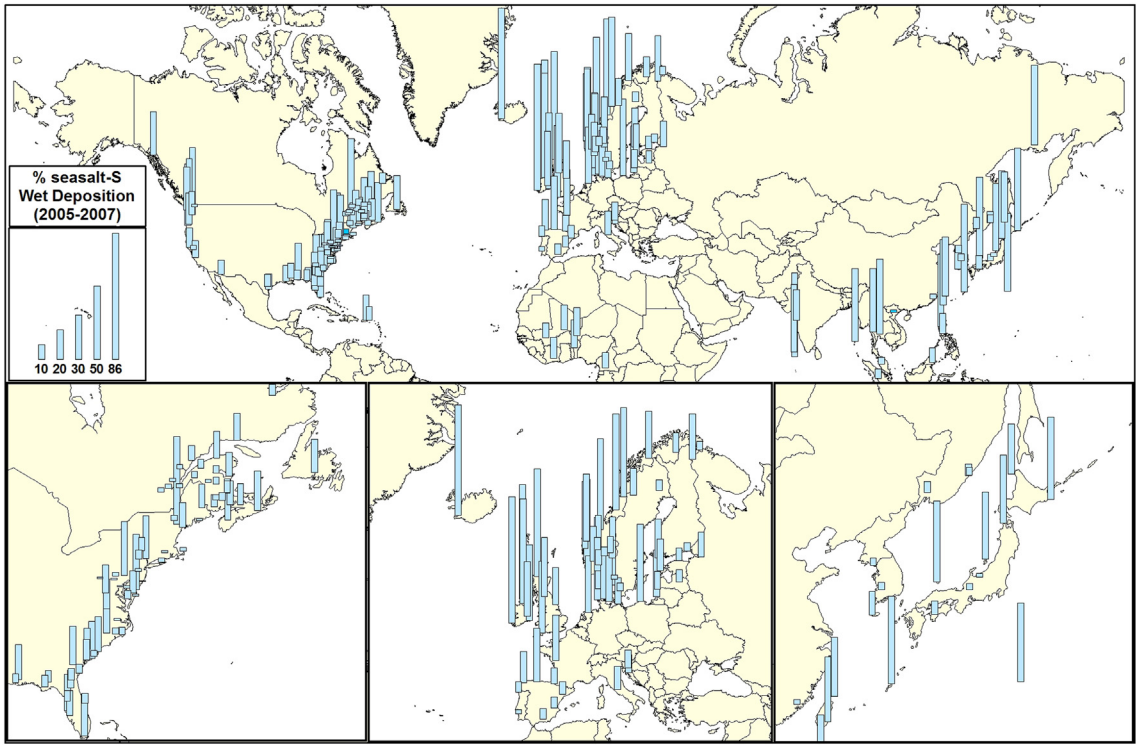

Fig. 3.4. Percent ssS contribution to measured S wet deposition based on 3-year average annual wet deposition values for 2005–2007.

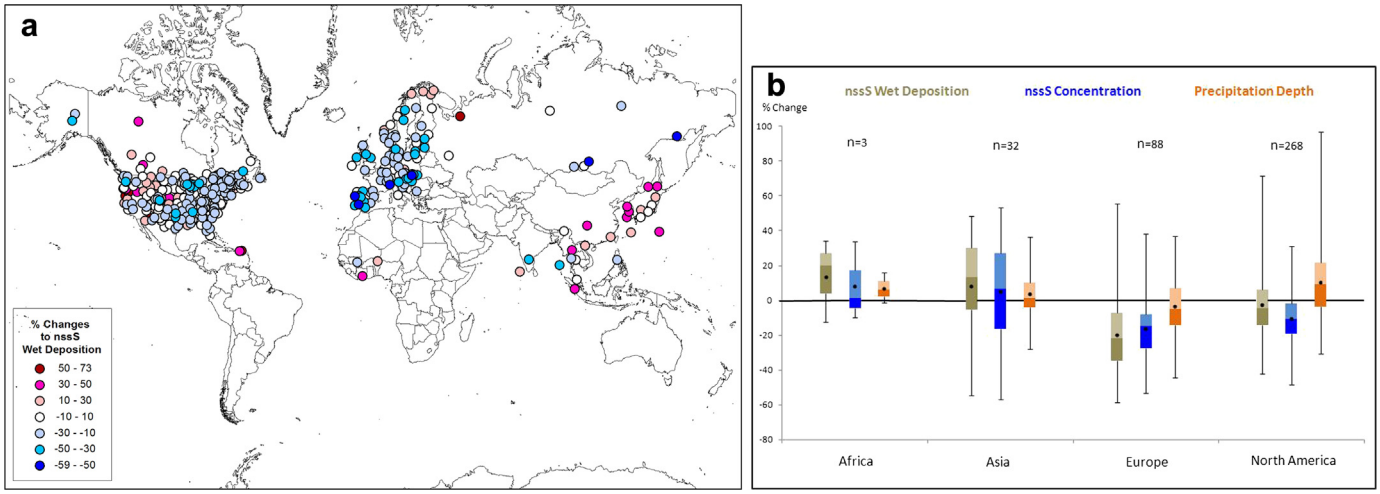

Fig. 3.5. (a) Global % change between the 2000–2002 and 2005–2007 3-year mean wet deposition fluxes of nssS (calculated as 100 $[D_{2005-2007} - D_{2000-2002}]/[D_{2000-2002}]$) and (b) box-and-whisker plots of the % changes of wet deposition (brown), concentration (blue) and precipitation depth (orange) at all sites in Africa, Asia, Europe and North America. The whiskers represent the minimum and maximum values, the bottom and top of the boxes represent the 25th and 75th percentiles, the centre line represents the median, the dot represents the mean and n equals the number of measurement sites.

that wet deposition changes reflect both concentration and depth changes.

Consistent with the North American SO_2–S emission reductions, Fig. 3.5a,b indicates that nssS wet deposition also decreased in North America (median % change of 268 sites = −4.5%) and Europe (median % change of 88 sites = −22.2%). More than 60% of the North American sites (166 of 268) showed decreases of 0–42%, and 82% of the European sites (71 of 88) showed decreases of 0–58%. Fig. 3.5b indicates that these decreases were due predominantly to decreasing concentrations of nssS (associated with the major reductions in S emissions on both continents) and not to decreasing precipitation depths. In fact, Fig. 3.5b shows that most sites in North America had greater concentration decreases than wet deposition decreases. Consistent with increasing S emissions in Asia, wet deposition in Asia increased by as much as 48% at one site in China, with 65% of the sites (20 of 32), showing increases from 0 to 48% and the other 35% of the sites showing decreases from 0 to 54%.

The map of % changes in precipitation depth (Addendum Fig. S2c) shows that major precipitation increases occurred in western North America, along the coast of Norway, and at a few sites in East Asia while major decreases occurred in east-central North America and much of Europe. At many sites in western North America, the increasing precipitation depths coupled with the decreasing precipitation-weighted mean concentrations of nssS (Addendum Fig. S2d), produced net decreases in wet deposition (Fig. 3.5a,b). In contrast, along the coast of Norway and in East Asia, the increased levels of wet deposition were largely due to increases in both concentration and precipitation depth.

The combined measurement and ensemble-mean model maps serve to enhance our understanding of global patterns of precipitation concentrations and wet deposition of S. On the assumption that measurement-model comparability is good, the modeled values provide estimates of values in the areas between the measurement points and over the oceans. To that end, the 2000–2002 3-year average measured values of nssS precipitation-weighted mean concentrations and nssS wet deposition are superimposed on the 2001 ensemble-mean nssS modeled patterns in Fig. 3.6a and c, respectively. Presented beside the maps are scatterplots (Fig. 3.6b and d) of the grid-average measured versus modeled values. It is important to note that the model-based pattern of precipitation-weighted mean concentrations (Fig. 3.6a) was produced by dividing the ensemble-mean annual wet deposition value for each $1^\circ \times 1^\circ$ grid square by its associated ensemble-mean annual precipitation depth (i.e., the precipitation-weighted mean concentrations were not modeled). As expected, the concentration and wet deposition patterns in Fig. 3.6a,c strongly mimic the emission patterns of S with allowances for long range transport, dispersion, chemical transformation, precipitation and deposition.

Fig. 3.6b shows considerable scatter between the measured and modeled *precipitation-weighted mean concentrations* of nssS ($r = 0.678$; $n = 428$ grid squares). Nevertheless, reduced scatter and high correlations occurred in Africa ($r = 0.986$; $n = 7$), North America ($r = 0.886$; $n = 273$), Europe ($r = 0.586$; $n = 106$) and Asia ($r = 0.742$; $n = 39$), which indicates that the lower global r value was due to a combination of over-predicted modeled values (but good correlations) in Europe and North America and under-predicted modeled values (but good correlations) in Asia. Fig. 3.6a suggests that a modeled global *background* nssS concentration would be <0.04 mg S L^{-1} over Antarctica and remote ocean areas. Several of the continental and offshore areas show modeled concentrations in the range of 0.1–1.0 mg S L^{-1} while the high emission areas of North America, Europe, and East Asia (see Fig. 3.1) have the highest global concentrations of 1.0–2.0 mg S L^{-1}. The maximum measured global concentrations were 3.2 and 2.9 mg S L^{-1} at the EANET sites of Chongquing-Jinyunshan and Tie Shan Ping (China), respectively, while the lowest measured value was 0.03 mg S L^{-1} at the Sagehen Creek NADP site in the western U.S.. Further measurement-model comparison statistics can be found in Addendum Table S3.

The measured and modeled values of nssS *wet deposition* shown in Fig. 3.6c compare better ($r = 0.793$) than do the concentrations ($r = 0.678$), with more uniform scatter about the one-to-one line (Fig. 3.6d). An analysis indicated that this was due to the HTAP model concentrations being over-predicted at many sites and the precipitation depths being under-predicted (or vice versa), leading to a net effect of better predictions of wet deposition. Fig. 3.6c and d show that slight model over-predictions of wet deposition occur in North America and Europe and under-predictions occur in Asia. The modeled wet deposition pattern has a global range of 0.01 kg S ha^{-1} a^{-1} in Antarctica to 20.40 kg S ha^{-1} a^{-1} in eastern China. In terms of measurements, three sites in eastern China recorded measured nssS wet deposition considerably higher than

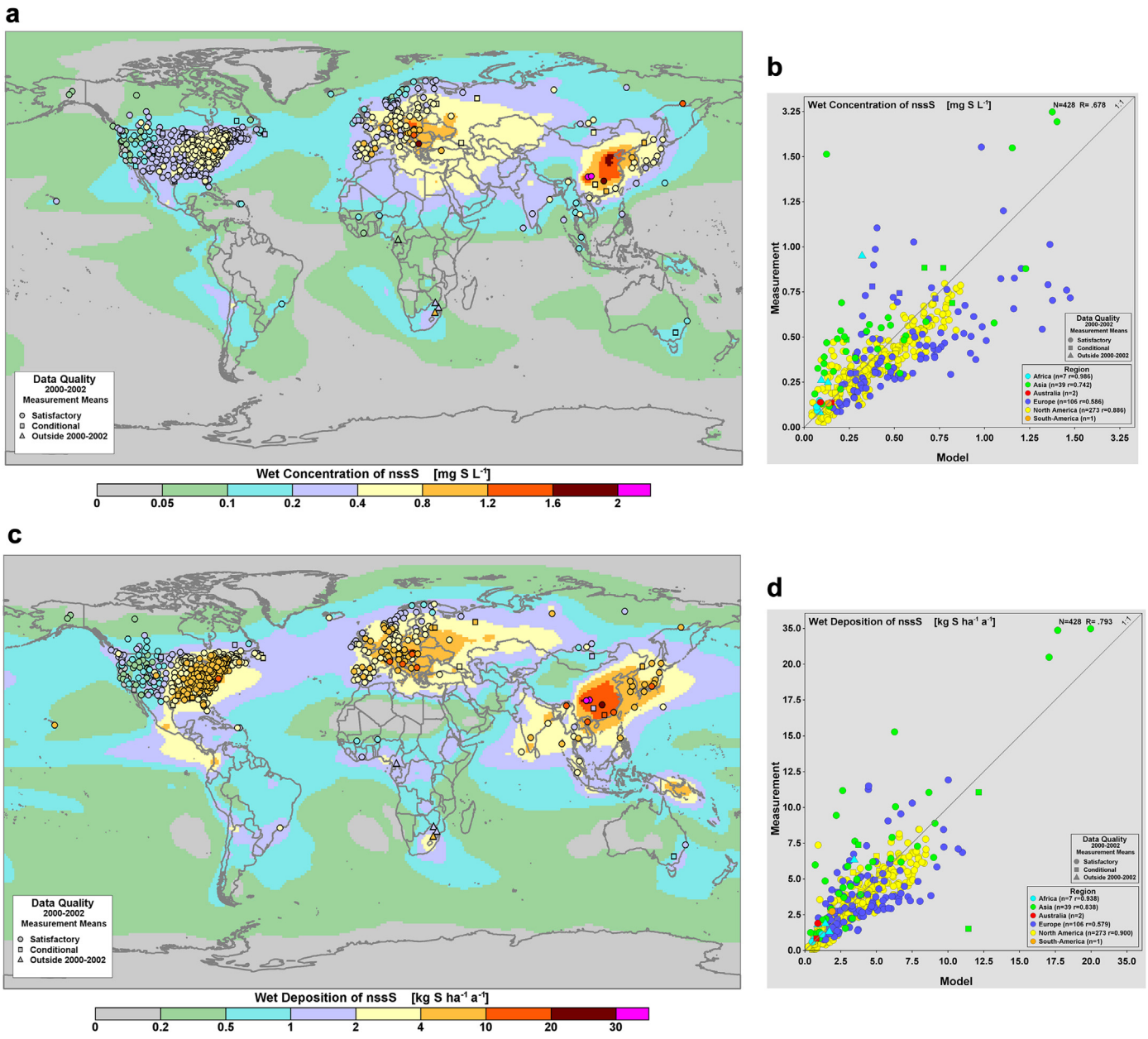

Fig. 3.6. (a) Measurement-model precipitation-weighted mean concentrations with (b) concentration scatterplot, and (c) measurement-model wet deposition of nssS in kg S ha^{-1} a^{-1} with (d) deposition scatterplot. Measurement values represent 3-year averages (2000–2002) of nssS; model results represent 2001 nssS values. Note the non-linear scale in the last increment of the scatterplot.

the modeled maximum, namely: Cai Jia Tang at 22.92 kg S ha^{-1} a^{-1}, Chongqing-Jinyunshan at 34.25 kg S ha^{-1} a^{-1}, Tie Shan Ping at 34.90 kg S ha^{-1} a^{-1}. Assuming that the modeling results in Fig. 3.6c captured the general pattern of wet deposition reasonably well, global background wet deposition levels are projected to range from <0.2 to 1.0 kg S ha^{-1} a^{-1} over the remote oceans. Considerably higher levels of 1.0–4.0 kg S ha^{-1} a^{-1} are modeled over the mid-latitudinal areas of the Atlantic and Pacific Oceans and the equatorial regions of the Atlantic, Pacific and Indian Oceans due to ship emissions and off-shore transport of continental emissions (see later discussion).

As expected from the global emission pattern (Fig. 3.1), the low-emission areas of the continents (specifically, northern and western North America, most of South America, most of Africa, northern Scandinavia, northern and central Asia and most of Oceania) received low levels of wet deposition in the range of 0.2–2.0 kg S ha^{-1} a^{-1} (modeled) while the continental areas within and adjacent to the high emission source regions received very high levels of 4.0–34.90 kg S ha^{-1} a^{-1} (measured).

3.3. Global dry deposition of S

Measurement-based inferential network estimates of S dry deposition were made in only a few countries worldwide using the *inferential technique* explained in Section 2. The long-term inferential estimates were available only in Canada, the U.S., Japan, Africa and Australia. The measurement techniques, the S species measured, the periods of measurement, and the dry deposition

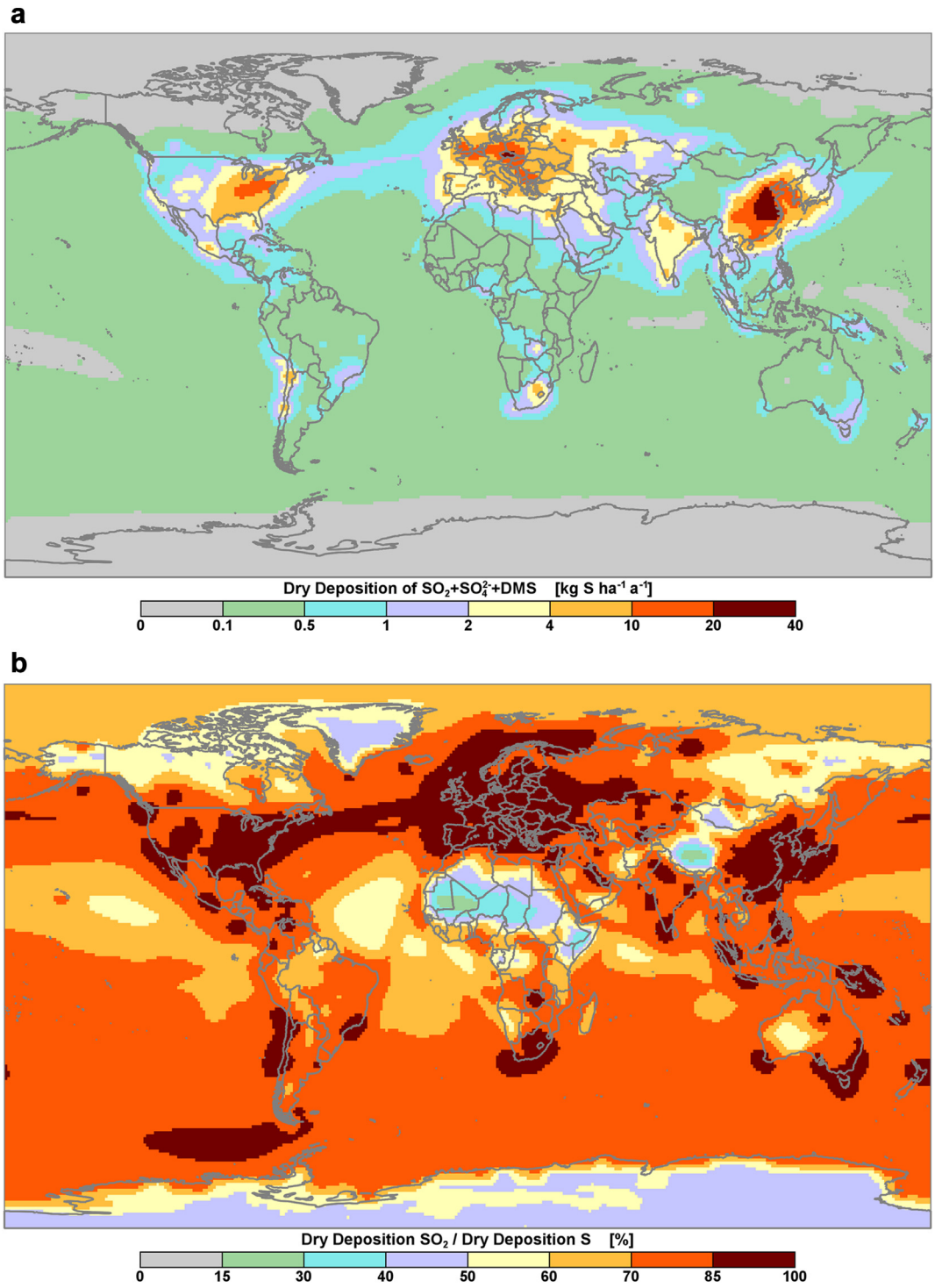

Fig. 3.7. 2001 ensemble-mean patterns of: (a) dry deposition of S (actually nssS) from SO_2 dry deposition, p-SO_4^{2-} dry deposition, and DMS-S in kg S ha^{-1} a^{-1} and (b) % ratio of SO_2–S dry deposition to S dry deposition as defined in (a).

velocity models varied considerably from country to country which made it difficult to produce a global map of dry deposition. For this reason, the following discussion on global dry deposition is based only on the 2001 HTAP ensemble-mean modeling estimates of S dry deposition (non-sea-salt-sulfur) and the reader is referred to the North America, Africa and Oceania sections for region-specific discussions of the measurement-based inferential dry deposition estimates.

The 2001 ensemble-mean pattern of nssS dry deposition is shown in Fig. 3.7a, along with the % contribution of SO_2–S to nssS dry deposition in Fig. 3.7b.

The global model-based pattern of nssS dry deposition in Fig. 3.7a closely mimics the global pattern of S emissions (Fig. 3.1) and nssS wet deposition (Fig. 3.6b). Maximum global dry deposition model estimates to range from 20.0 to 33.0 kg S ha^{-1} a^{-1} in the very high S emission areas of eastern China and the so-called Black

Triangle area of Germany, Poland and the Czech Republic (per Fig. 3.1). Levels from 4.0 to 20.0 kg S ha^{-1} a^{-1} appear on all continents (except Australia and Antarctica) in areas with emissions exceeding roughly 1 kg S ha^{-1} a^{-1}. Very low dry deposition levels of less than 0.5 kg S ha^{-1} a^{-1} appear in the low emission regions of the continents and over most of the remote oceans (not including the near-coastal regions and the major shipping lanes). The Arctic and Southern Oceans, as well as the continent of Antarctica, have modeled dry deposition levels of less than 0.1 kg S ha^{-1} a^{-1}.

The individual ensemble-mean modeled patterns of SO_2–S and SO_4^{2-}–S dry deposition are not shown here but appear in Fig. S3 of the Addendum. Fig. 3.7b, however, provides a model-based assessment of the importance of gaseous SO_2–S dry deposition relative to S dry deposition, where S consists of gaseous SO_2–S, nss particle SO_4^{2-}–S, and DMS-S. This map, presented as a % ratio, is useful for those who want to estimate S dry deposition but have access only to SO_2–S dry deposition values. Fig. 3.7b suggests that SO_2–S is the dominant contributor (>50%) to S dry deposition worldwide (both continents and oceans) with only a few exceptions, i.e., in very low emission areas of northern and eastern Africa, western China, western Mongolia, Greenland and Antarctica. In the high emission areas of the continents where emissions exceed roughly 2 kg S ha^{-1} a^{-1}, SO_2–S dry deposition appears to contribute >85% of the dry deposition of S. This percentage is expected to be high because the HTAP models do not include ssSO_4^{2-} aerosols and because high uncertainties exist in the dry deposition parameterizations of particle SO_4^{2-}.

3.4. Global total deposition of S

The 2001 ensemble-mean modeled pattern of total deposition of S is shown in Fig. 3.8a; again, measured values could not be superimposed on this figure because measurement-based inferential dry deposition values were not available for most of the globe. The deposition pattern exhibits four areas of very high total deposition: East Asia including eastern China and the Republic of Korea with values of 20.0–50.2 kg S ha^{-1} a^{-1} (the global maximum), western Europe including Germany, Poland, Czech Republic, Romania, Bulgaria, and Belgium with values of 20.0–32.0 kg S ha^{-1} a^{-1} and eastern North America (specifically the northeast U.S.) with values of 20.0–23.4 kg S ha^{-1} a^{-1}. Extensive areas of high deposition in the range of 4.0–20.0 kg S ha^{-1} a^{-1} are projected in the eastern U.S. and southeastern Canada, most of Europe, large sections of Pakistan, India and Bangladesh, and large sections of East Asia including Myanmar, Thailand, Laos, eastern China, the Democratic People's Republic of Korea, the Republic of Korea and Japan. Smaller areas in the same range are predicted on all continents including sections of southern Mexico, Colombia, Chile, and Nigeria, South Africa, western Russian Federation and the area of Oceania around Papua New Guinea. Very large areas of the continents (except Antarctica) and oceans have total deposition from 0.2 to 2.0 kg S ha^{-1} a^{-1} and most of Antarctica has very low levels from 0.1 to 0.2 kg S ha^{-1} a^{-1}, with the former value being the global minimum. Several coastal areas including off eastern North America, around Europe (Mediterranean, North and Baltic Seas), west, south and east of India and east of East Asia show relatively high total deposition levels in the range of 4.0–20.0 kg S ha^{-1} a^{-1} with areas of lower total deposition between 1.0 and 4.0 kg S ha^{-1} a^{-1} extending eastward across the Atlantic Ocean and the Pacific Ocean. These latter high deposition areas appear to be due to continental emissions being transported across the oceans, shipping emissions (Fig. 3.1) and high precipitation depths (Addendum Fig. S2a).

Scientists interested in the ecological effects of S usually need values of total deposition but, unfortunately, often have access only to wet deposition measurement data. In such cases, knowing the ratio of wet or dry deposition to total deposition allows them to estimate total deposition from the wet-only deposition values. Fig. 3.8b shows the ensemble-mean model estimated % contribution of dry deposition to total deposition of S. Not surprisingly, the areas with the highest % dry deposition (>70%) appear in the driest continental areas of the world as well as their nearby coastal zones, including the southwestern U.S., northern Mexico, northern Chile, northern and southern Africa, the Middle East, southwest Asia, and western and eastern Australia, all of which receive annual precipitation depths of <40 cm a^{-1} and, in some cases < 20 cm a^{-1} (see Addendum Fig. S2a). Other areas also appear to be dominated by dry deposition, but to a lesser degree, with ratios between 50 and 70%. These areas typically occur where emissions are relatively high and precipitation depths are relatively low, e.g., central and eastern U.S., southwestern Canada, most of Europe, northeastern South Africa, the Republic of Korea and northeastern China.

Wet deposition is dominant in areas where emissions range from low to moderate and precipitation depths range from moderate to high, e.g., northern Canada, northern Asia, central Africa, most of South America and most of the oceans. The contiguous U.S. and Mexico are unique in that most of their surface area is characterized by roughly equal contributions of dry and wet deposition

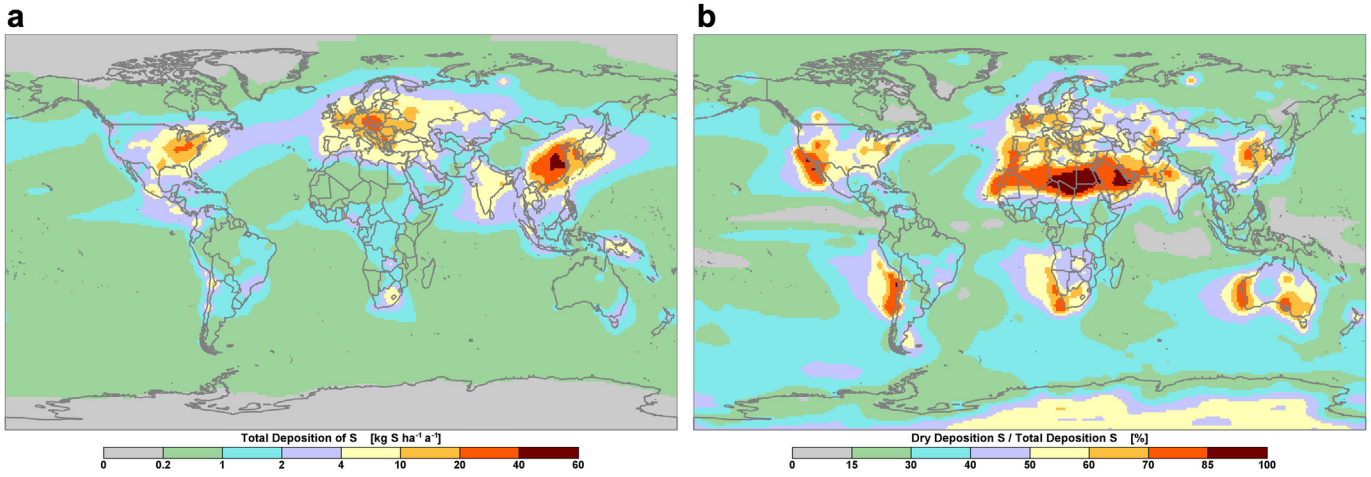

Fig. 3.8. 2001 ensemble-mean patterns of: (a) total deposition of S in kg S ha^{-1} a^{-1} and (b) % ratio of dry to total deposition of S.

(50% ± 10%). These ratios are very uncertain due to uncertainty in dry deposition parameterizations of the models and particularly so in the low deposition areas of the continents.

3.5. Area-integrated emissions and deposition of S

Area-integrated, model-based estimates of emissions and total deposition of nssS for 2001 are tabulated for the continents, oceans and coastal zones in Table 2. The area-integrated values provide a number of insights into the global atmospheric S budget:

- The 2001 global budget of nssS total deposition is estimated at 84.8 ± 6.1 Tg S with global emissions of 91.0 ± 7.3 Tg S (±numbers represent the ensemble standard deviation of all modeled values). The difference of 6.2 Tg S (or 7% of global emissions) is within ±1 standard deviation of the two estimates and is due to many of the TF HTAP models not being internally mass consistent and to inherent uncertainties in the models (HTAP, 2010). Mass inconsistency was confirmed for several models by comparing global emission totals to global deposition totals, with differences between the two falling in the range of +0.8% to −16.6% relative to the emission totals. Other sources of uncertainty include post-processing errors in the reported emissions, systematic uncertainties in the ensemble-mean averaging, and errors associated with the integration processes for the combined set of S species.
- Although non-coastal continental areas constituted only 26.3% of the global surface area, in 2001 they were estimated to have emitted 55.4% of the global S emissions and to have received 47.4% of the global S total deposition. The coastal zones constituted only 14.1% of the global area but emitted 23.5% of the S emissions and received 22.1% of the total deposition. Finally, the non-coastal ocean areas comprised 59.5% of the global surface area but emitted only 21.1% of the global emissions and received 30.5% of the global S total deposition.
- The total deposition of S to the non-coastal continental areas was highest in Asia (21.1% of global S deposition), Europe (9.6%) and North America (8.7%) and lowest in Oceania (1.1%) and Antarctica (0.1%) – a ranking consistent with the continent rankings of S emissions. The continental coastal zones were ranked in the same order, with Asia, Europe and North America accounting for 8.6%, 4.6%, and 3.6% of the global deposition, respectively. For the non-coastal oceanic areas, total deposition of S was greatest over the north Pacific (10.0%), the North Atlantic (6.2%) and the South Pacific (5.5%) and lowest over to the Southern Ocean (0.7%) and Arctic Ocean (0.3%). Total deposition of S to the non-coastal + coastal continental areas was highest in Asia at 29.7% of the global total – over double that to the next highest continent of Europe at 14.2% of the global total.
- Transport of continental and coastal zone S emissions appears to be an important source of atmospheric S input to the open oceans. For example, the modeled pattern of total deposition in Fig. 3.8a shows areas of high S total deposition extending into the oceans off the east coasts of North America, India and East Asia. Quantitative estimates of the amounts transported and deposited to the oceans were made in a manner similar to Galloway et al. (2004) by calculating the net export of S from the continental non-coastal and coastal areas to the non-coastal oceans (and vice versa for the import to the oceans) as the difference between the area-integrated emissions and estimated total deposition. The calculations indicate that, on a global scale, the export of S from the non-coastal continental and coastal areas to the non-coastal oceans was 12.9 Tg S and the import to the non-coastal oceans was roughly 6.7 Tg S. The difference of 6.2 Tg S represents the inherent uncertainty in the global mass balance estimates due to mass inconsistencies in several of the HTAP models.

Overall, the 2001 HTAP ensemble-mean model results indicate that the total deposition of S was highest in East Asia, Europe and eastern North America and lowest to the Southern and Arctic Oceans (Fig. 3.8a). They also suggest that between 15 and 50% of the S that was deposited on the non-coastal oceanic areas was of continental and coastal origin.

Comparing our global S deposition values to those of the 2000 ACCENT model comparison reported by Dentener et al. (2006), the global totals are within 4% of each other (i.e., 84.8 versus 81.8 Tg S, respectively). This difference is likely due to model and emission inventory differences between the two studies.

3.6. Regional aspects of S deposition

3.6.1. North America

3.6.1.1. Precipitation-weighted mean concentrations and wet deposition of S. The measurement-based average annual precipitation-weighted mean S concentrations in North America for the periods 2000–2002 and 2005–2007 are shown in Fig. 3.9a and b,

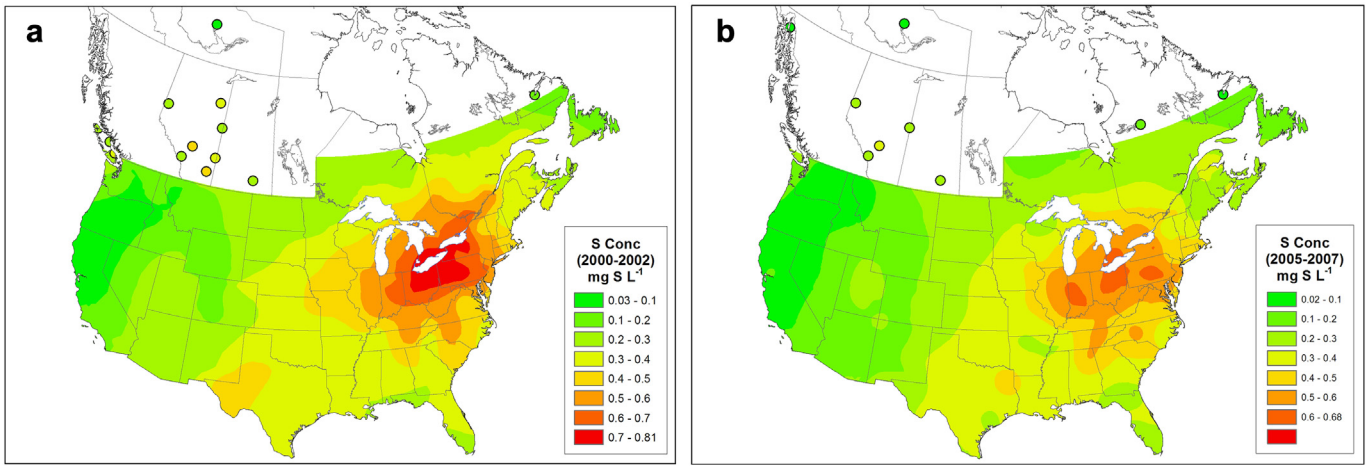

Fig. 3.9. Measured 3-year average annual precipitation-weighted mean concentrations of S in precipitation (in mg S L^{-1}) for (a) 2000–2002 and (b) 2005–2007. The minimum and maximum values on the color scales correspond to the minimum and maximum measured values.

respectively. No sea salt corrections were made to these data. The patterns differ from the global patterns shown earlier in that they show interpolated contours over areas with sufficient measurement site density. Given the paucity of measurement sites in western Canada, deposition values in this geographical area are shown as colored circles instead of contours.

The highest S concentrations in precipitation in both periods occurred in the area of the U.S. northeast and Canadian southeast adjacent to Lakes Erie and Ontario. This area had (and still has) the highest S emissions in the U.S., largely due to a large number of electrical generating sources and major urban centers in the Midwest and east coast of the U.S. as well as in southern Ontario and southern Quebec, Canada. Concentrations in the central and eastern parts of the continent ranged from 0.30 to 0.81 mg S L^{-1} in 2000–2002 and 0.30–0.68 mg S L^{-1} in 2005–2007 while concentrations in the western part of the continent were considerably lower, ranging from 0.03 to 0.50 mg S L^{-1} in 2000–2002 and 0.02–0.50 mg S L^{-1} in 2005–2007.

The measurement-based 3-year-mean annual wet deposition patterns of S for 2000–2002 and 2005–2007 are shown in Fig. 3.10a and b. Wet deposition estimates of S differ considerably between the eastern and western halves of North America. Considering the 2.0 kg S ha^{-1} a^{-1} isopleth as a rough boundary between east and west, wet deposition in the west was considerably lower with values of 0.1–2.0 kg S ha^{-1} a^{-1} in both periods than in the east with values of 2.0–8.5 kg S ha^{-1} a^{-1} in 2000–2002 and 2.0–7.8 kg S ha^{-1} a^{-1} in 2005–2007. As was the case with the spatial pattern of precipitation-weighted mean concentrations of S (Fig. 3.9a,b), the area of highest S wet deposition occurred on both sides of the Canada–U.S. border in the vicinity of Lakes Erie and Ontario where the pattern resembles an elongated bullseye stretched along a southwest to northeast axis with deposition ranging from 6.0 to 8.5 kg S ha^{-1} a^{-1}. From the center of the bullseye, wet deposition decreases along a gradient to values as low as 1 kg S ha^{-1} a^{-1} in Newfoundland and Labrador and northwestern Ontario (Canada) and 2.0–3.0 kg S ha^{-1} a^{-1} in southern/central Texas (U.S.) and 3.0–4.0 kg S ha^{-1} a^{-1} in Florida (U.S.).

The low density or complete lack of measurement data over large areas of North America makes the combination of measurement and model results particularly useful for assessing the continental pattern of wet deposition. Fig. 3.11a shows the 2001 ensemble-mean wet deposition pattern of nssS combined with the 3-year average annual wet deposition measurement values for 2000–2002 and Fig. 3.11b shows the associated scatterplot. The overall measurement-model comparability was quite good with a high correlation ($r = 0.916$; $n = 270$ grid squares) and uniform scatter of all points about the 1:1 line. The modeled pattern captures the measured area of highest wet deposition in eastern North America (eastern U.S. and southeastern Canada) but, in general, slightly overestimates the measured values in the eastern and western U.S.

The comparability between the model and measurement results provides reasonable comfort that the model-based pattern can be used to interpolate between measurement sites and to extrapolate to the areas where no measurements exist. In light of the latter, the model results suggest that a secondary hot spot of wet deposition (of 4.0–6.0 kg S ha^{-1} a^{-1}) exists in central Mexico in the vicinity of Mexico City, and that moderately high values (of 2.0–4.0 kg S ha^{-1} a^{-1}) exist in eastern Mexico, the Gulf of Mexico and over the Atlantic Ocean. While regional-scale measurements were not available from Mexico to confirm the wet deposition hotspot modeled around Mexico City, the associated modeled hotspot of precipitation-weighted mean concentration, with grid square values ranging from 0.4 to 1.0 mg S L^{-1} in Fig. 3.11a, was confirmed by on-site concentration measurements of 1.0 mg S L^{-1} in Mexico City in 2001–2002 published by Baez et al. (2007) and 0.9 mg S L^{-1} at a site 80 km from Mexico City published by Garcia et al. (2006). In most of western and northern Canada and the western U.S., the modeled pattern shows the same large area of low S wet deposition as the measurements with wet deposition estimates of $<$1.0 kg S ha^{-1} a^{-1} with the exception of the high emission areas of southwestern British Columbia, Alberta and Washington State. Further measurement-model comparison statistics are available in Addendum Table S3.

3.6.1.2. Dry deposition of S. North America is one of four continents that provided measurement-based inferential dry deposition estimates. The inferential estimates were made at regionally representative measurement sites of the United States Clean Air Status and Trends Network (CASTNET) and the Canadian Air and Precipitation Monitoring Network (CAPMoN). Schwede et al. (2011) determined that SO_2 and HNO_3 concentrations measured by the two networks are reasonably comparable (i.e., between-network median percent differences of 4.2% and 18.5% for SO_2 and HNO_3, respectively; CAPMoN higher), but the modeled dry deposition velocities and fluxes from the inferential models are markedly different. For example, the median % difference between the two countries' estimated inferential SO_2 dry deposition fluxes was

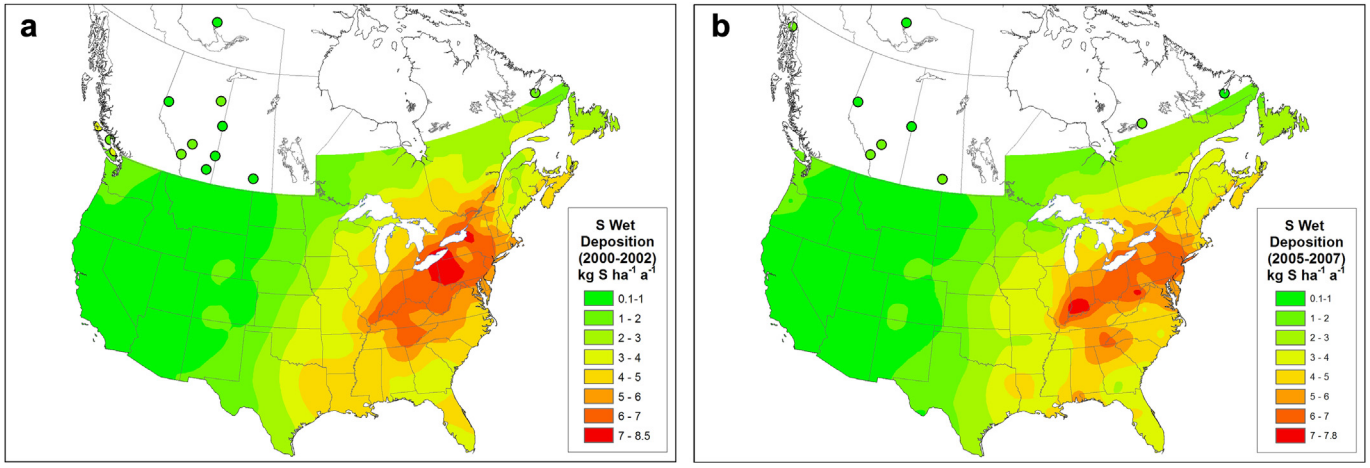

Fig. 3.10. 3-year mean annual wet deposition of S (in kg S ha^{-1} a^{-1}) in North America for (a) 2000–2002 and (b) 2005–2007.

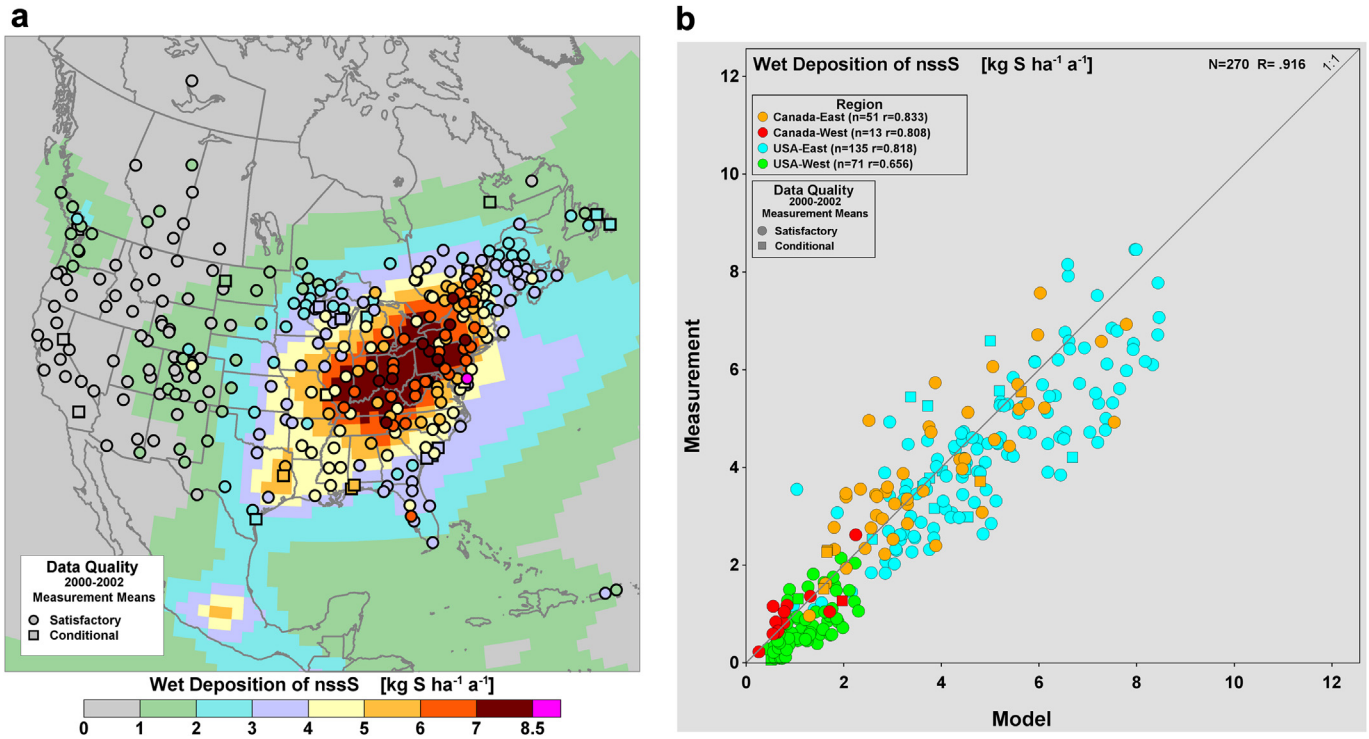

Fig. 3.11. (a) 2001 ensemble-mean model pattern of wet deposition of nssS combined with measured 3-year average annual wet deposition values for the period 2000–2002 (in kg S ha^{-1} a^{-1}) and (b) scatterplot of measured versus modeled values.

quantified at 53.8% (CAPMoN higher). These differences were attributed predominantly to differences in the estimated dry deposition velocities, where the median % difference for SO_2 was 49.3% (CAPMoN higher). The authors found that non-stomatal (ground and cuticle) resistance parameterizations in the two inferential models were the main cause of the differences in the SO_2 dry deposition velocities. Particle-SO_4^{2-} dry deposition velocities and fluxes were not considered in Schwede et al. (2011) and their between-country comparability has not been quantified to date.

Since true values of S dry deposition are not available in North America, it is not possible to determine which of the two networks' inferential dry deposition estimates is more accurate. A rough indication of the relative accuracy of the two models is given in Mitchell et al. (2011) who published watershed mass balance results for 15 watersheds in eastern Canada and the eastern U.S. For the 15 watersheds, the authors determined that the Canadian dry deposition estimates produced a lower average discrepancy between the atmospheric input of S and the total water discharge of S than did the U.S. estimates (i.e., the Canadian discrepancy was −2.2 kg ha^{-1} a^{-1} while the U.S. discrepancy was −3.5 kg ha^{-1} a^{-1}). While this suggests better accuracy of the Canadian inferential estimates, it is not conclusive because the input-discharge discrepancies might be real and related to the geochemical processes that affect the watersheds, e.g., mineral weathering and the mineralization of organic sulfur. Given the unknown accuracy of the models, the inferential dry deposition estimates of both Canada and the U.S. are included and merged here to represent the state-of-the-science in dry deposition estimation in North America.

The spatial pattern of S dry deposition (SO_2–S plus SO_4^{2-}–S) for the 2000–2002 period is shown in Fig. 3.12a as the 2001 HTAP ensemble-mean nssS dry deposition map with the 2000–2002 average annual CASTNET and CAPMoN measurement-based inferential S values superimposed. The associated scatterplot is shown as Fig. 3.12b and the 2005–2007 period measurement-based inferential results are shown in Fig. 3.12c. The measured dry deposition values include ssS while the HTAP modeled values do not. This has minimal effect on the comparability since only a few sites are located within 100 km of salt water and the relative contribution of particle-SO_4^{2-} deposition compared to gaseous SO_2–S is very low.

The inferential dry deposition estimates of S (both model- and measurement-based) are markedly lower in western North America than in eastern North America in both periods, e.g., in the 2005–2007 period, the measurement-based inferential dry deposition S fluxes at most sites in the western U.S. were ≤0.5 kg S ha^{-1} a^{-1} compared to 0.5–11.0 kg S ha^{-1} a^{-1} in the eastern U.S.. In Canada, the fluxes at the two western Canadian sites were 0.8 and 1.6 kg S ha^{-1} a^{-1} (notably higher than at sites in the western U.S.) and, at the 8 eastern sites, ranged between 0.7 kg S ha^{-1} a^{-1} in the remote north and 4.5 kg S ha^{-1} a^{-1} in the populated industrialized south. In both periods, the maximum measurement-based inferential dry deposition on the continent (both model- and measurement-based) occurred in the high SO_2 emission area of the U.S. northeast where the model-based dry deposition ranged from 10.0 to 16.0 kg S ha^{-1} a^{-1}. Two secondary hot spots of dry deposition were projected by the models, one in east Texas and the other around Mexico City with dry deposition ranging from 6.0 to 10.0 kg S ha^{-1} a^{-1}. The lowest modeled dry deposition estimates on the continent were <0.05 kg S ha^{-1} a^{-1} in northern Canada.

Although the ensemble-mean modeled pattern and measurement-based inferential S dry deposition in 2000–2002 (Fig. 3.12a) are well-correlated ($r = 0.838$; $n = 71$ grid squares), the modeled values are considerably higher than the measured values (average model-measured difference = 3.67 kg S ha^{-1} a^{-1}). This is due mainly to higher modeled values of SO_2–S dry

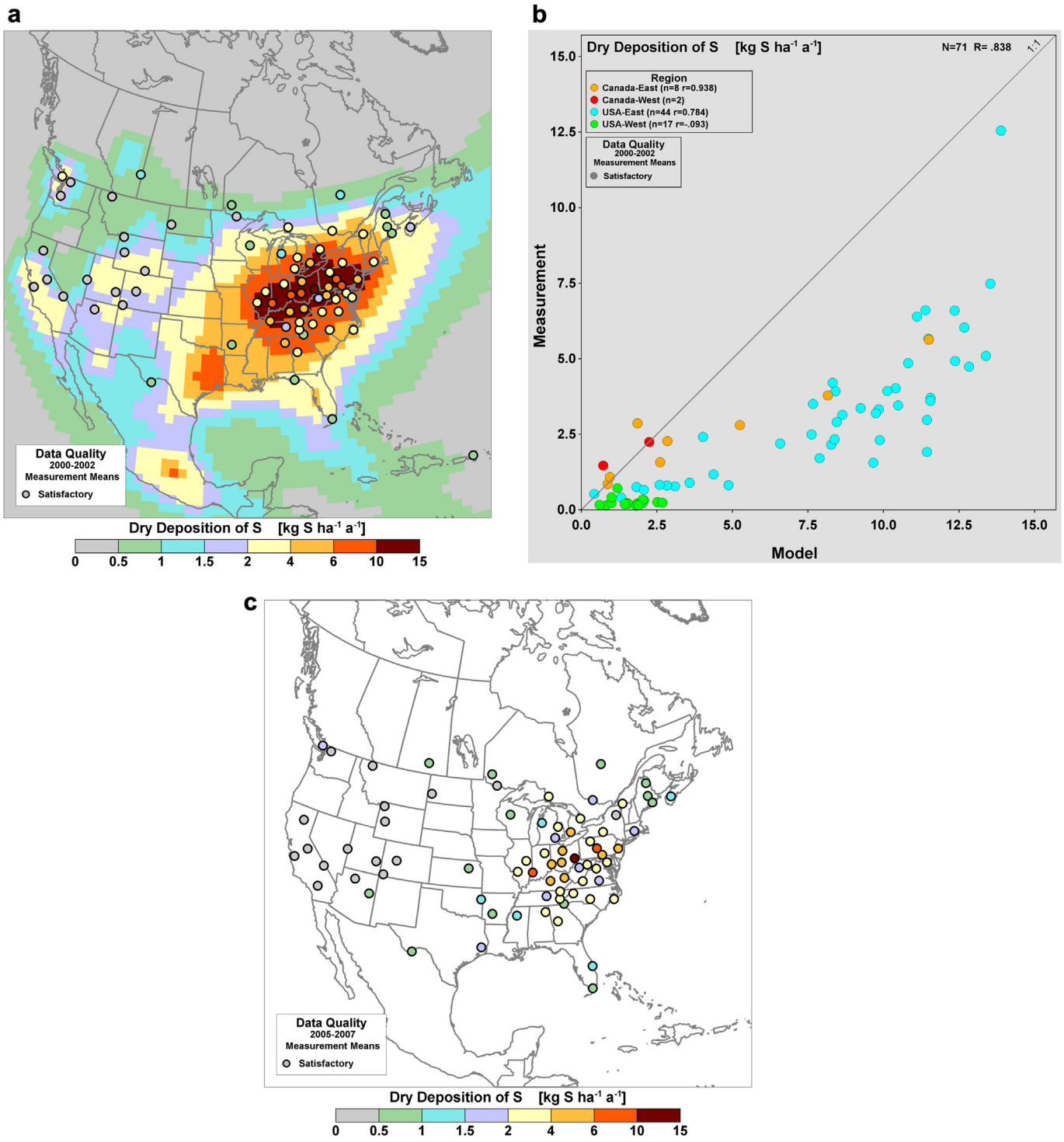

Fig. 3.12. (a) The 2001 ensemble-mean modeled pattern of dry deposition and measurement-based inferential estimates of 2000–2002 3-year average annual dry deposition of S including SO_2–S and SO_4^{2-}–S in kg S ha^{-1} a^{-1}; (b) associated scatterplot of measured versus modeled (grid square) values; (c) measurement-based inferential 2005–2007 3-year average annual dry deposition of S in kg S ha^{-1} a^{-1}.

deposition in the eastern U.S. where the average model-measured difference was 5.1 kg S ha^{-1} a^{-1} (versus 2.0 in eastern Canada). In the high emission area of the Ohio River Valley, the modeled values were as much as 200–300% times greater than the measurement-based inferential values (the same is true at the two sites in southern Ontario/Quebec in Canada). Since there are no direct dry deposition measurement data against which to compare the inferential dry deposition estimates, it is not possible to say which of the two inferential models is more accurate. Also unknown is whether the model-measurement differences are due to differences in ambient concentration measurements or estimated dry deposition velocities, and whether the HTAP model results are more accurate than the inferential results.

In spite of the foregoing uncertainties, the HTAP and inferential results have been merged in Fig. 3.12a to give the best-available estimates. The poor model-measurement comparability in Fig. 3.12b (i.e., modeled values > measurement-based inferential estimates) is due to a number of factors including uncertainties in the measurement-based inferential estimates and the dry deposition parameterizations of the HTAP and inferential models, plus the fact that modeled values are derived from grid square average emissions and concentration values while the measurement data apply to a single point typically located > 50 km from large emission sources.

3.6.1.3. Total deposition of S. The 2000–2002 S total deposition results are shown in Fig. 3.13a and b, and for 2005–2007 in

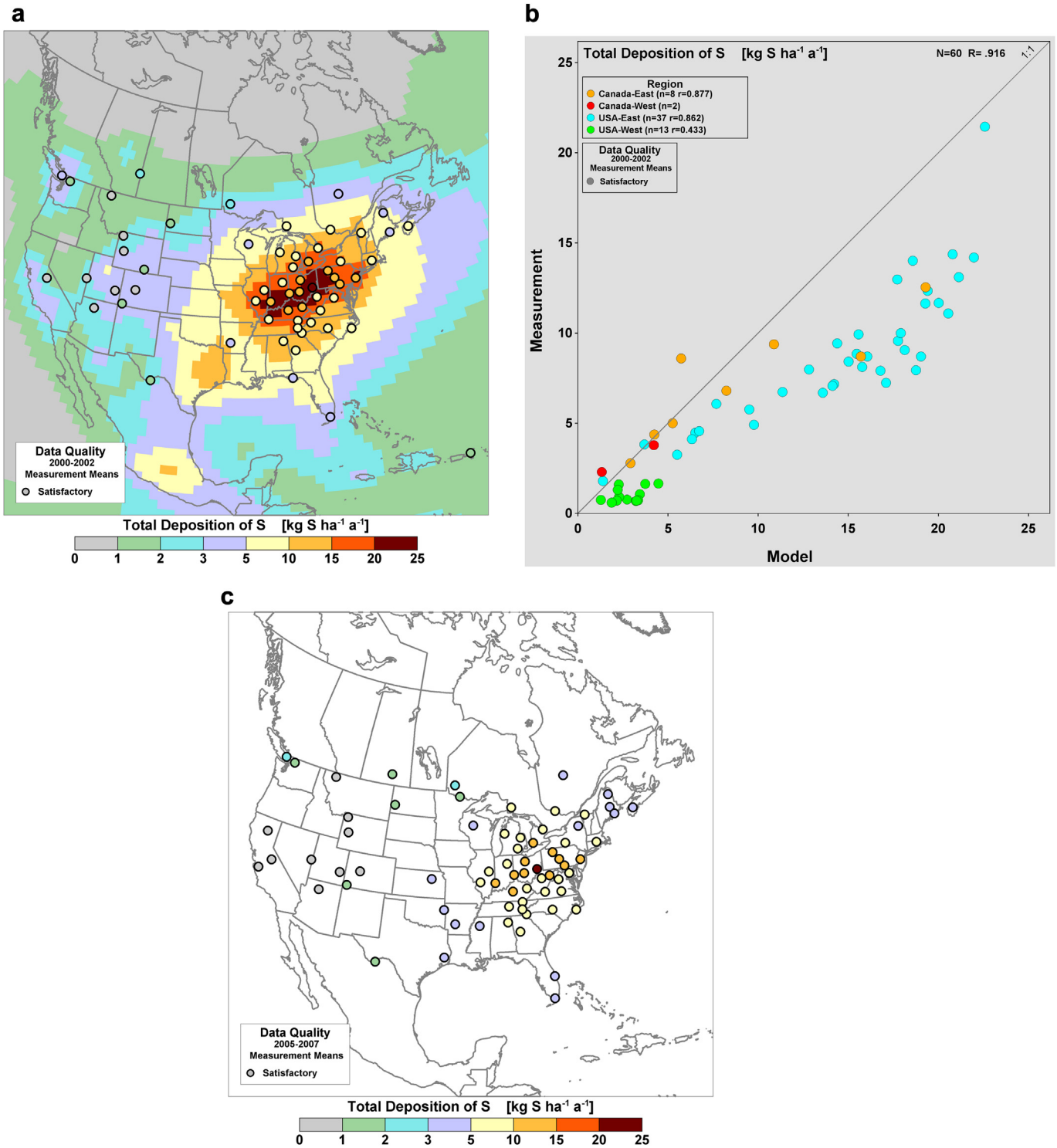

Fig. 3.13. (a) The 2001 ensemble-mean modeled pattern of total deposition of S with measurement-based 2000–2002 3-year average annual estimates, (b) the associated scatterplot of measured versus modeled (grid square average) values, (c) 2005–2007 measurement-based 3-year average annual estimates.

Fig. 3.13c. The spatial patterns of the 2001 modeled and 2000–2002 measurement-based results are quite similar, with a measurement-versus-model correlation of $r = 0.916$ for $n = 60$. The area of maximum total deposition occurs in the high S emission area that extends northward from Tennessee (U.S.) to southern Ontario (Canada), and westward from Illinois to New Jersey. The lowest deposition appears in the western U.S. and western/northern Canada. The measurement-based 3-year-average annual total deposition in 2000–2002 ranged from 0.4–3.8 kg S ha^{-1} a^{-1} in western North America to 1.8–21.5 kg S ha^{-1} a^{-1} in eastern North America and in 2005–2007 from 0.3 to 2.9 and 2.0 to 20.9 kg S ha^{-1} a^{-1}, respectively. The model-based estimates in 2001 ranged from a low of 0.4 kg S ha^{-1} a^{-1} in the west to a high of 22.6 kg S ha^{-1} a^{-1} in the east. Consistent with the patterns of wet and dry deposition, the total deposition pattern has the appearance of an elongated bullseye stretched along a southwest to northeast axis with secondary maxima in east Texas and central Mexico. Lowest continental levels of total deposition appear north of the 56th parallel in northern Canada with values <1 kg S ha^{-1} a^{-1}.

While the spatial patterns have similar shapes, the model-based total deposition estimates are systematically higher than the measurement-based estimates, due in large part to the systematically higher modeled dry deposition of SO_2 shown in Fig. 3.13a. As was the case with dry deposition, the largest measurement-model differences appear in the U.S. and at two sites in the high deposition area of eastern Canada; interestingly, the measurement and modeled values are roughly equal at the other 8 sites in Canada as seen in Fig. 3.13b. Considering the U.S. only, the measurement-based total deposition values are roughly 64% of the modeled values. It is not known whether the U.S. or Canadian flux estimates are more accurate. The better agreement of the Canadian flux estimates relative to the HTAP modeled estimates (outside the high deposition area) could be due to two factors: (1) better agreement between the HTAP ensemble-mean and CAPMoN-based inferential dry deposition velocity models (see discussion above) and (2) a lesser contribution of dry deposition to total deposition throughout the lower deposition Canadian domain.

3.6.1.4. Changes in S deposition over time due to changing SO_2 emissions. Anthropogenic SO_2 emissions in the U.S. and Canada decreased steadily from 1990 to 2007 in response to emission reduction programs according to documented emissions in both countries (IJC, 2010). In the U.S., SO_2 emissions declined 44% from 20.935 MT in 1990 to 11.757 MT in 2007 while emissions in Canada declined by 41%, from 3.201 MT to 1.905 MT (IJC, 2010). The largest emission decreases in both countries took place in the highest emission areas of the eastern U.S. and southeastern Canada. The decline in emissions resulted in a marked decline in nssS concentrations in air and precipitation and in nssS wet deposition in the eastern half of the continent – documented for the period from the early-1990s to the early-2000s by Holland et al. (1999), Sickles and Shadwick (2007), Lynch et al. (2000), Vet et al. (2005), Lehmann et al. (2005, 2007). Fig. 3.14a–c extend this period to 2007 by showing the annual wet deposition maps for 1990, 2000 and 2007

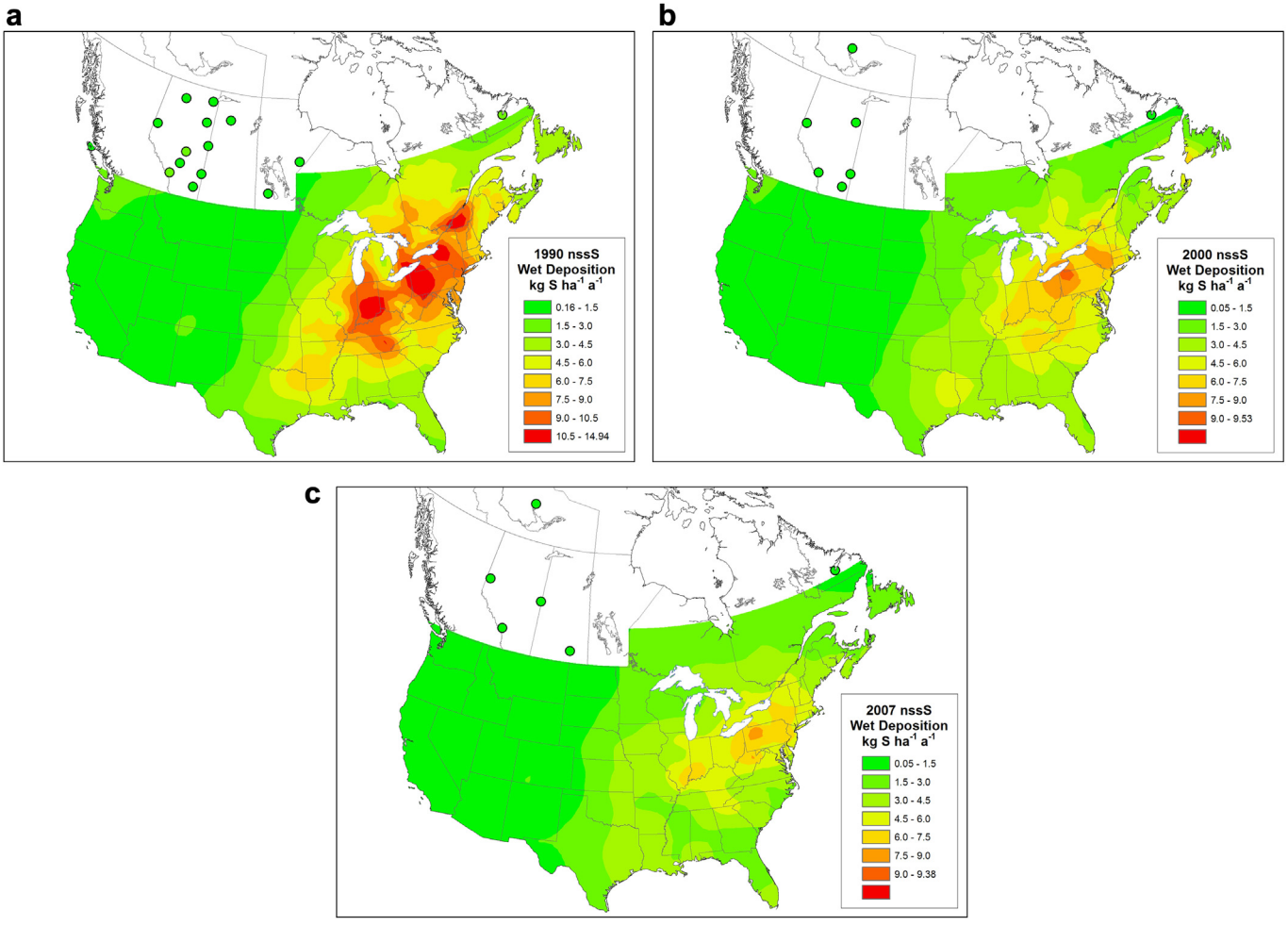

Fig. 3.14. Annual wet nssS deposition over North America in: (a) 1990, (b) 2000, and (c) 2007.

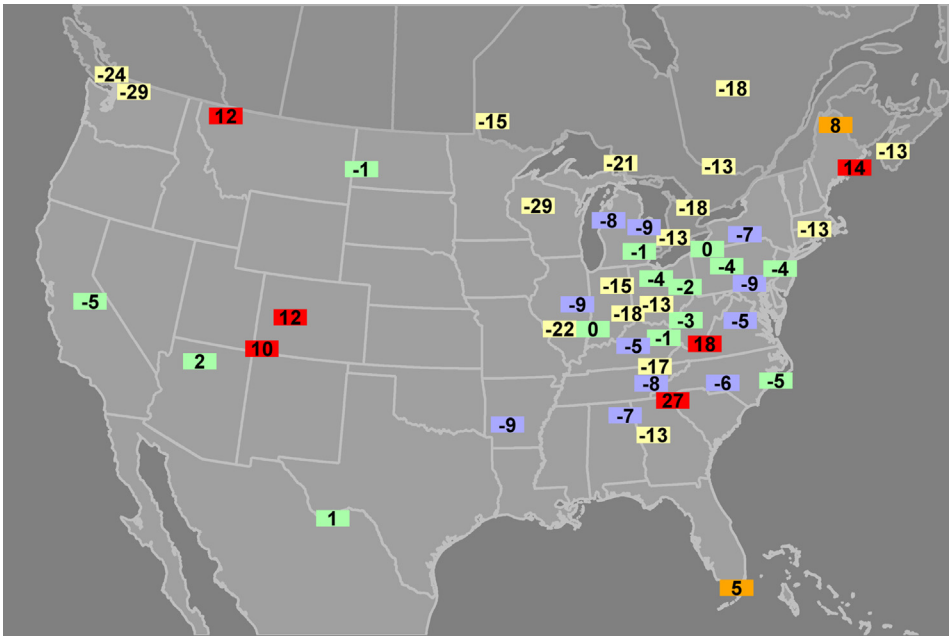

Fig. 3.15. Percent (%) change in measurement-based 3-year averages of S total deposition from 2000–2002 to 2005–2007 calculated as $100(D_{2005-2007} - D_{2000-2002})/D_{2000-2002}$.

which clearly illustrate that the emission reductions led to markedly lower wet deposition levels in the eastern half of the continent. These figures are consistent with Fig. 3.5a,b that show the global % changes of wet deposition from 2000–2002 to 2005–2007 in which >65% of North American sites showed decreases from 0 to 42%. Two of the most visible manifestations of the wet deposition declines are (1) the decrease of the continental maximum measured wet deposition from 14.9 kg S ha^{-1} a^{-1} in 1990 to 9.4 kg S ha^{-1} a^{-1} in 2007 and (2) the decreasing area encompassed by the 7 kg S ha^{-1} a^{-1} isopleth from 1658.8 $\times$ 10^3 km^2 in 1990 to 326.1 $\times$ 10^3 km^2 in 2000 and further to 51.4 $\times$ 10^3 km^2 in 2007.

Although based on more limited spatial coverage and site density than the wet deposition measurements, the total deposition estimates also showed a direct response to declining S emissions in the 2000s. Fig. 3.15 shows the % reduction of S total deposition at U.S. CASTNET and NADP sites and Canadian CAPMoN sites between 2000–2002 and 2005–2007. Sites in the western half of the continent showed reductions of total deposition between 0 and 29% (with the exception of 3 sites that showed increases) while sites in the eastern half showed reductions between 0 and 22% (with the exception of 3 sites that showed increases).

The decreases in measured North American precipitation-weighted mean concentrations, wet deposition and total deposition point to the success of Canadian and U.S. sulfur emission reduction programs.

3.6.2. South America

3.6.2.1. Precipitation-weighted mean concentrations and wet deposition of S. Relative to other continents (except Oceania), South America has comparatively low S emissions. For example, the 2001 annual emissions were estimated at 3.3 $\pm$ 0.8 Tg S a^{-1} (Table 2) with highest emissions occurring in the urban and industrial areas of Chile and Colombia (Fig. 3.1). In the last 30 years, most countries in South America underwent unprecedented population movement from rural areas to the major urban centers, the consequence of which was an increase in pollution levels in the urban atmospheres. This, in turn, led to precipitation chemistry monitoring studies focused on urban and industrial areas with only a few focused on regionally representative sites (see literature review at the beginning of this section). The urban/industrial studies are diverse in nature, covering a broad range of long-term and short-term periods, urban and industrial site locations, wet-only and bulk sampling methods, and different statistical metrics (e.g., arithmetic mean, precipitation-weighted mean). Overall, the urban and industrial concentrations of S in precipitation reported in the literature range from <0.1 mg S L^{-1}–3.8 mg S L^{-1} (Pelicho et al., 2006; Klockow et al., 1997 as cited in Forti et al., 2001; Fornaro and Gutz, 2006; Forti et al., 2005). The largest number of studies were carried out in and around the urban area of Sao Paulo, Brazil (Fornaro and Gutz, 2006; Forti et al., 2005).

The few regionally representative studies that have been published report on precipitation chemistry measurements in Venezuela, Uruguay and Brazil (in the latter case, mostly in Amazonia). Zunckel et al. (2003) reported arithmetic mean concentrations at three regionally representative sites in northeast Uruguay of 1.01, 0.82 and 0.24 mg S L^{-1} in 1999 and 2000. Morales et al. (2001a) reported annual precipitation-weighted mean concentrations at a number of rural sites in the Maracaibo Lake Basin of Venezuela in the same range, from 0.35 mg S L^{-1} in 1995–96 (Morales et al., 2001b as cited in Morales et al., 2001a) to 1.07 mg S L^{-1} in 1988–89 (Morales et al., 1995, 1998 as cited in Morales et al., 2001a). Lara et al. (2001) reported wet-only measurement values at a rural site in the Piracicaba River Basin of southeast Brazil of 0.3 mg S L^{-1} in 1997–1998. These values are higher than the remote background concentrations of 0.04 (1985) to 0.08 (1990–92) mg S L^{-1} reported in east Venezuela by Morales et al. (2001a) and of <0.1 mg S L^{-1} mg S L^{-1} in Amazonia, Brazil reported by Forti et al. (2000), Lesack and Melack (1991) and Pauliquevis et al. (2012).

For this assessment, data were included from the one regionally-representative monitoring site in South America (Brazil) that met our time period restrictions and quality acceptance criteria. The precipitation-weighted mean concentration and wet deposition values, as provided by C. Forti (personal communication, April 29, 2010), appear in Fig. 3.6a and b and were measured at a forest site in eastern Brazil (Cunha) for the period 1999 to

2001. The precipitation-weighted mean concentrations of S and nssS at Cunha were 0.162 mg S L^{-1} and 0.133 mg nssS L^{-1}, respectively, where the concentration is very close to the modeled grid cell value in that area (see Fig. 3.6b) and consistent with the modeled deposition hot spot in southeast Brazil. The sparse amount of data on the continent makes it necessary to use the HTAP model results to understand the concentration pattern across South America. To that end, the pattern (see Fig. 3.6a) closely resembles the pattern of S emissions (Fig. 3.1), with low concentrations in the range of <0.04 mg S L^{-1} in the remote areas of Amazonia and southern Argentina and high concentrations in the range of 0.1–1.0 mg S L^{-1} in Colombia, northern Chile, southeastern Brazil and northern Argentina (with an extension into the eastern Pacific Ocean). The lowest concentrations on the continent are in the same range as concentrations in other remote areas of the world.

The measured wet deposition of S and nssS (Fig. 3.6c) at Cunha were 3.34 kg S ha^{-1} a^{-1} and 2.73 kg nssS ha^{-1} a^{-1}, respectively. The nssS value compares well to the modeled nssS grid square value in Fig. 3.6d. The modeled pattern shows low wet deposition of 0.2–1.0 kg S ha^{-1} a^{-1} everywhere on the continent except in the northwest and central areas where values varied from 1.0 to > 6.0 kg S ha^{-1} a^{-1}. The highest modeled wet deposition value was 6.3 kg S ha^{-1} a^{-1} in the very high emission area of Colombia. At a remote site in central Amazonia, Pauliquevis et al. (2012) reported annual deposition values of 1.5 kg ssS ha^{-1} a^{-1} and 1.2 kg nssS ha^{-1} a^{-1} over a 3.5 year period between 1998 and 2001.

3.6.2.2. Dry deposition of S. The absence of measurement-based inferential dry deposition estimates in South America makes it necessary to evaluate the continental pattern of dry deposition based solely on the 2001 HTAP ensemble-mean modeling results (Fig. 3.7a). Again not surprisingly, the South American dry deposition pattern closely mimics the S emission pattern (Fig. 3.1) with the highest fluxes occurring in the 6.4–7.5 kg S $ha^{-1}a^{-1}$ range in Bolivia and northern Chile and the lowest fluxes in the 0.1–0.5 kg S ha a^{-1} range in the low emission areas (i.e., emissions <2 kg S ha^{-1} a^{-1}). Minimum modeled deposition occurs in the Amazon region of Brazil at 0.1 kg S ha^{-1} a^{-1}. Fig. 3.7b suggests that S dry deposition (i.e., SO_2–S plus p-SO_4^{2-}-S) is dominated by SO_2 dry deposition with contributions greater than 60% over most of the continent and greater than 85% in the high SO_2 emission areas.

3.6.2.3. Total deposition of S. As above, the discussion of total deposition of S must be based on the HTAP modeling results; the modeled pattern (Fig. 3.8a) closely resembles the S emission pattern. Highest fluxes of 8.8–10.4 kg S ha^{-1} a^{-1} are projected in the high emission areas of Bolivia, Chile and Colombia and lowest fluxes of 0.3–0.4 kg S ha^{-1} a^{-1} are projected in southern Argentina and Amazonia (the latter being slightly higher). In the high emission areas (emissions >4 kg S ha^{-1} a^{-1}), total deposition ranges from 2.0 to 10.4 kg S ha^{-1} a^{-1} while, in the central, northwestern coastal and northeastern coastal regions (including the coastal outflow regions), the fluxes vary from 1.0 to 2.0 kg S ha^{-1} a^{-1}.

3.6.3. Europe

3.6.3.1. Precipitation-weighted mean concentrations and wet deposition of S. Europe has an extensive network of wet deposition measurements from the EMEP programme and a few national programmes as described in Addendum Table S1. The measurement-based 3-year annual precipitation-weighted mean concentration patterns of nssS for 2000–2002 and 2005–2007 are shown in Fig. 3.16a and b, respectively, and for wet deposition in Fig. 3.17a and c. Concentration measurements from the earlier period are superimposed on the isopleth map of the 2001 HTAP model estimates. For S concentration and deposition maps that include ssS, the reader is referred to the figures and discussions in the global section.

Highest concentrations of about 1.9 mg S L^{-1} occurred in the first period and 1.2 mg S L^{-1} in the second period in Serbia in eastern Europe, with a few hotspots elsewhere such as Spain and Turkey. The lowest concentrations (~0.1 mg S L^{-1}) occurred in Scandinavia. The spatial patterns of nssS concentration and wet deposition in Europe share similar shapes. However, large variations in annual precipitation depth, related to coastal and topographical effects, result in localized heavy wet deposition. For example, sites in southern Norway and the region around the Alps experienced high wet deposition due to high annual precipitation depths (150–250 cm). The highest wet deposition levels appear in the southern part of eastern Europe, with values of about

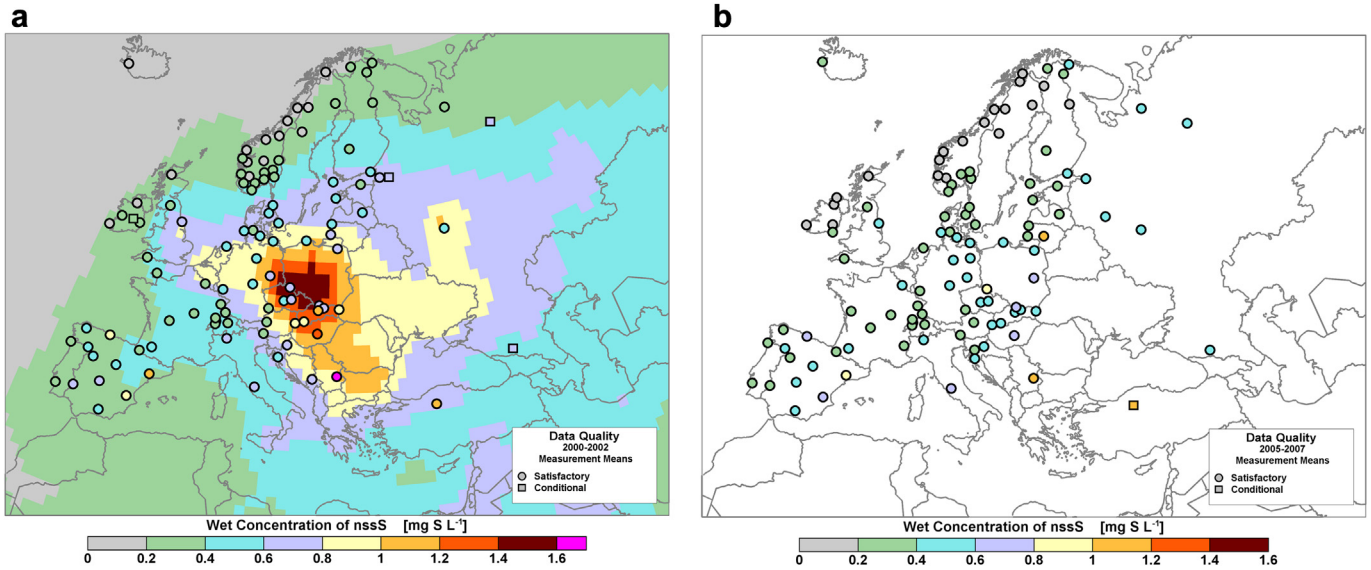

Fig. 3.16. (a) Measured and modeled precipitation-weighted mean concentration of nssS in Europe for 2000–2002 and (b) measured precipitation-weighted mean concentrations for the period 2005–2007 (units in mg S L^{-1}).

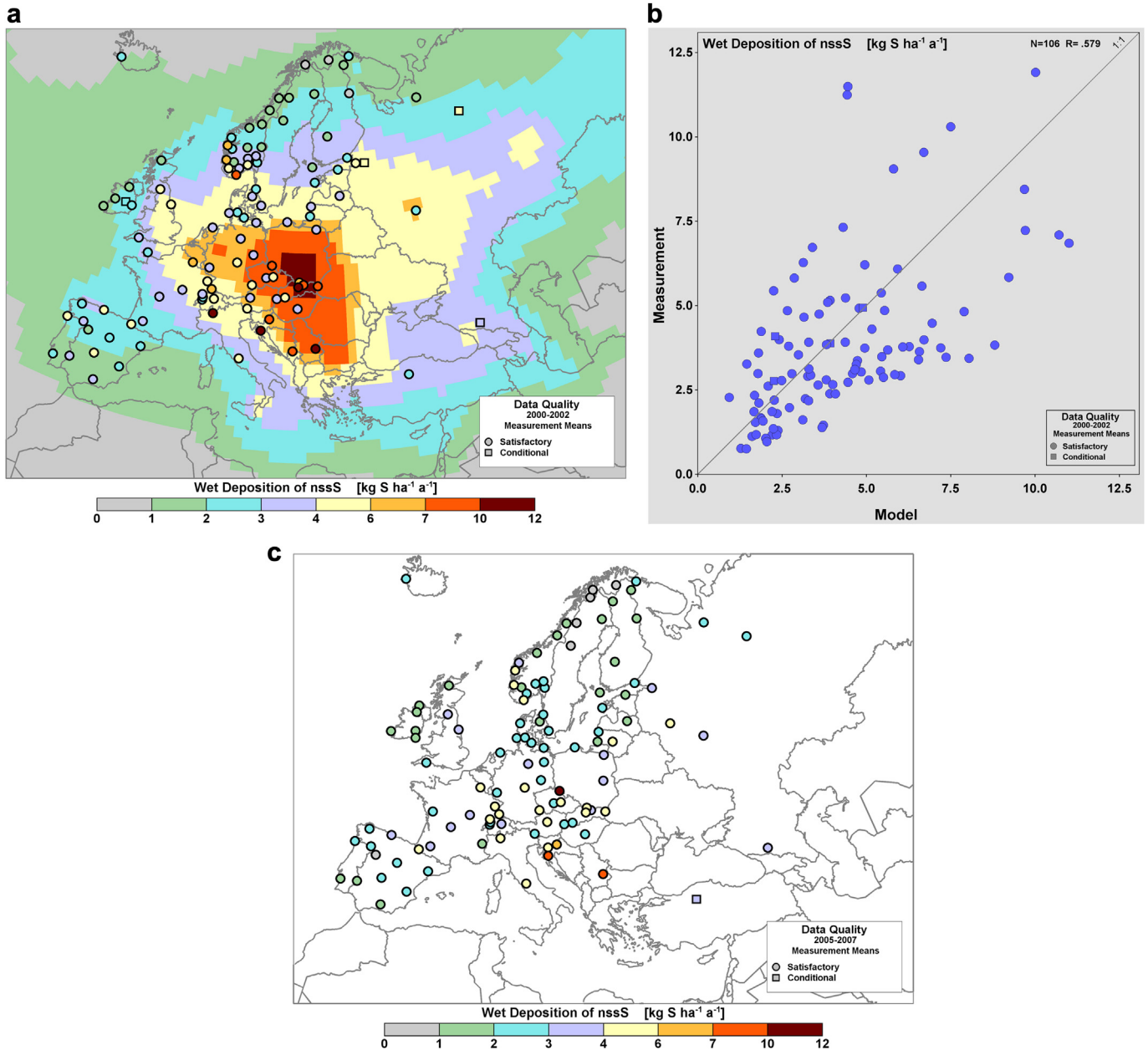

Fig. 3.17. (a) Measured and modeled wet deposition of nssS in Europe for 2000–2002 with (b) associated scatterplot of measured versus modeled (grid square) values, and (c) measured wet deposition for 2005–2007 in kg S ha^{-1} a^{-1}.

10.0 kg S ha^{-1} a^{-1}. The lowest wet deposition levels occur in Northern Scandinavia and northwest of the British Isles, with deposition < 2.0 kg S ha^{-1} a^{-1}. Some sites in Hungary, Russian Federation, and Spain with high S concentrations have relatively low annual precipitation (about 30–50 cm a^{-1}) and therefore experience low wet deposition levels. The model presents a general picture consistent with the measurements, but does not capture many of the finer scale effects resolved by the measurements (Fig. 3.17b).

There are obvious gaps in the monitoring networks in Eastern and Southeastern Europe. Some additional national measurements relevant for assessing deposition in these areas include: the Berezinsky Biosphere Reserve site in Belarus (Sanets and Chuduk, 2005), which had an average deposition of 5.6 kg S ha^{-1} a^{-1}, equivalent to the EMEP site in Belarus; the Romanian site in the forested area of the Retezeat Mountains, which had an average deposition of 4.7 kg S ha^{-1} a^{-1} for 2000–2002 (Bytnerowicz et al., 2005); and a site in the Carpathian Mountains in Ukraine with about 8 kg S ha^{-1} a^{-1} in 2008 (Oulehle et al., 2010). These results are in agreement with the spatial pattern shown by the HTAP model in Fig 3.17a.

3.6.3.2. Dry deposition of S. Dry deposition of S is not measured on a large scale in Europe. However, there have been a number of national and regional studies of dry deposition using either advanced micrometeorological flux measurements or more long term deposition monitoring using measured air concentrations combined with inferential models. For example, in a forested area near the German/Czech border, an average S deposition (SO_2 + particulate SO_4^{2-}) of 10.1 kg S ha^{-1} a^{-1} was estimated using

the inferential technique for 2002–2004 (Zimmermann et al., 2006). Perhaps the longest time series of dry deposition measurements anywhere in Europe exists in the UK, where SO_2 fluxes have been monitored continuously since the mid 1990's at two rural sites (Fowler et al., 2005, 2009). The average dry deposition of SO_2 at the site Auchencorth Moss in Scotland was 0.5 ± 0.2 kg S ha^{-1} a^{-1} in the period 1995–2006. Of special note with these long term measurements was the observation of an increase in the deposition velocity of SO_2 with time caused by a reduction in canopy resistance. The change in canopy resistance was attributed to a long term change in concentration ratios of SO_2:NH_3 related to ambient SO_2 concentrations decreasing faster than NH_3 concentrations (Fowler, 2009).

Dry deposition of S from the HTAP ensemble-mean model pattern (Fig. 3.7a) shows a clear gradient away from the highest flux areas in Southeastern Europe and parts of Poland. The highest HTAP dry deposition levels in 2001 were about 20.0 kg S ha^{-1} a^{-1} in 2001 and the lowest were <1 kg S ha^{-1} a^{-1} in Scandinavia. Further, the HTAP results show evidence of ship emissions around the English Channel. The coarse nature of the HTAP ensemble average model does not resolve the ship emissions along the coastlines of Southern Europe; however, in the Mediterranean and the Atlantic these emissions can be seen in other models with a finer resolution (i.e. Benedictow et al., 2009). The HTAP model results indicate that more than 85% of dry deposition of S in Europe is due to SO_2, with p-SO_4^{2-} of minor importance (Fig. 3.7b), but there are certainly regional differences and quite high uncertainties in this estimate. Nevertheless, the air concentrations of SO_2 in the EMEP network (Hjellbrekke, 2003) show a spatial pattern consistent with the dry deposition calculated by the HTAP model, even the small but significant signal along the northwestern coast of Spain.

3.6.3.3. Total deposition of S. Europe has a large scale network for routinely monitoring air concentrations that in principle could be used for inferring spatial patterns of dry deposition, but this has not been applied in a systematic way. An alternative approach for determining total deposition is to measure bulk deposition under a forest canopy, known as the *throughfall* method. This method can be used for chemical species, such as S, that are not irreversibly absorbed into the forest canopy. In Europe, ICP Forest coordinates a network of nearly 250 forest plots where throughfall is measured (Fischer and Lorenz, 2011; Lorenz and Granke, 2009). Throughfall S measurements, corrected for ssS, have been averaged for the two time periods, 2000–2002 and 2005–2007, and are shown in Fig. 3.18a and b, respectively, with nssS deposition from the earlier period superimposed on 2001 HTAP model pattern of total deposition.

The ICP Forest monitoring network is very dense, especially in Central Europe, and some outlying sites show relatively large differences, suggesting that not all sites are regionally representative. Nevertheless, the spatial pattern of S total deposition is similar in shape to the HTAP model results. The highest total deposition levels (>20.0 kg S ha^{-1} a^{-1}) appear in East Central Europe, decreasing toward Southeastern Europe and toward the northwest, around the English Channel (Fig. 3.18a). Throughout much of Central Europe, total deposition ranges between 10.0 and 20.0 kg S ha^{-1} a^{-1} and in northern and Southwestern Europe, S deposition is < 10.0 kg S ha^{-1} a^{-1}. The lowest deposition levels are seen in Scandinavia at about 1 kg S ha^{-1} a^{-1}. Relatively high deposition levels are seen in Bulgaria and Romania in 2000–2002, as shown by the HTAP model results, and although there were no measurements in this region for that time period, the 2005–2007 data confirm these enhanced levels. Similar results are reported in a study by Oulehle et al. (2010) who estimated total deposition of around 10 kg S ha^{-1} a^{-1} in the Carpathian Mountains in Ukraine and Romania in 2008.

The correlation between the model and grid-average throughfall measurements is quite good with $r = 0.734$, $n = 195$, but the model generally overestimates total deposition relative to the ICP Forest throughfall measurements (Fig. 3.18b). The throughfall data have been compared with the high resolution EMEP regional model (Simpson et al., 2006) which shows better agreement than the HTAP ensemble-mean model results shown here. As well, the EMEP coarse resolution hemispheric model in our HTAP model ensemble compared better with the ICP throughfall data than the HTAP ensemble-mean (data not shown). An analysis suggests that the better comparability of the EMEP models is due to higher estimates of wet deposition in Europe by the EMEP model relative to the HTAP ensemble-mean.

Based on HTAP model results (Fig. 3.8b), dry deposition contributes more than wet deposition to total deposition in much of Europe. The model results suggest that the dry deposition contribution is highest in the United Kingdom and Spain, where it accounts for >70% of the total deposition (Fig. 3.8b). In the Benelux countries and Northern Germany, the contribution of dry deposition is >60%, while in Scandinavia, the Baltic countries, and Russian Federation, wet deposition exceeds dry deposition. The reader should be aware that the TF HTAP ensemble-mean modeling results may overpredict dry deposition and its % contribution to total deposition in Europe. This is a reflection of the large variability in the different models in the TF HTAP ensemble. This is illustrated by the EMEP model, which suggests that dry deposition accounts for <30% of total deposition over most of Eastern Europe and Scandinavia and from 15 to 50% over most of Western Europe. Fig. 3.8 must therefore be interpreted with caution in Europe.

3.6.3.4. Changes in nssS deposition over time due to SO_2 emission changes. The spatial patterns of nssS wet deposition in 2000–2002 and 2005–2007 were roughly similar in shape (Fig. 3.17) but the wet deposition levels were considerably lower (i.e., median decrease of 23% for the 88 sites) in the latter period (Fig. 3.5b). Since the median decrease of precipitation depth was only 5%, the dominant cause of the lower wet deposition was the reduction in nssS concentrations, which had a median decrease of 15% (Fig. 3.5b). The decreases in wet deposition and concentration levels were generally higher at sites with high concentrations (Fig. 3.19). The wet deposition and concentration decreases were attributable to major reductions in S emissions across Europe, which were 24% lower in 2007 than in 2000 for the EMEP Parties (EMEP/CEIP, 2012). On the other hand, ship emissions increased by 10% over the same period and offset some of the decreases in anthropogenic S emissions on land, giving a net total emission reduction of 17% for the whole region (EMEP/CEIP, 2012).

There have been large reductions in S emissions in Europe over the last few decades. Most countries reduced their emissions by more than 60% between 1990 and 2004 and a quarter of these countries by more than 80% (Vestreng et al., 2007). Starting in the late 1970s, emission control programs included a number of measures like installation of flue gas desulfurization units at power plants and reduction of the sulfur content of fuel. However, it was not until the change in political and economical systems in eastern European countries that large reductions were observed (Lövblad et al., 2004; Vestreng et al., 2007; Tørseth et al., 2012). Presently, the largest source of SO_2 emissions in Europe is power generation (EMEP/CEIP, 2012). Ship emissions are of growing concern since they have the potential to counteract the benefits of reduced land-based anthropogenic emissions in several regions (Dore et al., 2007). In 2009, the ship emissions accounted for about 15% of the total emissions in Europe (EMEP/CEIP, 2012; Tørseth et al., 2012).

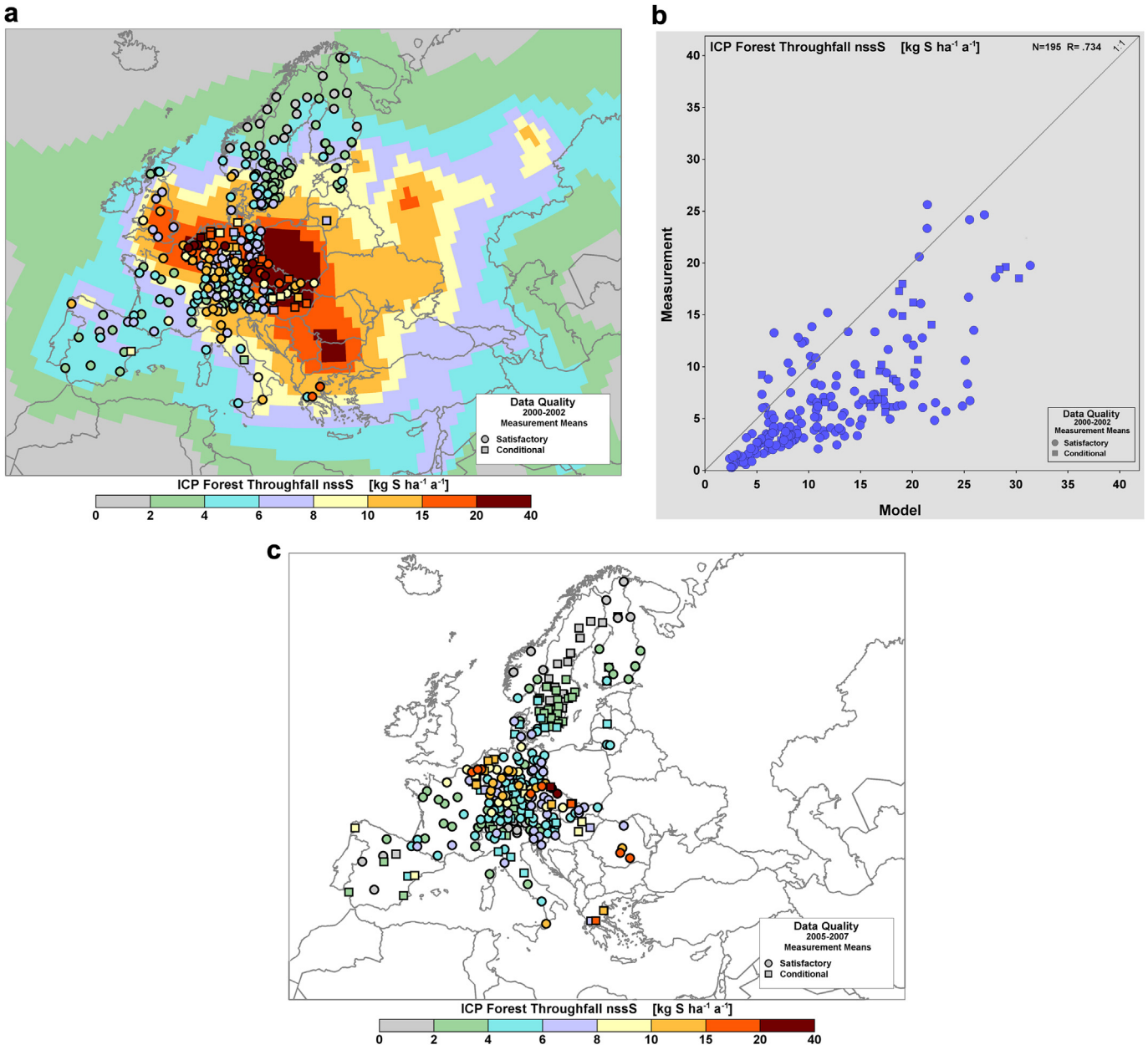

Fig. 3.18. (a) 3-year average (2000–2002) measured (by throughfall, ICP Forest) and 2001 modeled (by HTAP ensemble-mean) total deposition of nssS in Europe, (b) associated scatter plot and (c) annual average measured (by throughfall) total deposition for the period 2005–2007 in units of kg S ha^{-1} a^{-1}. Conditional data apply to sites with only two years of measurements.

Calculations have shown that in many coastal areas, ships will be responsible for more than 50% of S deposition by 2020, although expected emission controls on shipping (Cofala et al., 2007; Eyring et al., 2010) as well as the newly adopted UN International Maritime Organization (IMO) and European Union (EU) regulations (European Parliament, 2012) could lower these estimates considerably.

The EMEP monitoring results reflect the emission changes throughout Europe (Tørseth et al., 2012). For thirty EMEP sites with continuous measurements of S in air and precipitation since 1990, the average decreases were 75% for SO_2, and 56% and 64% for SO_4^{2-} in aerosol and precipitation, respectively, for the period 1990–2009 (Tørseth et al., 2012). It should be noted that sites with long term measurements are mainly situated in the north, west, and central parts of Europe and may not reflect the average trend over the whole region. Nevertheless, the emission reduction over the whole EMEP domain (including a large part of eastern Europe) was 65% for the same 1990–2009 period (EMEP/CEIP, 2012; Tørseth et al., 2012). The observation that SO_2 decreased more than SO_4^{2-} can be explained in part by the oxidation of SO_2 to SO_4^{2-}. With the oxidizing capacity of the atmosphere remaining unchanged and the amount of SO_2 available for oxidation growing smaller, the fraction of atmospheric SO_2 converted to SO_4^{2-} increases. This results in a larger decrease in SO_2 concentrations than in SO_4^{2-} concentrations. In addition, the SO_2 dry deposition rates may have changed during the time period due to changes in ambient ammonia concentrations which influence the sulfur dry deposition rates (Fowler, 2009 and references therein). The decreases in S wet and dry deposition

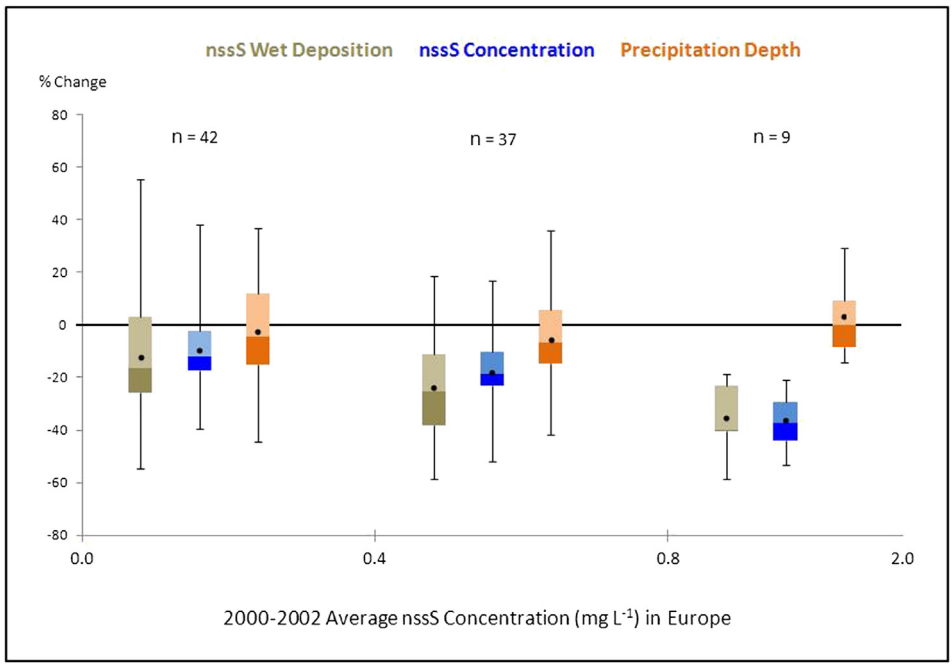

Fig. 3.19. % Changes in nssS wet deposition, concentration and precipitation depth from 2000–2002 to 2005–2007 as a function of 2000–2002 concentrations (mg S L^{-1}). Negative % changes indicate lower values in the 2005–2007 time period.

are also reflected in decreases in the size of the area receiving S wet and dry deposition, thereby reducing the problems of acidification due to sulfur deposition (Hettelingh et al., 2008).

3.6.4. Africa

Precipitation composition, wet deposition and dry deposition in Africa have been monitored at various times since the late-1990s at 10 IDAF sites, seven of which are located in west and central Africa and three in South Africa. These IDAF sites were specifically located in different African ecosystems (Fig. 3.20), which provide land use context for the discussion that follows. Unfortunately, large areas of Africa have never been monitored routinely and S deposition is largely unknown beyond the 10 IDAF sites.

3.6.4.1. Precipitation-weighted mean concentrations and wet deposition of S. Spatial patterns of multiple-year averages of precipitation-weighted mean concentrations of S are shown for the periods 2000–2002 and 2005–2007 in Fig. 3.2. Five of the IDAF measurement sites in west and central Africa operated for the 8 year period from 2000 to 2007 while the other two sites operated

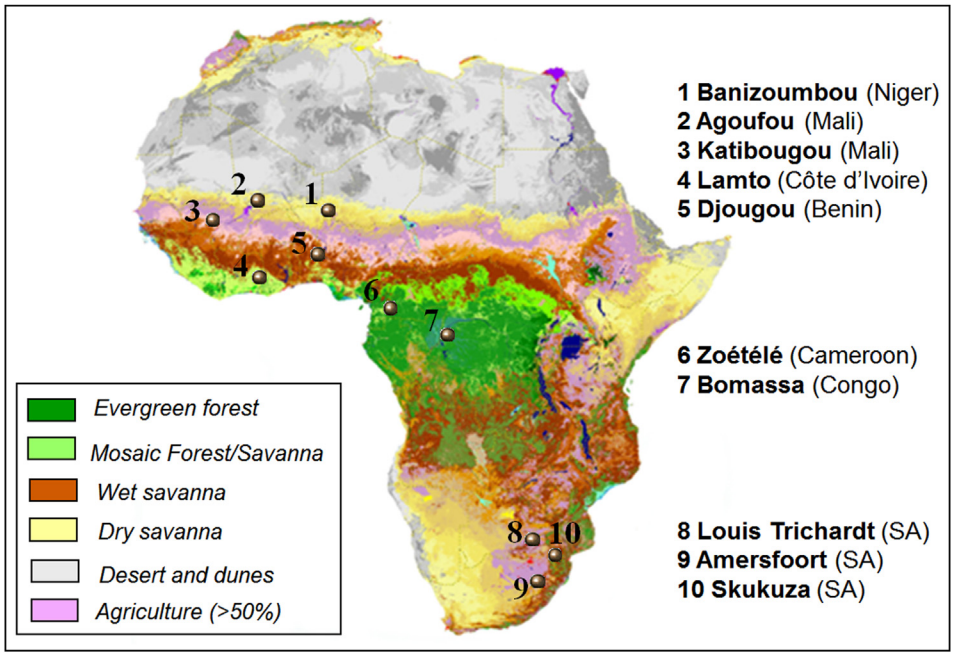

Fig. 3.20. Vegetation and location map of the 10 measurement stations of the IDAF network. (Vegetation map from Mayaux et al., 2003).

for only the 2005–2007 period. In the case of the three sites in South Africa, Amersfoort and Louis Trichardt operated for the period 1986–2000 and Skukuza for the period 1999–2002. Given the scarcity of data in Africa, we chose (as for nitrogen) to discuss the multi-year average precipitation-weighted mean concentrations measured for the whole studied period at each of the sites. It is worth noting that for the African sites, we have applied the correction for sea-salt-sulfate (ssS) even if sites were located further than 100 km of salt water bodies (see discussion below).

With respect to the various sites in west central Africa and their respective time periods, the mean annual precipitation-weighted concentrations of nssS ranged from a minimum of 0.10 to a maximum of 0.93 mg S L^{-1}. In the dry savannas, they varied from 0.09 to 0.12 mg S L^{-1}, in the wet savannas from 0.07 to 0.10 mg S L^{-1} and, in the forest region they were around 0.10 mg S L^{-1}. In contrast, the precipitation-weighted mean concentrations at the South African sites were higher, i.e., 0.93 mg S L^{-1} at Amersfoort in the industrialized area, and around 0.24 mg S L^{-1} in the dry savannas of Louis Trichardt and Skukuza.

The dominant pathway of air masses influencing the IDAF sites during the wet seasons was characterized based on back trajectories calculated using the Hysplit model (http://www.arl.noaa.gov/ready/hyspilt4.html) (Laouali et al., 2012; Mphepya et al., 2004, 2006). Results clearly indicated that monsoonal air masses coming from the Guinean Gulf rich in sea salt aerosols influence all of the sites and explains a 'marine signature' measured in the collected precipitation. The contribution of sea salt species to ion composition in precipitation was evaluated for each IDAF site using the Cl^-/Na^+ ratio and a global marine contribution was defined as the sum of the sea salt contributions of Mg^{2+}, Ca^{2+}, Cl^-, SO_4^{2-} and K^+. At the South African sites, Mphepya et al. (2004, 2006) demonstrated that the marine contribution (as defined previously) to the total ionic content of rainfall at Amersfoort, Louis Trichardt and Skukuza was 11, 23 and 25%, respectively, while the ssS contribution to measured S varied from 3% to 9% for Amersfoort and Louis Trichardt, respectively. At the west central Africa sites, the calculated marine contribution to total ion composition for the dry savanna, wet savanna and forest sites ranged from 10 to 16% and the ssS contribution to measured S ranged from 10 to 17%.

In west central Africa, a positive relationship exists between SO_4^{2-} and other non-marine species in precipitation including Ca^{2+}, K^+ and Mg^{2+} (Yoboué et al., 2005; Sigha-Nkamdjou et al., 2003; Galy-Lacaux et al., 2009; Laouali et al., 2012). This relationship confirms that the particles coming from the North African desert areas (Sahel and Sahara) and semiarid regions are probably the most important mineral aerosol sources in Africa (Kaufman et al., 2005). The dissolution of terrigenous soil dust species (calcite, dolomite, gypsum and other key minerals such as illite, smectite, palygorskite) that compose African dusts explain the enrichment of Mg^{2+}, SO_4^{2-} and K^+ (Avila et al., 1997). Thus, in addition to the marine source, the SO_4^{2-} content of west and central African precipitation is attributed to the terrigenous source. The decrease in SO_4^{2-} precipitation-weighted mean concentrations from dry savannas to forests is explained by the dust gradient across these ecosystems considering the distance to the source. In South Africa, Mphepya et al. (2004, 2006) found that SO_4^{2-} in precipitation at the three sites originates from soil dust, fossil fuel combustion and industrial emissions from the Highveld. At the Amersfoort and Louis Trichardt sites, NH_4^+, NO_3^- and SO_4^{2-} are highly correlated to each other and can be attributed to anthropogenic pollution. Assuming that the terrigenous SO_4^{2-} contribution is in excess of that supplied by gypsum (Delmas, 1981), Mphepya et al. (2004) determined that almost 80% of the SO_4^{2-} measured at Amersfoort and 50% of that measured at Louis Trichardt originates from industries in the Highveld (high altitude grassland region).

Spatial patterns of the 3-year average annual SO_4^{2-}–S and nssSO_4^{2-}-S wet deposition values are shown for 2000–2002 and 2005–2007 on the global maps of Fig. 3.3. To help fill the large gaps in measurements, we have chosen to include South African wet deposition data for years prior to our standard 3-year averaging periods. Wet deposition of S in west central Africa ranges from 0.61 to 6.2 kg S ha^{-1} a^{-1} for the periods indicated above. In terms of African ecosystem types (Fig. 3.20), in west-central Africa, wet deposition is low at the dry savanna sites (0.61–0.67 kg S ha^{-1} a^{-1}) and higher in the wet savanna and forest sites (0.68–1.5 kg S ha^{-1} a^{-1}) for the periods 2000–2002 and 2005–2007. In South Africa, wet deposition at Amersfoort and Louis Trichardt (1986–2000) and Skukuza (1999–2002) showed a positive gradient of concentration from the central Highveld region northward. Within this gradient, S wet deposition increased from a low of 1.6 kg S ha^{-1} a^{-1} at Louis Trichardt to 1.9 kg S ha^{-1} a^{-1} at Skukuza, to a maximum of about 6 kg S ha^{-1} a^{-1} at Amersfoort, which is located in the industrialized Highveld and in the same general area as a number of coal-fired power plants. In western and central Africa, measurements indicate that dust particle composition strongly influences wet SO_4^{2-}–S deposition. This terrigenous S source (i.e., SO_4^{2-} contained in dust) is associated with a marine S contribution and contributes an estimated 3–17% of wet deposition, thereby explaining a large part of the S content in rain and in wet deposition. It is important to note that the dust emission strength reaches its maximum in the dry season, and its minimum in the wet season with the consequence that the mean annual contribution of dust to S wet deposition is relatively low.

In a global context, concentrations and wet deposition of S in west and central Africa are relatively low compared to other areas of the world (Figs. 3.2 and 3.3) while in South Africa, they are considerably higher due to anthropogenic activities, especially at the Amersfoort site in the industrialized area (see emissions map in Fig. 3.1). However, we should note that in the analysis of S deposition, S chemistry in west and central Africa is less important compared to nitrogen chemistry. In South Africa, S is more important especially with higher SO_2 concentrations influencing the magnitude of S wet and dry deposition at all the sites.

Given the limited amount of data available in Africa, insight into the spatial pattern of nssS wet deposition across the continent can only be gained from the combined model-measurement global map shown in Fig. 3.6. Fig. 3.6c and d show reasonably good agreement between the modeled and measured nssS wet deposition values at the IDAF sites ($r = 0.938$; $n = 7$) and, although limited to a few measurement sites, supports the general pattern of low levels of wet deposition in most of west and central Africa with a decreasing gradient from central to northern Africa following the precipitation gradient. The highest simulated wet deposition is in South Africa where the maximum (3.6 kg S ha^{-1} a^{-1}) is located in the high emission area in the Highveld. The HTAP simulation underestimates the S wet deposition of 6.3 kg S ha^{-1} a^{-1} measured at Amersfoort – located close to the industrial emissions - by a factor of 2, although the measured and modeled periods are not exactly the same.

3.6.4.2. Dry deposition of S. Dry deposition estimates at the African sites were estimated using the inferential technique described in Section 2. Ambient particle- SO_4^{2-} concentrations were measured in Banizoumbou from 1996 to 2004; Katibougou from 1999 to 2003 and in Lamto from 1998 to 2005. In South Africa, p-SO_4^{2-} was measured only during intensive periods of 15 days in the summer and winter of 2005 and 2006 (Kleynhans et al., 2008). To estimate a range of particle-sulfate dry deposition, we used two dry deposition velocities, namely, 0.1 and 0.2 cm s^{-1} according to Zhang et al. (2009).

The estimated mean annual deposition of p-SO_4^{2-} in the semi-arid and wet savanna regions of west and central Africa ranged over the area from 0.1 to 0.3 kg S ha^{-1} a^{-1} and, in South Africa, from 0.5 to 1.1 kg S ha^{-1} a^{-1}. In other words, estimated dry deposition of p-SO_4^{2-} is low and of the same order of magnitude in all ecosystems, but are smaller by an order of magnitude than the wet S deposition. SO_2 dry deposition was estimated from monthly-integrated measured concentrations of SO_2 and monthly-average dry deposition velocities where the dry deposition velocities were estimated using the method described in Section 2. The resulting monthly-average dry deposition velocities for West Central Africa were: dry savannas 0.4 cm s^{-1}, wet savannas 0.6 cm s^{-1} and forest 0.9 cm s^{-1}, and for South Africa, 0.4 and 0.5 cm s^{-1}. SO_2 concentrations at the west and central Africa sites and for South African sites have been published, respectively, in Adon et al. (2010) and Martins et al. (2007). The annual average SO_2 concentrations for the period 2002–2007 at the sites in west central Africa and the period 1997–2005 at the sites in South Africa led to estimated annual dry deposition SO_2 fluxes ranging from 0.9 to 1.4 kg S ha^{-1} a^{-1} in west central Africa and from 1.7 to 5.2 kg S ha^{-1} a^{-1} in South Africa.

Fig. 3.7a shows reasonably good agreement between the modeled and measurement-based inferential S dry deposition values (SO_2 + p-SO_4^{2-}) at the IDAF sites (note, however, that the modeled p-SO_4^{2-} results do not include ssS while the measurements do). However, for the west and central African sites, the ensemble-mean HTAP simulation gives a range of S dry deposition of 0.2–1.0 kg S ha^{-1} a^{-1} – smaller by a factor 2 compared to the measured values of 1.0–1.5 kg S ha^{-1} a^{-1} in the dry savannas. Higher dry deposition is simulated in southern Africa with the maximum located in the South African Highveld due to power plant emissions, with comparable values between the modeled and measurement-based inferential dry S fluxes (2–10 kg S ha^{-1} a^{-1}).

On a continental scale, the HTAP model results (Fig. 3.7a) indicate that S dry deposition levels are highest in the high emission areas of South Africa (2–10 kg S ha^{-1} a^{-1}), the Mediterranean and Red Sea coasts (1–4 kg S ha^{-1} a^{-1}), Zambia (1–4 kg S ha^{-1} a^{-1}) and the Atlantic coastal areas of Nigeria and Cameroon (0.5–2 kg S ha^{-1} a^{-1}). The highest SO_2 emissions in the continent occur in the South African Highveld, in Zambia and near Lagos in Nigeria (Fig. 3.1). The main sources of these emissions are industrial activities (e.g., power generation, metal smelting) in the south African Vaal triangle, Lagos and industrial cities in the Copperbelt Mining-Smelting Area of Zambia (Mihaljevič et al., 2011; Ncube et al., 2012; Klimont et al., 2013; Smith et al., 2011; Liousse et al., 2013).

Dry deposition in these areas is highly efficient because gaseous S dry deposition velocities are high in the forested areas present in Zambia and Cameroon (Adon et al., 2013). The high S dry deposition over the eastern Mediterranean and Red Sea coasts are linked to high power production and industrial emissions in Egypt and Israel (http://edgar.jrc.ec.europa.eu) and pollution transport from Europe over the Mediterranean (Lelieveld et al., 2002). S dry deposition levels in the rest of the continent are low – ranging from 0.1 to 1 kg S ha^{-1} a^{-1}. Fig. 3.7b shows that the modeled dry deposition of S is dominated by SO_2 dry deposition in all of Africa except in the low emission/low precipitation areas of the Sahara Desert and the Horn of Africa. The measurement-based inferential dry deposition estimates in west central Africa and South Africa corroborate this with estimated contributions ranging from 76 to 90%.

3.6.4.3. Total deposition of S. The measurement-based estimates of total deposition of S (different periods for each) were estimated to be between 1.8 and 2.9 kg S ha^{-1} a^{-1} at the sites in West Central Africa and between 4.0 and 12.0 kg S ha^{-1} a^{-1} at the sites in South Africa. Based on these estimates, 45–60% of S total deposition is contributed by dry deposition in the forest, dry and wet savannas. In the forested ecosystem, wet deposition of nssS contributes more (55%) to total deposition of S; this decreases towards the dry savanna ecosystems where wet deposition contributes around 40% of the total. In South Africa, dry deposition of S contributes 48 and 56% at the Amersfoort and Louis Trichardt sites, respectively.

The continental pattern of modeled total deposition is shown in Fig. 3.8a. In north Africa, total deposition of S is very low in the Saharan region, with values ranging from 0.2 to 1 kg S ha^{-1} a^{-1}, and higher (1–4 kg S ha^{-1} a^{-1}) along the Mediterranean and Red Sea coastlines. In central and southern Africa, the levels generally range from 0.2 to 2 kg S ha^{-1} a^{-1} except in the high emission areas of South Africa (2–10 kg S ha^{-1} a^{-1}), Zambia (2–5 kg S ha^{-1} a^{-1}) and the Atlantic coastal areas of Nigeria and Cameroon (2–5 kg S ha^{-1} a^{-1}). The IDAF measurements in Mali and Niger give values around 1–2 kg S ha^{-1} a^{-1}, which are in the same range as the modeled values. The IDAF measurement-based estimates at the 3 sites in South Africa are between 4 and 12 kg S ha^{-1} a^{-1}. These values are in a similar range (4–10 kg S ha^{-1} a^{-1}) to the modeled values. Again, the modeled values of total deposition do not include the dry deposition of ssS but these values are known to be very low as discussed above.

3.6.4.4. Changes to S deposition over time due to changing SO_2 emissions. Changes to S wet deposition on the African continent are difficult to discuss because of the limited availability of deposition and emissions data. Only three of the IDAF monitoring sites, all of which are located in west central Africa, had sufficient data to calculate wet deposition changes from 2000-2002 to 2005–2007 (see Fig. 3.5). Between the two periods, Lamto (Republic of Côte d'Ivoire) and Banizoumbou (Niger) measured increases of 20 and 34% while Katibougou (Mali) measured a decrease of 12.4%. Unfortunately, it was not possible to put these changes in the context of changing S emissions in that area of the continent. In west and central Africa (except in Nigeria), we assume that S emission changes are related predominantly to annual variations in soil and biomass burning, where the latter include the burning of forest, grassland, and agricultural wastes (Macdonald et al., 2004; Arndt et al., 1997). Overall, anthropogenic S emissions in Africa related to thermal power stations, smelters, steel works, foundries, and fertilizer plants, have generally been increasing throughout recent decades (McCormick, 1997; UNEP, 2000). Moreover the rapid increase of the population of many African cities increases the energy demand and consequently S industrial emissions (Lamarque et al., 2011). Clearly, the long term deposition data sets collected by the IDAF program will be very important for quantifying the future effects of S emission changes on deposition.

3.6.5. Asia

Asia is considered here to be the area encompassed by Iran in the west to Japan in the east, and Russian Federation in the north to Thailand in the south. The density of precipitation monitoring sites throughout Asia is sparse, with no data available for this review over large areas of the continent (see Section 2 for data sources). The subsections that follow describe the available measurement-based and model-based results for S in precipitation and deposition in Asia.

3.6.5.1. Precipitation-weighted mean concentrations and wet deposition of S. The measurement-based 3-year average precipitation-weighted mean concentration and wet deposition patterns of S are shown for 2000–2002 and 2005–2007 in the global maps of Figs. 3.2a,b and 3.3a,b, respectively. As expected from the pattern of S emissions (Fig. 3.1), the precipitation-weighted mean concentrations of S in precipitation and S wet deposition were highest in the eastern part of the continent, viz., northeast India, northern

Vietnam, eastern China, the Republic of Korea and Japan (and nearby seas). In 2000–2002, the 3-year average precipitation-weighted mean concentrations in that area ranged from 0.5 mg S L^{-1} at the edges to 3.2 mg S L^{-1} at the EANET site at Chongqing-Jinyunshan, China and, in 2005–2007, from 0.5 to 4.6 mg S L^{-1} at Xi'an-Jiwozi site in China. Wet deposition values in this area ranged from 5.0 to 34.9 kg S ha^{-1} a^{-1} at Tie Shan Ping (near Chongqing, China) in 2000–2002 and 5.0–49.8 kg S ha^{-1} a^{-1} in 2005–2007 with the maxima occurring at Chongqing-Jinyunshan, China. In contrast to the high values in eastern China, wet deposition in Japan and the Republic of Korea was generally in the 5.0–15.0 kg S ha^{-1} a^{-1} range and in India, in the 4.0–11.0 kg S ha^{-1} a^{-1} range. In India, the maxima occurred at two locations: Mohanbari in northeast of India and at Portblair, an island site. In both cases, the maxima were due to very high precipitation depths.

The wet deposition pattern over all of Asia is strongly influenced by high precipitation depth, especially where S concentrations in precipitation were comparatively low such as the northeast, east, south and on the islands. The contribution of ssS to S wet deposition at coastal and island sites in Asia ranged from a low of 1.6% at the Hoa Binh site in Vietnam in 2005–2007 to a high of 77% at the Japanese island site of Hedo in 2000–2002.

Fig. 3.6c shows the 2000–2002 measured wet deposition of nssS superimposed on the 2001 ensemble-mean modeled pattern of wet deposition. As mentioned above, the modeled pattern fills the gaps between the measurement sites and can be used to estimate the values in those gaps on the assumption that the measurement-model comparability is good. In Asia, the measurement-to-model correlation coefficient (r) is 0.838 for $n = 39$ (Fig. 3.6d), with a tendency for the modeled values to underpredict the measured values. Maximum modeled nssS wet deposition of 17.0–20.4 kg S ha^{-1} a^{-1} appears in the high emission area of eastern China – considerably lower than the maximum measured values in Asia (and in the world) of 22.9, 34.3 and 34.9 kg S ha^{-1} a^{-1}. The modeled results also indicate a broad area of 5–10 kg S ha^{-1} a^{-1} over other parts of eastern China as well as north Vietnam, northeast India, Democratic People's Republic of Korea, the Republic of Korea and Japan. Here, the model-measurement comparison was quite good except at the EANET Hedo site in Japan which had very high deposition. Low wet deposition levels of <2 kg S ha^{-1} a^{-1} are modeled over most of Russian Federation, Mongolia, western China and to the west of India. The minimum modeled value of 0.15 kg S ha^{-1} a^{-1} occurred in Saudi Arabia, no doubt associated with low rainfall amounts in the area. Further measurement-model comparison statistics are available in Addendum Table S3.

3.6.5.2. Dry deposition of S. Long-term network-based measurements of dry deposition of S across Asia are not available. The only long-term characterization of S (and nitrogen) dry deposition was estimated for Japan (Endo et al., 2011; EANET, 2011) based on measurements at 10 EANET sites from 2003 to 2008. Dry deposition was calculated by the product of the air concentrations of SO_2 and p-SO_4^{2-} measured biweekly via filter-pack, and deposition velocities for forest and grass surfaces inferentially estimated by Matsuda (2008). Five-year mean annual dry deposition amounts for S were in the range of 1.6–11.8 kg S ha^{-1} a^{-1} with the highest concentrations at sites near the Sea of Japan and Western Japan. SO_2 was the largest contributor at each site (~40–70%) with a relatively small sea salt SO_4^{2-} contribution. A review of the SO_2 and particle-SO_4^{2-} dry deposition velocities published in Endo et al. (2011) indicated that they had higher maximum values than the two North American networks (CASTNET and CAPMoN) described in Section 3.6.1.

Some short-term measurement-based inferential estimates of dry S deposition were also published for other parts of Asia (Kominami et al., 2005; Kim et al., 2010). Kominami et al. (2005), for example, indicated that in 2001, S dry deposition levels at EANET sites throughout Asia (Russian Federation, Mongolia, Japan, China, Vietnam, Phillipines, Thailand and Malaysia) ranged from 0.1 to 8.0 kg S ha^{-1} a^{-1} except for China were the range was from 20 to 40 kg S ha^{-1} a^{-1}. Kim et al. (2010) estimated S dry deposition over the Yellow Sea and coastal area for the period 1999–2000 using ground, shipboard and aircraft ambient measurements. Annual dry deposition of S over the Yellow Sea was 3.84 kg S ha^{-1} a^{-1}.

The lack of long-term measurement-based inferential dry deposition values makes it necessary to rely on the 2001 model-based pattern of dry deposition, which is visible in the global pattern of Fig. 3.7a. Not surprisingly, the pattern of S dry deposition closely resembles the pattern of S emissions (Fig. 3.1). Modeled dry deposition is highest (20–33 kg S ha^{-1} a^{-1}) in eastern China and second highest (10–20 kg S ha^{-1} a^{-1}) in the Democratic People's Republic of Korea, the Republic of Korea and over the Yellow and South China Seas. Local hot spots, ranging from 2 to 10 kg S ha^{-1} a^{-1}, appear in parts of western Asia and in most of India and parts of Pakistan, Thailand, Vietnam and Japan. The area of minimum dry deposition occurred in northern Russian Federation where values reached as low as 0.05 kg S ha^{-1} a^{-1} and in the low precipitation, low emission areas of western China and Mongolia. Fig. 3.7b suggests that SO_2–S contributes > 50% of the dry deposition of S over all of Asia except in the dry, low emission areas of northwest China and western Mongolia where it contributes only 15–50%. In the high dry deposition areas of western Asia, India, eastern China, the Democratic People's Republic of Korea, the Republic of Korea, Japan and their surrounding seas, dry SO_2–S deposition is projected to be responsible for over 85% of the dry S deposition.

3.6.5.3. Total deposition. Five-year mean annual total deposition of S at EANET sites in Japan (Endo et al., 2011; EANET, 2011) was estimated in the range of 9–24.6 kg S ha^{-1} a^{-1} and was higher in the Sea of Japan and western Japan, and lower at Rashiri and Ogasawara. The contribution of dry deposition to total deposition was estimated to be 10–55%. Given the lack of measurement-based inferential dry deposition estimates for the Asian continent, we discuss here the 2001 HTAP model-based pattern of total deposition (Fig. 3.8a). The area of maximum total deposition (40.0–50.2 kg S ha^{-1} a^{-1}) occurred in the high emission area of eastern China with a secondary maximum (20–40 kg S ha^{-1} a^{-1}) also in eastern China and extending to the Democratic People's Republic of Korea and the Republic of Korea. The lowest total deposition occurred in northern Russian Federation with values of 0.2 kg S ha^{-1} a^{-1} with a secondary minimum of 0.4–1.0 kg S ha^{-1} a^{-1} in western China and Mongolia. Throughfall measurements from the IMPACTS sites in China (see Addendum Table S1) confirm the high deposition levels of S in this region, where the annual S deposition ranges from 20 to 160 kg S ha^{-1} a^{-1} (Larssen et al., 2006) and the maximum occurs in Tie Shan Ping (relatively close Chongquing). The contribution of dry deposition to total deposition in Asia can be seen in the global map in Fig. 3.8b. Wet deposition contributes more than dry deposition in most of Asia (i.e., ratios of <50%) but the opposite is true in areas around the Caspian Sea, Pakistan, India, eastern China, the Democratic People's Republic of Korea and the Republic of Korea.

3.6.5.4. Changes in S deposition over time due to changing SO_2 emissions. The measured differences in the 3-year average wet deposition of S between 2000–2002 and 2005–2007 are shown in Fig. 3.5a,b. The average % change for the 32 measurement sites was an increase of 8.5%, although both increases and decreases occurred. Of the 32 sites, 21 showed increases between 0 and 48%

and 11 showed decreases between 0 and 54%. During this period, SO_2 emissions in Asia are known to have increased at a phenomenal rate with a contribution to global SO_2 emissions of 50% in 2005 compared to 18% in 1980 (EANET, 2011). From 1980 to 2003, SO_2 emissions in India and China increased 3.2 times and 2.5 times, respectively. Since the 1990s, Chinese SO_2 emissions contributed about one-fourth of the global anthropogenic emissions and more than 90% of emissions in East Asia (Lu et al., 2010). SO_2 emissions in China have increased dramatically since 2000; however, they began to slow down around 2005 and decreased after 2006 due to the installation of flue-gas desulfurization equipment in power plants (Lu et al., 2010; EANET, 2011).

An analysis of annual mean concentration and deposition of nssS and other ions at selected EANET sites over the period 2000–2009 showed a high degree of variability with the conclusion that a longer period of observations will be required to elucidate temporal trends (EANET, 2011).

Between 2000–2002 and 2005–2007 in India (Fig. 3.5a,b), the minimum decrease in the 3-year average wet deposition of S of 5% occurred at the Mohanbari site in northeast India, the maximum decrease of 47% occurred at an island site Portblair over Bay of Bengal, and an increase of 20% occurred at an island site Minicoy over Arabian Sea. Consistent with the decreases, the Central Pollution Control Board's (CPCB) National Ambient Air Quality Monitoring (NAAQM) reports a decreasing trend in SO_2 levels in many cities like Delhi and Mumbai from 1995 to 2007. This trend was due to various emission measures such as the reduction of sulfur in fuel (e.g., the S content in gasoline was reduced from 0.1% to 0.05% in 2000 and in diesel fuel from 0.25% to 0.05% in 2005) and the use of LPG instead of coal as a domestic fuel (Ministry of the Environment and Forests, 2009). As well, Garg et al. (2006) report a decreasing trend in total SO_2 emissions from the transport sector in India from 0.138 Tg in 2000 to 0.085 Tg in 2005.

3.6.6. Oceania

Oceania is defined here as Indonesia, Malaysia, Australia, Papua New Guinea, New Zealand, and neighboring South Pacific islands. Oceania had only five regionally-representative monitoring sites that met our screening criteria: two in Malaysia, one in Indonesia and two in Australia. Two additional sites in Australia, Cape Grim and Burrup Peninsula, did not meet our screening criteria but are discussed below because of their importance for characterizing wet deposition in the area. Cape Grim data were screened out because they represented only the subset of precipitation events associated with the so-called "baseline" wind direction sector from the south, and Burrup Peninsula data were screened out because they did not fit conveniently within our standard 3-year measurement periods. Observations for these sites were provided by the Acid Deposition Monitoring Network in East Asia (EANET) and the Bureau of Meteorology/Australian Commonwealth Scientific and Industrial Research Organisation (CSIRO) Marine and Atmospheric Research (BoM/CMAR). No measurements exist for areas such as New Zealand, Papua New Guinea or other South Pacific Islands.

3.6.6.1. Precipitation-weighted mean concentrations and wet deposition of S. During the period 2000–2002, the lowest average nssS concentrations in precipitation were measured at Tanah Rata, Malaysia (0.13 mg nssS L^{-1}) and the highest at Bukit Kototabang, Indonesia (0.18 mg nssS L^{-1}). The same average precipitation-weighted nssS concentration (0.14 mg nssS L^{-1}) was observed at the Australian sites of Coffs Harbour and Wagga Wagga even though Coffs Harbour is on the coast and Wagga Wagga is 275 km from the coast. No data were available from Danum Valley for 2000–2002. Over the 2005–2007 period, the highest concentration was also observed at Bukit Kototabang (0.20 mg nssS L^{-1}) while the lowest was at Danum Valley, Malaysia (0.08 mg nssS L^{-1}), but no data were available for Coffs Harbour and Wagga Wagga. At the Burrup Peninsula (northwestern Australia), the average precipitation-weighted concentration for 2004/05, 2007/08 and 2008/09 was 0.11 mg nssS L^{-1}.

During the 2000–2002 period, the highest average nssS wet deposition in Oceania was observed at Tanah Rata (3.70 kg nssS ha^{-1} a^{-1}) and the lowest at Wagga Wagga (0.84 kg nssS ha^{-1} a^{-1}), although the latter is an annual average for 2000 (Fig. 3.3c). In the later 2005–2007 period, nssS wet deposition was highest at Bukit Kototabang (4.10 kg nssS ha^{-1} a^{-1}) and Tanah Rata (3.98 kg nssS ha^{-1} a^{-1}) and lowest at Danum Valley (2.47 kg nssS ha^{-1} a^{-1}) (Fig. 3.3d). No data were available for Coffs Harbour and Wagga Wagga. The average nssS deposition measured at the Burrup Peninsula over three years (2004/05, 2007/08 and 2008/09) was 0.38 kg nssS ha^{-1} a^{-1}. There was a large difference in the nssS deposition between 2004/2005 and 2007/2008; the period 2007/2008 had a larger sulfur wet deposition due in part to the higher rainfall amount and to one rainwater event that had a significant influence on the annual flux. Methane sulfonate was also measured in precipitation samples at these sites. The calculated annual deposition of methane sulfonate was found to be a very small fraction of the total S flux (0.034–0.058 kg S ha^{-1} a^{-1} at Coffs Harbour, 0.062 at Wagga Wagga and 0.004–0.016 kg S ha^{-1} a^{-1} at Cape Grim); thus, they were not included in the S wet deposition estimate.

The S concentration measurements made at the Cape Grim Baseline Air Pollution Station (Tindale et al., 2003; Cainey et al., 2004; Cainey et al., 2006; Cainey et al., 2007; Derek and Krummel, 2011), are particularly noteworthy because Cape Grim is a global baseline station within the Global Atmosphere Watch Programme of the World Meteorological Organization. At Cape Grim, the precipitation collector was turned on only for the subset of precipitation events having flow from the Southern Ocean (i.e., all other events from all other flow directions were not sampled). Thus, the concentrations presented here represent only the subset of so-called *Southern Hemisphere baseline events* and annual precipitation-weighted mean concentration and wet deposition values could not be calculated. Fig. 3.21a presents box-plots of nssS concentrations in baseline precipitation for the years 2000–2007. At Cape Grim the baseline nssS precipitation-weighted mean varied from 0.28 to 0.88 mg nssS L^{-1}, with an average value of 0.48 mg nssS L^{-1}, and during the 8 years of measurements no real temporal changes were observed. The annual wet deposition estimate for baseline nssS events at Cape Grim ranged from 0.31 kg nssS ha^{-1} a^{-1} in 2001 to 0.80 in 2006 with an average of 0.56 kg nssS ha^{-1} a^{-1} for all years, as Fig. 3.21b shows. Fig. 3.21b explains that the annual variation in baseline nssS wet deposition results from the variation in precipitation depth, rather than variation in the S concentration in precipitation.

As a consequence of the lack of remote sites, very little is known about the spatial distribution of S concentrations in precipitation and S wet deposition over Oceania. Modeled concentrations in precipitation aid in providing a regional-scale view (see Fig. 3.6). The highest nssS concentrations in Oceania are generally found near populated areas, which typically coincide with high emission areas; and the lowest concentrations over oceanic or remote continental areas. The highest concentrations of 0.1–0.2 mg nssS L^{-1} are found in several areas of Oceania including south eastern Australia; Auckland, New Zealand; northern Papua New Guinea and the Bismarck Sea, on Java near Jakarta; and Peninsula Malaysia, near Kuala Lumpur. The concentrations of nssS over Papua New Guinea and the Bismarck Sea are probably due to emissions of S from the copper and gold mines in Papua New Guinea rather than high population densities. The nssS concentrations decrease at the edges of these populated areas to 0.08–0.1 mg nssS L^{-1} and then to

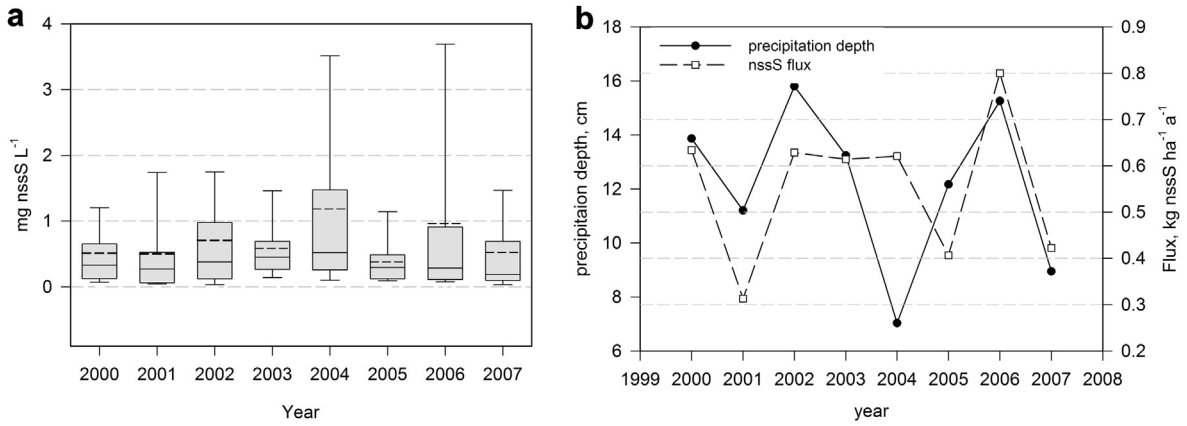

Fig. 3.21. (a) Concentrations of nssS and (b) annual nssS wet deposition and precipitation depth in baseline precipitation at the Cape Grim Baseline Atmospheric Pollution Station from 2000 to 2007. The median concentrations, mean concentrations (dotted line), the 25th and 75th quartiles and 10th and 90th percentiles are shown.

0.07–0.08 mg nssS L^{-1} due to decreases in population densities. In remote continental areas, the concentrations can be as low as 0.02–0.04 mg nssS L^{-1} in northwestern Australia and around the Indonesian islands of Sulawesi and the Moluccas archipelago. The lowest nssS concentrations of 0.015–0.02 mg nssS L^{-1} are found over the Bismarck Sea in the north west of Oceania. Other oceanic areas have concentrations of 0.05–0.06 mg nssS L^{-1} near continents that decrease to 0.02–0.04 mg nssS L^{-1} farther away from continental influences.

A comparison between modeled and measured concentrations (Fig. 3.6a) show that the average nssS measured concentration at Tanah Rata, Coffs Harbour and Wagga Wagga agree very well with the model predictions. The average concentration of nssS at Bukit Kototabang (0.18 mg S L^{-1}) is considerably higher than the modeled value (0.06 mg S L^{-1}).

At Cape Grim the modeled nssS concentration is in the range of 0.1–0.2 mg nssS L^{-1} compared with the measured baseline nssS values ranging from 0.28 to 0.88 mg nssS L^{-1}(Baseline 1999–2000, 2003; Baseline 2001–2002, 2004; Baseline 2003–2004, 2006; Baseline 2005–2006, 2007; Baseline 2007–2008, 2011). As mentioned above, the concentrations measured at Cape Grim represent only the subset of "*baseline*" precipitation events associated with winds from the Southern Ocean and were therefore screened out of the 3-year average data set mapped globally. The measured concentrations are somewhat higher than the model results, and this may be due to errors encountered in estimating the nssS fraction of S in rainwater at this site. Over the eight years of these measurements the nssS averaged 13.1% (standard deviation 12.7) of the total sulfate concentration in precipitation at Cape Grim. A relatively small change in sea-salt ratios can have a significant effect on the non sea-salt concentrations, and this may in part explain the disparity between the measured and modeled nssS concentrations at Cape Grim.

The 2001 modeled nssS wet deposition from TF HTAP as well as the measured wet deposition for 2000–2002 are presented in Fig. 3.6c. The modeled nssS wet deposition values for Tanah Rata, Bukit Kototabang and Wagga Wagga compare closely with the measured average fluxes; while the measured average sulfur deposition at Coffs Harbour is significantly higher than the model. The modeled deposition at the Burrup Peninsula is < 0.2 kg nssS ha^{-1} a^{-1}, which is of the same order as the average measured deposition of 0.38 kg nssS ha^{-1} a^{-1}, particularly considering the annual variation in the flux.

3.6.6.2. Dry deposition of S. Dry deposition of SO_2–S was estimated for two sites in Oceania (Tanah Rata and Burrup Peninsula) using measured SO_2 concentrations and a dry deposition velocity of 0.0028 m sec^{-1} as used by Manins (1994) for Malaysian conditions. Meyers et al. (1991) suggest the uncertainties of the predicted deposition velocities are generally within 30% of the measured velocities over short periods, and about 20% over longer periods of one week. The resulting average dry deposition of SO_2–S at the Burrup Peninsula for the two annual periods (2004/05 and 2007/07) was 0.17 kg SO_2–S ha^{-1} a^{-1}. At Tanah Rata the annual SO_2–S dry deposition for the period 2000–2001 was 1.04 kg SO_2–S ha^{-1} a^{-1}. Particulate phase SO_4^{-2} was measured at the Burrup Peninsula but only as total suspended particulate; thus, S deposition cannot be estimated since there is no information on the particle size distribution. No particulate data are available for Tanah Rata.

Model results from HTAP 2001 (Fig. 3.7a) show that the minimum SO_2 plus p-SO_4^{2-} fluxes of 0.1–0.15 kg S ha^{-1} a^{-1} are found in central Australia and the oceanic areas of the Bismarck Sea, north of Papua New Guinea and in the Indian Ocean west of Sumatra and Australia. The oceanic areas away from continental areas generally have SO_2 plus p-SO_4^{2-} fluxes in the range of 0.1–0.15 kg S ha^{-1} a^{-1}, and as low as 0.1 kg S ha^{-1} a^{-1} in the Bismarck Sea. Closer to continental areas dry deposition of SO_2 plus p-SO_4^{2-} can be up to 1–2 kg S ha^{-1} a^{-1}, such as in Peninsula Malaysia near Kuala Lumpur, and in south eastern Australia. In other less populated continental areas the dry deposition S flux ranges from 0.5 to 1.0 kg S ha^{-1} a^{-1}.

Fig. 3.7b shows the SO_2–S dry deposition as a fraction of dry SO_2–S to dry SO_2–S + dry p-SO_4^{2-}-S. In Oceania, most of the total S dry deposition is in the form of SO_2–S with lesser amounts from p-SO_4^{2-}-S and DMS-S. When compared to model estimates (Fig. 3.7a), the measurement-based inferential average dry SO_2–S deposition for Tanah Rata is within the modeled range of 1.0–2.0 kg SO_2–S ha^{-1} a^{-1}. At the Burrup Peninsula, the average measurement-based inferential SO_2–S flux compares closely to the model predicted range of 0.2–0.3 kg SO_2–S ha^{-1} a^{-1}.

The areas having the highest fraction of SO_2–S to the total flux of S are found in southeastern and southwestern Australia, the Bismarck Sea north of Papua New Guinea, the North Island of New Zealand, Sumatra and Java, Indonesia, where fluxes range from 85 to 100%. These areas have relatively high emissions of S in the forms of SO2, p-SO_4^{2-} and DMS-S as shown by the global sulfur emissions map in Fig. 3.1. Central Australia, where the lowest flux occurs, has areas where the SO_2–S percentage is 60–70% of the total flux of S.

3.6.6.3. Total deposition of S. Total deposition of S was estimated for Tanah Rata during 2000 and 2001 and at the Burrup Peninsula during 2004/05 and 2007/08. These estimates are the total of SO_2–S and p-nssSO_4^{2-}-S deposition. The average total deposition of S at

Tanah Rata for the period 2000–2001 was 4.57 kg S ha^{-1} a^{-1}. At the Burrup Peninsula, the average total deposition during 2004/05 and 2007/08 was 0.64 kg S ha^{-1} a^{-1}. The 2001 HTAP model results for total deposition are shown on the global map in Fig. 3.8a. The average total deposition at Tanah Rata (4.57 kg S ha^{-1} a^{-1}) falls within the range of 4.0–10 kg S ha^{-1} a^{-1} predicted by the HTAP 2001 model ensemble. In the Burrup Peninsula, the average total deposition (0.64 kg S ha^{-1} a^{-1}) is also very closely aligned with the model predicted range of 0.2–1.0 kg S ha^{-1} a^{-1}.

Not surprisingly, the modeled total deposition pattern of S over Oceania (Fig. 3.8a) closely reflects the S emission pattern shown in Fig. 3.1. The highest modeled total deposition fluxes of 4.0–10.0 kg S ha^{-1} a^{-1} were found in the Bismarck Sea in Northern Papua New Guinea and in Peninsula Malaysia near Kuala Lumpur. The HTAP model results predict S deposition of 2.0–4.0 kg S ha^{-1} a^{-1} in the populated areas of south eastern Australia, Sumatra, Java, Papua New Guinea, Sabah, Brunei and in the North Island of New Zealand. In less populated areas and in oceanic areas close to continents, the total deposition is predicted to be the range of 1.0–2.0 kg S ha^{-1} a^{-1}. The total deposition of S over the oceans ranged from 0.8-1.0 kg S ha^{-1} a^{-1} close to continental areas and dropped to 0.4–0.6 kg S ha^{-1} a^{-1} in the Indian Ocean and even to <0.4 kg S ha^{-1} a^{-1} in a section of the Indian Ocean in the west of Oceania.

S dry deposition as a percentage of total deposition was measured at Tanah Rata (2000–2001) and at the Burrup Peninsula (2004/05 and 2007/08). Tanah Rata had dry deposition contributions of 21% and 25% during those two years, giving an average of 23%. The predicted value from the HTAP 2001 model (Fig. 3.8b) is 30%–40%, which is somewhat higher than the measured percentage. The contributions measured at the Burrup Peninsula were 48% and 19%, respectively, during the two years, considerably lower than the modeled value of 60–70% (Fig. 3.8b).

The highest S dry deposition percentages modeled by HTAP 2001 are found on the Australian continent due to low rainfall depths compared to other regions of Oceania. Dry deposition fractions of 70%–85% are found in south west Australia and southern Australia, near Adelaide and Melbourne. In less populated areas of Australia, the dry deposition fractional contribution ranges from 60% to 70%, and as low as 30%–40% in remote areas. In other areas of Oceania the contribution ranges from 30% to 40% in populated areas and 15%–30% in less populated areas. In oceanic areas, the contribution is 40–50% close to the Australian continent, 30–40% farther away from the Australian continent (particularly in the Indian and Southern Oceans), and 15–30% over the ocean and continental areas of northern Oceania such as Papua New Guinea and parts of Indonesia and the South Pacific Ocean. The lowest percentage of dry to total deposition over the oceans is 0–15% near the Bismarck Sea.

Locations such as Tanah Rata and the Burrup Peninsula receive much of their rainfall from monsoonal systems. These systems often lead to significant variations in the total precipitation depth during a particular year. For example, over a six year period on the Burrup Peninsula, precipitation depth varied from 85.5 cm in 2006 to 9.5 cm in 2010. Tropical storms close to the area explain the large amount of precipitation during 2006 while during 2010 the monsoon almost completely failed to bring rain. It is difficult to model the precipitation depths in such locations, and this is probably the reason for the disparity between the measured and modeled percentage of sulfur dry deposition to the total of the wet and dry sulfur deposition.

3.7. Summary, gaps and uncertainties

An assessment of the spatial distribution of nssS in precipitation and wet deposition globally shows that S concentrations in precipitation are highest at sites in eastern China and lowest at sites in the western U.S., and wet deposition is highest in Asia (China, Japan, India, Taiwan), Europe (Croatia and Ireland) and North America (eastern U.S.) and lowest in western U.S.. Regional scale measurements of precipitation chemistry and deposition were not available for large parts of every continent; thus, HTAP ensemble-mean model estimates were used to fill information gaps in these geographical areas. High correlations between the observations and the ensemble-mean modeling results suggest that the modeled patterns of concentration ($r = 0.678$, $n = 428$) and wet deposition ($r = 0.793$, $n = 428$) are reasonable for filling the measurement gaps on a global basis, although not quite as well in Europe compared to the other continents. The ensemble-mean model estimates were also used to determine the S budget over the continents and oceans. Sea salt sulfur (ssS) was an important contributor to wet deposition in the coastal and island areas of the world.

The characterization of dry and total deposition on a global scale is only possible based on model estimates; however, regional measurement-based estimates are available for selected sites in North America, Europe (throughfall), Africa, Japan and Australia. As to be expected, the areas with the highest modeled % contribution of dry deposition to total deposition appear in the driest continental areas of the world as well as their nearby coastal zones. In North America and Europe, wet deposition levels have decreased significantly since 1990 and particularly between 2000–2002 and 2005–2007. This is attributed to the success of SO_2 emission reduction programs on these continents. Changes to S wet deposition in Asia were variable and difficult to discuss because of limitations in deposition and emissions data. The HTAP ensemble-mean global model results significantly overestimated total deposition of S in Europe as well as dry and total deposition in North America. There is a need to eliminate these biases in the global model through continued model development and evaluation against measured gas concentrations and dry deposition. There is also a pressing need to resolve the large differences in the inferential dry deposition models of Canada and the United States.

4. Nitrogen

Since the last global review (Whelpdale and Kaiser, 1996), publications on nitrogen composition and deposition on a global scale have been based largely on chemical transport model predictions because of the paucity of global measurement data. Model-based estimates (Rodhe et al., 2002; Bouwman et al., 2002; Dentener et al., 2006) show that areas of high N deposition coincide with those of high S deposition. These areas include southeastern China, northeastern India and Bangladesh, large parts of Europe, and northeastern North America. Ensemble-mean annual deposition patterns presented by HTAP (2010) show the largest deposition of reactive N[1] in parts of North America, Europe and East and South Asia, and demonstrate that reactive N deposition is dominated by domestic emissions with small intercontinental contributions.

Galloway et al. (2004), using a variety of data sets and model results, estimated global N budgets for 1860 and the early 1990s and projected them forward to 2050. They estimated that global emissions of NH_3–N in the 1990s were roughly 25% more than NO_x–N emissions and that approximately twice as much $N_{oxidized}$ was deposited to the continents as to the oceans. In contrast, a greater amount of $N_{reduced}$ was estimated to fall on the oceans

[1] Reactive N includes all nitrogen species (oxidized and reduced) except N_2; NO_y includes to all oxidized nitrogen species except N_2O. (Dentener et al., 2006).

compared to the continents. Based on 23 atmospheric models, Dentener et al. (2006) estimated that about 36–51% of NO_y and NH_x is deposited over the oceans with the balance over the continents. There was good agreement between ensemble model results and observations in Europe and North America, with a systematic overestimate of NH_x deposition in South Asia, and underestimated NO_y deposition in East Asia. In addition to its role in ecosystem acidification, model estimates of N deposition exceeded the eutrophication critical load of global natural ecosystems (Bouwman et al., 2002; Dentener et al., 2006).

Considerably more published information is available on a continental scale than globally. In North America, descriptions of N concentrations in precipitation and wet deposition reported for various long-term time periods (Environment Canada, 2005; NAPAP, 2005; Sickles and Shadwick, 2007; Lehmann et al., 2005; Baumgardner et al., 2002; Nilles and Conley, 2001; IJC, 2008; IJC, 2010; Zbieranowski and Aherne, 2011; Eshleman et al., 2013), show that the area of highest N (and S) deposition is just south of the Great Lakes. Measurements have also been used to determine spatial and temporal patterns of $N_{oxidized}$ and $N_{reduced}$ deposition in specific parts of the continent (e.g., Kvale and Pryor, 2006; Kelly et al., 2002; Luo et al., 2002; Martin et al., 2002; Willey et al., 2006; Lawrence et al., 2000; Peters et al., 2002; Golden and Boyer, 2009; Butler et al., 2003, 2005; Strayer et al., 2007; Poor et al., 2001; Scudlark et al., 2005; Walker et al., 2000; Stephen and Aneja, 2008; Anderson and Downing, 2006) and at high elevation sites (e.g., Clow et al., 2002; Hidy, 2003; Ingersoll et al., 2008; Beem et al., 2010).

In general, regional-scale and localized studies indicate that $N_{oxidized}$ in precipitation and wet deposition has varied over the last two decades with decreases occurring in the last 5–10 years in response to NO_x–N emission reductions. $N_{reduced}$, on the other hand, was found not to have decreased and, in fact, appeared to increase in certain areas. A number of studies also demonstrated that cloudwater deposition at high elevations can account for 20–60% of total wet deposition of $N_{oxidized}$ and $N_{reduced}$ and sometimes as much as 80% at the highest elevations (Anderson et al., 2006; Sickles and Grimm, 2003; Hutchings et al., 2009; Aleksic et al., 2009). Estimates of the influence of long range transboundary transport of NO_x–N emissions between the U.S. and Canada based on measurement data (Vet and Ro, 2008) show that between 62% and 83% of eastern Canadian $N_{oxidized}$ wet deposition in the 1990s was attributable to NO_x–N emissions from the eastern U.S., while a very low percentage of wet deposition in the eastern U.S. was attributable to considerably lower emissions from eastern Canada. Concentrations of $N_{oxidized}$ and $N_{reduced}$ in precipitation from short-term studies have been reported in Mexico, with much higher concentrations reported in Mexico City (Baez et al., 2007) than in the Mayan Riviera (Bravo et al., 2000).

Regionally-representative studies of $N_{oxidized}$ and/or $N_{reduced}$ concentrations in precipitation and wet deposition in South America are limited, with the majority conducted in Brazil. A summary of observations from this region based on published literature is presented later in this chapter.

In Europe, continental-scale spatial and temporal analyses of concentrations of major ions, including $N_{oxidized}$ and $N_{reduced}$, in precipitation and wet deposition are reported annually by the European Monitoring and Evaluation Programme (EMEP, http://www.emep.int/). The 2004 EMEP report (Lövblad et al., 2004) concluded that deposition of both $N_{oxidized}$ and $N_{reduced}$ decreased during the period 1980–2000 due to lower concentrations in air and precipitation resulting from NO_x and NH_3 emission reductions. $N_{oxidized}$ concentrations in precipitation exhibited considerable interannual variation due to changes in precipitation amount with the largest overall decreases taking place in Denmark and Poland. Regional-scale trends based on measurements at EMEP sites and model estimates over the 1980–2003 period showed statistically significant decreases of $N_{oxidized}$ and $N_{reduced}$ in precipitation at most sites (Fagerli and Aas, 2008). Tørseth et al. (2012) reported an average decrease of both $N_{oxidized}$ and $N_{reduced}$ concentrations in precipitation of about 25% from 1990 to 2009 with minor reductions since the late 1990s.

Large reductions of $N_{oxidized}$ deposition were achieved in the 1990s in parts of Europe, especially in Germany, Czech Republic and the eastern European countries such as Estonia, Lithuania, Latvia, Ukraine and Bulgaria (Fagerli et al., 2006). $N_{reduced}$ deposition was also reported to have declined in eastern Europe after 1990 but no large changes were observed elsewhere in Europe (Fagerli et al., 2006). Wet deposition of N ranged from less than 1 kg N ha^{-1} a^{-1} to more than 20 kg N ha^{-1} a^{-1}. $N_{reduced}$ and $N_{oxidized}$ contribute approximately equally to total N deposition, except at sites in the Benelux area and in Ireland (where $N_{reduced} > N_{oxidized}$) and Scandinivia and the Mediterranean (where $N_{reduced} < N_{oxidized}$). Despite decreases in the area and magnitude of exceedance of critical loads (Lövblad et al., 2004; Fagerli et al., 2006), eutrophication continues to be a major environmental problem in Europe. It is projected that it will continue to affect about 40% of the natural areas in Europe in 2020 under current emissions control legislation (WGE, 2011). In addition to monitoring under EMEP, numerous special studies have been conducted in European countries, generally of a short-term nature and designed to increase understanding of the sources and impacts of concentrations in precipitation and deposition. Given the focus of this assessment on regionally-representative long-term trends, these short-term studies are not discussed here.

In Asia, periodic regional assessments of the Acid Deposition Monitoring Network in East Asia (EANET) report on N concentrations in precipitation and deposition. Over the period 2000–2004, average $N_{oxidized}$ concentrations at remote and rural sites across Asia ranged from 0.05 to 1.06 mg N L^{-1} and $N_{reduced}$ concentrations ranged from 0.03 to 2.99 mg N L^{-1} (EANET, 2006). Siva Soumya et al. (2009) reported volumetric mean concentrations of major ions over the period 1978–2006 at a variety of rural, urban and suburban sites in India in relation to distance from the seacoast and showed that $N_{oxidized}$ remained constant at around 0.36–0.43 mg N L^{-1} with few sites showing higher concentrations. In Japan, Endo et al. (2011) estimated 5-year (2003–2008) averages of dry and total deposition of N at 10 EANET sites of 1–7 kg N ha^{-1} a^{-1} and 3.1–18.2 kg N ha^{-1} a^{-1}, respectively, with dry deposition estimated to contribute 13–56% of the total deposition. A characterization of the spatial and temporal pattern of N at a mix of urban and rural sites throughout China (Lu and Tian, 2007) showed that the wet and dry deposition rates for N ($N_{oxidized}$ plus $N_{reduced}$ and NO_2, respectively) increased significantly from 1990 to 2003 and peaked over central south China. The wet deposition maximum value was 62.25 kg N ha^{-1} a^{-1} and the average value was 9.88 kg N ha^{-1} a^{-1}. The peak values of dry deposition of >4.93 kg N ha^{-1} a^{-1} were centered in upper mideastern China, with a mean deposition rate of 3.03 kg N ha^{-1} a^{-1}. Numerous short-term studies have presented $N_{oxidized}$ and $N_{reduced}$ concentrations in precipitation and deposition in individual Asian countries; however, these are too local for the scope of this assessment and are thus not discussed here.

In Africa, reports of N concentrations in precipitation and deposition for different African ecosystems have been based on observations at regionally-representative sites in the following countries: South Africa (Mphepya et al., 2004, 2006), Republic of Côte d'Ivoire (Yoboué et al., 2005; Cameroon (Sigha-Nkamdjou et al., 2003), Benin, and Niger (Galy-Lacaux et al., 2009; Laouali et al., 2012). At these sites, $N_{reduced}$ was usually the dominant ion in precipitation, with the major source being emissions from

livestock. A continental assessment of wet and dry deposition of N species over a 3-year period (Galy-Lacaux et al., 2003) found higher wet deposition in wet zones than in dry savannas, except for one site in South Africa located near significant sources of anthropogenic emissions. They also found that dry deposition contributed approximately 60–70% of the total deposition. A comprehensive N budget for Sahelian dry savanna ecosystems in west central Africa has been published by Delon et al. (2010) where they estimate the total deposition to be 7.5 ± 1.8 kg N ha^{-1} a^{-1}, of which approximately 30% is attributed to $N_{oxidized}$ and 70% to $N_{reduced}$.

In Oceania, recent literature on N deposition and concentrations in precipitation is limited to measurements taken prior to the year 2000 and typically of short duration. In Australia, for example, Ayers et al. (2003) quoted $N_{reduced}$ concentrations in precipitation of 0.15–0.16 mg N L^{-1} at a site in southeastern Australia (New South Wales) in 1993–1994 and Likens et al. (1987) reported concentration of $N_{oxidised}$ and $N_{reduced}$ of 0.017 and 0.012 mg N L^{-1}, respectively, in north-central Australia (Katherine) in 1980–1984. In Hawaii and Kauai, total deposition of N (organic and inorganic) averaged 17 kg N $ha^{-1}a^{-1}$ with the major portion deposited via fog interception (Carillo et al., 2002). Precipitation contributed a maximum of 1 kg N $ha^{-1}a^{-1}$ in Hawaii and 0.2 kg N $ha^{-1}a^{-1}$ in Kauai, with a major contribution from fog interception (Carillo et al., 2002). NADP (2013) reported precipitation concentrations of $N_{reduced}$ and $N_{oxidized}$ of 0.02 and 0.015 mg N L^{-1}, respectively for the period 2002 through 2005 in Hawaii. NADP (2013) also reported wet deposition of $N_{reduced}$ and $N_{oxidized}$ of 0.38 and 0.44 kg N ha^{-1} a^{-1} for the same period.

In the Arctic, concentrations of $N_{oxidized}$ in precipitation from long-term observations at numerous sites were typically below 0.2 mg L^{-1} (AMAP, 2006; Hole et al., 2009). Significant trends of $N_{oxidized}$ concentrations in precipitation could not be detected by Hole et al. (2009) at 3 sites in the Arctic given that the power of the observations was too weak. Toom-Sauntry and Barrie (1994) collected snow for three years at Alert in the Canadian Arctic using a method that carefully avoided contamination from blowing snow. The data showed a strong seasonal variation that peaked in the spring with a maximum weekly concentration of 0.3 mg N L^{-1}.

Global and regional aspects of N emissions, N concentrations in precipitation and N wet and dry deposition are described in the sections that follow based on available precipitation chemistry measurement data and the 2001 HTAP ensemble mean modeling results from 16 $N_{oxidized}$ models and 7 $N_{reduced}$ models (see Section 2). The data presented herein are restricted to inorganic N compounds since measurements of organic N in air and precipitation are sparse and highly uncertain (Cape et al., 2011).

In order to ensure clarity in the discussion that follows, the terms used for the different N species and types of deposition are as follows: *NO_x-N emissions* refers to the sum of NO + NO_2 emissions expressed as nitrogen in Tg N a^{-1}; *NH_3–N emissions* refers to NH_3 emissions expressed as nitrogen in Tg N a^{-1}; $N_{oxidized}$ refers to the oxidized nitrogen species in air, precipitation and deposition expressed as N. In air and dry deposition, $N_{oxidized}$ includes some or all of the following species for which measurements are made: NO, NO_2, HNO_3, particle-NO_3^-, and PAN. In wet deposition, $N_{oxidized}$ refers to the NO_3^- ion expressed as nitrogen as measured in precipitation; $N_{reduced}$ refers to the reduced species of N in air, precipitation and deposition. In air and dry deposition, $N_{reduced}$ refers to gaseous NH_3 plus particle-NH_4^+; in precipitation and wet deposition, $N_{reduced}$ refers to the NH_4^+ ion resulting from precipitation scavenging of NH_3 and particle-NH_4^+. The sum of oxidized plus reduced nitrogen species (i.e., $N_{oxidized}$ + $N_{reduced}$) is referred to hereafter as "N" in wet, dry and total deposition.

4.1. Global and regional emissions of NO_x–N and NH_3–N

Global maps of 2001 NO_x–N, NH_3–N and NO_x–N + NH_3–N emissions are shown in Fig. 4.1a–c, respectively. The maps show $1^\circ \times 1^\circ$ grid square ensemble-mean emission rates in kg N ha^{-1} a^{-1} compiled from the emission inventories of the 16 HTAP $N_{oxidized}$ models and 7 $N_{reduced}$ models discussed in Section 2. The NO_x–N emission sources used to compile Fig. 4.1a include fossil-fuel generating units, vehicles, home heating, industry, shipping, biomass burning, soils and lightning. The NH_3–N emission sources in Fig. 4.1b include animals, biomass burning, domestic fires, forest fires, industry, and fertilizer application.

NO_x–N emissions (Fig. 4.1a) were highest in eastern North America, southern California, the United Kingdom, central Europe and East Asia, due in large part to fossil-fuel power production and vehicular emissions. Mid-range levels of NO_x–N emissions occurred as above and in parts of South America (Brazil, Colombia and Venezuela), central and southern Africa, western Russian Federation and India. Lowest emissions occurred over the oceans with the exception of major shipping channels which had low to moderate emission levels. NH_3–N emissions in 2001 (Fig. 4.1b) were highest in western Europe, Pakistan, India and eastern China, largely due to the intense agricultural activity in those regions. Moderate NH_3–N emissions occurred in the eastern half of North America, Mexico, northern and eastern South America, central Africa, western Russian Federation and parts of East Asia. Lowest emissions occurred over the remote oceans although the equatorial and temperate sections showed somewhat higher levels due to highly uncertain natural NH_3 emissions from oceans (Dentener et al., 2006).

The combined NO_x–N + NH_3–N emission fluxes in 2001 (Fig. 4.1c) were highest in eastern China (i.e., 40–60 kg N ha^{-1} a^{-1}) with next highest (20–40 kg N ha^{-1} a^{-1}) in eastern North America, Europe, Pakistan, India and south-central and northeast China. Lower emissions (4–20 kg N ha^{-1} a^{-1}) occurred in North America, northern and eastern South America, central and southern Africa, western Russian Federation, parts of East Asia and parts of Oceania. Lowest emissions (<0.2 kg N ha^{-1} a^{-1}) occurred over the remote oceans although the equatorial and temperate sections showed somewhat higher emissions (0.2–1 kg N ha^{-1} a^{-1}) derived from NH_3 oceanic emissions.

Area-integrated emissions of NO_x–N, NH_3–N and NO_x–N + NH_3–N (Table 3) were estimated as the sum of the ensemble-mean grid square emission values over the continents, coastal zones and oceans defined in Fig. 2.2 (also shown in Table 3 are total deposition values, which are discussed later). For the reasons given in Section 2, emissions are shown separately for the continental non-coastal, oceanic non-coastal, and coastal zones. Global total emissions of NO_x–N in 2001 were estimated at 46.6 ± 7.8 Tg N (where 7.8 represents the ensemble standard deviation of all model values), of which 71.2% were non-coastal continental, 23.0% were coastal zone, and 5.8% were non-coastal oceanic. Of the 46.6 Tg N total, non-coastal + coastal Asia accounted for 26.8%, with North America and Africa accounting for 18.7% and 16.7%, respectively. Oceanic non-coastal emissions were very low at 5.8%.

Global total emissions of NH_3–N in 2001 were estimated at 58.5 (±9.5) Tg N, of which 70.1% were non-coastal continental, 16.2% were coastal, and 13.7% were non-coastal oceanic. Of the 58.5 Tg N, non-coastal + coastal Asia accounted for the highest emissions at 39.4% of the global total, with Africa and South America the next highest at 12.5% and 10.4%, respectively. Oceanic non-coastal emissions of NH_3–N accounted for a higher proportion of global emissions (13.7%) than did oceanic non-coastal NO_x–N emissions (5.8%). The 2001 global total of NO_x–N + NH_3–N emissions was 105.1 Tg N, of which 70.6% was non-coastal continental, 19.2%

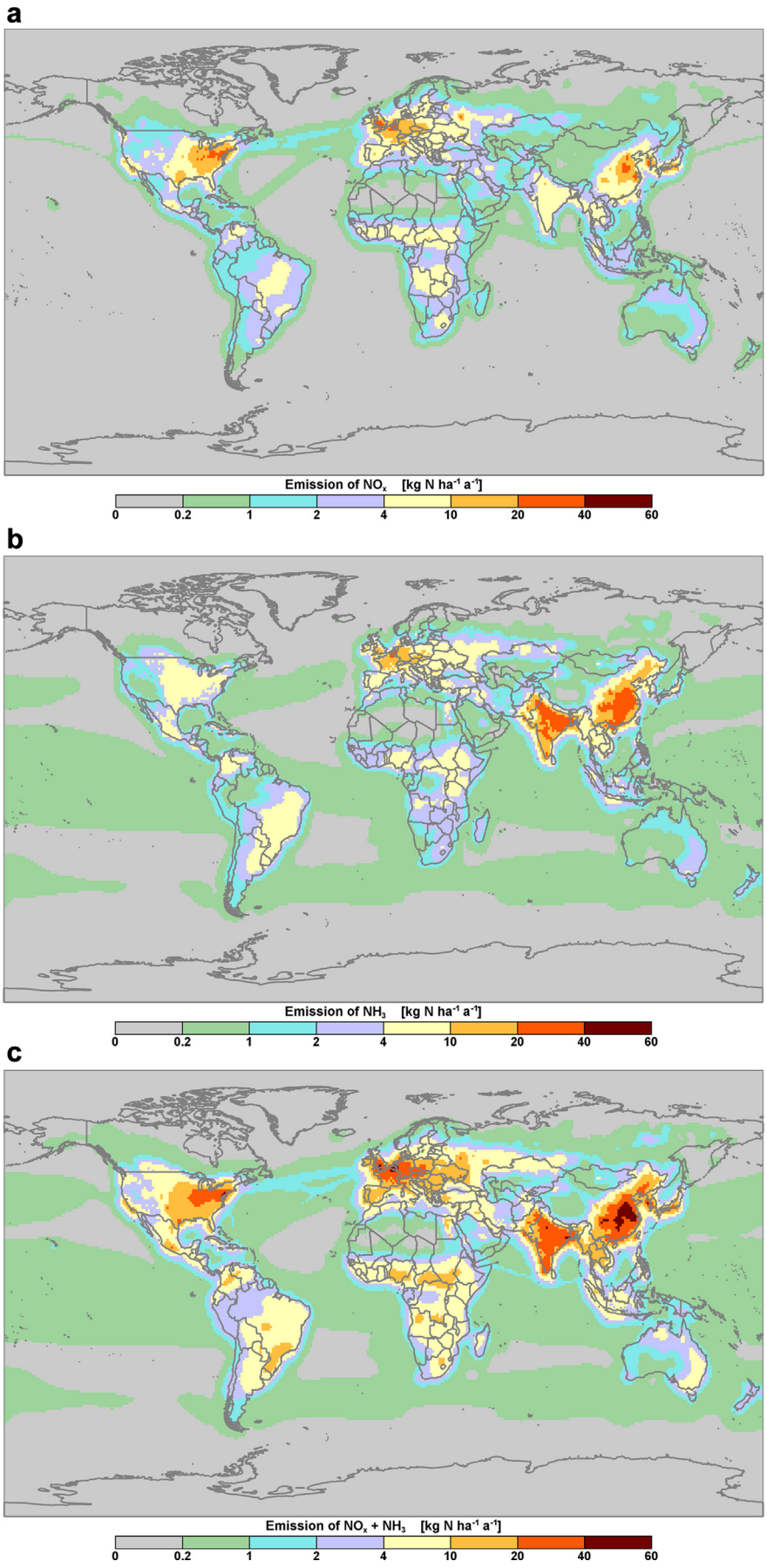

Fig. 4.1. 2001 ensemble-mean, 1° × 1°, emissions of: (a) NO_x–N, (b) NH_3–N and (c) NO_x–N + NH_3–N in kg N ha^{-1} a^{-1} obtained from the 16 HTAP NO_x models and 7 HTAP NH_3 models.

Table 3
Area-integrated 2001 estimates of NO_x–N + NH_3–N emissions and $N_{oxidized}$, $N_{reduced}$ and total deposition of N (Tg N) for Continents, Coastal zones and Oceans (as defined in Fig. 2.2). Values in parentheses represent the associated percentage of global $N_{oxidized}$, $N_{reduced}$ and N emissions and total deposition. Note that the Coastal Total emissions (and deposition) are the same for the Continents and Oceans. Thus, global Total emissions and deposition equal the sum of the Non-coastal Continents, Non-coastal Oceans and one of the Coastal Continents or Oceans.

Region	$N–NO_x$ emissions (Tg N)		$N_{oxidized}$ total deposition (Tg N)		$N–NH_3$ emissions (Tg N)		$N_{reduced}$ total deposition (Tg N)		N emissions (Tg N)		N total deposition (Tg N)	
	Non-coastal	Coastal	Non-coastal	Coastal	Non-coastal	Coastal	Non-coastal	Coastal	Non-coastal	Coastal	Non-coastal	Coastal
Continents												
Africa	6.9 (14.8)	0.9 (1.9)	5.2 (11.0)	1.0 (2.2)	6.5 (11.0)	0.9 (1.5)	5.4 (9.2)	1.0 (1.7)	13.4 (12.7)	1.8 (1.7)	10.6 (10.0)	2.0 (1.9)
Antarctica	0.0 (0.0)	0.0 (0.0)	0.0 (0.0)	0.0 (0.0)	0.0 (0.0)	0.0 (0.0)	0.0 (0.0)	0.0 (0.0)	0.0 (0.0)	0.0 (0.0)	0.0 (0.0)	0.0 (0.0)
Asia	9.1 (19.4)	3.4 (7.4)	7.7 (16.1)	3.3 (6.8)	19.4 (33.1)	3.7 (6.3)	15.9 (27.2)	4.3 (7.5)	28.4 (27.1)	7.1 (6.8)	23.6 (22.2)	7.6 (7.1)
Europe	4.7 (10.2)	2.3 (5.0)	3.6 (7.4)	2.0 (4.2)	4.5 (7.8)	1.4 (2.4)	3.7 (6.3)	1.5 (2.5)	9.3 (8.8)	3.7 (3.5)	7.2 (6.8)	3.5 (3.3)
North America	6.7 (14.4)	2.0 (4.3)	4.8 (10.1)	2.0 (4.1)	4.3 (7.3)	1.0 (1.7)	3.6 (6.2)	1.2 (2.0)	11.0 (10.5)	3.0 (2.9)	8.5 (8.0)	3.1 (3.0)
Oceania	1.4 (3.0)	1.4 (3.0)	0.8 (1.7)	1.2 (2.5)	1.2 (2.1)	1.6 (2.7)	0.9 (1.5)	1.6 (2.7)	2.6 (2.5)	3.0 (2.8)	1.7 (1.6)	2.8 (2.6)
South America	4.4 (9.4)	0.7 (1.4)	3.0 (6.2)	0.5 (1.1)	5.1 (8.8)	0.9 (1.6)	4.5 (7.6)	0.9 (1.5)	9.5 (9.0)	1.6 (1.5)	7.5 (7.0)	1.4 (1.3)
Σ Continents	**33.2 (71.2)**	**10.7 (23.0)**	**25.1 (52.5)**	**10.0 (20.9)**	**41.0 (70.1)**	**9.5 (16.2)**	**34.0 (58.0)**	**10.5(17.9)**	**74.2 (70.6)**	**20.2 (19.2)**	**59.1(55.6)**	**20.4 (19.2)**
Oceans												
North Atlantic	1.1 (2.3)	4.6 (9.8)	3.6 (7.5)	4.2 (8.8)	0.8 (1.3)	2.7 (4.7)	2.0 (3.4)	3.0 (5.2)	1.8 (1.8)	7.3 (6.8)	5.6 (5.2)	7.2 (6.8)
South Atlantic	0.2 (0.3)	0.4 (0.9)	1.2 (2.5)	0.4 (0.8)	1.0 (1.7)	0.6 (1.1)	1.6 (2.8)	0.6 (1.0)	1.2 (1.1)	1.0 (1.0)	2.8 (2.6)	1.0 (0.9)
N. Pacific	0.7 (1.7)	3.3 (7.2)	3.9 (8.2)	3.0 (6.2)	2.3 (3.9)	2.8 (4.8)	4.2 (7.2)	3.2 (5.5)	3.1 (2.9)	6.2 (5.8)	8.1 (7.7)	6.1 (5.8)
S. Pacific	0.2 (0.5)	0.6 (1.2)	1.5 (3.2)	0.5 (1.1)	2.0 (3.5)	0.7 (1.2)	2.5 (4.2)	0.7 (1.1)	2.2 (2.1)	1.3 (1.2)	4.0 (3.7)	1.2 (1.1)
North Indian	0.3 (0.6)	1.0 (2.2)	0.9 (1.9)	1.0 (2.1)	0.5 (0.9)	1.7 (2.8)	1.7 (2.9)	2.0 (3.3)	0.8 (0.7)	2.7 (2.6)	2.6 (2.5)	2.9 (2.8)
South Indian	0.2 (0.4)	0.8 (1.6)	1.4 (2.9)	0.7 (1.4)	1.3 (2.3)	1.0 (1.6)	1.9 (3.3)	0.9 (1.6)	1.5 (1.5)	1.7 (1.6)	3.3 (3.1)	1.6 (1.5)
Arctic	0.0 (0.0)	0.0 (0.1)	0.1 (0.3)	0.2 (0.5)	0.0 (0.0)	0.0 (0.0)	0.1 (0.1)	0.1 (0.2)	0.0 (0.0)	0.0 (0.0)	0.2 (0.2)	0.4 (0.3)
Southern	0.0 (0.0)	0.0 (0.0)	0.1 (0.1)	0.0 (0.0)	0.1 (0.1)	0.0 (0.0)	0.1 (0.2)	0.0 (0.0)	0.1 (0.1)	0.0 (0.0)	0.2 (0.2)	0.0 (0.0)
Σ Oceans	**2.7 (5.8)**	**10.7 (23.0)**	**12.7 (26.6)**	**10.0 (20.9)**	**8.0 (13.7)**	**9.5 (16.2)**	**14.1 (24.1)**	**10.5 (17.9)**	**10.7 (10.2)**	**20.2 (19.2)**	**26.8 (25.2)**	**20.4 (19.2)**
TOTAL	**35.9 (77.0)**	**10.7 (23.0)**	**37.8 (79.1)**	**10.0 (20.9)**	**49.0 (83.8)**	**9.5 (16.2)**	**48.1 (82.1)**	**10.5 (17.9)**	**84.9 (80.8)**	**20.2 (19.2)**	**85.9 (80.8)**	**20.4 (19.2)**

coastal, and 10.2% non-coastal oceanic. NH_3–N emissions accounted for 55.7% of the global NO_x–N + NH_3–N emissions and NO_x–N emissions 44.3%. Asia had the highest continental non-coastal plus coastal zone emissions at 35.6 Tg N or 33.9% of the global emissions, more than twice the next highest, Africa, at 15.2 Tg N or 14.5% of the global emissions.

4.2. Global N in precipitation and wet deposition

The measurement-based 3-year-average patterns of precipitation-weighted mean annual concentrations of N are shown in Fig. 4.2a and b for the periods 2000–2002 and 2005–2007, respectively. As with sulfur, large areas of the globe have had (and continue to have) little or no measurement coverage. In order to fill one of the largest data gaps, i.e., South Africa, several measurement points were included on the maps for periods slightly outside (but near) the 2000–2002 period. The screened-in data set in Fig. 4.2a comprised 433 Satisfactory, 32 Conditional and 4 Non-Conforming-Period data points; the data set in Fig. 4.2b consisted of 469, 15 and 0 data points, respectively.

Globally, the highest 3-year-average precipitation-weighted mean concentrations of N ranged from 1.50 to 1.88 mg N L^{-1} in the 2000–2002 period and from 1.50 to 1.93 in the 2005–2007 period. In both periods, the highest values, 1.88 and 1.93 mg N L^{-1} respectively, were measured at the Ust-Vym site in western Russian Federation and the Chongqing-Jinyunshan EANET site in eastern China. The other sites, characterized by concentrations greater than 1.50 mg N L^{-1}, were located in China, Russian Federation and Italy. The lowest concentrations measured in the two periods ranged from 0.03 to 0.04 mg N L^{-1} and were located in the United States (including Hawaii) and Malaysia. Overall, the measured concentrations varied over two orders of magnitude. Not unexpectedly, the spatial pattern of concentrations bears a close resemblance to the global pattern of NO_x–N + NH_3–N emissions with high concentrations occurring in high emission areas and low concentrations in low emission areas. Although not shown here, the

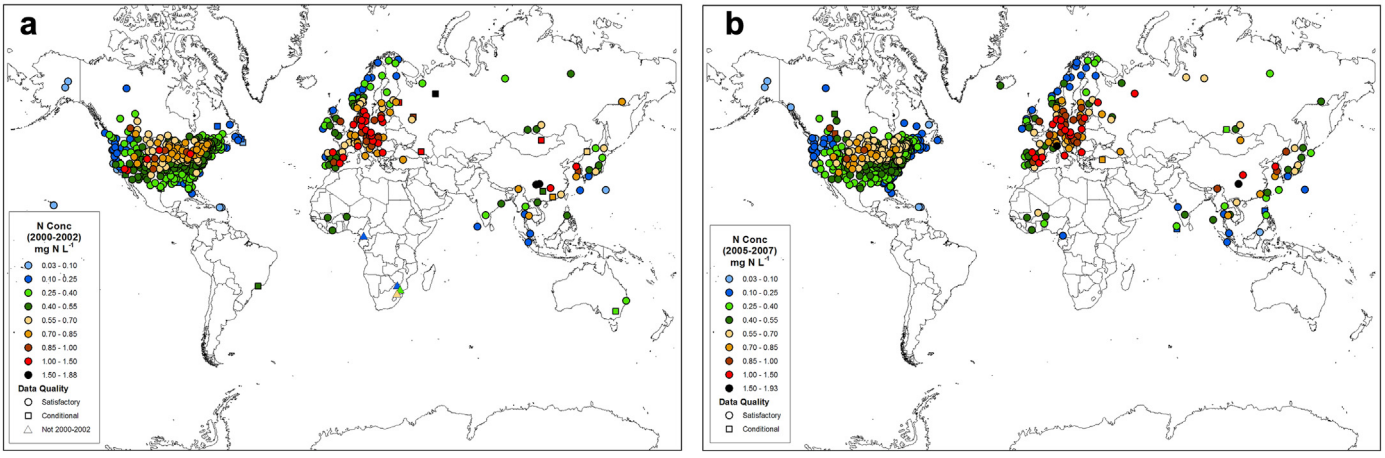

Fig. 4.2. Measurement-based patterns of 3-year average precipitation-weighted mean concentrations of N in mg N L^{-1} for: (a) 2000–2002 and (b) 2005–2007.

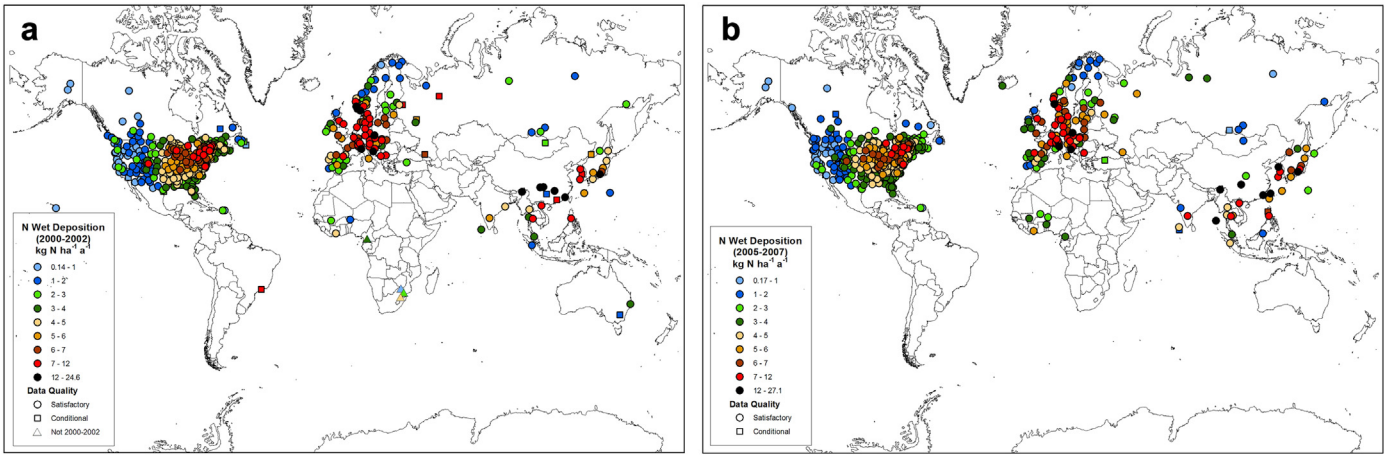

Fig. 4.3. Measurement-based patterns of 3-year average wet deposition of N in kg N ha^{-1} a^{-1} for: (a) 2000–2002 and (b) 2005–2007.

individual $N_{oxidized}$ and $N_{reduced}$ concentration maps are included as Addendum Figs. S4–S7.

The measurement-based 3-year average patterns of N wet deposition for 2000–2002 and 2005–2007 are shown in Fig. 4.3a and b, respectively. As was the case for the precipitation-weighted mean concentrations, the wet deposition patterns mimic the general NO_x–N + NH_3–N emissions pattern (Fig. 4.1c) with the additional influences of long range transport and precipitation amount. In 2000–2002 and 2005–2007, the highest 3-year average measured wet deposition occurred in Europe and Asia, ranging from 12.00-24.55 kg N ha^{-1} a^{-1} and 12.00–27.07 kg N ha^{-1} a^{-1}, respectively. The highest global values in the two periods were measured at the Ispra EMEP site in Italy in 2000–2002 and the EANET site at Chongquing-Jinyunshan, eastern China in 2005–2007. The lowest 3-year average wet deposition values measured globally were 0.14 kg N ha^{-1} a^{-1} in 2000–2002 at the Joshua Tree National Park NADP site in the western U.S. and 0.17 kg N ha^{-1} a^{-1} in 2005–2007 at the NADP Denali National Park site in Alaska, U.S.. The global maximum values were 175 and 159 times higher than the global minimum values, respectively, during the two periods. Overall, the lowest levels of wet deposition (<1.0 kg N ha^{-1} a^{-1}) occurred in western North America, northern Europe, and Russian Federation and the highest values (>7 kg N ha^{-1} a^{-1}) occurred in eastern North America, southern Europe, northeast India, Southeast Asia and northern Oceania – again a reflection of the NO_x–N + NH_3–N emissions (Fig. 4.1c).

$N_{oxidized}$ and $N_{reduced}$ wet deposition maps are not shown here but are available as Addendum Figs. S8–S11. The screened-in $N_{oxidized}$ wet deposition data set in Figs. S8 and S9, respectively, consisted of 434 and 470 Satisfactory, 32 and 14 Conditional, and 4 and 0 Non-Conforming-Period data points. Similarly, the screened-in $N_{reduced}$ wet deposition data set in Addendum Figs. S10 and S11 consisted of 435 and 469 Satisfactory, 30 and 15 Conditional, and 4 and 0 Non-Conforming-Period data points, respectively. $N_{oxidized}$ wet deposition in the two periods ranged from a minimum of 0.06 kg N ha^{-1} a^{-1} in 2000–2002 at Joshua Tree National Park in the western U.S. to a maximum of 17.3 kg N ha^{-1} a^{-1} in 2005–2007 at Mohanbari in northeastern India, the latter being due to both a very high concentration (0.71 mg N L^{-1}) and precipitation depth (242 cm). Measured $N_{reduced}$ wet deposition ranged from 0.08 kg N ha^{-1} a^{-1} in 2000–2002, again at Joshua Tree National Park in the western U.S., to 19.8 kg N ha^{-1} a^{-1} in 2005–2007 at the EANET

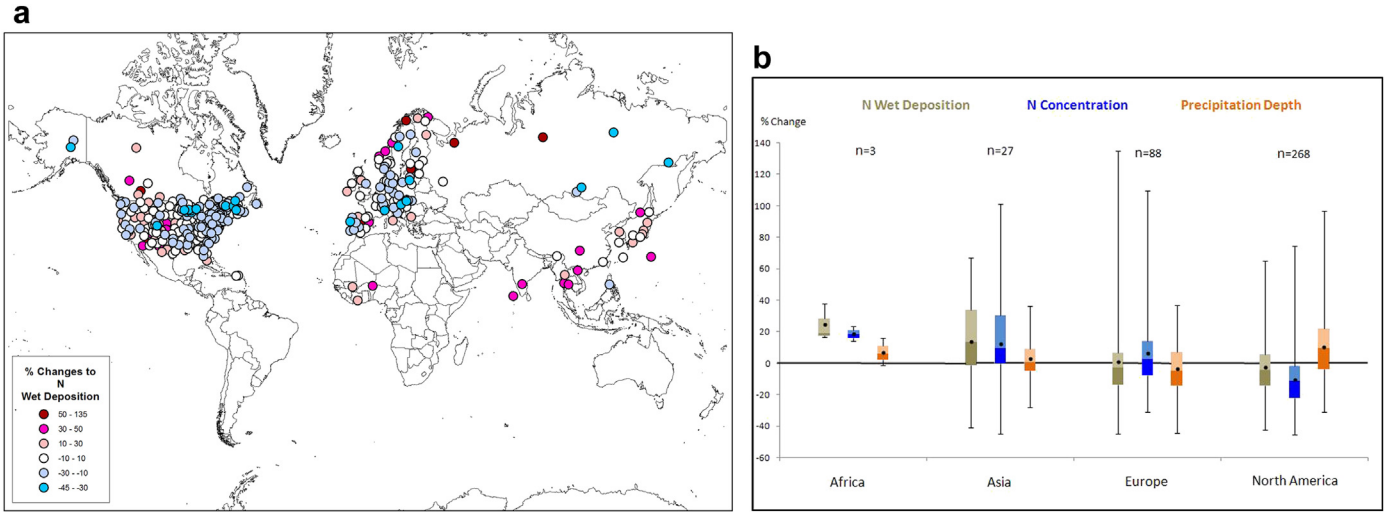

Fig. 4.4. (a) Global % change between 2000–2002 and 2005–2007 3-year mean wet deposition of N (calculated as 100 $[D_{2005-2007} - D_{2000-2002}]/[D_{2000-2002}]$) and (b) box-and-whisker plots (per Fig. 3.5b) of % changes in wet deposition (brown), concentration (blue) and precipitation (orange) at all sites in Africa, Asia, Europe and North America (n = number of sites).

site of Chongquing-Jinyunshan in eastern China, the latter reflecting the extremely high NH_3–N emissions in eastern China (Fig. 4.1b).

Major changes in the anthropogenic emissions of NO_x–N and NH_3–N from 2000 to 2007 have occurred and been documented in various parts of the world. For example, major NO_x–N emission reductions occurred in Europe, eastern Canada, and the eastern U.S. (Tørseth et al., 2012; IJC, 2010), and major NO_x–N and NH_3–N emission increases occurred in India and China (Garg et al., 2006; Gu et al., 2012). As context for the assessment of the observed changes in the 3-year average wet deposition values from 2000–2002 to 2005–2007, continental-scale NO_x–N + NH_3–N emission changes were calculated between the same 3-year periods from the EDGAR emission inventory (European Commission, 2011). The emission changes were as follows: Africa +56%; Asia +15%; Europe −2.7% and North America −4% (where the plus sign represents an increase from the early to late period). Consistent with the emission changes, the median wet deposition changes were: Africa +19.0%; Asia +13.6%; Europe −2.7% and North America −4.3% (calculated per Fig. 3.5 in the sulfur chapter). The spatial distribution of theses changes at the global sites is shown in Fig. 4.4a (and for $N_{oxidized}$ and $N_{reduced}$ in Figs. S13 and S14 of the Addendum). Fig. 4.4b presents the associated box-and-whisker plots of the % changes in wet deposition, concentrations and precipitation depths at the measurement sites on the four continents. From the figure, it can be seen that the increases in wet deposition in Africa and Asia were due predominantly to increases in N concentrations. In Europe and North America, the small changes in wet deposition at most sites were related to offsetting increases and decreases in the concentrations and precipitation depths.

The combined measured data and ensemble-mean model results provide a useful tool for understanding the global concentration and wet deposition patterns of N and to assess the comparability of the measured and modeled results. To that end,

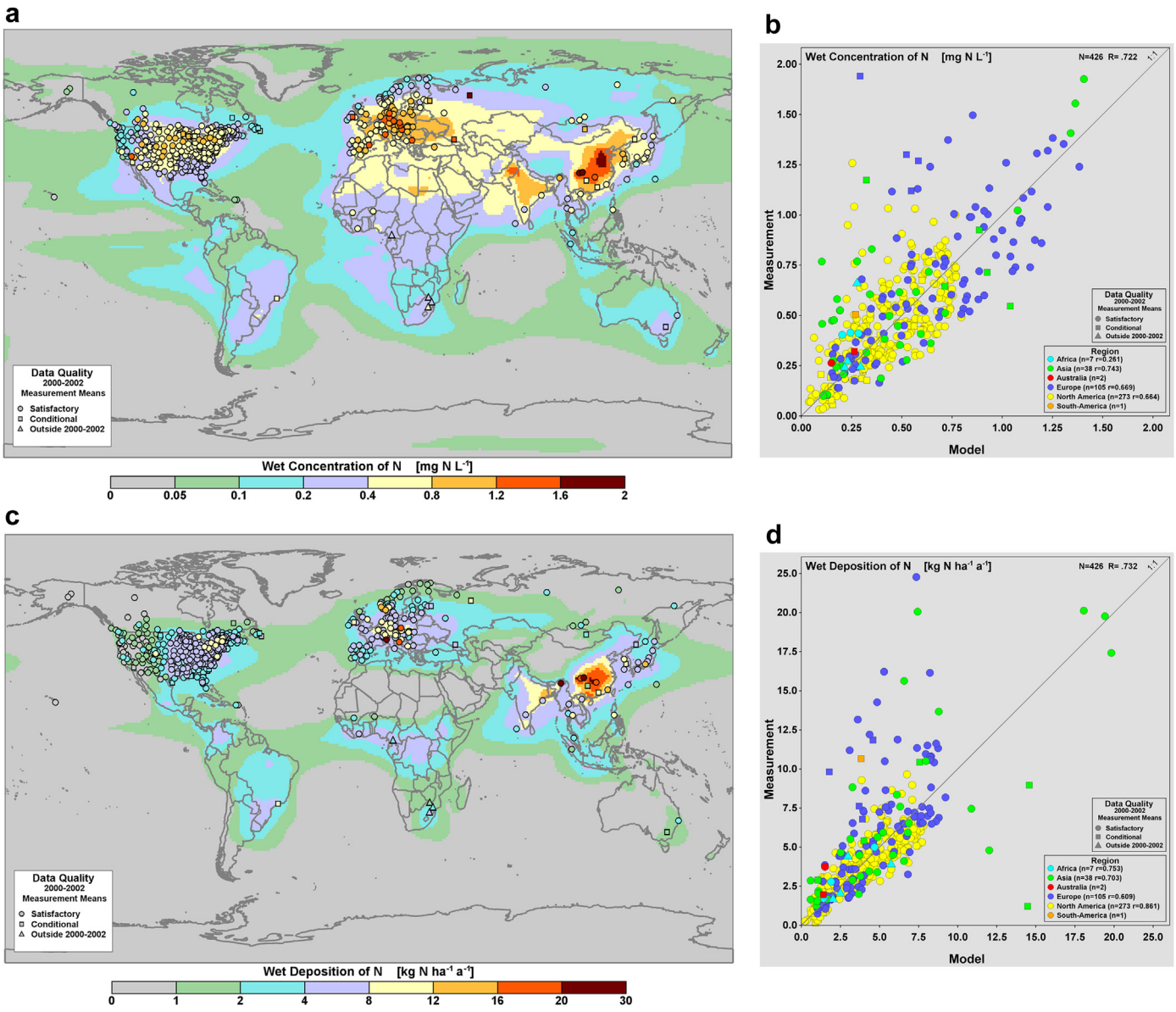

Fig. 4.5. (a) Measurement-model precipitation-weighted mean concentration with (b) associated concentration scattergram, and (c) measurement-model wet deposition of N in kg N ha^{-1} a^{-1} with (d) associated deposition scattergram. Measurement values represent the 3-year averages for 2000–2002; model results represent the 2001 model year. Note the non-linear scale in the last increment of the scattergram.

the 2000–2002 3-year average measured values are superimposed on the 2001 ensemble-mean modeled patterns of N precipitation-weighted mean concentrations and wet deposition in Fig. 4.5a and c, respectively, along with their associated scattergrams of measured versus ensemble-mean modeled (grid square) values (Fig. 4.5b,d). The model-based pattern of precipitation-weighted mean concentration (e.g., Fig. 4.5a) was produced by dividing the ensemble-mean annual wet deposition value at each $1^\circ \times 1^\circ$ grid square by its associated ensemble-mean annual precipitation depth. As expected, the concentration and wet deposition patterns in Fig. 4.5a and c strongly mimic the emissions patterns of NO_x–N and NH_3–N with allowances for transport, dispersion, chemical transformation, precipitation and deposition.

Globally, the measured and modeled precipitation-weighted mean concentrations compare reasonably well with an overall r value of 0.722 ($n = 426$ grid squares) and with even scatter on both sides of the one-to-one line except at high measured concentration values. The r values for the individual continents were: North America $r = 0.664$, $n = 273$; Europe $r = 0.669$, $n = 105$; Asia $r = 0.743$, $n = 38$; and Africa $r = 0.261$, $n = 7$. The average and standard deviation of the measurement-minus-model differences for the 426 points was 0.04 ± 0.22 mg N L^{-1} broken down as follows: North America $= 0.03 \pm 0.17$, Europe $= 0.05 \pm 0.29$, Asia $= 0.22 \pm 0.46$, Africa 0.13 ± 0.14 mg N L^{-1}. However, there is evidence of model underprediction at a number of sites in North America (Canada and the western U.S.), extreme southern and northern Europe, central Africa, Brazil, northern Oceania and parts of East Asia. In fact, the model results always underpredicted the measured values at sites where the measured concentrations exceeded 1.25 mg N L^{-1} (North America, Europe and Asia). In light of the good measurement-model comparability at all sites with deposition < 1.25 mg N L^{-1}, the modeled pattern appears to describe quite reasonably the concentrations in areas between measurement sites.

The pattern in Fig. 4.5a indicates that global minimum N concentrations < 0.05 mg N L^{-1} occur over large swaths of the South Pacific, South Indian, Southern and Arctic Oceans. Large regions of the major continents and several near-continent off-shore areas exhibit moderate concentrations in the range of 0.2–1.2 mg N L^{-1} while high concentrations, from 1.2 to 2.0 mg N L^{-1}, are predicted in the high emission areas of Europe, Pakistan, northern India and eastern China. The maximum measured global value was 1.93 mg N L^{-1} at the Chongqing-Jinyunshan EANET site in eastern China. The individual measurement-model maps of $N_{oxidized}$ and $N_{reduced}$ precipitation-weighted mean concentrations are not shown here but appear as Addendum Figs. S4–S7.

For N *wet deposition*, the measured and modeled pattern in Fig. 4.5c compare reasonably well, with $r = 0.732$ ($n = 426$) and uniform scatter about the one-to-one line except for serious underprediction at sites where the measured wet deposition > 8.0 kg N ha^{-1} a^{-1} (eastern North America, Brazil, Europe and Asia). Globally, the average and standard deviation of the measurement-minus-model differences for the 426 grid squares were 0.36 ± 2.28 kg N ha^{-1} a^{-1} broken down as follows: North America $= -0.06 \pm 1.09$ ($r = 0.861$, $n = 273$), Europe $= 1.36 \pm 3.17$ ($r = 0.609$, $n = 105$), Asia $= 0.47 \pm 4.14$ ($r = 0.703$, $n = 38$) and Africa 0.03 ± 1.06 ($r = 0.753$, $n = 7$) kg N ha^{-1} a^{-1}. These numbers indicate relatively high model underprediction in Europe and moderate underprediction in Asia. The underprediction in Europe is largely due to underpredictions of precipitation depth in the high deposition areas of the continent (see Sections 3.6.3 and 4.6.3). The cause of the underprediction in Asia is unknown but there is a body of literature suggesting that Asian emissions are underestimated (Wang et al., 2007; Q. Zhang et al., 2007; Lu et al., 2010; Wang et al., 2012).

The spatial pattern has a global range from <0.2 kg N ha^{-1} a^{-1} over the Arctic and Southern Oceans to just over 24 kg N ha^{-1} a^{-1} in northern Italy and eastern China. Again, assuming that the wet deposition pattern in Fig. 4.5c is reasonable in all areas with loadings <0.8 N kg ha^{-1} a^{-1}, one can use the modeled pattern to establish wet deposition levels in those areas of the globe with little to no measurement data. This being the case, low wet deposition levels range from 0.2 to 1 kg N ha^{-1} a^{-1} over the large sections of the oceans. Considerably higher levels of 1–4 kg N ha^{-1} a^{-1} occur over the mid-latitudinal areas of the northern oceans and equatorial regions of the Atlantic, Pacific and Indian Oceans. These relatively high levels are attributable to ship emissions and off-continent transport of continental emissions (see later discussion). As expected from the global emission patterns (Fig. 4.1a–c),

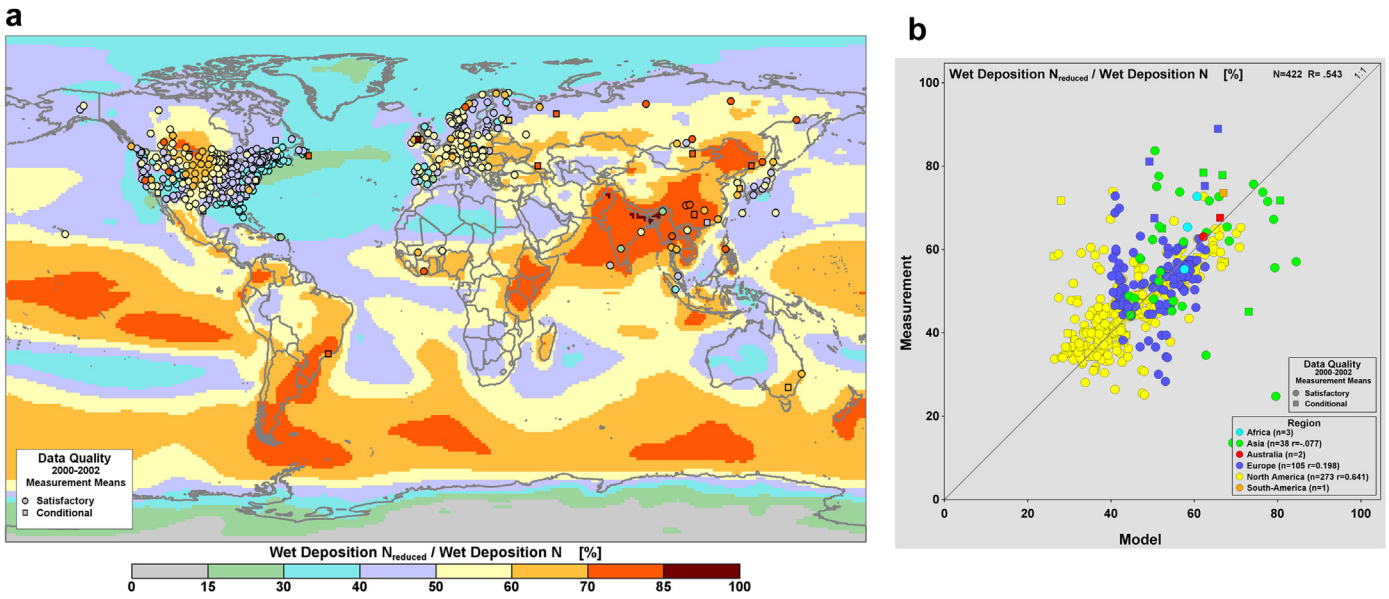

Fig. 4.6. (a) Measurement-modeled pattern and (b) scattergram of % ratio of $N_{reduced}$ to N wet deposition. Measurement values represent the 3-year average wet deposition for 2000–2002 and the model values represent the ensemble-mean wet deposition for 2001 (all units in kg N ha^{-1} a^{-1}).

the low-emission areas of the continents (specifically, northern and western North America, western and southern South America, northern and southern Africa, northern Scandinavia, northern and central Asia and most of Oceania) received low levels of wet deposition in the range of 0.2–2 kg N ha^{-1} a^{-1} while the densely populated and/or intensively cultivated areas of the continents received very high levels in the range of 2–24.55 kg N ha^{-1} a^{-1}.

The relative contribution of $N_{reduced}$ to N wet deposition is shown in Fig. 4.6a, which plots the measurement-based ratios of $N_{reduced}$ to N wet deposition superimposed on the model-based pattern. Fig. 4.6b shows the associated measurement versus modeled scattergram of the ratios, with $r = 0.543$ ($n = 422$) and the global average measurement-model difference and standard deviation of the ratios = 1.18 ± 10.62. Correlation coefficients were low for Asia ($r = -0.077$) and Europe ($r = 0.198$) but high for North America ($r = 0.641$) and Africa ($r = 0.931$). The measurement and model-based results suggest that large areas of the globe receive approximately equal portions of $N_{reduced}$ and $N_{oxidized}$ (i.e., ratio = 50% ± 10%). $N_{reduced}$ is the dominant contributor to N wet deposition (i.e., ratios > 60%) in: (1) the intensive agricultural areas that include central North America and Mexico and most of South America, India, and East Asia and (2) the low deposition areas of the southern Atlantic, southern Pacific and Southern Oceans that receive very low levels of wet deposition (i.e., <0.2 kg N ha^{-1} a^{-1}). In contrast, $N_{oxidized}$ is the dominant contributor (with $N_{reduced}$ < 40%) in the NO_x–dominated emission areas of the world including the far eastern and western regions of the U.S., the northern Atlantic Ocean and the areas of very low precipitation including the major deserts, Antarctica and the Arctic. Two areas of globe where the measurement-based ratios compare poorly to the model-based estimates are in the Russian Federation and India, with no apparent explanation (Fig. 4.6a). The measurement-based ratios for 2005–2007 are shown in Fig. S12 of the Addendum.

The patterns suggest that NO_x–N and NH_3–N emissions are transported off the continents where they are subsequently wet deposited on the off-coastal regions of the major oceans, most notably off the east coast of the U.S., the west coast of Europe, the west coast of central Africa, all coasts of India and northern Oceania and, off the east coast of southern Asia. Wet deposition of $N_{oxidized}$ and $N_{reduced}$ appears to be roughly equivalent over large areas of the globe but $N_{reduced}$ is dominant in two areas – the continental areas with intensive agricultural activity and the oceans with low N wet deposition (although this is highly uncertain given limited of knowledge of NH_3 emitted from oceans).

4.3. Global dry deposition of N

Routine measurement-based inferential estimates of dry deposition are made only in North America, Africa and Oceania. These estimates are based on the *inferential technique* described in Section 2. Unfortunately, the low number of measurement sites and the major differences in measured species and dry deposition velocity models make it impossible to map the dry deposition estimates on a global scale. As a result, this section on global dry deposition is based solely on the 2001 HTAP ensemble-mean modeling results (note however that the regional sections for North America, Africa and Oceania contain details of the measurement-based inferential dry deposition estimates). The HTAP 2001 ensemble-mean pattern of N dry deposition is shown in Fig. 4.7a, along with the % contribution of $N_{reduced}$ to N dry deposition in Fig. 4.7b.

The global pattern of N dry deposition in Fig. 4.7a bears a close resemblance to the global patterns of NO_x–N + NH_3–N emissions (Fig. 4.1c) with latitude for the effects of long range transport, dispersion, chemical and physical transformation and deposition. Highest dry deposition levels (10–20 kg N ha^{-1} a^{-1}) are predicted in the highest emission areas of the eastern U.S. (Pennsylvania and New York), western Europe (England, Belgium, Netherlands, and Germany), northern India, Bangladesh, and eastern China. The maximum modeled value worldwide was 19.1 kg N ha^{-1} a^{-1} in eastern China. Moderately high levels from 4 to 10 kg N ha^{-1} a^{-1} were predicted on all continents except Australia and Antarctica - corresponding roughly to the areas with emissions from 10 to 20 kg N ha^{-1} a^{-1}. Very low levels of dry deposition are predicted for the low emission and/or low precipitation areas of the continents, with values of 0.1–0.5 kg N ha^{-1} a^{-1} over the major deserts (Sahara, Taklimakan, Great Victoria). Dry N deposition to the oceans was generally quite low (<0.5 kg N ha^{-1} a^{-1}) except in the near-coastal regions. The Arctic and Southern Oceans, as well as the continent of Antarctica, had dry deposition levels of less than 0.1 kg N ha^{-1} a^{-1}.

The individual ensemble-mean modeled patterns of $N_{oxidized}$ and $N_{reduced}$ dry deposition are not shown here but are included as Addendum Figs. S15 and S16. Fig. 4.7b, shows the % ratio of $N_{reduced}$ to N dry deposition. The figure is quite similar in shape to the pattern of % $N_{reduced}$ to N in wet deposition (Fig. 4.6a). It can be seen here that $N_{reduced}$ dominates over $N_{oxidized}$ by >60% in the major agricultural areas of the world (i.e., central North America; northern, eastern and southern South America; east-central Africa; India; Pakistan; China; and parts of Oceania), as well as over the oceans of the Southern Hemisphere where N dry deposition is very low. In contrast, $N_{oxidized}$ dominates in the non-agricultural continental areas as well as over the oceans of the Northern Hemisphere.

The lack of inferential measurement-based estimates of $N_{oxidized}$ and $N_{reduced}$ dry deposition is a major problem worldwide. Routine measurements of oxidized and reduced species in air at regionally representative stations are needed on all continents. Ambient air measurements of NO_2 and NH_3 for the estimation of nitrogen dry deposition have been called for in acid rain programs for decades and are still badly needed. Existing filter-based measurement methods used at most regional sites suffer from volatilization/absorption artifacts and more accurate measurements are required. Inferential dry deposition models must be improved, tested and used routinely with the ambient air measurements and the models must include bidirectional surface exchange of NO_2 and NH_3.

4.4. Global total deposition of N

The 2001 ensemble mean modeled pattern of total deposition of N is shown in Fig. 4.8a. As with dry deposition, measurement-based data could not be superimposed. This is because measurement-based inferential dry deposition estimates were not available globally due to the scarcity of air concentration observations outside of Europe and North America and the lack of inferential dry deposition models outside of Africa and North America. The model-based pattern identifies three regions of the globe where total deposition is very high: western Europe (Belgium, Netherlands, Germany) with levels from 20.0 to 28.1 kg N ha^{-1} a^{-1}; South Asia (Pakistan, India and Bangladesh) from 20.0 to 30.6 kg N ha^{-1} a^{-1}; and East Asia from 20 to 38.6 kg N ha^{-1} a^{-1} in eastern China (the global maximum). Extensive areas of high deposition from 10 to 20 kg N ha^{-1} a^{-1} appear in the eastern U.S. and southeastern Canada as well as most of central Europe, large sections of Pakistan, India and Bangladesh, and large parts of East Asia including Myanmar, Thailand, Laos, Cambodia, eastern China, the Democratic People's Republic of Korea, the Republic of Korea, and Japan. Small areas of total deposition of N from 10 to 20 kg N ha^{-1} a^{-1} appear in Mexico, southern Brazil, and Nigeria. Very large areas of the continents (except Antarctica) have deposition from 2 to 10 kg N ha^{-1} a^{-1}; as do ocean areas off the coastlines of all the continents except Antarctica. Total deposition from 4 to

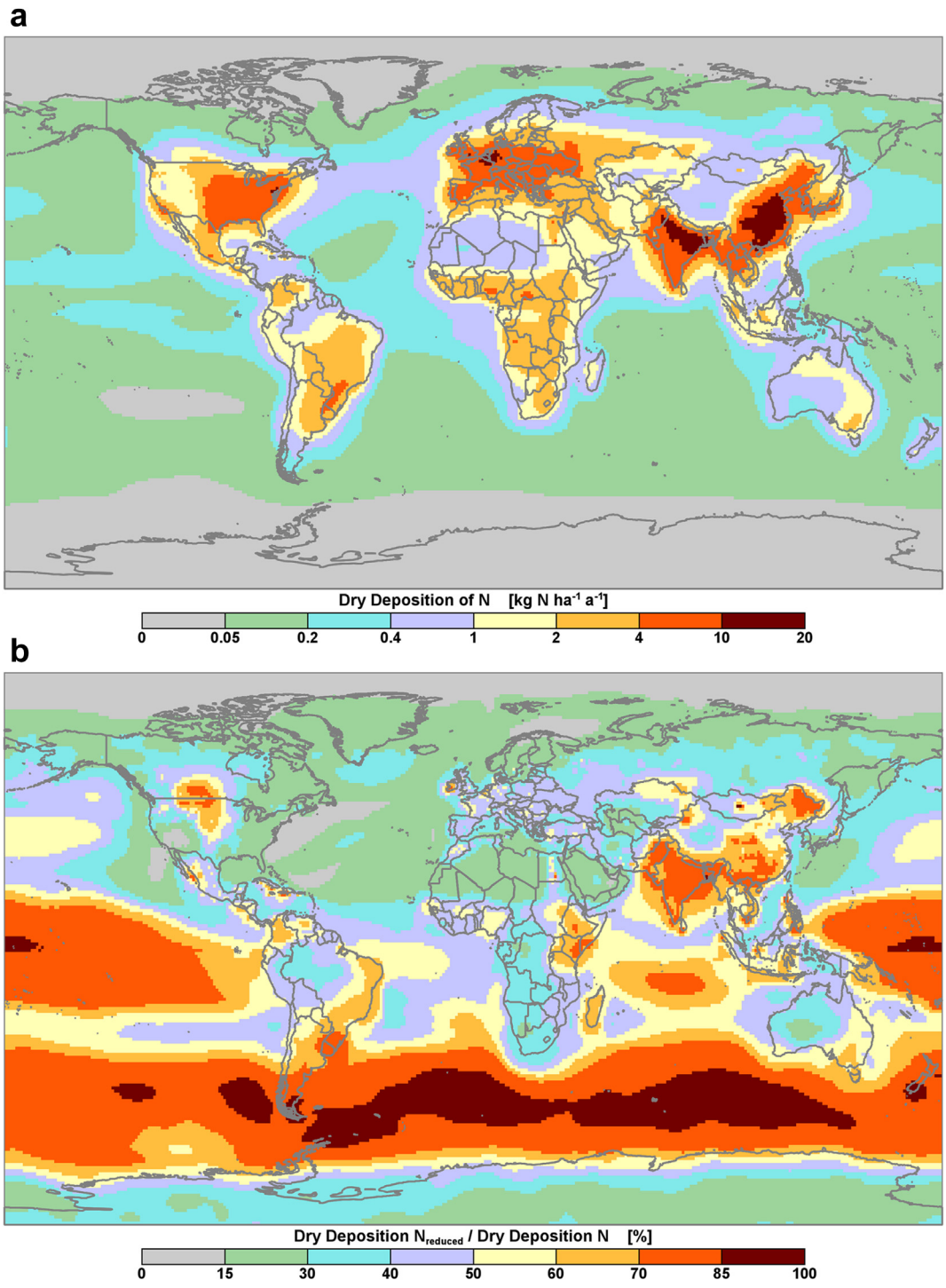

Fig. 4.7. 2001 ensemble-mean patterns of: (a) dry deposition of N in kg N ha^{-1} a^{-1} and (b) % ratio of $N_{reduced}$ to N in dry deposition.

10 kg N ha^{-1} a^{-1} appears over several ocean areas including: (1) the northern Atlantic Ocean off the east coast of North America and the west coast of Europe, (2) the Northern Indian Ocean and (3) the northern Pacific Ocean off the east coast of Asia. Based on the NO_x–N + NH_3–N emissions map (Fig. 4.1c), these high levels are likely the result of ship emissions as well as transport of continental emissions off the coastlines. In contrast to the foregoing near-coastal areas, most of the open oceans and the remote continental areas received low levels from 0.2 to 2.0 kg N ha^{-1} a^{-1}, while the Arctic Ocean, Southern Ocean and Antarctica received global background levels of <0.2 kg N ha^{-1} a^{-1}.

As was the case with S, scientists interested in the ecological effects of N need quantitative estimates of total deposition of N. Unfortunately, they typically have access only to wet deposition measurements; thus, knowing the ratio of dry deposition to total deposition allows scientists to estimate the fluxes of total deposition from the wet-only deposition values. Fig. 4.8b shows the estimated % contribution of dry deposition to total deposition of N.

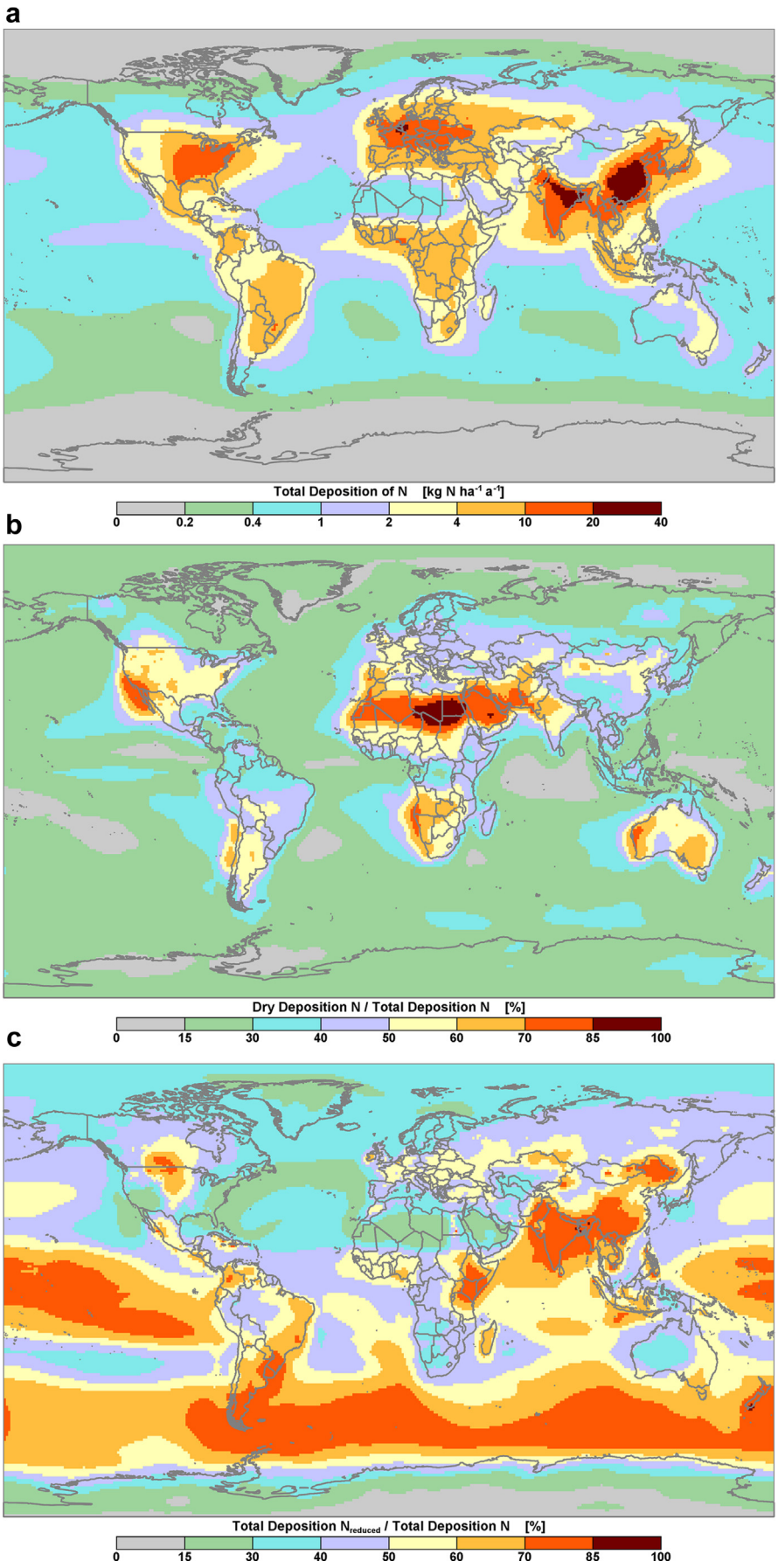

Fig. 4.8. 2001 ensemble-mean patterns of (a) total deposition of N in kg N ha^{-1} a^{-1}, (b) % ratio of dry/total deposition of N and (c) % ratio of total deposition of $N_{reduced}$/total deposition of N.

Not surprisingly, the highest (>70%) dry deposition is predicted in the driest areas of the world including southwest North America, southwest South America, and southwest and northern Africa, all of which are characterized by annual precipitation depths of <40 cm a^{-1}. With the exception of the foregoing areas, very large sections of all of the continents were predicted to receive roughly equal contributions of dry and wet deposition (i.e., 50% ± 10%). Such areas typically had NO_x–N + NH_3–N emissions greater than 2 kg N ha^{-1} a^{-1} and precipitation depths greater than 40 cm a^{-1}. Most of the oceans and the remote low-emission areas of the continents were dominated by wet deposition.

Fig. 4.8c shows the global pattern of % ratio of $N_{reduced}$ to N in total deposition. This pattern bears a striking resemblance to the % ratio pattern in wet deposition (Fig. 4.6a) such that $N_{reduced}$ total deposition is roughly equivalent to $N_{oxidized}$ total deposition (i.e., 50% ± 10%) over large areas of all continents except Antarctica. This is consistent with the 2001 global emission inventory in which NH_3–N emissions represent 56% of the global total of NO_x–N + NH_3–N emissions in 2001. $N_{reduced}$ dominates over $N_{oxidized}$ (i.e., >60% of N) throughout the major agricultural areas of the world, particularly in the Prairies/Great Plains of central North America, large areas of northern, eastern and southern South America, east-central Africa, almost all of India, a large portion of East Asia, and many of the island states of Oceania. As expected, $N_{oxidized}$ total deposition dominates over $N_{reduced}$ total deposition (i.e., $N_{reduced}$ <40%) in the high NO_x–N emission areas of the continents. Over the oceans, large regions of the southern Atlantic, southern Pacific and Southern Oceans that receive low levels of N total deposition (<2 kg N ha^{-1} a^{-1}) are dominated by $N_{reduced}$. The Indian Ocean is also dominated by $N_{reduced}$ but here the total deposition levels are considerably higher, ranging from 2 to 10 kg N ha^{-1} a^{-1}. In contrast, the Antarctic and Arctic regions are predicted to be dominated by $N_{oxidized}$ in spite of the fact that they receive the lowest levels of total deposition on the globe (<0.4 kg N ha^{-1} a^{-1}). Individual maps of $N_{oxidized}$ and $N_{reduced}$ total deposition are not included here but can be found as Addendum Figs. S17 and S18.

4.5. Area-integrated emissions and deposition of N

Ensemble-mean area-integrated estimates of total deposition of $N_{oxidized}$, $N_{reduced}$ and N are given for the non-coastal continents, the non-coastal oceans and the continental and oceanic coastal zones in Table 3. The area-integrated values were calculated as the sum of the ensemble-mean grid square deposition values within the continents, oceans and coastal zones based on the outputs of the 16 HTAP $N_{oxidized}$ and 7 HTAP $N_{reduced}$ models.

The area-integrated ensemble-mean emission and deposition of N in Table 3 provide insight into the global atmospheric N budget for 2001, most notably:

- Global total deposition of N was estimated at 106.3 Tg N, comparable to the global emissions of NO_x–N + NH_3–N at 105.1 Tg N. The difference of 1.2 Tg N (or 1% of the global emission total) is within the uncertainty of the emissions and deposition estimates.
- Although the continental non-coastal areas of the globe constitute only 26.3% of the global surface area, in 2001 they were responsible for 70.6% of the global N emissions and received 55.6% of global total deposition of N. The coastal zones constituted only 14.1% of the global area but emitted 19.2% of global N emissions and received the same percentage, 19.2%, of total deposition. Finally, the non-coastal areas of the oceans constituted 59.5% of the global surface area but emitted only 10.2% of the global emissions and received 25.2% of the global total deposition of N.
- On the non-coastal portions of the continents, total deposition of $N_{reduced}$ was approximately one third higher than $N_{oxidized}$ (34.0 versus 25.1 Tg N a^{-1}, respectively) due mainly to Asia where the deposition of $N_{reduced}$ was double that of $N_{oxidized}$ – a reflection of the relative emissions of NH_3–N and NO_x–N. In comparison, total deposition of $N_{reduced}$ and $N_{oxidized}$ over the coastal zones was roughly equivalent (10.5 versus 10.0 Tg N, respectively), and to the non-coastal oceans (14.1 versus 12.7 Tg N, respectively).
- Total deposition of N to the non-coastal continental areas was highest in Asia (22.2% of global N deposition), Africa (10.0%) and North America (8.0%) and lowest in Oceania (1.6%) and Antarctica (0.0%) – a ranking consistent with the continental rankings of N emissions. The coastal zones of the continents were ranked slightly differently with Asia, Europe and North America accounting for 7.1%, 3.3%, and 3.0% of the global total deposition, respectively. For the non-coastal oceanic areas, total deposition of N was highest over the North Pacific (7.7%), the North Atlantic (5.2%) and the South Pacific (3.7%) and lowest over to the Southern (0.2%) and Arctic (0.2%) Oceans. Total deposition of N to the non-coastal continental areas plus coastal zones was highest in Asia, which received 29.3% of the global total or approximately 2.5 times as much as the next highest continent, Africa, at 11.9%.
- Transport of N emissions from the continental non-coastal and coastal zones to the oceans is an important source of oceanic N input. The pattern of total deposition in Fig. 4.8a, for example, shows large areas of high N total deposition extending off the east coasts of North America, India and East Asia onto the adjacent oceans. Quantitative estimates of the transported and deposited amounts to the oceans were made in a manner similar to Galloway et al. (2004), by calculating the net export of N from the continental non-coastal and coastal areas to the non-coastal oceans (and vice versa for the import to the oceans) as the difference between the area-integrated emissions and deposition based on Table 3. The calculations suggest that, on a global scale, the N export from the non-coastal continental areas and coastal zones to the non-coastal oceans was 14.9 Tg N, while the import into the non-coastal oceans was 16.3 Tg N. The 1.2 Tg N difference is well within the uncertainty of these fluxes.

Overall, the 2001 HTAP ensemble-mean model results indicate that the gridded total deposition of N was highest in East Asia, South Asia, Europe and eastern North America and lowest over the Southern and Arctic Oceans. They also suggest that just over half (i.e., between 56 and 61%) of N total deposition on the non-coastal oceanic areas was due to continental and coastal zone emissions.

4.6. Regional aspects of N deposition

4.6.1. North America

4.6.1.1. Precipitation-weighted mean concentrations and wet deposition of N. The measurement-based 3-year mean annual precipitation-weighted mean concentration patterns of N for 2000–2002 and 2005–2007 are shown in Fig. 4.9a,b, respectively, and for wet deposition in Fig. 4.9c,d. The patterns differ from the global patterns shown earlier in that they include interpolated contours where measurement sites were sufficiently dense to support interpolation and colored dots in areas where they were not.

The highest precipitation-weighted mean concentrations of N (0.6–1.0 mg N L^{-1}) occurred in four locations: a hot spot in the western U.S., the Prairie region of western Canada, the Great Plains area of the central U.S., and the lower Great Lakes area of eastern

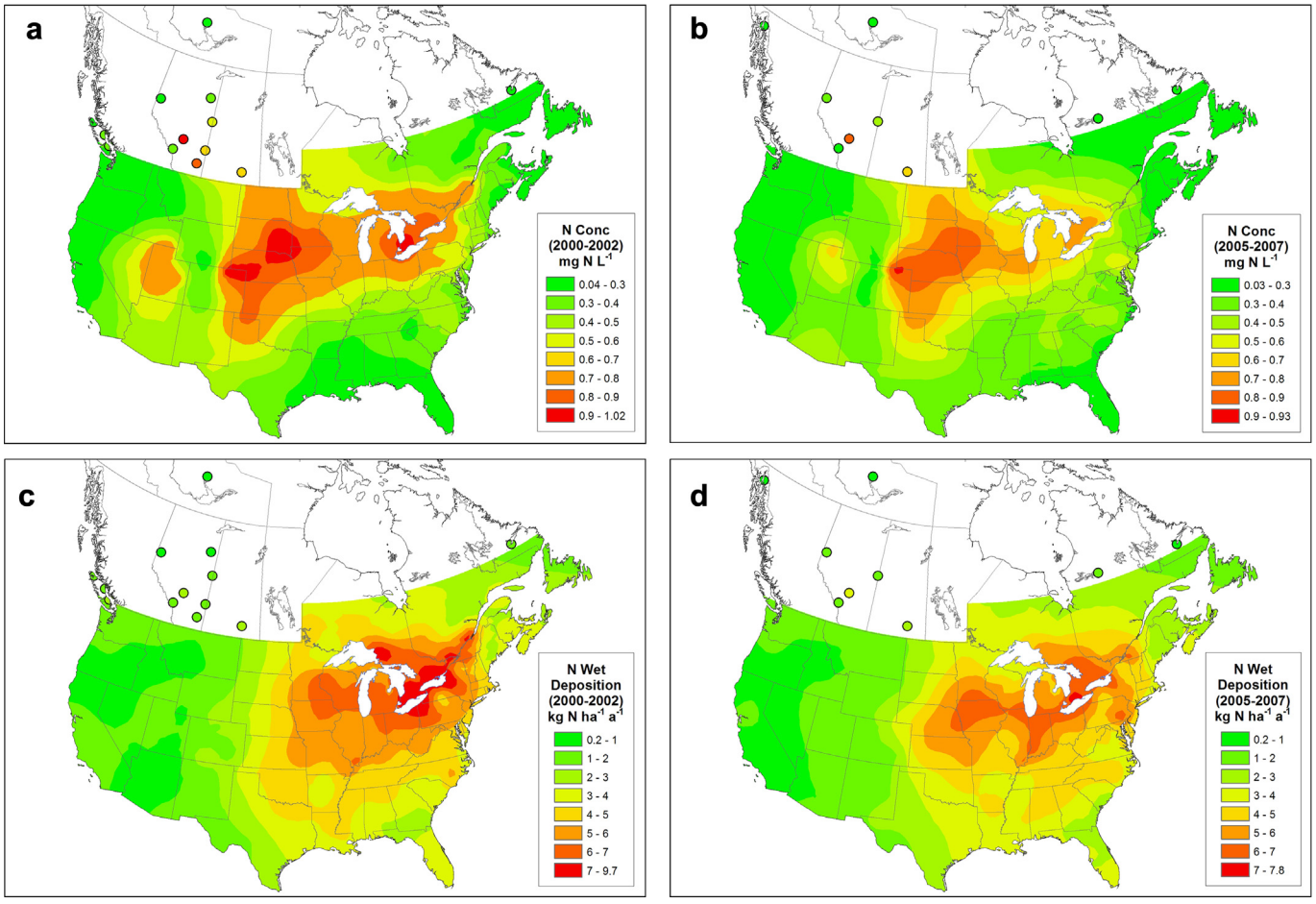

Fig. 4.9. 3-year average annual precipitation-weighted mean concentrations (in mg N L^{-1}) of N for (a) 2000–2002 and (b) 2005–2007 and wet deposition of N (in kg N ha^{-1} a^{-1}) for (c) 2000–2002 and (d) 2005–2007.

Canada/U.S. (Fig. 4.9a,b). These areas are characterized by high emissions of both NO_x–N and NH_3–N. High agricultural emissions of NH_3–N occur in the Prairie and Great Plains regions, and high emissions of both species in the Great Lakes region (Fig. 4.1a,b). Western U.S. is characterized by several large point sources of NO_x–N emissions as well as some regions of intensive agriculture resulting in high NH_3–N emissions. Low precipitation-weighted mean concentrations (<0.4 mg N L^{-1}) occurred in the western, southeastern and northeastern U.S. and in northern and eastern Canada (Fig. 4.9a,b).

For wet deposition (Fig. 4.9c,d), the large scale patterns differ from the patterns of precipitation-weighted mean concentration reflecting the fact that wet deposition depends on both concentration and precipitation depth. In the western half of the continent where precipitation depths are considerably lower than in the eastern half (typically 25–70 cm a^{-1} versus 70–160 cm a^{-1}, respectively), 3-year average annual wet deposition of N is low, ranging from 0.2 to 4 kg N ha^{-1} a^{-1}, even in areas such as Utah where the annual concentrations in precipitation are high. The lowest values of N wet deposition on the continent occurred in the U.S., with a 3-year average in 2000–2002 of 0.14 kg N ha^{-1} a^{-1} at the desert site of Joshua Tree National Park (southern California) and a 2005–2007 value of 0.17 kg N ha^{-1} a^{-1} at Denali National Park (Alaska). Wet deposition in the eastern half of the country is considerably higher, ranging from 3.0 to 9.7 kg N ha^{-1} a^{-1} in 2000–2002 and 3.0–7.8 kg N ha^{-1} a^{-1} in 2005–2007 over a very large area. In both periods, the highest wet deposition levels occurred in the areas to the west of and around the Great Lakes in both eastern Canada and the eastern U.S.

Fig. 4.10a–d show the individual wet deposition patterns of $N_{oxidized}$ and $N_{reduced}$ for the 2000–2002 and 2005–2007 periods. The $N_{oxidized}$ wet deposition patterns differ markedly from the $N_{reduced}$ patterns in a manner consistent with the NO_x–N and NH_3–N emissions patterns shown on Fig. 4.1a,b. Specifically, as was the case with N wet deposition, both $N_{oxidized}$ and $N_{reduced}$ wet deposition levels were higher in the eastern half of North America than in the western half, and the areas of maximum $N_{oxidized}$ wet deposition (i.e., >3.0 kg N ha^{-1} a^{-1}) were east of the areas of maximum $N_{reduced}$ wet deposition (also > 3.0 kg N ha^{-1} a^{-1}). Again, this is a direct reflection of the emission patterns of NO_x–N and NH_3–N.

The modeled and measured patterns of N wet deposition are shown in Fig. 4.11a and the scatterplot of model-versus-measured values is shown in Fig. 4.11b. The comparability of the measured and modeled results is quite reasonable with $r = 0.857$ ($n = 270$). However, the modeling results generally underestimate the measured deposition values of >6 kg N ha^{-1} a^{-1} in eastern Canada around Lakes Superior, Erie, and Ontario in the eastern U.S. and overestimate the measured values in the range of 4.0–6.0 kg N ha^{-1} a^{-1} in the agricultural area of the central U.S. (i.e., the states of Nebraska, Kansas, Illinois, Michigan, Indiana and Kentucky) as well as at a few individual sites across the continent. In most of western and northern Canada and the western U.S., the modeled pattern shows the same large area of low N wet

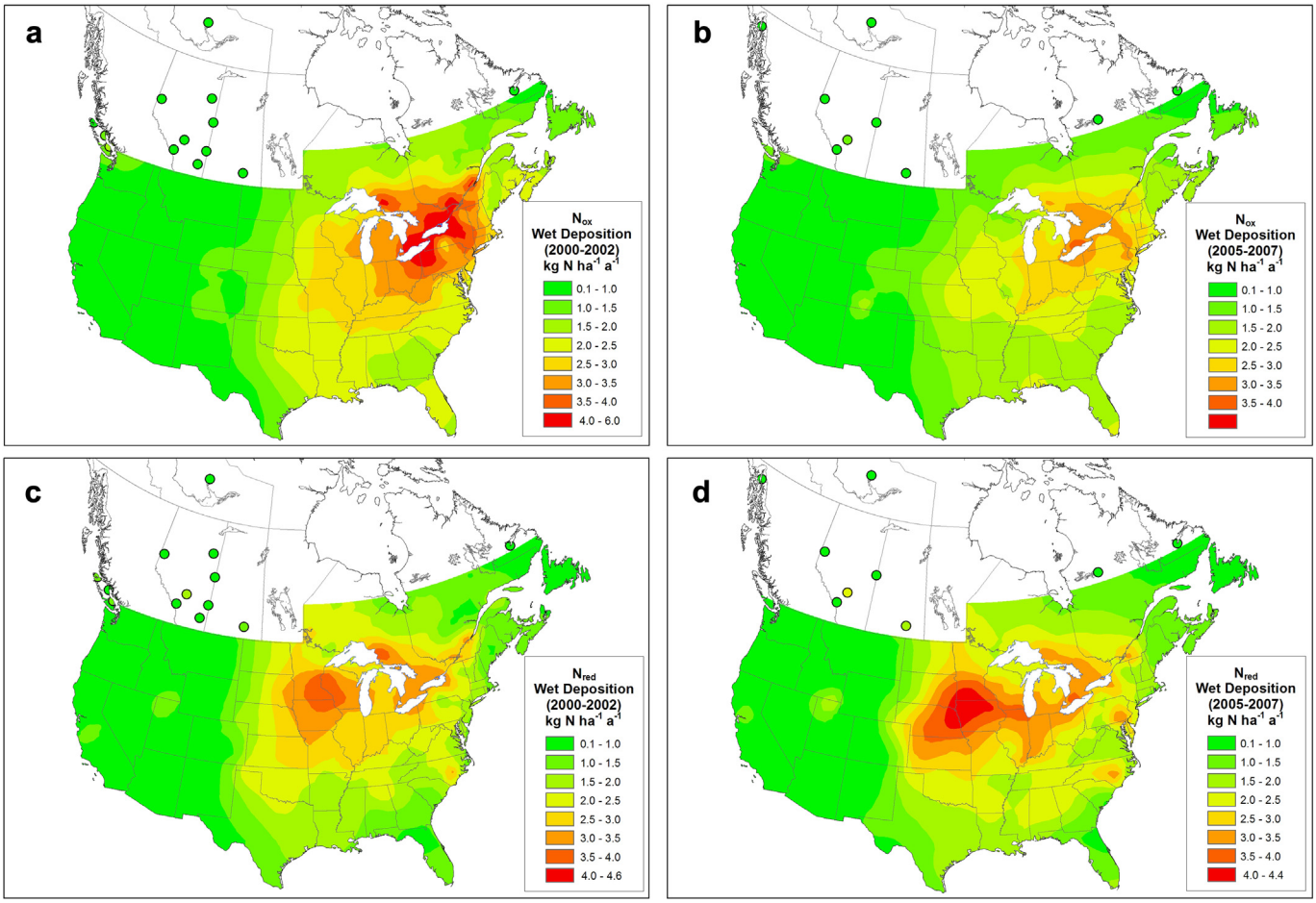

Fig. 4.10. 3-year average annual wet deposition of $N_{oxidized}$ for (a) 2000–2002 and (b) 2005–2007 and of $N_{reduced}$ for (c) 2000–2002 and (d) 2005–2007 in kg N ha^{-1} a^{-1}.

deposition as the measurements, with levels < 2.0 kg N ha^{-1} a^{-1}. The comparability between the model and measurement results provides reasonable assurance that the model-based pattern can be used to interpolate between measurement sites and to extrapolate to areas where no measurements exist.

Based on the modeling results, the continental background level of N wet deposition is less than 0.5 kg N ha^{-1} a^{-1} and occurs in the western U.S., northern Canada and northwestern Mexico. In Mexico where no measurement data were available, moderate wet deposition levels (2.0–4.0 kg N ha^{-1} a^{-1}) were estimated by the HTAP models although very high values (4.0–6.0 kg N ha^{-1} a^{-1}) were predicted near Mexico City. Wet deposition levels over vast (unmeasured) sections of western and northern Canada range from <0.5 kg N ha^{-1} a^{-1}–6.0 kg N ha^{-1} a^{-1}. Large areas of Canada located to the north and east of the Great Lakes received relatively high levels of wet deposition in spite of having low emissions of NO_x–N + NH_3–N, a fact consistent with many transport studies that indicate emissions are transported over long distances before being wet deposited (Vet et al., 2005; Vet and Ro, 2008). The coastal regions of the Gulf of Mexico and the Atlantic Ocean are predicted to have relatively high levels of wet deposition (1.5–6.0 kg N ha^{-1} a^{-1}) due to ocean-based ship emissions and off-continent transport of continental N emissions.

Fig. 4.12a shows the model and measurement patterns of the % ratio of $N_{reduced}$ to N in wet deposition and Fig. 4.12b shows the associated measurement-versus-model scattergram (r = 0.641, n = 270). $N_{reduced}$ appears as the major contributor to N wet deposition (i.e., ratios > 50%) in and near the agriculturally-dominated areas of central U.S., central Canada and Mexico. Alternatively, $N_{oxidized}$ is the major contributor (i.e., $N_{reduced}$ < 50%) along the western and eastern regions of the U.S. and Canada, northwest Mexico and off the Atlantic coast of Canada and U.S.. The measurement-based ratios for the 2005–2007 period (not included) show a marked increase in the % contribution of $N_{reduced}$ to N in wet deposition relative to 2000–2002, which is consistent with documented decreases in Canadian and U.S. NO_x emissions and increases in NH_3 emissions (IJC, 2010).

4.6.1.2. Dry deposition of N. Dry deposition estimates of $N_{oxidized}$, $N_{reduced}$ and N are available weekly in North America from the U.S. CASTNET network and daily from the Canadian CAPMoN network, in both cases based on the inferential technique described in Section 2. The gaseous (HNO_3) and particle (p-NO_3^-, p-NH_4^+) concentration measurements in the two countries/networks are comparable, but their associated dry deposition velocities and flux values are different (Schwede et al., 2011), with Canadian velocities and fluxes being systematically higher than the U.S. values (Schwede et al., 2011). In the absence of known *true* dry deposition estimates at the measurement sites, it is not possible to say which of the two countries' estimates is the more accurate, so we have included the dry deposition values of both countries as estimated by their specific inferential calculation techniques.

It is important to note that the CASTNET and CAPMoN inferential dry deposition estimates are very likely underestimated and highly uncertain (Zhang et al., 2009): the former because ambient concentrations of NO_2 and NH_3 are not measured by the networks and

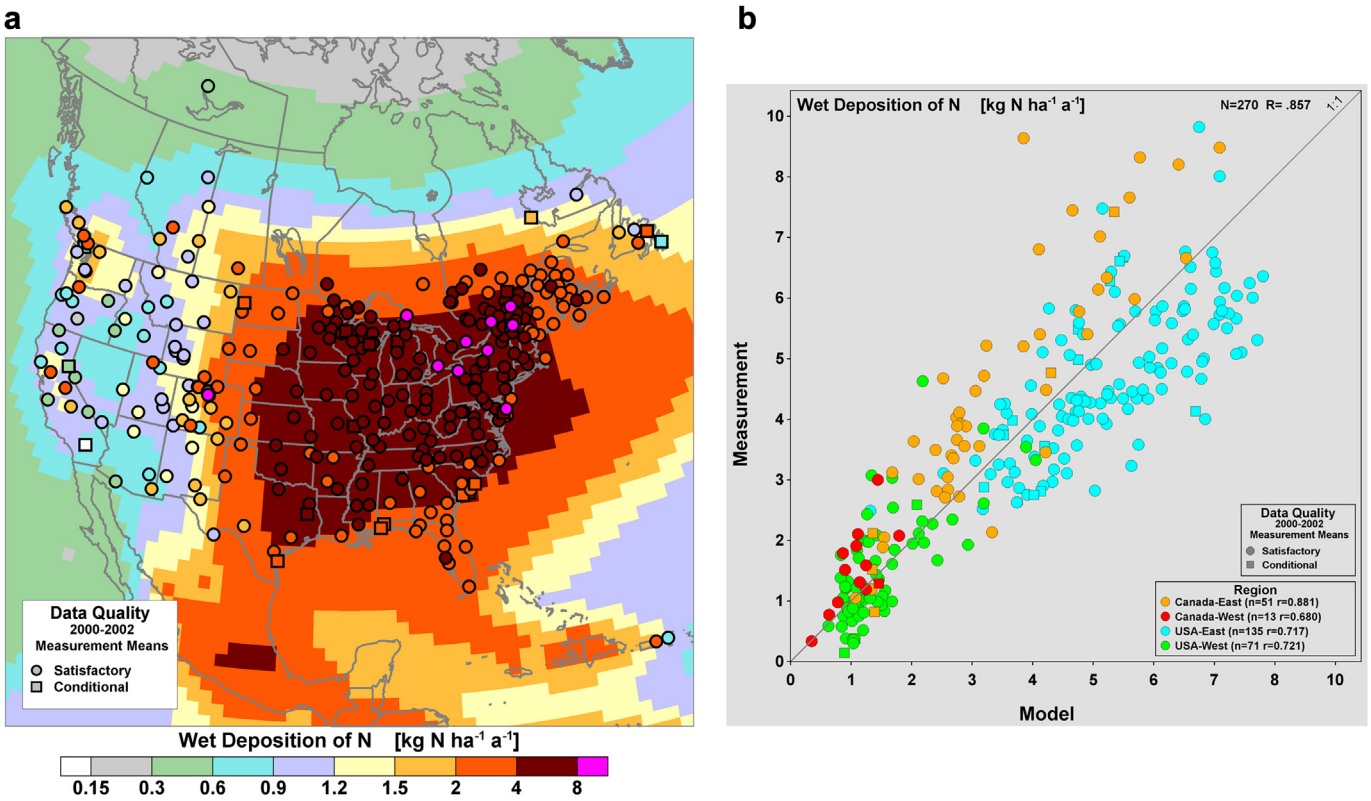

Fig. 4.11. (a) 2001 ensemble-mean model pattern of wet deposition of N, combined with measured 3-year average annual wet deposition values for the period 2000–2002 (in kg N ha^{-1} a^{-1}) and (b) scattergram of measured versus modeled (grid square average) values.

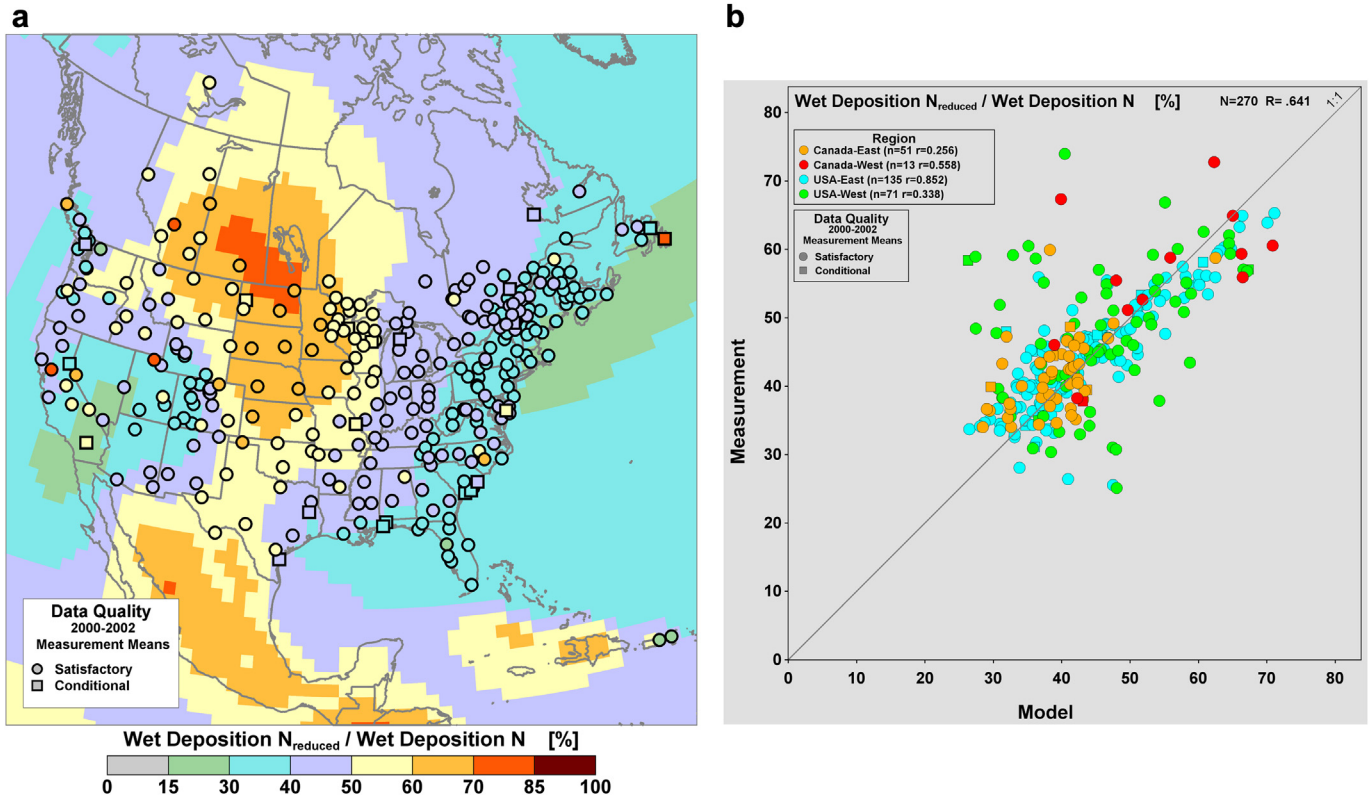

Fig. 4.12. (a) 2001 ensemble-mean model pattern of wet deposition of the ratio of $N_{reduced}$ to N combined with measured 3-year average annual wet deposition ratios for the period 2000–2002 (in %) and (b) associated scattergram of measured (site) and modeled (grid cell average) values.

are therefore not included in the estimates of N dry deposition; the latter because NH_4NO_3 is known to volatilize from particle collection filters causing uncertainty in the gas-particle partitioning of HNO_3, NO_3^- and NH_4^+ (Sickles et al., 1999). In spite of these limitations, the CASTNET and CAPMoN dry deposition estimates are presented here since they represent the state-of-the-art science for continental-scale, routine, measurement-based inferential estimates of dry deposition.

Fig. 4.13a–c show the 2000–2002 measurement-based inferential 3-year annual mean dry deposition estimates

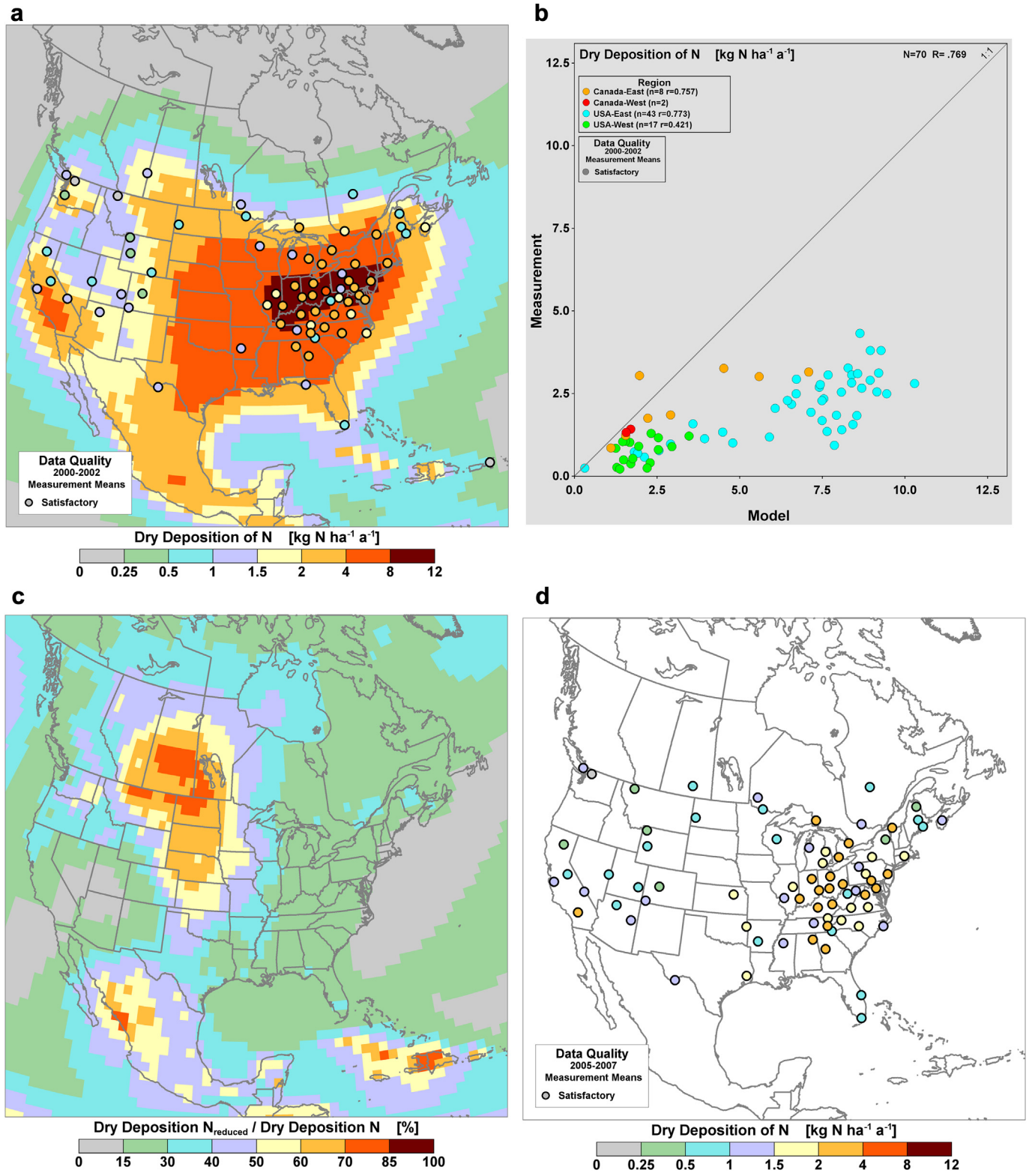

Fig. 4.13. (a) 2001 ensemble-mean modeled pattern of dry deposition and measurement-based inferential estimates of 2000–2002 3-year average annual dry deposition (not including the dry deposition of NO_2 and NH_3) for N in kg N ha^{-1} a^{-1} and (b) associated scattergram of measured versus modeled (i.e., grid square average) values of N; (c) 2001 ensemble-mean modeled % ratio of $N_{reduced}$ to N dry deposition; (d) 2005–2007 measurement-based inferential 3-year average annual estimates.

superimposed on the 2001 HTAP modeled dry deposition pattern of N, the associated scatterplot and the % ratio of $N_{reduced}$ to N dry deposition. Fig. 4.13d shows the measurement-based inferential 3-year annual mean fluxes for 2005–2007. The measurement-versus-model comparability clearly shows the aforementioned overestimation of the HTAP modeled fluxes, although the correlation is relatively high at $r = 0.769$ ($n = 70$). The mean of the HTAP modeled dry deposition values exceeds the measurement-based inferential dry deposition mean by 4.11 ± 2.20 kg N ha^{-1} a^{-1} (212% higher than the measurement mean) in eastern North America and 1.14 ± 0.63 kg N ha^{-1} a^{-1} (222% higher than the measurement mean) in western North America. Individual comparisons for $N_{oxidized}$ and $N_{reduced}$ dry deposition (not shown) indicate that the HTAP model-based estimates for both variables are higher than the measurement-based inferential dry deposition values. The causes of the discrepancy are thought to be due in part to the lack of routine $NO_x$and NH_3 measurements used to generate the measurement-based inferential fluxes.

The measurement-based inferential and model-based dry deposition estimatesof N are lower in western North America than in eastern North America in both periods, with the exception of southern California. Dry deposition of N at most sites in the western U.S. is <2 kg N ha^{-1} a^{-1} compared to < 5 kg N ha^{-1} a^{-1} in the eastern U.S.. In both periods, the maximum dry deposition on the continent (both model- and measurement-based) occurred in the high NO_x emission area of the U.S. northeast where the model-based dry deposition ranged from 7.0 to 11.0 kg N ha^{-1} a^{-1}. In Canada, the highest dry deposition values ranged from 3 to 7 kg N ha^{-1} a^{-1} in the urban and agricultural areas of southern Ontario and southern Quebec, immediately adjacent to the maximum area in the U.S. northeast. Secondary hot spots of dry deposition are modeled in southern California (3–7 kg N ha^{-1} a^{-1}) and central Mexico (3–5 kg N ha^{-1} a^{-1}). The lowest modeled dry deposition estimates on the continent were <0.5 kg N ha^{-1} a^{-1} in northern Canada where NO_x and NH_3 emissions are low. Fig. 4.13c shows that $N_{reduced}$ dry deposition dominates $N_{oxidized}$ dry deposition in the predominantly agricultural areas of west-central Canada, central U.S., western Mexico and the southern Caribbean.

4.6.1.3. Total deposition of N. The measurement-based 3-year average annual estimates of N total deposition for 2000–2002 (not including NO_2 and NH_3 dry deposition) are superimposed on the 2001 HTAP ensemble mean model pattern (including NO_2 and NH_3 dry deposition) and shown in Fig. 4.14a. A scatterplot of the measured and modeled deposition is shown in Fig. 4.14b and the 2005–2007 measurement-based results are shown in Fig. 4.14c. Modeled values of total deposition range from 0.10 to 17.67 kg N ha^{-1} a^{-1} and the modeled area of highest deposition (ranging from 15.0 to 17.67 kg N ha^{-1} a^{-1}) occurs in the densely populated, highly industrialized and intense agricultural areas of the northeastern U.S. south of the Great Lakes. The lowest deposition occurs in the western U.S. and western/northern Canada. Most of the western portion of the continent except for southern California, an area of Nevada, Oregon, Idaho, and all of northern Canada, exhibit moderate levels of total deposition from 2.0 to 4.0 kg N ha^{-1} a^{-1} while the central and eastern portions have very high levels ranging from 4.0 to 17.67 kg N ha^{-1} a^{-1}. In Mexico, deposition is in the 2.0–10.0 kg N ha^{-1} a^{-1} range except on the Baja Peninsula where it drops below 2.0 kg N ha^{-1} a^{-1}. The Mexican area of highest deposition corresponds to the intensely populated agricultural area around Mexico City.

The measurement-based 3-year-average annual estimates of N total deposition for 2000–2002 and 2005–2007 (with their built-in underestimation) are typically lower in western North America with means of 2.3 and 2.1 kg N ha^{-1} a^{-1} (and ranges of 0.4–3.9 and 0.3–3.7 kg N ha^{-1} a^{-1}), respectively, than in eastern North America with means of 7.3 and 6.5 kg N ha^{-1} a^{-1} (and ranges of 1.2–12.4 and 2.7–10.3 kg N ha^{-1} a^{-1}), respectively. The area of highest total deposition in both periods occurred in the major NO_x and NH_3 emission areas of the U.S. Midwest, Ohio River Valley and Boston-New York corridor, and in southern Ontario and southern Quebec of Canada. The area of lowest measurement-based total deposition was in the western half of the continent where the lowest site values ranged from 1.1 to 1.7 kg N ha^{-1} a^{-1}. In the eastern half of the continent, the lowest values occurred in northern Quebec (Canada) and Maine and Florida (U.S.) where the range was from 3.1 to 4.9 kg N ha^{-1} a^{-1} in 2000–2002 and 2.6–4.2 kg N ha^{-1} a^{-1} in 2005–2007.

As seen in Fig. 4.14b, the measured and modeled total deposition estimates correlate well ($r = 0.793$, $n = 59$) but, due to the lack of NO_2 and NH_3 measurements, the measurement-based total deposition values are in general lower than the modeled values. This is predominantly so in the U.S., where the measurement-based estimates represent about 56% of the modeled values (where 0.56 = slope of the regression line through zero; $r = 0.7457$; $n = 55$). In Canada, the measurement-based values compare better to the modeled values with a zero-forced regression slope of 1.03 ($r = 0.9563$; $n = 10$). The better agreement in Canada is thought to be due to three reasons: (1) NO_2 and NH_3 dry deposition are generally lower in Canada than the U.S., (2) the Canadian inferential dry deposition velocity and flux model produces higher estimates of HNO_3 than the U.S. model (Schwede et al., 2011), and (3) dry deposition is a smaller contributor at most of the Canadian sites than at many of the U.S. sites. With regard to #2, the ambient concentrations of HNO_3 compared reasonably well between the two networks (median % difference = 18.5%; Canada higher) but the Canadian dry deposition velocities and fluxes were considerably higher (median % differences = 34.7% and 46.6%, respectively). The higher estimates by the Canadian model were attributed to lower aerodynamic resistances of HNO_3 (Schwede et al., 2011).

The HTAP ensemble-mean modeling results provide useful information about the relative contribution of dry deposition to total deposition of N (as seen globally in Fig. 4.8b) and the relative contribution of $N_{reduced}$ to total deposition of N (Fig. 4.8c). Fig. 4.8b shows that modeled dry deposition values of N are approximately equal (i.e., ratios = 50% ± 10%) across most of the U.S., Mexico and central Canada. Dry deposition is the dominant contributor (60–85%) in the southwestern U.S.A., northwestern Mexico, over the Pacific Ocean off the west coast, and over selected areas of western and central U.S. while wet deposition is the dominant contributor (0–40% dry deposition) over most of Canada, especially in the north and east.

Based on Fig. 4.8c, $N_{reduced}$ is the main contributor to total deposition of N (50%–85%) in the agricultural areas of central U.S., central Canada, Mexico and in the eastern Caribbean while $N_{oxidized}$ is the main contributor (15%–50% $N_{reduced}$) in the eastern and western parts of Canada and the U.S. as well as northern Canada and over the North Atlantic Ocean off the east coast of the continent.

4.6.1.4. Wet deposition changes in the 2000s. Anthropogenic NO_x–N emissions decreased markedly in U.S. beginning in 1999 and in Canada in 2003 due to emission control regulations in both countries (IJC, 2010). The 3-year average NO_x–N emissions in the U.S. decreased 15% from 6.01 MT N a^{-1} in 2000–2002 to 5.10 MT N a^{-1} in 2005–2007 and, in Canada, decreased 7% from 0.76 MT N a^{-1} to 0.71 MT N a^{-1}. The largest NO_x–N emission changes occurred in the high-emission region that encompasses much of southeast Canada

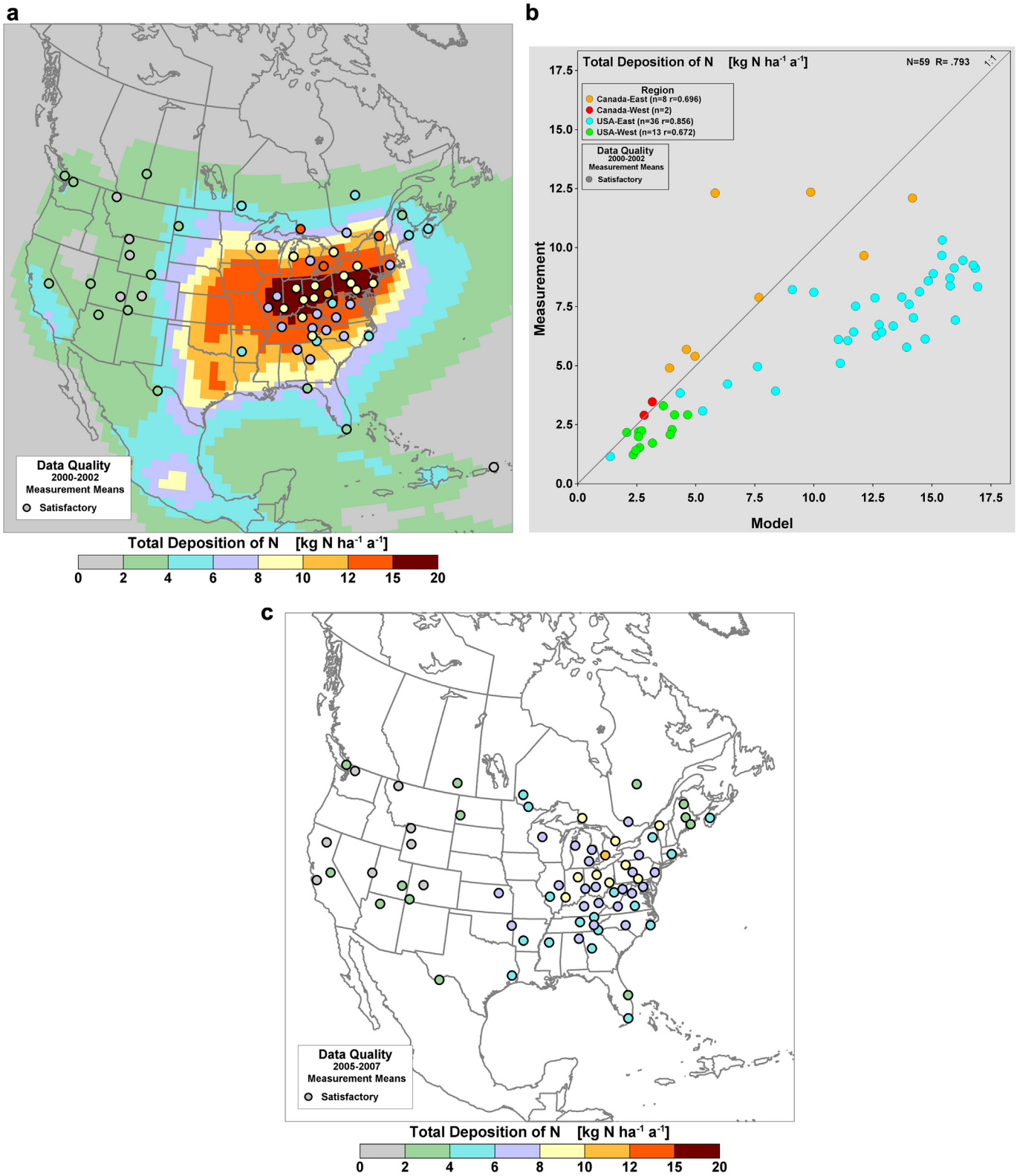

Fig. 4.14. (a) The 2001 ensemble-mean modeled pattern of N total deposition in kg N ha^{-1} a^{-1} with measurement-based 2000–2002 3-year average annual estimates (without NO_2 and NH_3 dry deposition); (b) the associated scatterplot of measured versus modeled (grid cell average) values; (c) 2005–2007 measurement-based 3-year average annual estimates.

and the northeast U.S. where annual emissions decreased by 29% and 28%, respectively, from 2000 to 2007 (IJC, 2010).

An extensive body of literature has been published that links the foregoing emission reductions to major declines in observed $N_{oxidized}$ wet deposition (IJC, 2010; Sickles and Shadwick, 2007; Likens et al., 2005; Butler et al., 2005, 2003; Eshleman et al., 2013), $N_{oxidized}$ air concentrations (Butler et al., 2011; Canada, 2011; IJC, 2010; Sickles and Shadwick, 2007), and inferential

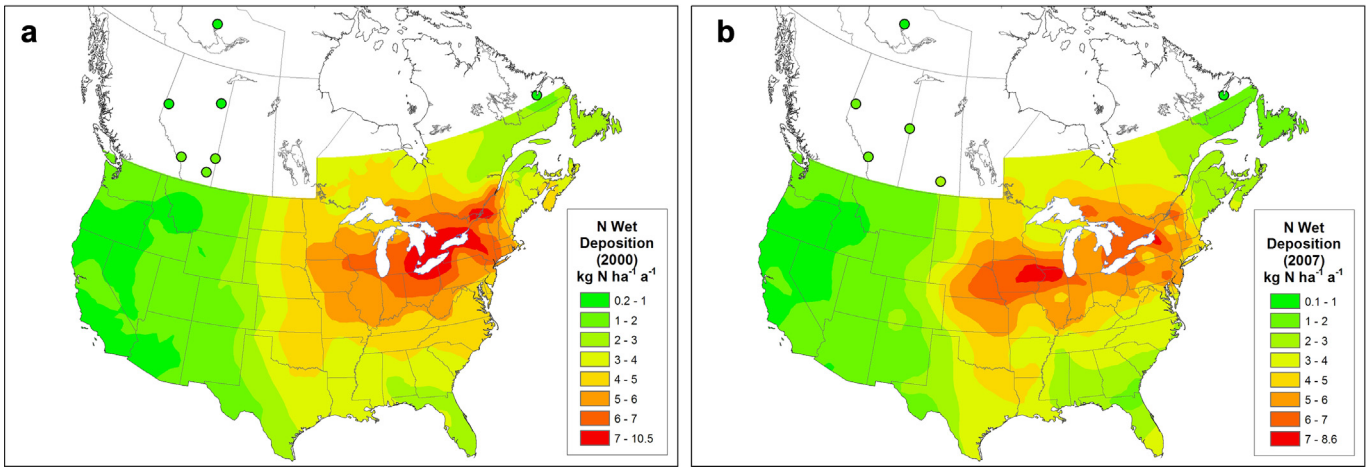

Fig. 4.15. Annual wet deposition of N over North America in (a) 2000 and (b) 2007.

$N_{oxidized}$ dry deposition (Sickles and Shadwick, 2007; Butler et al., 2005). The 2000–2002 and 2005–2007 measurement-based wet deposition patterns shown in Fig. 4.10a,b confirm that $N_{oxidized}$ wet deposition decreased in both Canada and the U.S. concomitant with the decreases in NO_x–N emissions. The largest wet deposition decreases of 10–50% occurred in the northeastern U.S. and southeastern Canada with more moderate decreases 3 of 10%–30% over most of the continent with the exception of a few sites in the U.S. and western Canada where wet deposition increased in response to increasing regional emissions.

Ammonia emission trends in Canada and the U.S. during the 1990s and 2000s are difficult to quantify because the U.S. methodology for estimating NH_3–N emissions changed in 2001 (EPA, 2004). However, the U.S. Environmental Protection Agency indicates that national total emissions of NH_3–N remained relatively constant at about 3.01 MT N a^{-1} from 2002 to 2007 (http://www.epa.gov/ttn/chief/eiinformation.html). In Canada, the National Pollutant Release Inventory similarly indicates that the 3-year average NH_3–N emissions in the 2000–2002 and 2005–2007 periods were roughly constant, with values of 0.4339 MT a^{-1} and 0.4298 MT a^{-1}, respectively (http://www.ec.gc.ca/inrp-npri/default.asp?lang=en&n=0EC58C98#Emission_Summaries). Agricultural sources accounted for 90% of NH_3–N emissions in 2007 in both countries (IJC, 2010). Fig. 4.10c,d above indicate that $N_{reduced}$ wet deposition increased (calculated as 10 to >50%) in the central U.S. and selected parts of the eastern U.S., but decreased (calculated as 0–30%) in most of the eastern part of the continent.

Changes in annual N wet deposition patterns from 2000 to 2007 are shown in Fig. 4.15a,b. These patterns reflect the combined effects of $N_{oxidized}$ and $N_{reduced}$ emission changes. Most of the eastern and western sites show decreasing wet deposition due to decreases in NO_x–N and NH_3–N emissions. Most of the central sites show increases or no change due to increasing or relatively minor changes to NH_3–N emissions. In the eastern part of the continent, the decrease in wet deposition is most visible from the marked reduction in the area encompassing the ≥7 kg N ha^{-1} a^{-1} contour, corresponding to a decrease from 241,900 km^2 in 2000 to 77,700 km^2 in 2007. As was the case with SO_2 emission reductions in Canada and the U.S. (Section 3), NO_x emissions reductions were very effective at reducing N wet deposition in the eastern half of North America.

4.6.2. South America

4.6.2.1. Precipitation-weighted mean concentrations and wet deposition of N. Emissions of NO_x–N and NH_3–N in South America are relatively low compared to other parts of the world, e.g., the HTAP ensemble-mean NO_x–N + NH_3–N annual emissions in 2001 were 9.5 Tg N or 9.0% of the global emissions (Table 3). NO_x–N and NH_3–N 2001 annual emissions are highest in the central and southeastern parts of Brazil, parts of Venezuela, Colombia and Argentina (as well as Paraguay and Uruguay for NH_3–N emissions). South America in general stands out as the global region with the highest inputs of reactive N from naturally-occurring biological nitrogen fixation (Galloway et al., 2004). Increasing cultivation of nitrogen-fixing crop species, biomass burning, use of synthetic N fertilizer and urbanization contribute to the increase in N emissions in the region (Galloway et al., 2004; Martinelli et al., 2006). The EDGAR emission inventory suggests a continental-scale increase in the 3-year average NO_x–N and NH_3–N emissions from 2000–2002 to 2005–2007 of 6% and 15%, respectively (calculated from EDGAR emission inventories published in European Commission, 2012).

Studies in South America that report measured concentrations of N in precipitation are predominantly from Brazil and Venezuela and are short-term in nature with a focus on industrial and urban areas. Concentrations of N in precipitation reported in the literature for the Brazilian Amazon basin (Goncalves et al., 2003; Pauliquevis et al., 2012) are < 0.1 mg N L^{-1} and are comparable to those observed in other remote sites in tropical forests (Pauliquevis et al., 2012). In southern Brazil, reported N concentrations in precipitation at sites near industrial and/or urban areas range from 0.1 to 0.4 mg N L^{-1} for NO_3^--N and <0.1–0.5 mg N L^{-1} for NH_4^+-N (Casartelli et al., 2008; Pelicho et al., 2006; Migliavacca et al., 2004, 2005; Flues et al., 2002; Lara et al., 2001). Concentrations of NO_3^--N and NH_4^+-N at sites in the Itataia National Park (De Mello and De Almeida, 2004), 150 km from Rio de Janeiro and 200 km from Sao Paulo, were at the lower end of this range (0.1 and 0.2 mg N L^{-1} at high and low elevation sites, respectively, in the case of both species), while concentrations from the large metropolitan areas of Sao Paulo (Fornaro and Gutz, 2003, 2006; Rocha et al., 2003) and Rio de Janeiro (De Mello, 2001) were at the higher end (0.2–0.3 mg N L^{-1} for NO_3^--N and 0.2–0.5 mg N L^{-1} for NH_4^+-N). Notably higher concentrations were reported by Forti et al. (2005) at an Atlantic forest site within Sao Paulo, at 0.9 mg N L^{-1} and 0.8 mg N L^{-1} for NO_3^--N and for NH_4^+-N, respectively. A Venezuelan study (Morales et al., 2001a) assessed the impact of urban and industrial sources on the Lake Maracaibo basin and found that NO_3^--N and NH_4^+-N concentrations ranged from 0.34 to 1.20 mg N L^{-1} and 0.09–0.32 mg N L^{-1}, respectively, contributing to NO_3^--N + NH_4^+-N concentrations of 0.97–2.0 mg N L^{-1}.

In this assessment, measurement data were included from only a single regionally representative site in South America (Brazil) that met the time period restrictions and quality acceptance criteria. The precipitation-weighted mean concentration and wet deposition values, as provided by Forti (personal communication, April 29, 2010), appear in Figs. 4.2a and 4.3a and were measured at a forest site in eastern Brazil (Cunha) for the period 1999 to 2001. The precipitation-weighted mean concentrations at Cunha were 0.1 mg N L^{-1} for NO_3^--N and 0.4 mg N L^{-1} for NH_4^+-N, for a total concentration of N of 0.5 mg N L^{-1}. These values are reasonably close to the modeled values of 0.09, 018 and 0.27 mg N L^{-1} in the Cunha grid square (Fig. 4.5a).

The sparse amount of data in South America makes it necessary to rely on the HTAP model results to understand the concentration pattern across South America. To that end, the HTAP concentration pattern (Fig. 4.5a) generally resembles the pattern of NO_x–N + NH_3–N emissions (Fig. 4.1c), with low concentrations in the range of <0.04 mg N L^{-1} in southern Argentina, higher concentrations in the range of 0.1–0.4 mg N L^{-1} in Venezuela, Colombia, Ecuador, northern Chile, central Amazonia, southeastern Brazil and northern Argentina (with an extension into the eastern Pacific Ocean), and hotspots of 0.4–1 mg N L^{-1} in southern Brazil. The lowest concentrations on the continent are in the same range as concentrations in other remote areas of the world.

The measured 3-year average wet deposition of NO_3^--N and NH_4^+-N at Cunha were 2.8 kg N ha^{-1} a^{-1} and 7.8 kg N ha^{-1} a^{-1}, respectively, producing a wet deposition of N of 10.6 kg N ha^{-1} a^{-1} (Fig. 4.3a). As was the case for the precipitation-weighted mean concentrations, the 2001 ensemble-mean model results (Fig 4.5b) underestimated the measured $N_{oxidized}$, $N_{reduced}$ and N wet deposition at Cunha, with values of 1.26, 2.55 and 3.81 kg N ha^{-1} a^{-1} as grid square average values, respectively. Overall, the modeled pattern (Fig. 4.5c) of N wet deposition shows low fluxes of <2 kg N ha^{-1} a^{-1} over most of the continent except for two higher deposition areas in the range of 2–10 kg N ha^{-1} a^{-1} encompassing the northwest and east-central areas of Venezuela, Colombia, central and southern Brazil, Paraguay, Uruguay and parts of Bolivia and Argentina. Low values in central Amazonia have been confirmed by Pauliquevis et al. (2012) who report annual deposition of 2.0 kg N ha^{-1} a^{-1} for NO_3^--N and 1.4 kg N ha^{-1} a^{-1} for NH_4^+-N over a 3.5 yr period between 1998 and 2001 (slightly higher than the 2001 modeled values of 0.83 and 0.97 kg N ha^{-1} a^{-1}).

4.6.2.2. Dry deposition of N. The only recent publications examining N dry deposition in South America have originated in Brazil (Trebs et al., 2006; Allen et al., 2011) and Argentina (Pineda Rojas and Venegas, 2008, 2009). These studies assess the influence of emissions from urban and industrialized areas on dry deposition by applying different modeling techniques and do not report annual dry deposition values that can be compared here. The absence of regionally-representative measurement-based inferential dry deposition estimates in South America makes it necessary to evaluate the continental pattern of dry deposition based on the 2001 HTAP ensemble-mean modeling results (Fig. 4.7a). Again not surprisingly, the South American dry deposition pattern closely mimics the NO_x–N + NH_3–N emission pattern (Fig. 4.1c) with the highest dry deposition occurring in the 2.0–4.0 kg N $ha^{-1}a^{-1}$ range in Venezuela, Colombia, Bolivia, Paraguay, Uruguay, central and southern Brazil and northern Argentina, and the lowest fluxes in the 0.2–1.0 kg N ha^{-1} a^{-1} range in the low emission areas of the continent (i.e., emissions <2 kg S ha^{-1} a^{-1}). Maximum modeled dry deposition occurs in southern Brazil at 4.0–10 kg N ha^{-1} a^{-1}. Fig. 4.7b suggests that N dry deposition is dominated by $N_{reduced}$ dry deposition, with ratios of $N_{reduced}$ to N > 50% over most of the continent.

4.6.2.3. Total deposition of N. The HTAP modeling results for total deposition of N in South America (Fig. 4.8a) also closely resemble the NO_x–N + NH_3–N emissions pattern (Fig. 4.1c). Fluxes greater than 4 kg N ha^{-1} a^{-1} are modeled in the high emission areas of Venezuela, Colombia, Ecuador, central and southeastern Brazil, Bolivia, Paraguay, Uruguay and northern Argentina. Fluxes over the rest of the continent are in the 0.4–4.0 kg N ha^{-1} a^{-1} range. Maximum total deposition of >10 kg N ha^{-1} a^{-1} is projected for a small area in southern Brazil.

In South America, reliance on global model emission and deposition estimates not validated by observations is an unsatisfactory benchmark for assessing ecosystem impacts of nitrogen from human and natural activities. Several long-term, regionally representative air and precipitation monitoring stations are needed throughout the continent. At the time of writing, a coordinated effort was underway to establish such a multi-country network of sites.

4.6.3. Europe

4.6.3.1. Precipitation-weighted mean concentrations and wet deposition of N. Europe has an extensive network of wet deposition measurements, mainly from the EMEP Programme and a few additional national programmes as described in Section 2. The measurement-based 3-year annual precipitation-weighted mean concentrations of $N_{oxidized}$ + $N_{reduced}$ for 2000–2002 and 2005–2007 are shown in Fig. 4.16a and b, respectively, and for wet deposition in Fig. 4.17a and b, respectively. Concentration measurements from the 2000–2002 period are superimposed on the isopleth map of 2001 HTAP modeled pattern in Fig. 4.16a with a model-measurement correlation coefficient of 0.669 for $n = 105$ (Fig. 4.5b). Highest measured concentrations of 1–2 mg N L^{-1} occurred throughout Europe, typically in regions of major agricultural activity and/or high traffic (Denmark, Italy, Serbia, Poland, Spain, and parts of the Russian Federation). The poorest model performance (underprediction) occurred at a number of the high concentration sites in Spain, UK, Serbia and the Russian Republic, many of which had conditional data. Low concentrations of <0.4 mg N L^{-1} occurred on the outer edges of Europe, i.e. Scandinavia, Ireland and Portugal.

Measured wet deposition of N ranged from <1 to 25 kg N ha^{-1} a^{-1} while the modeled wet deposition ranged from <1 to <12 kg N ha^{-1} a^{-1} (Fig. 4.17a,b). Overall, the modeled and measured values compared reasonably well ($r = 0.609$, $n = 105$; Fig. 4.5d) except in south-central and north-central Europe where the model seriously underpredicted wet deposition (Fig. 4.17a). The higher measurement-model correlation for concentrations ($r = 0.669$) compared to wet deposition ($r = 0.609$) indicates that precipitation depth was not modeled well in parts of Europe. This was confirmed by the very narrow range of modeled precipitation depths, from 28.9 to 118.5 cm, compared to the range of measured values from 23.9 to 306.9 cm.

Modeled estimates of measured wet deposition were particularly poor in areas of high annual precipitation depth (>150 cm), most notably in the Alps and along the coast of southwestern Norway. This is not surprising since precipitation depths in coastal and mountainous areas vary substantially over short distances while the global models predict precipitation depths on coarse grid resolutions of $1^\circ \times 1^\circ$ or more. Thus, the poor measurement-model comparability of wet deposition in these areas is likely related to a large degree to different spatial representativeness of measurements and models rather than to poor model performance. This is an important consideration when interpreting HTAP modeled wet deposition in high precipitation areas of Europe and elsewhere.

In eastern Europe, the model results showed elevated wet deposition in Ukraine, but there were no measurements with

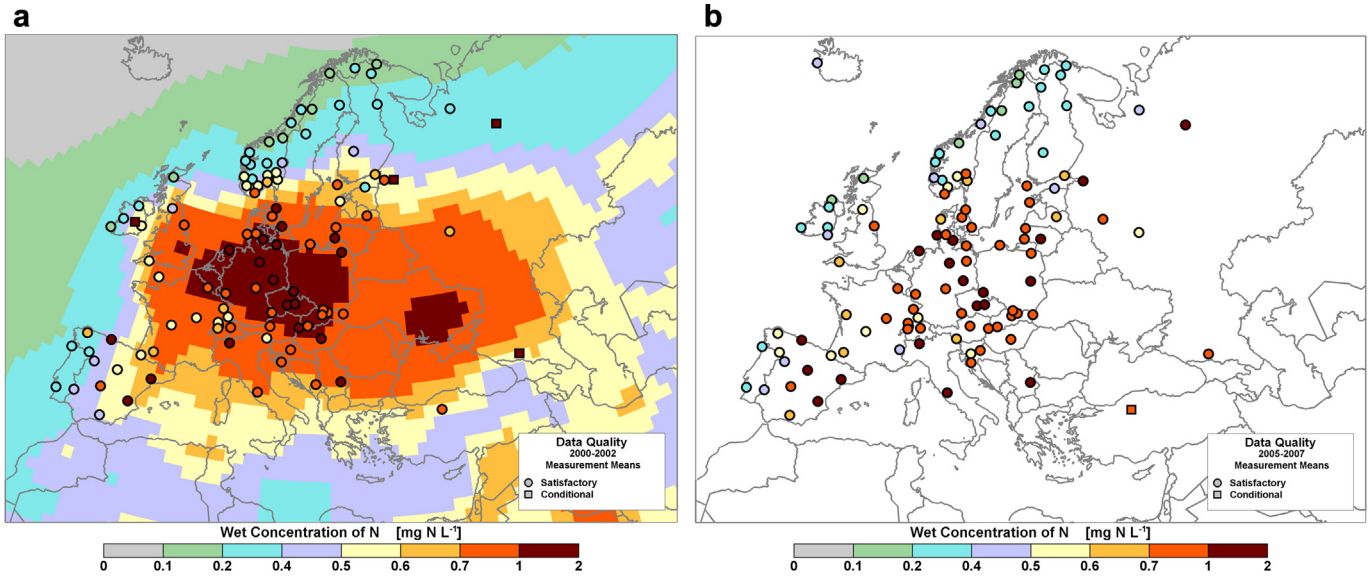

Fig. 4.16. (a) 2001 ensemble-mean model pattern of precipitation-weighted mean concentration of N in Europe combined with measured 3-year average annual precipitation-weighted mean concentration values for the period 2000–2002 and (b) measured 3-year average annual precipitation-weighted mean concentrations for the period 2005–2007 (mg N L^{-1}).

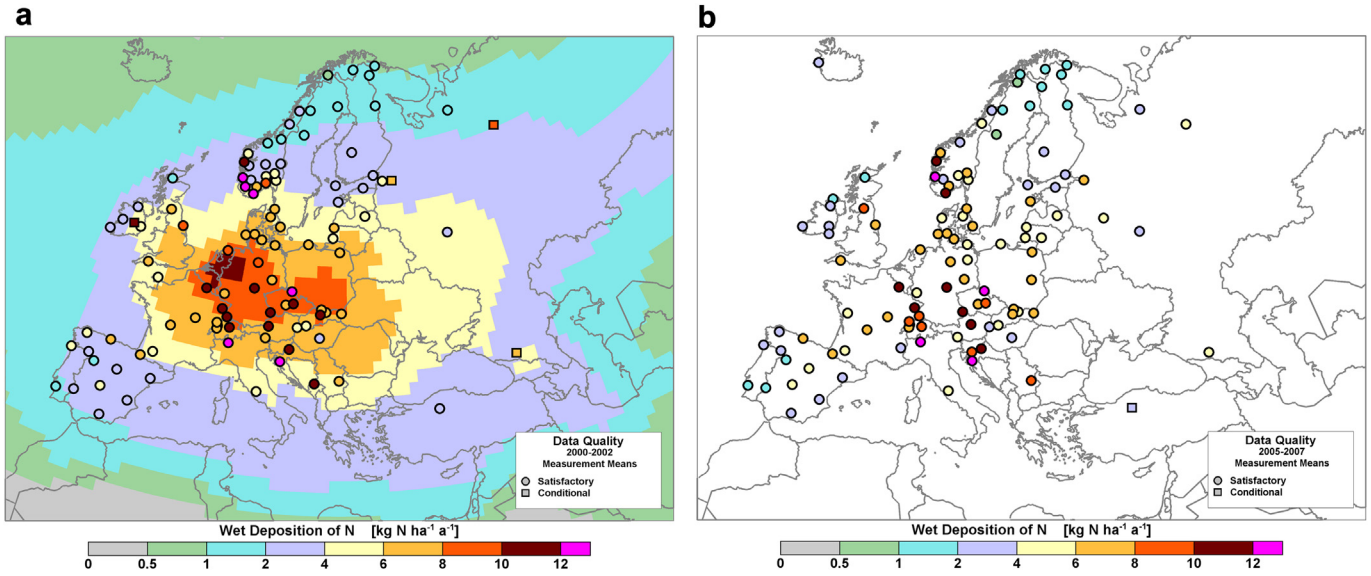

Fig. 4.17. (a) 2001 ensemble-mean model pattern of wet deposition of N, in Europe combined with measured 3-year average annual wet deposition values for the period 2000–2002 and (b) measured 3-year average annual wet deposition for the period 2005–2007 (kg N ha^{-1} a^{-1}).

which to confirm this except for a 2008 study at the Pop Ivan site in the Carpathian Mountains in Ukraine where the observed bulk (wet $N{-}NO_3 + N{-}NH_4$) deposition was 5.7 kg N ha^{-1} a^{-1} (Oulehle et al., 2010). For comparison, the home grid square 2001 HTAP ensemble-mean value was 7.35 kg N ha^{-1} a^{-1}. The lowest levels of wet deposition occurred in northern Scandinavia, western and northern British Isles, and parts of the Russian Federation and Spain. The low deposition in parts of the Russian Federation and Spain is a reflection of the very low precipitation amounts in these areas rather than low concentrations.

On average, the contributions of $N_{oxidized}$ and $N_{reduced}$ to N wet deposition are about the same (Fig. 4.6a,b). However, in the Benelux (*Be*lgium–*Ne*therlands–*Lux*embourg) region and in Ireland, the contribution of $N_{reduced}$ wet deposition exceeds that of $N_{oxidized}$. Furthermore, individual sites in Norway, Russian Federation and Portugal show elevated $N_{reduced}$ compared to $N_{oxidized}$ due to local sources. In eastern Europe (Romania, Ukraine and Belarus) the HTAP model results show a higher relative contribution of $N_{reduced}$. In contrast, there is a higher contribution of $N_{oxidized}$ wet deposition in the Nordic countries and the Mediterranean.

4.6.3.2. Dry deposition of N. Dry deposition is important to the total deposition budget of N in Europe, but unfortunately the EMEP network has no specific measurements of dry deposition and no routine application of an inferential model to the EMEP measurements of ambient gaseous and particulate N. Furthermore, the most common method to measure air concentrations of $N_{oxidized}$ and $N_{reduced}$ (except for NO_2) in the EMEP network is the filter pack

method, which has issues of proper gas-particle partitioning (see Section 2). Since the dry deposition velocities of gaseous and particulate species are so different, unbiased concentration measurements are essential for calculating accurate estimates of N dry deposition. That said, air concentrations of the various gaseous and particulate N compounds measured in the EMEP network (Hjellbrekke and Fjæraa, 2009) show a similar, though more scattered, spatial pattern than the HTAP modeled dry deposition (Fig. 4.7a). The highest modeled dry deposition of N occurred in central Europe and UK, with a maximum in the Benelux region. In general, the relative contribution of $N_{oxidized}$ is somewhat higher than $N_{reduced}$, and the highest difference among the two appears in the Nordic countries. Conversely, dry deposition of $N_{reduced}$ is higher than $N_{oxidized}$ in Ireland and the Benelux region (Fig. 4.7b).

The European Union project, NitroEurope, has established a network of advanced flux measurements at a few selected sites and a large-scale network of low cost denuders (Skiba et al., 2009). These measurements have been combined with various inferential models to calculate dry deposition (Flechard, 2011). For the period November 2006–December 2007, the first results from these measurements showed that net N dry deposition at a selection of these sites across Europe ranged from 0.5 to 18 kg N ha^{-1} a^{-1}. The highest fluxes were measured at agricultural sites in the Netherlands and Italy and the lowest at forest and wetland sites in Finland with values of ~7–8 kg N ha^{-1} a^{-1} at arable and grassland sites in the UK, Switzerland, Hungary and France (Skiba et al., 2009).

An extended study using data from all 55 NitroEurope sites for the period 2007–2008 (Flechard, 2011) showed that different inferential models yielded quite different fluxes of nitrogen. Four different inferential models were compared, and the annual dry deposition estimates for all the sites varied typically by a factor 2 to 3 (Flechard, 2011). The most significant differences were found for NH_3 for all vegetation types, and for fine particles (NH_4^+ and NO_3^-) over forests. There were large differences between the models in their parameterizations of stomatal conductance and non-stomatal resistances. Further, the authors showed that the uncertainties in the inferential dry deposition estimates could be reduced by on-site recording of vegetation parameters like leaf area index and canopy height. To validate and improve these models, it is necessary to compare the results to direct long-term micrometeorological flux measurements over different vegetation types, but few of these datasets are available (Flechard et al., 2011). Data from a national study on the German/Czech border yielded an average inferential dry deposition of 6.1 kg N ha^{-1} a^{-1} for the period 2002–2004 (Zimmermann et al., 2006). This is consistent with the modeling results in Fig. 4.7a, showing a value of 4–10 kg N ha^{-1} a^{-1}.

These results indicate the importance of dry deposition in large parts of Europe and illustrate the challenge in estimating dry deposition. To date, no inferential estimates of dry deposition have been made using the extensive ambient concentration measurements of the EMEP network. Additionally, no inferential dry deposition models have been evaluated or developed for this purpose. Such work would be extremely valuable.

The 2001 HTAP ensemble-mean model results (Fig. 4.7a) show an N dry deposition pattern similar in shape to the NitroEurope network, although the model results are from an earlier time period. Maximum dry deposition in the HTAP modeled results is lower than calculated by the measurement-based inferential method. On the other hand, one should note that some of the high deposition sites in NitroEurope are situated in agricultural areas, which may not be regionally-representative. The HTAP modeling results indicate that the Nordic countries receive < 1 kg N ha^{-1} a^{-1} from dry deposition; central and eastern Europe receive 5–10 kg N ha^{-1} a^{-1} and the hot spot areas of the Netherlands, UK, and Germany receive >10 kg N ha^{-1} a^{-1}.

4.6.3.3. Total deposition of N. Given that there are few long-term measurements of dry deposition and that the short-term projects and campaigns are not necessarily conducted where wet deposition is measured, it is difficult to estimate the total deposition of N from measurements in Europe. Estimates from a throughfall measurement network in Europe (Lorenz et al., 2007) generally underestimate N total deposition due to the considerable uptake of nitrogen in the forest canopy. This is especially true for $N_{reduced}$. Furthermore, throughfall is measured in forests, which typically have higher deposition rates than other land surfaces and may not necessarily be representative of Europe as a whole.

Notwithstanding these shortcomings, throughfall data can serve as a useful guide to examine spatial gradients of total deposition. Lorenz et al. (2007) estimated that the average $N_{oxidized}$ deposition in throughfall for the period 2002–2004 ranged from 0.2 to 19 kg N ha^{-1} a^{-1} and for $N_{reduced}$ from 0.2 to 24 kg N ha^{-1} a^{-1}. Highest N throughfall fluxes were mainly seen in central Europe, while lowest levels were seen in northern Europe and in the Alps (Lorenz et al., 2007). The highest model-based total deposition of N (Fig. 4.8a) appears in central Europe and the UK with more than 10 kg N ha^{-1} a^{-1}, and in the Benelux area with >20 kg N ha^{-1} a^{-1}. Scandinavia, southern Europe, and major parts of the Russian Federation receive <10 kg N ha^{-1} a^{-1}. Throughfall measurements were not compared with the HTAP model estimates in scatterplots, as was done for sulfur, because the loss of N in the canopy exchange makes deposition estimates of N very uncertain.

Based on Fig. 4.8b, the relative contributions of wet and dry nitrogen deposition vary across Europe. The HTAP model results show that the percentage of dry deposition exceeds 50% in central, western and southern Europe and is less than 50% in northern and eastern Europe. The largest relative contribution of dry deposition relative to total deposition (>60%) occurred in Spain and Portugal, while the lowest occurred in Scandinavia (<40%). Based on Fig. 4.8c, $N_{reduced}$ appears to be relatively more important in large parts of central and eastern Europe, while $N_{oxidized}$ is more important in southern and northern Europe.

4.6.3.4. Temporal changes to N deposition. In Europe, nitrogen oxides (NO_x–N) are emitted mainly from stationary combustion sources (power plants and industrial processes) and transportation sources (road, off-road and ship traffic). NO_x–N emissions increased in the 1980s due to increased traffic and started to decrease in the mid-1990s (Lövblad et al., 2004).

From 1990 to 2009, NO_x–N emissions in Europe decreased by 31% (EMEP/CEIP, 2012; Tørseth et al., 2012), due mainly to the conversion from coal and gas burning to nuclear power (Lövblad et al., 2004). Economic recovery in eastern Europe resulted in increased NO_x–N emissions from road traffic in this area after 2000 (Vestreng et al., 2009). On the other hand, NO_x–N emissions from traffic in western European decreased, even though fuel consumption increased. These reductions were due to the implementation of increasingly strict NO_x emission control measures commonly known as EURO-standards (Vestreng et al., 2009).

NO_x–N emissions trends in Europe are reflected in ambient NO_x measurements. From 1990 to 2009, the average decrease of NO_2 concentrations at long term measurement sites was 23% (Tørseth et al., 2012). Over this same time period, $N_{oxidized}$ in precipitation decreased by 25% (Tørseth et al., 2012). Interestingly, the concentrations of airborne $N_{oxidized}$ (nitric acid vapor + particulate nitrate) measured in the EMEP network decreased on average only 8% in the same period (Tørseth et al., 2012). These differences in trends can partly be explained by a shift in equilibrium towards more

particulate ammonium nitrate relative to nitric acid caused by a reduction in SO_2 emissions (Fagerli and Aas, 2008; Monks et al., 2009) and possibly more rapid oxidation of NO_x (Monks et al., 2009). Furthermore, the measurements of oxidized nitrogen in air and precipitation were not made at the same sites so the differences in trends may also have been influenced by the different site locations (Tørseth et al., 2012).

NH_3–N emissions decreased by 29% in Europe from 1990 to 2009 (EMEP/CEIP, 2012; Tørseth et al., 2012), but there were large regional differences. The largest reductions occurred in countries of central and eastern Europe (Lövblad et al., 2004). A majority of EMEP sites showed a decreasing trend in $N_{reduced}$ concentrations in both air and precipitation – on average 25%. The sum of gaseous ammonia and particulate ammonium ($NH_3+NH_4^+$) decreased similarly with an average of 24% for the twenty year period from 1990 to 2009 (Tørseth et al., 2012).

The median observed reduction in N wet deposition between 2001–2002 and 2005–2007 at the 88 European sites was −2.7% for N (Fig. 4.4). This was due mainly to reductions in $N_{oxidized}$ wet deposition (i.e., median change = −8.3%) rather than $N_{reduced}$ wet deposition (median change = −1.1%) (Note that the median values are not additive). The reduction of NO_x–N emissions by EMEP Parties was 5% over this same period but the ship emissions increased by 16%, resulting in a small reduction (2%) in total NO_x–N emissions in Europe (EMEP/CEIP, 2012).

4.6.4. Africa

4.6.4.1. Precipitation- weighted mean concentrations and wet deposition of N. The measurement-based 3-year mean annual precipitation-weighted mean concentrations of N for 2000–2002 and 2005–2007 at African sites are shown in Fig. 4.2a,b. Given the scarcity of data in Africa, a decision was made to discuss the multi-year average precipitation-weighted mean concentrations measured for the whole studied period at each of the sites: 2000–2007 for west and central Africa, except for Djougou, Benin (2005–2007) and Agoufou, Mali (2004–2006); and 1986–1999 for South Africa, except for Skukuza (1999–2002) (see Fig. 3.19 for site locations).

The average $N_{oxidized}$ precipitation-weighted mean concentrations at the five west and central African sites over the respective time periods ranged from 0.1 to 0.2 mg N L^{-1}. A concentration gradient was observed along a north-south transect from 0.2 mg N L^{-1} in the dry savanna to around 0.1 mg N L^{-1} in the wet savanna and forests of west and central Africa. Sites in South Africa had concentrations in the lower part of the range, i.e., 0.1 mg L^{-1} in the rural dry savanna areas of Louis Trichardt and Skukuza and 0.4 mg N L^{-1} at the Amersfoort site in the vicinity of South Africa's coal-fired power plants.

Galy-Lacaux et al. (2001) demonstrated that heterogeneous processes between nitric acid and mineral particles occur all over the African continent and help explain the concentration of $N_{oxidized}$ in precipitation. Nitric oxide (NO), in the non-burning season from June to September, is the major N compound released from savanna soils (Serça et al., 1998; Otter et al., 2001). A large fraction of NO produced is oxidized in the atmosphere through photochemical reactions into HNO_3 or organic nitrates. HNO_3 is extremely soluble in water and easily scavenged by clouds and hydrometeors. Heterogeneous processes decrease from the semi-arid regions to the forested ecosystem. This is because dust particles present in the semi-arid regions neutralize all of the HNO_3. This gradient coincides with the observed gradient in $N_{oxidized}$ concentrations in precipitation. At South African sites, $N_{oxidized}$ in precipitation is also attributed to NO emissions from biomass burning (Mphepya et al., 2004, 2006). The flux of emissions of biogenic NO from infertile soils in the semiarid savanna of South Africa is equal to the amount of NO generated by biomass burning, but slightly less than that from industry (Otter and Scholes, 2005). This result is in agreement with what was found in the Sahel, where biogenic soils emissions perturbed by grazing activities are high (Serça et al., 1998). The seasonal pattern of NO_2 concentration clearly shows rain-induced NO emissions from semi-arid savanna soils in the Sahelian region centered on the June maxima (Adon et al., 2010). The highest values of $N_{oxidized}$ in the rain of the anthropogenic dry savanna at the Amersfoort site are undoubtedly related to the influence of the Highveld industrial NO_x–N emissions.

The $N_{reduced}$ concentrations in precipitation in the forested, wet savanna and semi-arid ecosystems of west and central Africa were relatively high, ranging from 0.1 to 0.3 mg N L^{-1}. As the land type varies from dry savanna to wet savanna to forest, the concentrations of $N_{reduced}$ also changes. In the wet savanna of Lamto (Republic of Côte d'Ivoire), the 8-year annual average precipitation-weighted mean concentration of $N_{reduced}$ is around 0.3 mg N L^{-1} and comparable to concentrations in the dry savanna. The wet savanna of Benin (Djougou) had a lower precipitation-weighted annual mean concentration of 0.2 mg N L^{-1}. In South Africa, the $N_{reduced}$ content of the dry savannas precipitation ranged from 0.1 to 0.2 mg N L^{-1} and the two rural dry savannas had roughly comparable concentrations around 0.15 mg N L^{-1}. The chemical composition of rain over the long term 1986–1999 period reported by Mphepya et al. (2004) indicated that the Amersfoort site (dry savanna near industrial sites) had higher concentrations of $N_{reduced}$ (0.3 mg N L^{-1}), likely attributable to industrial emissions.

In Africa, the major emission sources of NH_3–N include bacterial decomposition of urea in animal excreta, emissions from natural or fertilized soils (Schlesinger and Hartley, 1992), savanna fires, and domestic fuel wood burning (Delmas et al., 1991; Brocard et al., 1996). The highest concentrations of $N_{reduced}$ compounds in precipitation measured in the semi-arid regions have been attributed to strong sources of NH_3–N from domestic and pastoral animals during the wet season in west central Africa (Galy-Lacaux and Modi, 1998; Galy-Lacaux et al., 2009; Adon et al., 2010; Delon et al., 2010). In South Africa, in the arid savanna around the Skukuza site, the large population of wild animals in Kruger National Park is the main source of NH_3–N (Mphepya et al., 2006). Also in South Africa, Mphepya et al. (2004) related $N_{reduced}$ concentrations to agricultural activities and petrochemical plants on the Mpumpalanga Highveld, which have been found to emit NH_3–N (Van der Walt, 1998 as cited in Mphepya et al., 2004).

The multi-year average (2000–2007) precipitation-weighed mean concentrations of N in west and central Africa ranged from 0.4 to 0.5 mg N L^{-1} in dry savannas to 0.2 mg N L^{-1} in forests, with higher values in dry savannas in accordance with high NO_x–N biogenic soil emissions combined with high NH_3–N emissions from livestock. In wet savannas, concentrations ranged from 0.3 to 0.4 mg N L^{-1}. In South Africa, annual precipitation weighed mean concentrations of N ranged from 0.3 to 0.6 mg N L^{-1}, with a maximum measured value in the dry savanna of Amersfoort influenced by the Highveld industrial emissions of gaseous nitrogenous compounds.

The 3-year average annual wet deposition of N for 2000–2002 and 2005–2007 is presented in Fig. 4.3a,b. A comparison of three of the sites in west Africa between the two 3-year averaging periods shows an absolute increase in wet deposition of N of <1 kg ha^{-1} a^{-1} (Fig. 4.4b) corresponding to a percentage change of +16 to +38% (note that the % increases are very high because wet deposition is so low). These wet deposition changes are at least consistent in sign with the estimated continental emission change of +56% calculated from the EDGAR emission inventory (European Commission, 2011) based on NO_x–N and NH_3–N emission changes of +65% and +20%. Given projected increases in N emissions and deposition in tropical

and subtropical regions by Galloway et al. (2008) and Dentener et al. (2006), as well as over forested areas from increasing fossil fuel combustion by Lamarque et al. (2005), it is important to quantify the processes that contribute to the changing levels of N deposition. In addition to changes in NO_x–N and NH_3–N emissions, the annual and seasonal rate and distribution of precipitation are also important to understand changes in N deposition over Africa. In dry areas, for example, N volatilization as NH_3 and NO is strongly dependent on soil moisture and consequently on the precipitation regime (Delon et al., 2012, 2014; Galy-Lacaux et al., 2014). Dentener et al. (2006) used the IDAF measurements to validate modeled deposition estimates over the African continent and showed that only 9.3% of the tropical forests have N deposition greater than 10 kg N ha^{-1} a^{-1}, a critical load over which a negative effect on sensitive vegetation types is expected (Phoenix et al., 2006; Dentener et al., 2006). Little is known about critical loads in the tropics, which may be less N limited than temperate forests and show different responses to elevated N deposition (e.g., Bobbink et al., 2010).

The multi-year average $N_{oxidized}$ wet deposition in west and central Africa (2000–2007) and in South Africa (1986–1999) ranged from 0.7 to 2.0 kg N ha^{-1} a^{-1}. The lower deposition estimates occurred in the rural dry savannas of west central Africa and South Africa and the highest fluxes in the industrial dry savanna area of South Africa (at the Amersfoort site). In the wet savanna and forested areas, wet deposition was generally around 1.5 kg N ha^{-1} a^{-1}. The multi-year average wet deposition of $N_{reduced}$ ranged from 0.5 to 3.8 kg N ha^{-1} a^{-1}. Higher values of $N_{reduced}$ deposition were measured in west and central Africa with maxima in the wet and dry savannas.

The multi-year average wet deposition of N ranged from 1.0 to 5.3 kg N ha^{-1} a^{-1}. At the dry savanna sites, N wet deposition varied from 1.7 (Agoufou, Mali) to 3.4 kg N ha^{-1} a^{-1}, with the maximum occurring in the dry savanna area of Mali. In the wet savannas and forested areas, the wet deposition ranged from 3.6 to 5.3 kg N ha^{-1} yr^{-1}. N wet deposition in west central Africa is dominated by N in the form of NH_4^+, which represents around 63–70% of the N wet deposition measurements at the paired IDAF stations (dry and wet savannas). In South African dry savannas, N wet deposition varies from 1.0 kg N ha^{-1} a^{-1} in Skukuza to 1.7 kg N ha^{-1} a^{-1} at Louis Trichardt to a maximum of 4.4 kg N ha^{-1} a^{-1} in the industrialized area of South Africa (at the Amersfoort site). As mentioned above, the latter two dry savannas are impacted by industrial emissions through air mass recirculation and we found an equal contribution of $N_{oxidized}$ and $N_{reduced}$ to the N wet deposition budget at these sites. In the dry savannas of Skukuza, located in the wild Kruger National Park, natural biogenic sources of $N_{oxidized}$ prevail and contribute up to 62% of the N wet deposition. In west and central Africa including dry ecosystems, in spite of very low industrial and transportation emission sources, nitrogenous compounds in precipitation are in the same range as in the industrialized region of South Africa, albeit at the lower end.

A more comprehensive depiction of N wet deposition across Africa is found in the combined model-measurement maps of N in Fig. 4.5c. This map shows the 2001 ensemble mean modeled wet deposition pattern combined with the 2000–2002 mean annual wet deposition observations in west central Africa and the 1996–1999 observations in South Africa. The modeled wet deposition ranges from lows of less than 0.5 kg N ha^{-1} a^{-1} in the Sahara to highs of 4.0–5.0 kg N ha^{-1} a^{-1} in the wet savannas and forests. Alternatively, precipitation-weighted mean concentrations show a negative gradient of $N_{oxidized}$ from the dry savanna to the forest (Fig. 4.5a). The gradient of wet deposition is opposite to the precipitation-weighted mean concentrations because of the strong rainfall gradient along the ecosystems transect with about 50–70 cm in dry savannas, 120 cm in the wet savanna and 150 cm in the forested ecosystem of Cameroon.

The combined model-measurement results for N wet deposition agree well with observations in the wet savannas and forests; however, in the Sahelian region of Mali and in the dry savanna of Skukuza in South Africa, the modeled mean is lower by a factor of two. This result is also correlated to model predictions of precipitation-weighted mean concentrations underestimated in dry ecosystems of the northern hemisphere.

4.6.4.2. Dry deposition of N. Dry deposition estimates for the African sites were obtained from the DEBITS program, which used the inferential technique for calculating dry deposition velocities (see Section 2) and measured concentrations of gaseous and particle nitrogen species. Monthly-integrated concentrations of NO_2, NH_3, and HNO_3 were obtained through passive sampling (Adon et al., 2010; Martins et al., 2007) and concentrations of water soluble p-NH_4^+ and p-NO_3^- through filter-based sampling (Kleynhans et al., 2008). Particulate-NH_4^+ and p-NO_3^-concentrations were measured in Banizoumbou, Niger from 1996 to 2004, in Katibougou, Mali from 1999 to 2003 and in Lamto, Republic of Côte d'Ivoire from 1998 to 2004. In South Africa, p-NH_4^+ and p-NO_3^- were measured during intensive 15-day periods in the summer and winter of 2005 and 2006 (Kleynhans et al., 2008). To estimate dry deposition of nitrogenous particles, two dry deposition velocities were used, namely 0.1 and 0.2 cm s^{-1} according to Zhang et al. (2009). The estimated dry deposition of p-NH_4^+ and p-NO_3^- are low and of the same order of magnitude for all of the ecosystems. The estimated mean annual deposition of p-NH_4^++p-NO_3^- in the semi-arid and wet savanna regions of west and central Africa is in the range of 0.1–0.2 kg N ha^{-1} a^{-1}. In South Africa, deposition of p-NH_4^++p-NO_3^- is estimated to be around 0.4–0.7 kg N ha^{-1} a^{-1} at Amersfoort and 0.2–0.4 kg N ha^{-1} a^{-1} at Louis Trichardt. The estimated dry deposition of particle-N is smaller by an order of magnitude than the wet deposition of N.

Gaseous N dry deposition was calculated as the sum of the dry deposition estimates of NH_3, HNO_3 and NO_2. The major uncertainty in the estimation of dry deposition of trace gases is due to the computation of the dry deposition velocities. Table 4 presents the range of dry deposition velocities (V_d) for each type of ecosystem calculated using the method described in Section 2. A range is given for the three sites in South Africa. The deposition velocities for dry and wet savannas in western central Africa can also be found in Delon et al. (2010). The total uncertainty for deposition is 70% for NO_2, 31% for NH_3 and 38% for HNO_3 (Delon et al., 2010).

NO_2 dry deposition varies only slightly according to the type of ecosystem, with fluxes ranging from 0.8 to 1.0 kg N ha^{-1} a^{-1} in the dry savannas, from 0.5 to 0.7 kg N ha^{-1} a^{-1} in the wet savannas and from 0.8 to 1.1 kg N ha^{-1} a^{-1} in the forested ecosystem. NH_3 dry deposition is higher and dominates the gaseous N dry deposition budget. In the dry savannas, in spite of a lower dry deposition velocity due to the low vegetative cover, NH_3 dry deposition ranges from 3.4 to 3.5 kg N ha^{-1} a^{-1}. In the wet savannas and the forest, the NH_3 fluxes are around 3 and 6 kg N ha^{-1} a^{-1}, respectively. Dry

Table 4
Range of dry deposition velocities (cm s^{-1}) for NO_2, NH_3 and HNO_3 for each type of ecosystem in west central Africa (WCA) and for South African sites.

Land type	Dry deposition velocity (cm s^{-1})		
	NO_2	NH_3	HNO_3
Dry savannas (WCA)	0.20–0.23	0.28–0.30	0.32–0.73
Wet savannas (WCA)	0.31–0.35	0.37–0.42	0.35–0.70
Forests (WCA)	0.47–0.53	0.39–0.79	1.54–1.78
South African sites	0.38–0.42	0.52–0.60	1.07–1.42

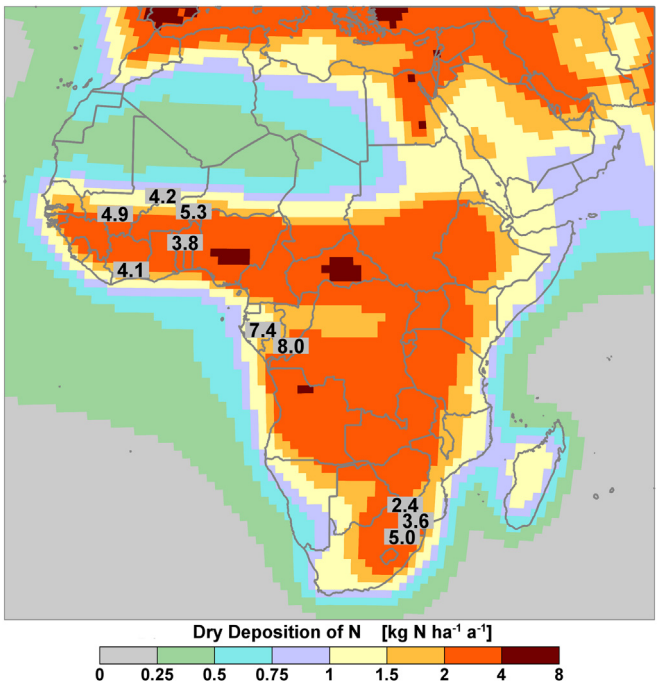

Fig. 4.18. 2001 HTAP modeled dry deposition of $N_{oxidized}$ + $N_{reduced}$ with measurement-based inferential estimates from 2000 to 2007 superimposed.

deposition of HNO_3 varies from 0.5 to 1.8 kg N ha^{-1} a^{-1} for all of the ecosystems.

Combining dry deposition of N coming from the gaseous and the particulate phase, the total dry N deposition for the period 2002–2007 is estimated to be in the range of 4.2–5.3 kg N ha^{-1} a^{-1} in dry savannas, 3.8–4.1 kg N ha^{-1} a^{-1} in wet savannas and 7–8 kg N ha^{-1} a^{-1} in forested ecosystems. In South African dry savannas, dry N deposition varies from 2.4 at Louis Trichardt to 5.0 kg N ha^{-1} a^{-1} at Amersfoort. As continental context, results for all the IDAF sites over various years are superimposed on the 2001 HTAP modeling results in Fig. 4.18. The combined model-measurement results for dry deposition of N show an underestimation of dry deposition over west and central Africa ecosystems, from 25% in wet savannas and forest to 50% in dry savannas and quite good agreement with dry N deposition measured in South Africa. Dry deposition of N is predicted to vary from 0.6 to 1.0 kg N ha^{-1} a^{-1} in dry savannas and from 2.0 to 5.0 kg N ha^{-1} a^{-1} in wet savannas, forests and in South Africa. Model results (Fig. 4.18) indicate that $N_{oxidized}$ is dominant compared to $N_{reduced}$ for the whole continent, given the importance of the distribution of anthropogenic NO_x–N emission sources (biomass burning and industries in South Africa). The model-based pattern of dry $N_{reduced}$ shows maximum fluxes around 1.0–2.0 kg N ha^{-1} a^{-1} with a latitudinal distribution similar to $N_{oxidized}$. This indicates that NH_3–N sources taken into account are also mainly related to anthropogenic emission sources (traffic, domestic, biomass, biofuel). We assume that the difference between model results and measurements representative of the African ecosystems relate to (1) the underestimation of NH_3–N emissions from livestock (mainly for dry savanna ecosystems) and from other agricultural activities and (2) the underestimation of dry deposition rates over forested ecosystems.

4.6.4.3. Total deposition of N. The measurement-based multi-year total deposition of N is estimated at approximately 7–8 kg N ha^{-1} a^{-1}, 7–9 kg N ha^{-1} a^{-1} and 11 kg N ha^{-1} a^{-1}, in the dry savanna, humid savanna and forested areas, respectively. In comparison, the flux calculated for the Petit-Saut station in the Amazonian forest is about 6 kg N ha^{-1} a^{-1} (C. Galy-Lacaux, personal communication, March 14–20, 2010). At the South African sites, total deposition of N at Amersfoort is estimated to be around 10 kg N ha^{-1} a^{-1}. Louis Trichardt and Skukuza present lower values between 4 and 6 kg N ha^{-1} a^{-1}. These are in the same order of magnitude as estimated for grasslands by Lowman and Scholes (2002) at 13.1 kg N ha^{-1} a^{-1}.

The foregoing measurement-based estimates of total deposition of N, coupled with the 2001 HTAP ensemble-mean global modeling results provide a tool for assessing the contribution of dry and wet deposition to total deposition of N in Africa (Fig. 4.19). Globally, model results underestimate total deposition of N in forested and dry savanna ecosystems in west and central Africa. The measurement-based estimates indicate the major importance of dry deposition in west central Africa, especially for nitrogenous gaseous compounds (Fig. 4.18). In the dry savanna, the fractional contribution of dry to total deposition of N ranges between 60 and 70%. In the wet savannas and forested ecosystems, this contribution is around 40–60% and 70%, respectively (Delon et al., 2012, 2014; Galy-Lacaux et al., 2014). In South Africa, dry deposition at the industrial site of Amersfoort is roughly equivalent to wet deposition. In the rural dry savannas of Louis Trichardt and Skukuza, dry and wet N deposition represent 60% and 40% of the total, respectively. This was also the case for the dry savanna in west central Africa. The dry N deposition values reported above are based only on gaseous deposition estimates of NO_2, NH_3 and HNO_3 and the wet deposition values on precipitation measurements of $N_{oxidized}$ and $N_{reduced}$. They do not include the contribution of organic nitrogen species such as PAN and the deposition of nitrogen-containing particles that could probably contribute significantly to the atmospheric burden of N, resulting in a possible underestimation of the total deposition of N.

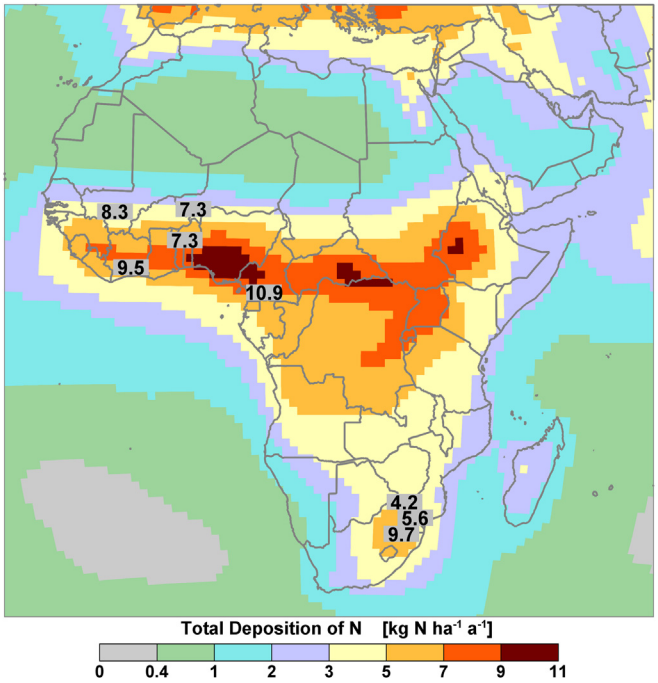

Fig. 4.19. 2001 HTAP modeled total deposition of N with measurement-based estimates from 2000 to 2007 superimposed.

4.6.5. Asia

4.6.5.1. Precipitation-weighted mean concentrations and wet deposition of N. Measured N precipitation-weighted mean concentrations across Asia are shown in Fig. 4.2a, b for 2000–2002 and 2005–2007, respectively. The measurement data were provided by EANET as well as networks in the Russian Federation and Taiwan and WMO GAW sites and selected national sites in India. The 3-year average measured concentrations in 2000–2002 and 2005–2007 ranged from lows of 0.10 mg N L^{-1} in Japan and the Maldives to highs of 1.85 and 1.93 mg N L^{-1} in eastern China (EANET Chongqing-Jinyunshan site) – a range of two orders of magnitude. The highest concentrations of >1.0 mg N L^{-1} occurred at EANET sites in eastern China (both periods), the Republic of Korea (both periods) and Mongolia (first period). Many sites throughout East Asia had concentrations in the 0.5–1.0 mg N L^{-1} range and many of the small island sites had concentrations in the range of 0.1–0.4 mg N L^{-1}.

Measured wet deposition values of N on a global scale are shown in Fig. 4.5c for 2000–2002 (superimposed on the 2001 model pattern) and in Fig. 4.3b for 2005–2007. In 2000–2002, three sites in eastern China and one site in northeast India measured among the highest N wet deposition on the globe with values of 17.4–20.3 kg N ha^{-1} a^{-1} (the only higher measured valued being from the Ispra site in Italy with a value of 24.55 kg N ha^{-1} a^{-1}; this site may be affected by agricultural and animal sources of NH_3). In 2005–2007, measurements from two sites in China, one site in Japan and one in India were the highest on the globe with values ranging from 14.83 to 27.07 kg N ha^{-1} a^{-1} (again with the exception of the Ispra site in Italy with a value of 16.40 kg N ha^{-1} a^{-1}). Lowest wet deposition in 2000–2002 ranged from 1.21 to 1.64 kg N ha^{-1} a^{-1} in western China and the eastern Russian Federation and, in 2005–2007, from 0.97 to 1.0 kg N ha^{-1} a^{-1} in the eastern Russian Federation. The range of wet deposition from lowest to highest was 1.21–20.25 kg N ha^{-1} a^{-1} in 2000–2002 and 0.97–27.07 kg N ha^{-1} a^{-1} in 2005–2007.

Insight into the spatial distribution of N precipitation-weighted mean concentrations and wet deposition in Asia can be gained from the combined model-measurement patterns of Fig. 4.5a and c, respectively. As expected from the emissions patterns, highest concentrations of 1.0–2.0 mg N L^{-1} were modeled in Pakistan, northern India, eastern China and Korea and very low concentrations of <0.2 mg N L^{-1} were predicted and measured in the northern Russian Federation and western China. The correlation coefficient between the HTAP ensemble-mean modeling results and the measured concentrations is 0.743 ($n = 38$) (see Fig. 4.5b). The model results generally underpredict the measured concentrations, particularly in Mongolia, the Russian Federation and Thailand.

The wet deposition pattern of N (Fig. 4.5c) shows high wet deposition (10–30 kg N ha^{-1} a^{-1}) in a large area of eastern China and somewhat lower deposition (2.0–10.0 kg N ha^{-1} a^{-1}) elsewhere in the eastern domain. The modeled results appear to underestimate the wet deposition levels slightly at sites in the Russian Federation, Mongolia, Korea and Japan but, overall, the measurement-model comparability is reasonable with $r = 0.703$ ($n = 38$). In India, higher $N_{oxidized} + N_{reduced}$ wet deposition at sites in the northeast part of the country and on the island location in the Bay of Bengal are attributed to precipitation depths, which appear to be higher than other parts of India.

The relative contribution of $N_{reduced}$ to N wet deposition in Asia is shown in Fig. 4.6a. Overall, the modeled and measured ratios do not compare well with $r = -0.077$ ($n = 38$) due largely to model underestimation in the northern Russian Federation and overestimation in India relative to measurements. Nonetheless, the modeling results suggest that $N_{reduced}$ is the major contributor to N wet deposition (with ratios > 60%) in India and most of East Asia – a fact consistent with the emission patterns of NO_x–N and NH_3–N (Fig. 4.1a and b). $N_{oxidized}$ is modeled as the major contributor only in the northern Russian Federation, parts of Kazakhstan, Uzbekistan and Turkmenistan, western Mongolia and Japan. At two of the four Indian locations, $N_{reduced}$ deposition was considerably lower than $N_{oxidized}$ deposition suggesting the dominance of anthropogenic NO_x–N emissions over agricultural NH_3–N emissions in those areas.

Temporal changes to N wet deposition from 2000–2002 to 2005–2007 are shown in Fig. 4.4a, b. Although the measurement data in Asia are sparse, the 27 sites showed a median increase of 13.6% between the two periods with roughly 70% of the sites having higher wet deposition in the later period. This is consistent with an overall 15% increase in the EDGARv4.2 emissions for Asia between the two periods (European Commission, 2011). Fig. 4.4a shows that most of the sites in Southeast Asia had increasing (or roughly constant) wet deposition of N while most sites in the Russian Federation had decreasing wet deposition. This is also consistent with the EDGARv4.2 emission inventory that shows a 25% increase in NO_x–N + NH_3–N emissions in Asia-without-Russian Federation but a 32% decrease in the Russian Federation (note that country statistics in EDGARv4.2 may not capture regional differences in growth). The lack of measurement sites in eastern China makes it impossible to quantitatively assess the impact on wet deposition of well-documented major increases in NO_x–N emissions in China between the two periods (Gu et al., 2012).

4.6.5.2. Dry deposition of N. At the time of writing, the only long-term measurement-based inferential estimates of N dry deposition in Asia were for Japan. These were based on published results from measurements at 10 EANET sites from 2003 to 2008 (Endo et al., 2011). Dry deposition was calculated as the product of ambient air concentrations of HNO_3, NH_3, p-NO_3^-, and p-NH_4^+ (measured biweekly by the filterpack method) times dry deposition velocities for forest and grass surfaces inferentially estimated by Matsuda (2008). Five-year mean dry deposition of N was in the range of 1–7 kg N ha^{-1} a^{-1} with the highest concentrations at sites near the Sea of Japan and western Japan (roughly equivalent to S dry deposition). A review of HNO_3, particle-NO_3^- and particle-NH_4^+ dry deposition velocities published in Endo et al. (2011) indicated that they had higher maximum values than the two North American networks (CASTNET and CAPMoN) described in Section 4.6.1. Unlike North America, Africa and Australia, where data were available for evaluation, data from this study were not available for use in this assessment. Most other measurements of dry deposition were made over short time periods at specific locations, e.g., Shen et al. (2009) and Kim et al. (2010). These two publications show different seasonal patterns of dry deposition depending on the N species and document annual dry deposition of N of up to 55 kg N ha^{-1} a^{-1} in north China and 3.08 kg N ha^{-1} a^{-1} over the Yellow Sea.

The lack of measurements makes it necessary to assess dry deposition on the basis of the 2001 HTAP ensemble-mean modeling results, which are shown in Fig. 4.7a for N. Fig. 4.7a identifies two areas of maximum N dry deposition in Asia with values ranging from 10 to 20 kg N ha^{-1} a^{-1}. The first area is located in northeast Pakistan, northeast India and Bangladesh and the second in eastern China. Moderately high levels of dry deposition in the 4–10 kg N ha^{-1} a^{-1} range are predicted in the rest of Pakistan, India, and most of East Asia in general. Low levels of dry deposition < 1 kg N ha^{-1} a^{-1} are predicted over most of western China, Mongolia and the Russian Federation except in the southwest, and very low values of <0.2 kg N ha^{-1} a^{-1} over the northern Russian

Federation and the adjacent Arctic/north Pacific Oceans. The minimum and maximum dry deposition values were 0.03 kg N ha^{-1} a^{-1} in the northeastern Russian Federation and 19.1 kg N ha^{-1} a^{-1} in eastern China. Of note is the fact that high levels of dry deposition are predicted in the coastal zones of the Indian and North Pacific Oceans – indicating a major influence of transported emissions from the continent and ocean-going ship emissions. In general, the dry deposition pattern for Asia corresponds closely to the large scale pattern of NO_x–N + NH_3–N emissions (Fig. 4.1c) with allowances for the transport and deposition of continental emissions to the coastal ocean zones.

The relative contribution of $N_{reduced}$ to N dry deposition is shown in Fig. 4.7b. As expected from the NO_x–N and NH_3–N emission patterns (Fig. 4.1a and b), $N_{reduced}$ appears as the main source of N dry deposition in and near the intensive agricultural areas of Asia, especially in India and East Asia where the ratio of $N_{reduced}$ to N exceeds 60%. $N_{oxidized}$ is the major contributor in the rest of Asia, particularly in the northern Russian Federation and Japan where the ratio of $N_{reduced}$ to N is less than 30%.

4.6.5.3. Total deposition of N. As with dry deposition, total deposition can be assessed only from the 2001 HTAP ensemble-mean modeling results. The total deposition pattern of N is shown in Fig. 4.8a. Total deposition levels over Asia range from <1 kg N ha^{-1} a^{-1} in the northern Russian Federation and the deserts of China and Mongolia, to 40 kg N ha^{-1} a^{-1} in the intensely cultivated and populated areas of northern India and eastern China. The latter areas, in fact, are predicted to receive the highest deposition of nitrogen on the globe (see Fig. 4.8a). As with wet and dry deposition, large sections of the Indian and Pacific Oceans near the continental coastlines are shown to receive high deposition values in the range of 10–20 kg N ha^{-1} a^{-1}.

Fig. 4.8b and c provide further insight into total deposition in Asia. Fig. 4.8b, which shows the % ratio of dry to total deposition of N, indicates that dry deposition is more important than wet deposition in the southwest portion of the domain, i.e., from Iran to northern India and along the northern border of China. Elsewhere, wet deposition is the major contributor, particularly in the northern Russian Federation and the Arctic Ocean where deposition levels are very low. Fig. 4.8c, which shows the % ratio of $N_{reduced}$ to N, indicates that total deposition is strongly dominated by $N_{reduced}$ in the intensive agricultural areas of Pakistan, India and most of East Asia including the eastern half of China (ratios > 60%). The rest of Asia, in general, has roughly equal contributions of $N_{oxidized}$ and $N_{reduced}$ (ratios = 50 ± 10%) with $N_{oxidized}$ being the major contributor ($N_{reduced}$ < 40%) in parts of Iran, Turkmenistan, Uzbekistan and Kazakhstan, the Republic of Korea, Japan and the Arctic Ocean.

4.6.6. Oceania

Oceania is defined as Indonesia, Malaysia, Australia, Papua New Guinea, New Zealand and the South Pacific region. The number of sites in Oceania where precipitation has been collected is small, and the areal coverage is sparse. The sites that met this assessment's screening criteria are located in Australia (Wagga Wagga and Coffs Harbour) and in Southeast Asia (Bukit Kototabang in Indonesia and Tanah Ratah and Danum Valley in Malaysia). Two sites in Australia (Cape Grim and Burrup Peninsula) did not meet our screening criteria principally because of short data records, but are discussed below because of their importance for the characterization of deposition in the area. Measurement data were provided by the Acid Deposition Monitoring Network in East Asia (EANET) and the Bureau of Meteorology/Australian Commonwealth Scientific and Industrial Research Organisation (CSIRO) Marine and Atmospheric Research (BoM/CMAR). No data exist for areas such as New Zealand, Papua New Guinea or the South Pacific islands.

4.6.6.1. Precipitation-weighted mean concentrations and wet deposition of N. The measured 3-year average (2000–2002) precipitation-weighted mean concentrations of N at Coffs Harbour and Wagga Wagga (Australia) were 0.26 and 0.32 mg N L^{-1}, respectively, and 0.11 mg N L^{-1} at both Bukit Kototabang (Indonesia) and Tanah Rata (Malaysia) (Fig. 4.2a). The highest wet deposition of N measured in Oceania was at Coffs Harbour (3.73 kg N ha^{-1} a^{-1}), followed by Tanah Rata (3.13 kg N ha^{-1} a^{-1}), Bukit Kototabang (1.99 kg N ha^{-1} a^{-1}), and Wagga Wagga (1.95 kg N ha^{-1} a^{-1}) (Fig. 4.3a).

In 2005–2007, concentrations of N in precipitation were 0.21 mg N L^{-1} for Bukit Kototabang, 0.12 mg N L^{-1} for Tanah Rata, and 0.04 mg N $L^{-1}$for Danum Valley. Wet deposition of N was highest in Bukit Kototabang (4.61 kg N ha^{-1} a^{-1}) followed by Tanah Rata (3.47 kg N ha^{-1} a^{-1}) and Danum Valley (1.09 kg N ha^{-1} a^{-1}). No data are available from regionally-representative sites in Australia for 2005–2007.

Wet deposition measurements were made, however, at a site in northwest Australia (Burrup Peninsula) for two 1-year periods (September 2004 to August 2005 and September 2007 to August 2008). The 1-year precipitation-weighted mean concentrations and wet deposition estimates of N at this site during each of those periods were 0.13 mg N L^{-1} and 0.17 mg N L^{-1} and 0.23 kg N ha^{-1} a^{-1} and 0.74 kg N ha^{-1} a^{-1}, respectively. The difference in the deposition flux for the two annual periods was due largely to differences in precipitation depth, i.e., 17.1 cm in the first period and 44.0 cm in the second.

Although not included in our database because of the urban nature of the site, N wet deposition of 21.09 kg N ha^{-1} a^{-1} was measured at Serpong, Indonesia. It is mentioned here to show that N wet deposition in areas with large anthropogenic impacts is more than an order of magnitude higher than in areas such as Tanah Rata or Bukit Kototabang, which are largely free from anthropogenic influences.

Measured and modeled N wet deposition (Fig. 4.5c) are generally in good agreement, with measured deposition at Tanah Rata and Bukit Kototabang-closely matching with the model-predicted range of 2–4 kg N ha^{-1} a^{-1}. The modeled wet deposition is 1–2 kg N ha^{-1} a^{-1} both for Wagga Wagga and Coffs Harbour. The flux for Wagga Wagga is in this range and that at Coffs Harbour is only slightly higher at 3.42 kg N ha^{-1} a^{-1}. The model-predicted deposition over the Burrup Peninsula is 0.2–0.3 kg N ha^{-1} a^{-1}, close to the measured value of 0.48 kg N ha^{-1} a^{-1} averaged over the two annual periods. This comparison is compromised by the variation in precipitation depth for the two years, although the average precipitation depth was 30.6 cm which is close to 27.5 cm, the average from 1972 to 2009.

The $N_{oxidized}$, $N_{reduced}$ and N measurements made at the Cape Grim Baseline Air Pollution Station (not discussed above) are particularly noteworthy because Cape Grim is a global baseline station of the Global Atmosphere Watch Programme of the World Meteorological Organization. By definition, the concentrations of N in precipitation measured at this site represent the subset of Southern Hemisphere "baseline" concentrations because they were collected only during so-called "baseline" precipitation events when the precipitation was not influenced by local or regional anthropogenic N emissions (or, to be specific, when the wind direction was from the Southern Ocean). As mentioned in Section 3.6.6, precipitation events from other wind directions were not sampled so it was not possible to estimate annual precipitation-weighted mean concentration and wet deposition values for this site.

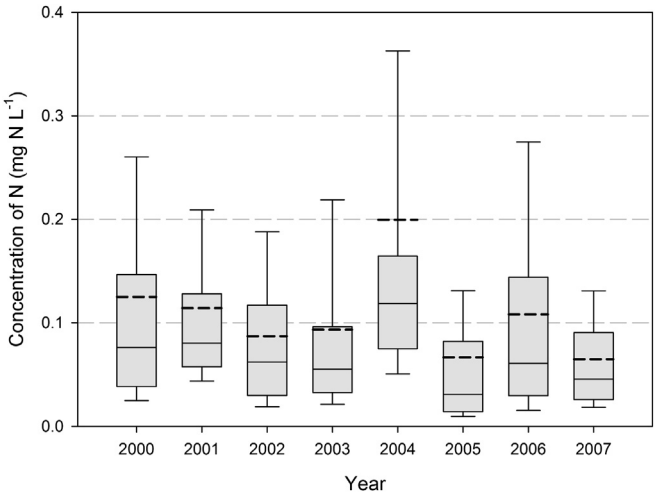

Fig. 4.20. Concentrations of N in baseline rain at the Cape Grim Baseline Atmospheric Pollution Station from 2000 to 2007, showing the median and mean (dotted line) concentrations, the 25th and 75th percentiles and the 10th and 90th percentiles.

Fig. 4.20 presents the annual median and mean (dotted line) concentrations, the 25th and 75th percentiles and the 10th and 90th percentiles of N in the *baseline* rain events from 2000 until 2007. The lowest annual median concentration was recorded in 2005 when the median, maximum and minimum concentrations were 0.031, 0.362 and 0.004 mg N L^{-1}, respectively, for 25 events. The highest median was recorded in 2004 when for 26 events the median, maximum and minimum concentrations were 0.119, 1.686 and 0.032 mg N L^{-1}, respectively. Over the 8 years of sampling, the total annual average precipitation depth at the Cape Grim station was 63.4 cm while the total *baseline* depth averaged 12.2 cm or 19.6% of the total. The fraction of baseline depth to the total precipitation depth varied over the years from 13.0% to 31.7%. The concentration of N in baseline precipitation is therefore representative only of precipitation falling on the southern Indian Ocean west of Australia and not the total annual precipitation. The HTAP modeling results in Fig. 4.5a show N concentrations in the range of 0.05–0.1 mg N L^{-1} for this marine environment, and this is in accord with the observations that range from 0.03 to 0.12 mg N L^{-1} and average 0.11 mg N L^{-1}. The observations of N concentrations at the Cape Grim station are consistent with the model outputs for areas in the Atlantic, Pacific and Arctic oceans.

The relative contribution of $N_{reduced}$ to N wet deposition is shown in Fig. 4.6a. The lowest ratios of $N_{reduced}$ to N wet deposition in the range of 30–40% occur in central Australia and some oceanic areas. The highest ratios of 70–85% occur near Jakarta, New Zealand and an area of the Southern Ocean. Oceanic areas south of Australia and large areas of Java, Sumatra and southern Kalimantan have ratios in the range of 60–70%.

4.6.6.2. Dry deposition of N. Oceania is one of the four regions that routinely estimated measurement-based N dry deposition using the inferential technique (see Section 2). Estimates were made at one site in Australia (Burrup Peninsula) for the periods 2004–2005 and 2007–2008, and at one site in Malaysia (Tanah Rata) for the annual periods 2000 and 2001. The estimates at both sites were based on monthly passive sampler measurements of gaseous NO_2, HNO_3 and NH_3 (Ferm, 1991; Ayers et al., 1998). The dry deposition velocities applied at Burrup Peninsula and Tanah Rata were 0.0021 m sec^{-1}, 0.0090 m sec^{-1-} and 0.0095 m sec^{-1-}, respectively, for NO_2, HNO_3 and NH_3. For NO_2 and HNO_3, the velocities were taken from an inferential model (Manins, 1994) and were used previously to estimate dry deposition in Indonesia (Gillett et al., 2000); the dry deposition velocity for NH_3 was taken from Puxbaum and Gregori, (1998). The monthly calculated fluxes were summed to give the estimated annual dry deposition. There are large uncertainties inherent with passive sampling measurements (10%) and deposition velocities (15% according to Puxbaum and Gregori, 1998); nevertheless, the dry deposition of $N_{oxidized}$ (NO_2, HNO_3) and $N_{reduced}$ (NH_3) presented here allows a comparison of the N dry deposition with the N wet deposition. The overall uncertainty of the dry deposition estimates is around 25% and the estimates do not include the dry deposition estimates of p-NO_3^-, p-NH_4^+ or organonitrates, which are very difficult to quantify. This is mainly due to the uncertainty in the deposition velocities as a function of particle size, the particle size distribution during the measurement period and the chemical composition of the particle.

The average annual dry deposition values of $N_{oxidized}$ and $N_{reduced}$ at the Burrup Peninsula for the 2004–2005 and 2007–2008 annual periods was 0.55 ± 0.14 kg N ha^{-1} a^{-1} and 0.67 ± 0.17 kg N $ha^{-1}a^{-1}$, respectively, giving a dry deposition of N of 1.22 ± 0.31 kg N ha^{-1} a^{-1}. The estimated average annual dry deposition of $N_{oxidized}$ at Tanah Rata for the period 2000 and 2001 was 1.15 ± 0.28 kg N ha^{-1} a^{-1}, about double the flux measured at the Burrup Peninsula, while the median annual deposition of $N_{reduced}$ was 12.81 ± 3.20 kg N ha^{-1} a^{-1} giving a dry deposition of N of 13.96 ± 3.48 kg N ha^{-1} a^{-1}. This very high dry deposition estimate of $N_{reduced}$ is consistent with the high wet deposition measured at that site and represents about 92% of the N dry deposition. The reason for the high $N_{reduced}$ wet and dry deposition during 2000 and 2001 is likely the use of fertilizer in the tea plantations and market gardens that abound in the area.

The 2001 HTAP ensemble-mean modeled pattern of dry deposition of N over Oceania (Fig. 4.7a) provides detailed insight into the spatial distribution of N dry deposition over the region. The model results show that at Tanah Rata the dry deposition of N was in the range of 2–3 kg N $ha^{-1}a^{-1}$ in 2001. The flux at Burrup Peninsula 0.4-1.0 kg N ha^{-1} a^{-1} during the 2004–2005 annual period. The measurement-based inferential annual dry deposition estimates at Tanah Rata during 2001 (17.01 kg N $ha^{-1}a^{-1}$) and at Burrup Peninsula for the period 2004–2005 (0.81 kg N ha^{-1} a^{-1}) were considerably higher than the HTAP modeled estimates. It is not clear how much of this difference is due to measurement versus model uncertainty and how much is due to the different time periods in the case of the Burrup Peninsula.

Considering Oceania as a whole, the 2001 ensemble-mean dry deposition pattern of N in Fig. 4.7a shows that the highest fluxes correspond to the high population centers in Oceania. This is true for southeastern Australia near Sydney and Melbourne, near Christchurch and Wellington in New Zealand, and the large population centers of Kuala Lumpur and Jakarta. In Australia, the dry deposition of N will be influenced by biomass burning events in the summer period, particularly in the north and down the southeast in the 1–2 kg N ha^{-1} a^{-1} areas of the continent. The $N_{oxidized}$ flux is due primarily to NO_x emissions from motor vehicles, power generation from fossil fuels, industry and domestic heating. The emission sources of $N_{reduced}$ deposition are to the same as sources of $N_{reduced}$ with the additional source of fertilizer use.

Fig. 4.7b shows the relative contribution of $N_{reduced}$ to N dry deposition across Oceania. The highest ratios in the 85%–100% range are found mainly in the southern Ocean and the south Island of New Zealand. The former is mainly due to lower NO_x–N emissions relative to NH_3–N emissions in the oceanic areas (as shown in Fig. 4.1a,b) and the latter is mainly due to agricultural activities such sheep farming in the area. The lowest ratio of $N_{reduced}$ to N is in the range of 15–20% and is found in the center of Australia where the ground cover and precipitation depth are both low and agricultural

activities are nonexistent, resulting in low emissions of NH_3–N compared with other parts of the continent. The ratio increases over southern and eastern Australia due to increased NH_3–N emissions from crops, pastures and from higher densities of naturally occurring biomass. Generally the modeled ratios of $N_{reduced}$ to N are greater than 50% in areas of higher population centers such as southeastern Australia, Java, Sumatra and peninsular Malaysia. The annual average of the measured ratios of $N_{reduced}$ to N at the Burrup Peninsula and Tanah Rata are 54% and 92%, respectively. These ratios are high at both sites compared with the ensemble-mean modeled outputs of 40%–50% and 30%–40% at the Burrup Peninsula and Tanah Rata respectively, as shown in Fig. 4.7b.

4.6.6.3. Total deposition of N. Fig. 4.8a shows the 2001 ensemble-mean modeled pattern of N total deposition. Measurement-based estimates of total deposition of N are available only at the Burrup Peninsula site for the two 1-year periods in 2004–05 and 2007–08, and Tanah Rata for the two 1-year periods of 2000 and 2001. The fluxes were 1.58 kg N ha^{-1} a^{-1} and 1.82 kg N ha^{-1} a^{-1}, respectively, at the Burrup Peninsula and 14.23 kg N ha^{-1} a^{-1} and 19.79 kg N ha^{-1} a^{-1}, respectively, at Tanah Rata. The measured values at the Burrup Peninsula compare reasonably to the model-based range of 0.8–1.0 kg N ha^{-1} a^{-1}, shown in Fig. 4.8a, albeit for the different period of 2001. At Tanah Rata, total deposition of N was higher than the model-based range of 4–10 kg N ha^{-1} a^{-1}. Note, however, that this pattern includes both gaseous and particulate dry deposition whereas the measurement-based inferential estimates include only the gaseous species NO_2, HNO_3 and NH_3.

The model-based pattern of deposition indicates that the highest deposition occurs over areas of high population density such as Java, Sumatra, Peninsula Malaysia and the southern area of Kalimantan which have fluxes of 4–10 kg N ha^{-1} a^{-1}. As expected, the lowest fluxes are found over oceanic areas where there is little anthropogenic influence and the flux varies from 0.2-0.4 kg N ha^{-1} a^{-1}. The fluxes over the oceanic areas increase to 0.4–0.5 kg N ha^{-1} a^{-1} and then to 1–2 kg N ha^{-1} a^{-1} near continental areas. The east coast of Australia has a flux of 2–4 kg N ha^{-1} a^{-1} as have the more populated areas around Christchurch and Wellington in New Zealand. Most of the remaining continental areas in Oceania have fluxes of 1–2 kg N ha^{-1} a^{-1}, as shown in the ensemble-mean model predictions of Fig. 4.8a. The highest fluxes of total deposition of N suggested by the HTAP model are 4–10 kg N ha^{-1} a^{-1}. These high fluxes appear over the continental areas of Sumatra, Java, Malaysia and southern Kalimantan. This is due to a combination of higher population densities with emissions of 4–10 kg N ha^{-1} a^{-1} for NO_x–N + NH_3–N (Fig. 4.1c), and higher precipitation depths compared to the Australian continent.

Fig. 4.8b shows the 2001 modeled pattern of the % dry deposition to total deposition of N across Oceania. The pattern shows that the highest ratios for this measure occur over the Australian continent. They range from 70 to 85% along the west coast and 60–70% in the west and southeast of the continent. Most of the rest of the Australian continent has a ratio of 50–60%. The oceanic areas close to continental shelves are 30–40% and reduce to 15–30% over the open ocean. The ratio over most of the other continental areas in Oceania is 30–40%, with some small areas of 40–50% over Kalimantan. The lowest percentage of dry deposition is in the range of 0–15%, and occurs in the northeast of Oceania around the Bismarck Sea, and southwest of Sumatra, in the Indian Ocean. The Burrup Peninsula has measured ratios of 86% and 59% for the two annual periods in 2004–05 and 2007–08. The mean of these is 72% which is close to the HTAP modeled ratio of 60–70% for this area. At Tanah Rata the ratios of dry deposition to total deposition of N are 76% and 86% in 2000 and 2001, respectively. This is significantly higher than the 30–40% suggested by the HTAP model results in Fig. 4.8b. This is probably due to the high dry deposition of $N_{oxidized}$ at this site compared to the ensemble mean suggested by the model.

Fig. 4.8c shows the 2001 modeled pattern of the % ratio of total deposition of $N_{reduced}$ to total deposition of N across Oceania. The pattern shows that the lowest ratio of 30–40% is found over the center of Australia and the Indonesian provinces of West Papua and North Maluku. This may be due to the low emissions of NH_3–N over central Australia and possibly due to high NO-N emissions from lightening over the Indonesian provinces. The highest ratio of 85–90% is found only in the east coast of the south island of New Zealand, and may be due to intensive sheep farming on the Canterbury Plains. The oceanic areas have ratios of 50–60% near the continental shelves and increase to 60–70% further south and then to 70–85% over the Southern Ocean. In general the more populated areas of Oceania have ratios of $N_{reduced}$ to N in the range of 60–70%.

At the Burrup Peninsula the annual average ratio of $N_{reduced}$ to N in total deposition is 55%, which compares quite closely with the modeled value of 40–50% presented in Fig. 4.8c. At Tanah Rata the ratios for 2000 and 2001 are 81% and 85% respectively, and as Fig. 4.8c shows, this is higher than the modeled value of 50–60%. The higher ratio shown by the measurements compared to the model is probably due to higher $N_{reduced}$ dry deposition values at this site.

4.7. Summary, gaps and uncertainties

Globally, the 3-yr average precipitation-weighted concentrations of N within the 2000–2007 period are highest in eastern China, western Russian Federation and northern Italy (Ispra) and lowest in parts of the United States (including Hawaii) and Malaysia. The highest levels of N deposition occurred in eastern North America, southern Europe, northeast India, southeast Asia and northern Oceania and the lowest levels in western North America, northern Europe, and the Russian Federation. Not unexpectedly, the broad features of the spatial patterns of global concentrations and deposition bear a close resemblance to those of the global pattern of NO_x–N + NH_3–N emissions with high values occurring in high emission areas and low values in low emission areas.

Large areas of the globe continue to have little or no measurement coverage; thus, model estimates are needed to fill the spatial gaps between sites. Globally, the measured and modeled precipitation-weighted mean concentrations and wet deposition compare reasonably well – with evidence of model underprediction of concentrations at sites in North America (Canada and western U.S.), extreme southern and northern Europe, parts of East Asia, central Africa, Brazil, and northern Oceania, and of wet deposition in Europe and particularly Asia. Ensemble-mean model estimates were used to determine the N budget over the continents and oceans. Major changes in the anthropogenic emissions of NO_x–N and NH_3–N occurred from 2000 to 2007 and have been documented in various parts of the world, including major NO_x–N emission reductions in Europe, eastern Canada, and the eastern U.S., and major NO_x–N and NH_3–N emission increases in India, China and Africa. Consistent with the aforementioned continental changes in emissions, median wet deposition declined in North America and Europe and increased in Asia and Africa.

In general, $N_{oxidized}$ accounts for greater than 50% of N wet deposition in the far eastern and western regions of the U.S., the northern Atlantic Ocean and the areas of very low precipitation including the major deserts, Antarctica and the Arctic. In contrast, $N_{reduced}$ accounts for >50% in most of Europe and the intensive agricultural areas of central North America, Mexico and large parts of South America, India, and East Asia, as well as in the low deposition areas of the southern Atlantic, southern Pacific and Southern

Oceans. As was the case for S, routine measurement-based inferential estimates of N dry deposition were only available in North America, Africa, Australia and Japan. Similarly, measurement-based estimates of N total deposition were limited to these four locations plus Europe (via throughfall estimates). In spite of Europe's long history of routine ambient concentration measurements, inferential dry deposition estimates have yet to be made.

Based on the HTAP ensemble-model patterns, the highest ratio of dry to total deposition is predicted in the driest areas of the world including southwestern North America, southwestern South America, and southwestern and northern Africa. Other regions of the world receive roughly equal contributions of dry and wet deposition. Projected increases of N emissions from agricultural soils (e.g., from the increasing use of synthetic fertilizers), over tropical forests (e.g., from biomass burning), and in rapidly developing locations around the globe emphasize the need for long-term observations of wet and dry deposition to understand the future impacts.

The lack of inferential measurement-based estimates of $N_{oxidized}$ and $N_{reduced}$ dry deposition is a major problem and routine measurements of oxidized and reduced nitrogen species in air are needed at regionally representative stations worldwide. Routine measurements of NO_2 and NH_3 in air have been called for in acid rain programs for decades and are still not in place. Filter-based measurement methods used today suffer from volatilization and absorption artifacts and more accurate measurements are needed. Inferential dry deposition models, including bidirectional surface exchange of NO_2 and NH_3, must be improved, evaluated and applied routinely to the ambient air measurements to estimate the dry deposition of these species.

5. Sea salt and base cations

This section addresses two specific qμestions:

- What do measurements and models tell us about the global deposition of sea salt?
- What do measurements tell us about the deposition of the sum of the following base cations: Na^+, Ca^{2+}, Mg^{2+} and K^+?

The major sources of Na^+, Ca^{2+}, Mg^{2+} and K^+ in the atmosphere are sea salt aerosols, aeolean dust, biomass burning, volcanic dust, industrial emissions, and transportation-related particulate matter (i.e., road and off-road dust and vehicle emissions). Both sea salt and aeolean-derived dust exist as coarse and fine particles in the atmosphere. Base cations in aerosols and hydrometeors are important to gas-particle partitioning, heterogeneous chemistry and radiative transfer in the atmosphere (Sofiev, 2011; Erickson et al., 1999; Erickson and Duce, 1988).

Rodhe et al. (2002) present global-scale estimates of mineral deposition based on the model-simulated deposition of soil-derived calcium. They show that deposition is heaviest in and downwind of arid regions, especially northern Africa and central and south Asia. Calcium derived from industrial and agricultural activities, as well as magnesium and potassium, were not included in this simulation. An evaluation of modeled and measured base cation deposition in Europe by Lee et al. (1999) confirms that soil-derived calcium from arid regions is an important contributor to base cation deposition, but also suggests that agricultural activities are a major regional source of airborne calcium. Authors of both studies point to large uncertainties in quantifying the sources and deposition rates of base cations.

In North America, a number of publications present regional and large-scale spatial and temporal patterns of base cations and sea salt ions in the United States based on long-term observations from national networks. Brahney et al. (2013) determined that Ca^{2+} wet deposition increased significantly from 1994 to 2010 in three areas of the western U.S. They attributed these increases to increasing mineral aerosol emissions caused by increased aridity, more frequent dust storms and increasing influences of human activity upwind. Lehmann et al. (2005) concluded that from 1985 to 2002, earth crustal cation (sum of calcium, magnesium and potassium) concentrations in precipitation increased significantly at 23% of the National Trends Network sites in the U.S. (virtually all in interior southern and midwestern states), and decreased at 40% ($p \leq 0.10$) of sites, with the largest decreases occurring in the northeastern and northwestern states. Tessier et al. (2002) examined base cation changes in precipitation in the northeastern U.S. over a 15-year period (1985–1999) during which there were substantial SO_2 emission reductions. Focusing on base cation concentrations at 12 NTN sites sufficiently inland to minimize the potential confounding effects of sea salt, they found significant decreases of Mg^{2+} at all 12 sites, of Ca^{2+} at 11 of 12 sites and of K^+ at 6 of 12 sites. In a similar study that compared $Ca^{2+} + Mg^{2+}$ concentrations in 1990–1994 with 1995–1998, Butler et al. (2001) found concentration increases at most eastern U.S. sites. Each of these studies examined somewhat different time periods and different sets of sites.

The fact that the temporal changes conflict in space and time across North America indicates the complexity of the source–receptor relationships for base cations and the clear need for additional studies to focus on the sources and scavenging mechanisms of base cations. These regional-scale studies were complemented by local, site-specific, and/or shorter-term studies of mineral base cations in precipitation (Aleksic et al., 2009; Grimshaw and Dolske, 2002; Kelly et al., 2002) in cloud-water (Hutchings et al., 2009; Aleksic et al., 2009; Anderson et al., 1999), and in snow cores at high elevation sites in the U.S. (Hidy, 2003; Clow et al., 2002; Turk et al., 2001) and Canadian Rocky Mountains (Lafreniere and Sinclair, 2011).

In South America, recent studies have been undertaken because of concerns over the effects of population growth, urbanization, increased fossil fuel consumption and industrialization, land/forest clearing, and forestry and agricultural biomass burning. The possibility that lower air quality might result in increased acidic precipitation or other deleterious impacts led to numerous short-term, exploratory studies, especially in Brazil (Lara et al., 2001; Pelicho et al., 2006; De Mello and De Almeida, 2004; Migliavacca et al., 2004; Germer et al., 2007; Schroth et al., 2001; Coelho et al., 2011). Most investigators collected wet-only samples, either by using automated collectors or by manually exposing funnel/bottle collectors only during precipitation. Many of these studies identified soil dust, agriculture, and biomass burning as sources of mineral base cations in precipitation. Base cation measurements in precipitation have also been published for other sites in South America by Zunckel at al. (2003), Gonzalez and Aristizabel (2012), Grigholm et al. (2009), Germer et al. (2007), Campos et al. (2007) and Grigholm et al. (2009). Other studies addressed specific point, area and urban sources on deposition chemistry but these are not within the scope of this assessment.

In Europe, spatial and temporal analyses of base cations and sea salt in precipitation and wet deposition are presented in a few regional studies based on measurements and model estimates (Lövblad et al., 2004; Van Loon et al., 2005; Hellsten et al., 2007; Tsyro et al., 2011; Tørseth et al., 2012). In most areas of Europe, the anthropogenic contribution of mineral base cations is small, although it is relatively larger in northern Europe compared to the more arid south (Tørseth et al., 2012). Saharan dust outbreak events have a large impact on levels of base cation wet deposition (and ambient particulate matter) in the south of Europe (Querol et al.,

2009), and occasionally, when atmospheric transport conditions are favorable, lead to observable episodes in Scandinavia (Stuut et al., 2009). Base cations have decreased over the past 30 years (Tørseth et al., 2012), with an average decreasing trend of calcium in precipitation of 47% from 1980 to 2009 and 26% from 1990 to 2009 (Tørseth et al., 2012). In the early 1990s, the closing of many lignite-fired power stations and iron and steel smelters as well the implementation of effective abatement technologies for sulfur also led to a reduction of base cation emissions (Lövblad et al., 2004; Hellsten et al., 2007).

The level of deposition of sea salt ions in Europe is, to a large extent, determined by the distance from the sea and the significance of sea salt episodes. Highest deposition episodes are seen at coastal sites in Norway, Island, Ireland, UK, France and Spain (Tsyro et al., 2011). In addition to these regional studies, several country-scale and short-term studies were carried out aimed at characterizing the relative composition and sources of major ions, including mineral and sea-salt, at a variety of locations throughout Europe, for example: Belgium (Andreacute; et al., 2007), Romania (Bytnerowicz et al., 2005), Spain (Avila and Rodà, 2002), France (Deboudt et al., 2004), Italy (Aiuppa et al., 2003), Greece (Nastos et al., 2007), Switzerland (Thöni et al., 2008), Serbia (Goloboèanin et al., 2008), and Turkey (Tuncer et al., 2001; Topcu et al., 2002).

A recent regional scale assessment of precipitation composition and deposition in East Asia (EANET, 2011) documented that Na^+ and Cl^- concentrations are elevated at remote islands and coastal sites. A regional modeling study on acidic deposition in East Asia during the wintertime (Han et al., 2006) showed relatively high wintertime concentrations of non-sea-salt Ca^{2+} in western and northern China, as well as southern Mongolia. A number of local-scale studies, most of which were short-term campaigns often designed around precipitation events (e.g. monsoon), were conducted throughout Asia at a variety of non-urban sites, for example: India (Singh et al., 2006); China (Aas et al., 2007), Tibet (Li et al., 2007); Japan (Seto and Hara, 2006; Rahman et al., 2006); Jordan (Al-Momani, 2003; Al-Khashman, 2005a, 2005b, 2009), Israel (Herut et al., 2000). A large majority of these studies found that Ca^{2+} was the dominant ion in precipitation across Asia, along with SO_4^{2-}, as a result of the influence of crustal material. In India, concentrations of Ca^{2+} in precipitation were usually observed to be highest at the start of the monsoon season, declining thereafter as suspended dust washed out. At coastal sites throughout Asia, the predominant ions were Ca^{2+}, Cl^- and Na^+ due to the influence of sea salt.

In Africa, long-term studies of the chemical composition of precipitation and wet deposition over the last decade are based on precipitation event measurements at IDAF network sites (Yoboué et al., 2005; Mphepya et al., 2004, 2006; Galy-Lacaux et al., 2009; Sigha-Nkamkjou et al., 2003). According to these studies, Ca^{2+} is the most important species among base cations in precipitation over Africa, with the exception of Skukuza, South Africa where Cl^- and Na^+ were higher than Ca^{2+} due to the influence of sea salt (Mphepya et al., 2006). The concentration gradient for $nssCa^{2+}$ decreases from the dry savanna to wet savannas to equatorial forests (Yoboué et al., 2005). Calcium in the west-central African ecosystems of dry and wet savannas was significantly correlated with total carbonates, Mg^{2+} and SO_4^{2-} (Yoboué et al., 2005; Sigha-Nkamkjou et al., 2003; Galy-Lacaux et al., 2009), confirming the important influence of particles from the Sahara desert and semi-arid regions on the chemical composition of African rainfall.

Published studies of sea salt and base cation composition of precipitation in Oceania over the last decade are scarce and most were short-term campaigns with variable objectives and results. One of these, Carillo et al. (2002) measured total deposition of base cations (K^+, Mg^{2+}, and Ca^{2+}) for up to seven years in Hawaii and found sea salt to be the main source of cations with biomass burning and Asian dust also being significant in some years. Jickells et al. (2005) determined that the supply of dust to the oceans is very important in maintaining oceanic primary production and CO_2 uptake but is sensitive to climate change. They also show that the dust supply from the North African and Asian deserts directly affects the tropical North Atlantic and temperate North Pacific, with different effects. A composite of three published modeling studies was used to generate a map of dust fluxes to the world's oceans. Their analysis points to possible impacts that could amplify or diminish future global climate change, noting that current understanding contains considerable uncertainties and suggesting several research priorities including the need to better understand dust deposition processes.

5.1. Global deposition of sea salt

Salt water bodies are the dominant source of airborne sea salt aerosols. Winds over the water form breaking waves which, in turn, lead to the formation of bubbles. The bubbles, upon bursting, are responsible for the injection of sea water droplets into the atmospheric surface layer (Sofiev et al., 2011; Vignati et al., 2009; O'Dowd and Leeuw, 2007; Fairall et al., 1983). Since oceans constitute the world's main salt water bodies, they are the dominant source of sea salt particles.

As mentioned above, this section addresses the question: what do measurements and models tell us about sea salt deposition? Fig. 5.1a displays the 2001 HTAP ensemble-mean wet deposition of sea salt based on the outputs of 8 models. In most areas of the world, deposition over the oceans is more than an order of magnitude higher than over the land surfaces. Heaviest wet deposition (>100 kg ha^{-1} a^{-1}) occurs in the northernmost and southernmost open (and generally ice-free) oceans. Both the number and size of sea salt particles emitted by breaking waves increase with wind speed (Sofiev et al., 2011; Vignetti, 2010; O'Dowd and Leeuw, 2007), and these areas are where high winds generate large breaking waves that produce large mass concentrations of airborne sea salt particles. Models apply these relationships in order to compute sea salt emission fluxes (e.g., Gong et al., 1997; Gong et al., 2003, Sofiev et al., 2011), and in general, sea salt deposition patterns closely parallel the emission patterns. As a result, the pattern of wet deposition over the oceans generally tracks mean windspeeds. Lowest deposition occurs in the vicinity of the tropical doldrums, where winds are frequently calm or light, and highest deposition accompanies the strong winds over mid and high-latitude oceans.

Superimposed on the modeled wet deposition pattern in Fig. 5.1a are measurement-based estimates of sea salt wet deposition (3-year average) at sites located within 100 km of salt water coastlines. These estimates were derived from measured values of Na^+ wet deposition using the WMO method (WMO/GAW, 2004) developed originally by Keene et al. (1986). The conversion equation is as follows:

$$\text{Sea Salt}_{wd} = Na^+_{wd}/0.307 \quad (5.1)$$

where "*wd*" represents wet deposition and Na^+_{wd} represents the 3-year annual average wet deposition of sea salt mass (in kg ha^{-1} a^{-1}) and 0.307 is the ratio of Na^+ to total sea salt mass (Pilson, 1998). Cl^- was not included in Eq. (5.1) because Cl^- is a non-conservative ion in sea salt aerosols when acidified by S or N species (Keene et al., 1986). The use of Na^+ in Eq. (5.1) assumes that its origin is from sea salt alone. There are, however, other sources of Na^+ in precipitation including crustal dust, road salt, and terrestrial sources. The potential for the non-sea-salt sources of Na^+ grows with distance

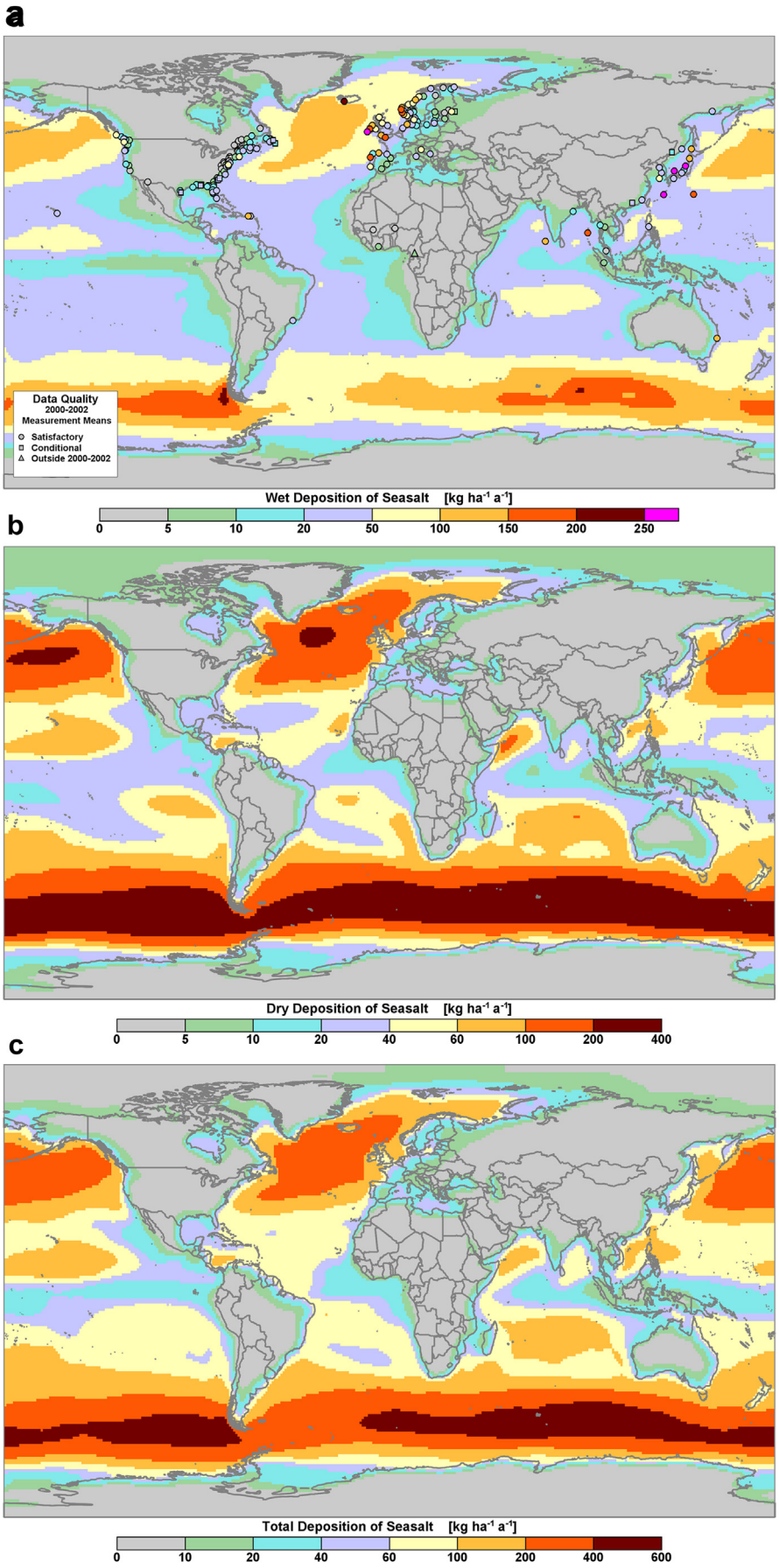

Fig. 5.1. Sea salt (a) wet deposition derived from annual average 2000–2002 precipitation measurements of Na^+ (see text) at coastal sites, superimposed on a map of 2001 ensemble-mean modeled wet deposition of sea salt, (b) modeled dry deposition and (c) modeled total deposition (kg ha^{-1} a^{-1}).

inland from the coast, so the measured estimates of sea salt wet deposition in Fig. 5.1a are shown only for those sites located within 100 km of the coast or where researchers have independently confirmed the presence of sea salt influences in precipitation further afield (most notably west central Africa). At the 170 sites plotted on Fig. 5.1a, more than 60 percent of the measurement-based wet deposition values are higher than the model-generated grid-square values, with the largest differences occurring at coastline and island locations. This is undoubtedly due to measurements being location-specific while grid-square values are areal averages.

Fig. 5.1b presents a map of the ensemble-mean estimates of sea salt dry deposition. Spatially, the distributions of dry and wet deposition mimic each another, although virtually everywhere the estimated dry deposition equals or exceeds wet deposition, even over continental margins. As with wet deposition, dry deposition decreases rapidly with distance from coastlines to the middle of continents, where it is estimated at < 5 kg ha^{-1} a^{-1}. The rate of decrease depends on the size of the sea salt aerosols, the near-coastal sea salt emission strength, the presence of topographic features, mean wind velocities, and the strength and inland penetration of coastal storms (Gong et al., 1997; Gong et al., 2002). Sea salt aerosols have been observed and modeled in both the supermicron and submicron size ranges (O'Dowd et al., 1997; Vignati et al., 2010; Sofiev et al., 2011) and modeling suggests that coastal surf-zones are important sources of sea salt aerosol emissions in addition to open oceans (Im, 2013). Thus, the modeled dry deposition of sea salt deep into the continents in Fig. 5.1b is reasonable and consistent with others (Im, 2013; Sofiev et al., 2011).

Fig. 5.1c shows the total deposition of sea salt from the sum of the 2001 HTAP ensemble-mean wet plus dry deposition estimates. Extremely high deposition, from 200 to 600 kg ha^{-1} a^{-1}, occurs in a band that encircles the earth in the southernmost open oceans. A similar feature, but with slightly lower deposition from 100 to 400 kg ha^{-1} a^{-1}, occurs in the oceans of the northern hemisphere. Although most sea salt is deposited over its oceanic source, it is deposition of sea salt to inland lakes and forests that is of ecological significance. Total deposition of sea salt to continental areas of 10 kg ha^{-1} a^{-1} or more is modeled at distances of more than 500 km inland from the oceanic sources. This is most evident in western Europe, where total deposition of sea salt of 20–40 kg ha^{-1} a^{-1} occurs at 500 km from the Atlantic coast and in southern Asia where monsoons transport and deposit sea salt hundreds of kilometers onto the Indian subcontinent (Madhavan et al., 2008). Continental saline water bodies such as Hudson Bay, the Mediterranean Sea, and the Black and Caspian Seas show sea salt total deposition footprints that extend inland from their respective shorelines, similar to along oceanic coastlines. Fig. 5.1c is particularly valuable for researchers interested in assessing the impact of sea salt on oceanic and continental ecosystems, especially those within 500 km of coastlines.

5.2. Base cations in atmospheric deposition

As mentioned earlier, precipitation chemistry measurements typically include the most abundant alkali and alkaline earth metals in precipitation: Ca^{2+}, Mg^{2+}, Na^{+}, and K^{+}. All are in particulate form in the atmosphere and none have significant gaseous precursors. Each is present in sea salt in relatively fixed proportions and in crustal dust in highly variable proportions. Some are present in plant matter, K^{+} being the most abundant and chemically available, and in other natural and anthropogenic sources. The distribution of these particle sources of mineral base cations is location-dependent and the concentrations are highly variable.

The objective of this section is to address a question related specifically to ecosystem critical loads: What do measurements and models tell us about the deposition of the following sum of base cations: $Na^{+} + Ca^{2+} + Mg^{2+} + K^{+}$? The focus is on the deposition of the base cation sum because this is a variable in the equation for calculating critical loads of forest and aquatic ecosystems (ICP, 2004; UNECE, 2004; Ouimet et al., 2006; Environment Canada, 2005; Whitfield et al., 2010). High deposition of these base cations into aquatic and terrestrial ecosystems increases the critical load of the systems and low deposition decreases the critical load. Base cation deposition reduces the effect of acidification by increasing the base cation pool in soils and, when associated with carbonates or oxides, by adding alkalinity to the soils (EMEP, 2004). In this section, the global measurement data is coupled with the TF HTAP model results to provide insight into base cation wet deposition for consideration by the critical loads community. It is important to point out that the base cation deposition term in the calculation of critical loads is for total deposition, which we cannot provide at this time. This is because total deposition requires two types of measurements: wet deposition (which are currently available) and dry deposition (which are currently not available). The latter would require routine long-term measurements of size-resolved, ion-specific, particle concentrations in air coupled with an inferential size-resolved dry deposition velocity model. Such measurements and inferential models are not available regionally or globally, so we are limited in this assessment to presenting only wet deposition estimates of the base cation sum.

Fig. 5.2a and b show the 3-year-average wet deposition of the base cation sum (in keq ha^{-1} a^{-1}) for the 2000–2002 and 2005–2007 periods, respectively. As in previous sections, several data points slightly outside the 3-year periods (i.e., non-conforming-period data) were included on the maps to improve the spatial coverage. These points appear as triangles on the maps. The screened-in wet deposition data set for the cation sum in Fig. 5.2a consisted of 436 Satisfactory, 28 Conditional and 4 Non-Conforming-Period data points and the data set in Fig. 5.2b consisted of 469 Satisfactory, 11 Conditional and 0 Non-Conforming-Period data points. Individual cation wet deposition maps appear as Figs. S19–S22 in the Addendum.

Globally, wet deposition of the base cation sum ranged from 0.01 to 11.7 keq ha^{-1} a^{-1} in 2000–2002 (Fig. 5.2a) and 0.01 to 8.5 in 2005–2007 (Fig. 5.2b). Most of the high deposition sites (i.e., >1 keq ha^{-1} a^{-1}) are located in coastal zones or islands – a reflection of the importance of sea salt Na^{+} to the sum of the base cations. The influence of land-based sources of base cations increases with distance inland from the coast. This is largely due to the influence of aeolian soil dust, road dust, biomass burning, etc. since Na^{+} is not a major constituent of most soils (except in areas covered by large salt flats such as in the western U.S.). Measurement data are too sparse in and downwind of the major aeolian dust sources of the world (e.g., the Sahara and Gobi Deserts) to identify the soil-derived pattern of base cation wet deposition in those areas. A major exception to this is wet deposition of 0.1–0.3 keq ha^{-1} a^{-1} in the central U.S., which is related to the influence of soil dust from agricultural sources.

Dry deposition estimates of base cations are not available and, at the time of writing, neither the deposition monitoring community nor the modeling community is able to provide quantitative large-scale estimates of wet, dry and total deposition of base cations needed by the critical loads community. This is an unsatisfactory situation that needs resolution through a combined monitoring and modeling effort. For monitoring, it requires an extensive network of regionally-representative collocated measurements of base cations in precipitation plus size-resolved, ion-specific, particle concentrations in air. The air concentrations would have to be used with an

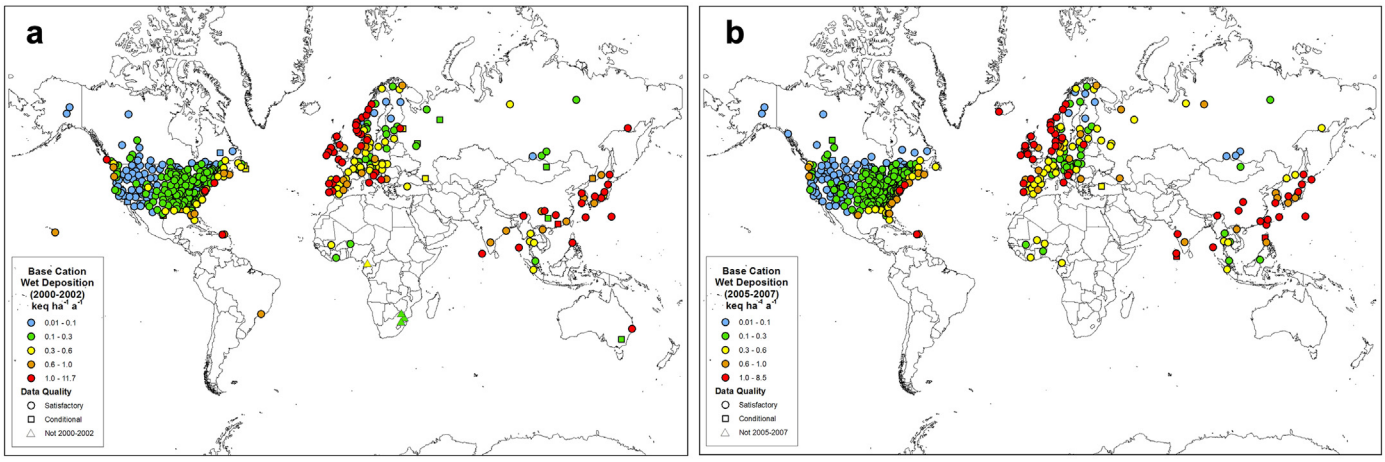

Fig. 5.2. Three-year average wet deposition of the sum of base cations (keq ha^{-1} a^{-1}) for (a) 2000–2002 and (b) 2005–2007.

inferential dry deposition velocity model to calculate dry deposition fluxes. For modeling, this will require models for the individual base cations from emission to deposition, followed by model evaluation against measurement data. Both the monitoring and modeling communities need a coordinated international effort to accomplish this.

5.2.1. Summary, gaps and uncertainties

In summary, model- and measurement-based maps of sea salt wet deposition are available, but only model-based estimates of total deposition are available. Both the measurement and modeling results show that sea salt is an important source of Na^+ wet deposition along ocean and inland sea coastlines, and the model results suggest that sea salt can be transported and deposited more than 500 km inland from coastlines. For base cations, rmeasurement-based maps of the wet deposition of $Na^+ + Mg^{2+} + Ca^{2+} + K^+$ are available to the critical loads community as partial estimates of the total deposition of the base cation sum. Neither the existing monitoring programs nor the existing models are capable of estimating wet and dry deposition of all four of these base cations or their sum. Dry deposition data are lacking worldwide and will require specialized measurements of size-resolved and ion-specific particle concentrations in air. Coordinated measurement and modeling efforts are needed worldwide to fill the large global monitoring gap and to provide estimates of total deposition. It remains for future assessments to address other important topics related to the deposition of sea salt, base cations and atmospheric dust, e.g., the influence of sea salt and soil dust on precipitation acidity and the role of deposition on the biogeochemical cycling of Aeolian dust.

6. Organic acids

Organic compounds play an important role in many atmospheric chemical processes and have a significant influence on a large number of biogeochemical processes. Global anthropogenic emissions of non-methane volatile organic compounds to the atmosphere have been estimated at 110 to 150 Tg C a^{-1} (Muller, 1992; Piccot et al., 1992) and the global biogenic emissions have been estimated at 1100 Tg C a^{-1} (Guenther et al., 1995). These emissions are of importance to the geochemical cycling of carbon (Guenther, 2002) and play an important role in the atmospheric chemical processing of ozone (Williams et al., 1997) and hydroxyl radicals (Lelieveld et al., 2008). In the oxidation processes of these compounds, organic particulate matter is formed which, in turn, affects the radiative and cloud nucleation properties of aerosols (Goldstein et al., 2009; Pöschl et al., 2010).

Recent research suggests that a substantial fraction of total atmospheric organic compounds have not been, or have very rarely been, directly measured (Goldstein and Galbally, 2007). Although our knowledge of these compounds is limited, organic material clearly influences the reactive chemistry of the atmosphere and the formation, composition, and climate impact of aerosols. Current global budget estimates of organic gases cannot account for the loss of approximately half of the non-methane organic compounds in the atmosphere (Goldstein and Galbally, 2007).

One of the first references to the contribution of organic acids to the free acidity of precipitation was made by Galloway et al. (1982) in a report on the composition of precipitation in remote areas of the world. In their assessment, a calculated anion deficiency was attributed to either an analytical error or an unmeasured anion, such as an organic anion. Follow up studies (Keene et al., 1983; Keene and Galloway, 1986; Likens et al., 1987) confirmed the presence of weak organic anions in precipitation and Keene et al. (1983) reported that formic acid (HCOOH) and acetic acid (CH_3COOH) were the dominant weak acids, contributing, on a volume-weighted basis, 63% of the total acidity in 12 samples from remote areas around the world. Other organic acids, most notably, oxalic, lactic, succinic, malonic, pyruvic, propionic, butyric, valeric, glycolic, maleic and methanesulfonic acids have also been observed in precipitation (Kawamura and Kaplan, 1983; Likens, 1983; Keene et al., 1983; Toom-Sauntry and Barrie, 2002; Brooks Avery et al., 2006), but, in general, at much lower concentrations than formic and acetic acids.

The acidity contributed by organic acids in rainwater has been estimated to be greater than or equal to the acidity due to mineral acids in the tropical rain forests of Africa (Lacaux et al., 2003), about 50% of the free acidity at several remote locations in Australia (Gillett et al., 1990), and up to 80–90% of the total acidity in the Amazon forest of South America (Andreae et al., 1988). Although a large number of mono- and dicarboxylic acids are found in rain (Kawamura et al., 2001), formic and acetic acids were found to comprise approximately 60% (from Table 1 in Kawamura et al., 2001) of the total molar quantity of carboxylic acids in rainwater in Los Angeles. These two carboxylic acids are the only two organic acids reported in most deposition papers and are therefore the only ones focused on in this report. As with other species in this assessment, the data are mainly from regionally-representative

(non-urban) sites measured in the time period from the late 1990s to the late 2000s. Some exceptions have been made in light of the scarcity of data.

Organic acids in precipitation are not routinely monitored on a long term basis at regionally representative (background) sites anywhere except in the IDAF project in Africa (IDAF is the **I**GAC (International Global Atmospheric Chemistry) **D**EBITS **Af**rica project where DEBITS represents the IGAC Deposition of Biogeochemically Import Trace Species. Formate and acetate anions, and, in some instances, propionate and oxalate anions, have been measured on a routine basis in rain water in this project since 1994. Due to the fact that these compounds biodegrade rather rapidly at room temperature in water, treatment of precipitation samples with a biocide (e.g. thymol, mercury or chloroform) or freezing during (or immediately after) collection is required at the site (Ayers and Gillett, 1988; Lacaux et al., 1992). The concentrations reported from the literature in this assessment have all been taken from reports in which preservation techniques have been used to avoid biodegradation. The typical analytical method used to quantify these anions has been ion chromatography, which requires the acids to be fully dissociated during the analytical process. Dissociation is normally accomplished using a gradient mode of different NaOH eluent solutions which means that the reported concentrations represent total organic anions rather than the dissociated fraction at a given pH. The buffering effect of organic acids in rain samples from remote regions can be significant and Keene and Galloway developed formulas by which it can be calculated (Keene et al., 1983). To date, no international inter-laboratory comparisons of precipitation samples have included organic acid anions, e.g., the WMO/GAW/Science Activity Centre laboratory intercomparison program (http://qasac-americas.org/lis/all/44/rings). Thus, direct comparisons of literature values are less standardized than other chemical species reported in this assessment.

6.1. Sources of organic acids in the atmosphere

Organic acids are important constituents of the global troposphere and contribute ~25% to the non-methane atmospheric mixture (Khare et al., 1999). Many different sources of atmospheric organic acids exist. Direct emissions of formic and acetic acids by vegetation have been suggested by a number of investigations (Talbot et al., 1990; Kesselmeier et al., 1991; Schäfer et al., 1992) with direct emissions from trees being estimated to be responsible for 15–30% of the atmospheric organic acid budget in Europe (Kesselmeier et al., 1998). Formic and acetic acids are also formed indirectly in the atmosphere via the oxidation of ethane and propene by ozone (Calvert and Stockwell, 1983), and the oxidation of isoprene produces formic and pyruvic acids (Andreae et al., 1987.) Additionally, formic and acetic acids are formed in the reaction of ozone with olefins like ethene, propene, and butene, which are predominantly of anthropogenic origin (Calvert and Stockwell, 1983; Atkinson et al., 1995). Carbon isotope analyses also suggest that 80–100% of formic acid in the atmosphere originates from biogenic VOCs emitted from terrestrial sources (Glasius et al., 2000), with the balance emitted by biomass burning (Talbot et al., 1988; Helas et al., 1992), dry soils (Sanhueza and Andreae, 1991), oceans (Graedel and Weschler, 1981) and formicine ants (Johnson and Dawson, 1993). On the basis of the vertical distribution of organic acids measured by using a mist scrubber on an aircraft in experiments in tropical regions in Africa (Helas et al., 1992), direct emission by vegetation was not considered to be the dominant source of organic acids in the atmosphere. Biomass burning and photochemical oxidation of biogenic precursors were concluded to be the major processes contributing to the enhancement of organic acids observed in the boundary layer. The organic acids profile also correlated with that of ozone and CO, which suggests that their generation processes are closely related.

Further indications of both primary and secondary sources of organic acids in the atmosphere were obtained from stable carbon isotope ratio ($\delta^{13}C$) data collected in Zurich, Switzerland in August–September 2002 and March 2003 (Fisseha et al., 2009). Anthropogenic sources were indicated by high-resolution ice core measurements from the French Alps that showed a strong increase in formate and acetate concentrations from 1950 to 1980 (Legrand et al., 2003). Legrand et al. (2003) calculated that 6% of formic acid and 25% of the acetic acid in the European boundary layer was of anthropogenic origin, mainly from direct vehicle emissions and secondary production from aliphatic alkanes oxidized by ozone. In light of the fact that the gas-phase oxidation of these acids is rather slow, i.e., five to ten days in summer (Legrand et al., 2003), their removal from the atmosphere is likely due largely to wet and dry deposition (Paulot et al., 2011) although the irreversible uptake on dust can also be an important regional removal mechanism (Falkovich et al., 2004). Ayers et al. (2003) reported that formic and acetic acids in precipitation can be lost as neutral molecules within one or two days due to biological consumption. Unless rainwater samples are preserved against bacterial loss they are not detected by the usual protocols such as ion balance checks (Ayers et al., 1998).

On a global scale, the photochemical oxidation of biogenic volatile organic compounds, in particular isoprene, dominates the bottom-up estimates of global sources of formic and acetic acids of ~1200 and ~1400 Gmol C a^{-1} published by Paulot et al. (2011). These authors propose that a long-lived secondary source of formic and acetic acid, of the order of ~2000 Gmol C a^{-1}, has yet to be identified. A strong correlation of aerosol organic content and formic and acetic acids hints at a possible relationship between aerosol aging and carboxylic acid production.

6.2. Measured global patterns of organic ion concentrations

The paucity of routine organic acid measurements in global precipitation monitoring networks made it impossible to create global and regional maps of deposition and precipitation concentrations for the two 3-year periods used for the major ions in earlier sections of this assessment. Fig. 6.1 provides an alternative integrated global view of organic acid concentrations in precipitation by showing a synthesis of historically published information and current (but limited) measurement data. The figure illustrates that annual precipitation-weighted mean formate and acetate concentrations in precipitation fall between 0.5 and 17.6 μeq L^{-1}, which suggests that the sources of formic and acetic acid in rain are reasonably well distributed throughout the world. Although not seen in the figure, it is important to note that seasonal variations at sites are, in most cases, greater than between-site differences (remote or urban) in different regions of the globe. Care was thus taken to exclude measurements of short time durations in this global overview to avoid potentially skewed results.

It follows from Fig. 6.1 that the reported concentrations are strongly associated with land use and land cover type. Higher concentrations are in general observed in forested tropical areas near the equator with a gradual drop toward the poles. This global map supports the current understanding discussed above that both formic and acetic acid in the atmosphere originate primarily from the photo oxidation of biogenic compounds (Paulot et al., 2011). The available data, sampling periods and references for remote or rural sites are listed in Table 5. The Table contains only concentrations from data sets collected over one or more years (to avoid seasonal

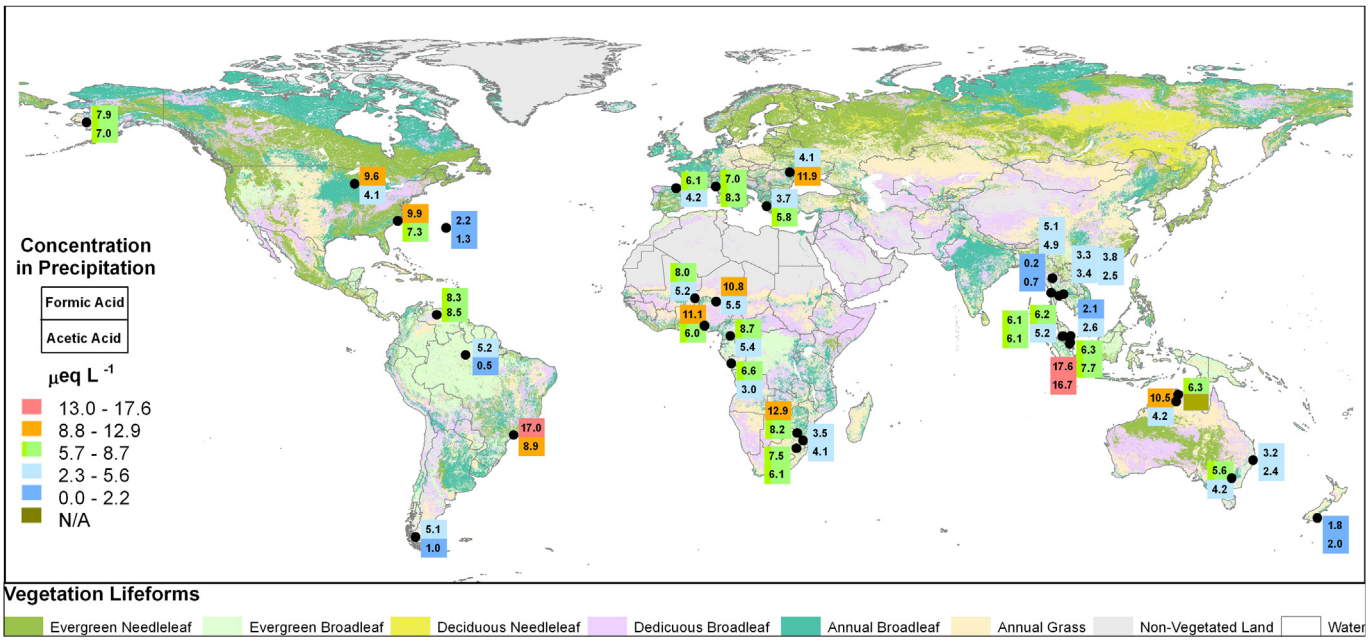

Fig. 6.1. Annual precipitation-weighted mean concentrations (μeq L^{-1}) of formate and acetate reported in non-urban precipitation (see Table 5 for representative time periods). Global Land Cover Characterization data courtesy of the U.S. Geological Survey.

fluctuations) and in which the use of suitable preservation techniques was reported.

6.3. *Regional aspects of organic acid concentrations in precipitation*

Long term measurements of organic acids in precipitation exist at only a few sites worldwide. Most of these sites are located in Africa where measurements were initiated in the late 1980's (Lacaux et al., 1992) and have been continuously monitored since 2002 at nine IDAF sites representative of major African ecosystems, i.e., in Niger, Mali, Republic of Côte d'Ivoire, Central African Republic, Cameroon, Congo and South Africa (3 sites). A tenth IDAF site, located in South America, has been operated at Petit Saut in French Guyana. Reports from these sites (Lacaux et al., 1992; Galy-

Table 5
Summary of available precipitation-weighted mean annual concentrations of formic (F) and acetic (A) acids in precipitation (in μeq L^{-1}) and wet deposition of formic plus acetic acid (in kg C ha^{-1} a^{-1}) at remote or rural sites. Blank spaces indicate no data or insufficient information to generate estimates.

Country	Site	[HCOOH] (μeq L^{-1})	[CH_3COOH] (μeq L^{-1})	Formate + acetate wet deposition (kg C ha^{-1} a^{-1})	Period	Reference
Niger	Banizoumbou	8.0	5.2	1.31	1994–2005	Galy-Lacaux et al., 2009.
Mali	Katibougou	10.8	5.5	2.03	1997–2005	Galy-Lacaux et al., 2009
Côte d'Ivoire	Lamto	11.1	6.0	4.92	1995–2002	Yoboué et al., 2005
Cameroon	Zoétélé	8.7	5.4	4.55	9/1996–4/2000	Sigha-Nkamdjou et al., 2003.
Congo	Dimonika	6.6	3.0		11/1986–9/1987	Lacaux et al., 1992
South Africa	Amersfoort	7.5	6.1	2.53	1986–1999	Mphepya et al., 2004
South Africa	Loius Trichardt	12.9	8.2	3.29	1986–1999	Mphepya et al., 2004
South Africa	Skukuza	3.5	4.1	1.52	1999–2002	Mphepya et al., 2006
Romania	Cuza University of Iasi	4.1	11.9	2.09	3/2003–12/2006	Arsene et al., 2007
Greece	University of Patras	3.7	5.8		3/2000–5/2001	Moschonas and Glavas, 2002
Spain	Galicia	7.0	8.3		8/1996–8/1997	Pena et al., 2002
Spain	Olaeta	6.1	4.2		1989–1990	Durana et al., 1992
U.S.	Wilmington	9.9	7.3		9/1996–5/1998	Brooks et al., 2006
U.S. (Alaska)	Bethel	7.9	7.0		7/1988–8/1988	Talbot et al., 1992
Brazil	Sao Paulo	17.0	8.9		2/2000–10/2000	Fornaro and Gutz, 2003
St. Georges	Bermuda	2.2	1.3		1980–1984	Galloway et al., 1989
U.S.	Wisconsin	9.6	4.1		4/1982–6/1984	Chapman et al., 1986
Chili	Torres del Paine	5.1	1.0		1984–1991	Galloway et al., 1996.
Venezuela	Calabozo	6.5	3.5		1990–1993	Sanhueza et al., 1996
Australia	Katherine	10.5	4.2		1980–1984	Likens et al., 1987
Australia	Jabiru	6.3			1983–1984	Gillett et al., 1990
Amsterdam Island	France			3.70	5/1980–1/1987	Moody et al., 1991
Singapore	Singapore	17.6	16.7	17.38	8/1997–12/1997	Zhong et al., 2001
New Zealand	Dunedin (South Island)	1.8	2.0		4/1999–3/2000	Kieber et al., 2002
Thailand	Patumthani	3.3	3.4	2.66	2006–2007	Nakayama, 2009
Thailand	Khanchanaburi	0.2	0.7	0.44	2007	Nakayama, 2009
Thailand	Chiang Mai	5.1	4.9	3.62	2005–2006	Nakayama, 2009
Thailand	Nakhon Ratchasima	3.8	2.5	2.32	2006–2007	Nakayama, 2009

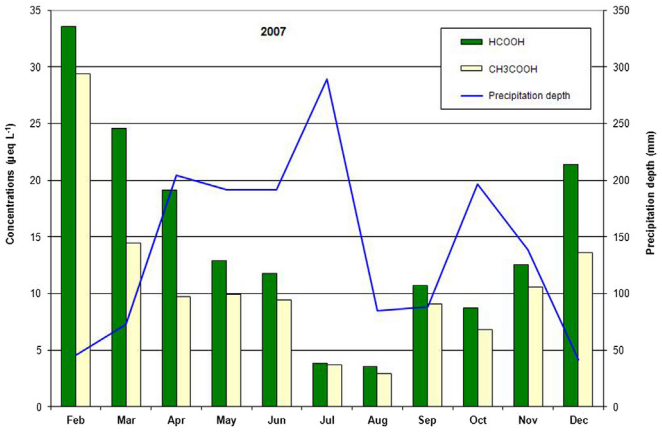

Fig. 6.2. Long-term concentrations (μeq L^{-1}) of organic acids in precipitation at Lamto, Republic of Côte d'Ivoire (data from the IDAF/DEBITS network. Galy-Lacaux, personal communication, March 14–20, 2010).

Lacaux and Modi, 1998; Galy-Lacaux et al., 2009; Sigha-Nkamdjou et al., 2003; Mphepya et al., 2004, 2006; Yoboué et al., 2005) give a range of concentrations of formate from 3.5 to 12.9 μeq L^{-1} and acetate from 3.1 to 8.2 μeq L^{-1}. The lowest concentrations were observed in Kruger National Park in South Africa (Bushveld land type) and at Banizoumbou in Niger (Sahelian savanna) during the rainy season. The highest concentrations occurred at Louis Trichardt in South Africa (tall grass savanna) and Lamto in the Republic of Côte d'Ivoire (wet savanna). In all cases the organic acids were found to make a substantial contribution to the overall acidity of precipitation. At the sites in the Republic of Côte d'Ivoire, South Africa (specifically Louis Trichardt) and Cameroon, formate concentrations were equivalent to or exceeded the concentrations of sulfate and nitrate in precipitation. In most of the reported studies, the average concentration of formate exceeded that of acetate by a factor of up to about 1.5. A 13-year data set for the Lamto site in the Republic of Côte d'Ivoire is unique and provides the best example of large inter-annual variations in formate and acetate concentrations linked to the amount of rainfall (i.e., more or less dilution) and variations in biogenic emissions (Fig. 6.2). The data at Lamto also show strong intra-annual variations (Fig. 6.3) indicating the importance of maintaining long term monitoring sites globally. These observations are not unique to the Lamto site in the Republic of Côte d'Ivoire as most sites that operated within the IDAF/DEBITS network show seasonal and interannual variations.

Concentrations of organic anions in other parts of the world have largely been determined during short term (campaign) studies. The following discussion relies heavily on these short term studies. In the early eighties, Keene et al. (1983) found the concentration of formate at Katherine, northern Australia (tropical savanna with scattered small eucalyptus trees) to be 10.5 μeq L^{-1}, and acetate 4.2 μeq L^{-1} during the period 1980–1984 (volume-weighted concentration of 12 samples). In New Zealand, near Dunedin on the South Island, concentrations were found to be less than 2 μeq L^{-1} for both formate and acetate, with concentrations from April 1999 to March 2002 being slightly higher in the winter than the summer (Kieber et al., 2002). In South America, Fornaro and Gutz (2003, 2006) reported formate concentrations of 17.0 μeq L^{-1} in the Sao Paulo metropolitan area between February (end of the rainy summer) and October (beginning of spring) 2000, making a contribution to the overall acidity equivalent to that of sulfate. Acetate was also significant at 8.9 μeq L^{-1}.

In Asia, reported concentrations have generally been lower, e.g., of the order of 5–6 μeq L^{-1} in north-central India at a regionally representative site with only grass, wild herbs, and Acacia trees in the vicinity (Singh et al., 2006); 6.1 μeq L^{-1} for formate and 4.5 μeq L^{-1} for acetate in Hong Kong at a residential site at the City University of Hong Kong (Tanner and Law, 2003); and 4.94 μeq L^{-1} for formate and 5.89 μeq L^{-1} for acetate in Singapore (Balasubramanian et al., 2001). However, much higher values were observed in Singapore at a residential site at the National University of Singapore between August and December 1997 (Zhong et al., 2001), with volume-weighted means of 17.6 μeq L^{-1} for formate and 16.7 μeq L^{-1} for acetate. During this study the measurement area was impacted by the plume of large forest fires in Indonesia, and peak concentrations of 105.6 μeq L^{-1} for formate and 62.8 μeq L^{-1} for acetate were observed, providing further evidence that biomass burning contributes to the formation of formic and acetic acid in the atmosphere.

High concentrations of organic anions have also been reported in the U.S., e.g., by Brooks Avery et al. (2001, 2006) for North

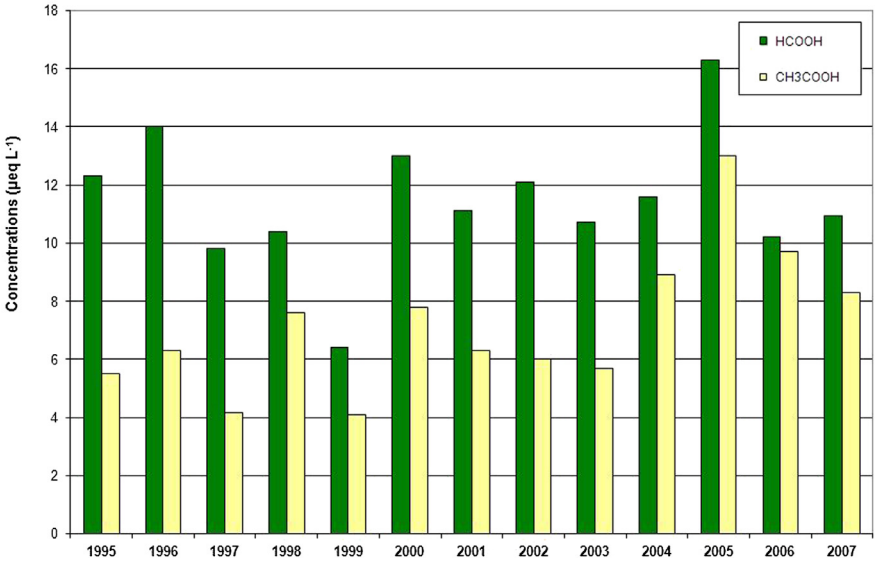

Fig. 6.3. Monthly variations in the concentrations (μeq L^{-1}) of organic acids in precipitation and precipitation depth (Ht in mm) at the Lamto site, Republic of Côte d'Ivoire (data from the IDAF/DEBITS network. Galy-Lacaux, personal communication, March 14–20, 2010).

Carolina, where samples were stratified by morning and afternoon and growing and non-growing seasons. The highest concentrations, 12 μeq L^{-1} for formate and 9 μeq L^{-1} for acetate, were found in afternoon samples during the growing season. Collett et al. (2008) found that 26% of the dissolved organic carbon content of fog water in California was acetate, with formate representing another 7%. In Virginia, U.S., Talbot et al. (1988) reported a strong seasonal signal whereby formate and acetate concentrations in rain during the growing season were about 4 times higher than in the non-growing season, with values of 6.81 and 5.09 μeq L^{-1} for formate and acetate, respectively, during the growing season and 1.57 and 2.05 μeq L^{-1} during the non-growing season.

In Europe, in contrast to findings elsewhere, measured concentrations of acetate were higher than formate. For example, in Romania, formate and acetate concentrations were 4.08 and 11.9 μeq L^{-1}, respectively (Arsene et al., 2007); in Greece, 3.77 and 4.81 μeq L^{-1}, respectively (Moschonas and Glavas, 2002); and, in northwest Spain, 7.0 and 8.3 μeq L^{-1}, respectively (Pena et al., 2002). The latter concentrations represent a volume-weighted mean of 272 rainwater samples collected at nine monitoring sites during a one year period (August 1996–1997).

Few studies have been carried out in the polar regions of the world and the available data are from the 1980s and 1990s. In the Canadian high Arctic (Alert, Northwest Territories), Toom-Sauntry and Barrie (2002) measured median formate and acetate concentrations of 0.48 and 0.47 μeq L^{-1} in 19 low-windspeed snowfall events from September, 1993 to May, 1994. During this period, the highest concentrations of formate and acetate were 2 μeq L^{-1} and 1 μeq L^{-1}, respectively, occurring after polar sunrise (March to May) rather than in the dark of winter. On average, the organic acid anions amounted to only 1.7% of the total anion equivalents in the 19 samples. Snowfall concentrations at Barrow, Alaska contrast the results from a set of special study samples collected in the Central Amazon Basin of Brazil where formate and acetate represented roughly one half the anion equivalents. At Poker Flat, Alaska in the sub-Arctic boreal forest, Keene and Galloway (1986) reported summertime volume-weighted mean concentrations of about 4.3 μeq L^{-1} for formate and 1.2 μeq L^{-1} for acetate in rain samples collected during the summer of 1982. At Bethel, Alaska on the sub-Arctic tundra, Talbot et al. (1992) measured summertime (July–August, 1988) volume-weighted mean concentrations of 7.9 μeq L^{-1} for formate and 7.0 μeq L^{-1} for acetate in rainfall. The authors noted the presence of very high concentrations of carboxylic acids in the first few samples collected after an extended dry period followed by low concentrations thereafter. Their estimated ratio of formate to acetate on an equivalents basis from the individual samples was 1.91 - considerably less than the rainfall ratio of 3.31 observed at Poker Flat in 1982 by Keene and Galloway (1986). No data were found on organic acids in Antarctica.

The foregoing observations are consistent with the expectation that the major emission sources of organic anions are biogenic, with biomass burning a significant seasonal source in many environments (Paulot et al., 2011).

6.4. Wet deposition of carbon from formate and acetate organic acids

Literature estimates of wet deposition of C due to organic acids are not available. To fill this void, wet deposition was estimated from concentration and precipitation depth values published in the literature. The wet deposition was calculated by multiplying the sum of the measured annual average concentrations of acetic and formic acids in g C L^{-1} (from Table 5) times the average annual precipitation depth values (in cm) that were published with the concentrations. The calculated wet deposition estimates are shown in Table 5 and mapped globally in Fig. 6.4. Many of the published concentrations were not accompanied by precipitation depths which made it impossible to calculate wet deposition. These cases appear as blanks in Table 5 and account for the low number of deposition estimates in Fig. 6.4. To our knowledge, this is the first time that wet deposition of C from organic acids has been estimated globally.

It follows from the estimates reported in Fig. 6.4 that the annual mean precipitation depth has a strong influence on total C from acetate + formate in wet deposition.

It must be emphasized that the wet deposition of formic plus acetic acid does not represent total C in total atmospheric deposition (i.e., dry deposition and other carbonaceous compounds are

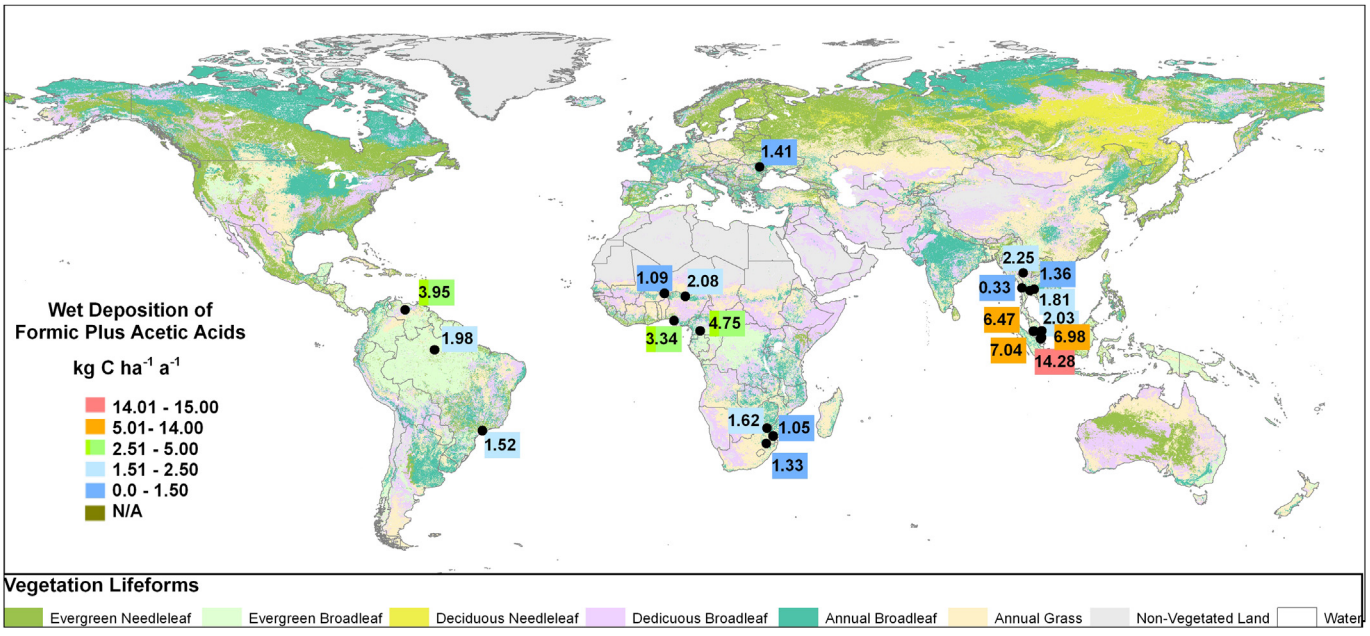

Fig. 6.4. Global wet deposition of C from formic and acetic acids (kg C ha^{-1} a^{-1}). Global Land Cover Characterization data courtesy of the U.S. Geological Survey.

not accounted for) but it does give us for the first time an estimate of dissolved C in rain water. These values can now be compared to dissolved values of N, S and other species found in rainwater. At the African DEBITS sites, carbon wet deposition from these two compounds exceeds that of sulfur at most sites and is comparable to the reported nitrogen wet deposition. It is expected that the relative ratios of these compounds are important to the sustainability of various ecosystems.

6.5. Summary, uncertainties and gaps

It is clear from the many reports cited in this review that organic acids play an important role in controlling atmospheric acidity in many regions of the world. The contribution of these acids is more pronounced in remote areas but is a factor in all regions. The very important role that carbon, and especially the deposition of dissolved carbon-containing compounds, plays in ecosystems is well known (Fillion et al., 1999) and it is therefore important to take note of the wet deposition estimates reported for the first time in this review.

It is also well known that the monitoring of organic acids in rain is complicated because they are extremely sensitive to biodegradation. Special care must be taken in sampling and storage to avoid biodegradation and to ensure reliable data. Apart from the IDAF sites, several sites in the EANET network, and a few sites in Australia, no routine long term measurements of organic acids in wet deposition have been reported. Biogenic source strengths of both precursors and the organic acids themselves seem to play a major role in the global distribution of these acids in rainwater. In order to enhance our understanding of the impact of wet deposition as a global distributor of nutrients, including carbon, wet deposition monitoring networks must start including measurements of formic and acetic acids.

Finally, although it is clear from this assessment that anthropogenic emissions of organic acids and/or their precursors are increasing, biogenic sources and natural processes still dominate the emissions. The study of the budget of these acids offers a glimpse into the interaction of the biosphere and the atmosphere (Paulot et al., 2011). It is also important to note that there are no dry deposition estimates of acetic and formic acids so dry deposition has not been discussed here.

7. Acidity and pH

The acidity of precipitation is determined by the relative amounts of acids and bases in solution (Daum et al., 1984; Sequeira, 1982; Hobbs, 1995; Noguchi et al., 1995; Noguchi and Hara, 2004; WMO/GAW, 2004; Wang et al., 2012). The dominant strong acids affecting global precipitation are sulfuric, nitric and hydrochloric and the dominant weak acids are the major organic acids formic, acetic and, to a lesser degree, other carboxylic acids. Organic acids play a significant role in precipitation acidity when strong acid concentrations are low, but wet deposition of organic acids is considered to be of minor importance to ecosystems because of their consumption by microorganisms on the earth's surface (Rodhe et al., 2002). On a global scale, the only recent assessment of precipitation pH and H^+ wet deposition was published by Rodhe et al. (2002) who applied a chemical transport model to predict the geographical distribution of pH and the wet deposition of H^+ and bicarbonate. Rodhe et al. (2002) estimated that the lowest pH values occurred in Europe, China and eastern North America because of high concentrations of sulfuric acid. Their estimated pH values showed fair agreement with observed pH values in most parts of the world with the exception of western North America, southwestern Europe, and northern China, where the model-estimated pH values were lower than the observed values.

In North America, only a few studies since 2000 have reported measurement-based pH trends at the regional or national scale. Lynch et al. (2000) reported that the concentration of H^+ in precipitation at regionally-representative sites in the eastern U.S. decreased due to SO_2 emission reduction regulations (Phase I of Title IV of the 1990 Clean Air Act), with maximum reductions of H^+ and SO_4^{2-} occurring in the same areas immediately downwind of most of the major stationary sources targeted by the emission regulations. Vet et al. (2005) mapped the spatial distribution of the pH of precipitation in southeastern Canada and the eastern U.S. Based on precipitation-weighted mean concentrations of H^+ over the period 1996–2000, they reported a minimum 5-year average pH of 4.4 near and downwind of the major SO_2 and NO_x emission areas, and a maximum of 5.0–5.4 in the upwind direction northwest of the major sources. No regionally-representative trends of H^+ in precipitation have been reported in Mexico.

In Brazil, Pauliquevis et al. (2012) reported a volume-weighted mean pH of 4.90 over a 3.5 year period at a remote site in central Amazonia, with the most important contribution to acidity being attributed to weak organic acids. Other short-term precipitation pH studies in Brazil and other parts of South America focused on urban or industrial areas and were not regionally-representative; thus, they are not discussed here.

In Europe, Torseth et al. (2012) examined average spatial and temporal trends in the precipitation composition of major ions at EMEP sites. Results showed that the lowest pH in Europe occurs in the eastern part, which has relatively high sulfate deposition and low base cation deposition, and the highest is observed in Spain and parts of Italy. They found that from 1980 until 2009, pH had increased by 0.5–0.6 pH units and H^+ concentrations had declined by 74%, attributable to larger declines in sulfate concentrations relative to base cations. At the sub-regional scale, Ryaboshapko et al. (2010) showed a spatial constancy in precipitation acidity at EMEP stations in the northwestern European Russian Federation over the period 2000 to 2007, with a difference of 0.3 units between the maximum and minimum pH. They also demonstrated an increase in pH over the last 25 years attributed to the implementation of the LRTAP Convention, with maximum pH values changing from around 5 to around 6. Several other published studies report precipitation pH at sites in individual European countries, but these are either not regionally-representative or are short-term in nature.

The latest regional assessment of acidic deposition in East Asia (EANET, 2011) reported annual rainwater pH values ranging from 4.18 to 6.94 over the period 2000–2009 at 42 EANET stations (including both rural and urban sites as both are integrated into the network). They also reported 5-yr averages (2005–2009) ranging from 4.4 to 6.2, with pH < 5.0 at 62% of the sites. Average rainwater pH values below 4.6 were recorded at specific urban sites in Malaysia, China (Chongqing) and Indonesia, and at several rural/remote sites in the Republic of Korea and Japan. In contrast, average values higher than 6.0 were observed in China (Xi'an) and Mongolia (Ulaanbaatar). These high values were attributed to the increased contribution of alkaline species such as ammonia from agriculture and calcium carbonate from soil dust, respectively. Sulfuric acid contributed more to precipitation acidity than nitric acid while other acids including hydrochloric and organic were suggested to explain the observed wet deposition chemistry. The highest annual wet hydrogen ion (H^+) deposition was seen exclusively in Petaling Jaya, Malaysia ranging from 1.73 kg ha^{-1} a^{-1} in 2001 to 1.34 kg ha^{-1} a^{-1} in 2009. The lowest annual wet H^+ deposition ($<7 \times 10^{-4}$ kg ha^{-1} a^{-1}) was observed in Mongolia (Ulaanbaatar and Terelj), and China (Jiwozi and Weishuyuan). Several other observational studies were carried out in Asia (Kulshrestha et al., 2005; Chudaeva et al., 2008; Lu et al., 2010; Ge et al., 2011; Yang et al., 2012) but were mainly focused on urban/

suburban/industrial measurements and so are not described in detail here.

In Africa, the recent literature on observed precipitation pH and H^+ deposition is based on measurements at the IDAF sites representing different ecosystems. In the wet savanna, Yoboué et al. (2005) reported a multi-year average pH of 5.16 with 40% of acid neutralization explained by acid gas-alkaline soil particle interaction and the remainder by inclusion of gaseous ammonia. The high contribution of organic acids to total acidity of precipitation was consistent with observations made at other wet savanna locations. Average precipitation pH at remote sites in the South African dry savanna ranged from 4.4 to 4.72 (different sites and measurement periods) with an almost equal contribution of inorganic and organic acidity (Mphepya et al., 2004, 2006). In the Nigerian dry savanna, the reported median pH was 6.06 due to neutralization by mineral dust, mainly carbonates, and/or dissolved gases such as NH_3 (Galy-Lacaux et al., 2009). In the case of a forest ecosystem site, pH was seasonally variable (lower in the dry season) with an average value of 4.92 and H^+ concentration of 12 μeq L^{-1} (Sigha-Nkamdjou et al., 2003). Wet deposited H^+ was only reported for sites in the wet savanna and forest ecosystems and were 0.084 kg ha^{-1} a^{-1} (Yoboué et al., 2005) and 0.243 kg ha^{-1} a^{-1} (Sigha-Nkamdjou et al., 2003), respectively.

No long-term studies of precipitation pH and H^+ in Oceania were found in the literature post-2000. The composition of baseline precipitation has been measured at the Cape Grim Baseline Air Pollution Station in Australia since 1993 and is available at http://www.bom.gov.au/inside/cgbaps/, but has not been published in the scientific literature.

A regional assessment of measured precipitation pH in the European Arctic (AMAP, 2006) showed an upward trend in pH from 1990 to 2003 that did not appear to be coupled to sulfate or nitrate. Hole et al. (2009) concluded that acidity is generally reduced at many monitoring stations in the European Arctic while the precipitation amount was either increasing or stable. In the Canadian Arctic, precipitation pH values as low as 4.4 were observed in low windspeed snowfall at Alert from September to May, 1990–1994 (Toom-Sauntry and Barrie, 2002).

7.1. Global patterns of pH and H^+ wet deposition

Global maps of 3-year average precipitation pH and H^+ wet deposition for 2000–2002 and 2005–2007 are shown in Fig. 7.1a,b and 7.2a,b, respectively. Each 3-year mean pH value was calculated as the negative logarithm of the average of the three annual precipitation-weighted-mean H^+ concentrations (WMO/GAW, 2004). All calculations were based on laboratory-measured pH values. The accepted pH and H^+ wet deposition data in Fig. 7.1a and 7.2a consisted of 437 Satisfactory, 30 Conditional and 4 Non-Conforming-Period data points; the data in Fig. 7.1b and 7.2b consisted of 470, 14 and 0 points, respectively.

The global patterns of pH and H^+ wet deposition generally mimic the global emission patterns of SO_2 and NO_x (Fig. 3.1 and 4.1) and S and N wet deposition (Fig. 3.3a,b and 4.3a,b, respectively) due to the strong influence of sulfuric and nitric acids on precipitation acidity in most areas of the world. Areas of lowest pH and highest acidity (pH = 4.1–5.2) occurred within and adjacent to the high SO_2 and NO_x emission areas of eastern North America, Europe, East Asia and central Africa. Parts of northeast Canada and northern Scandinavia associated with low SO_2 and NO_x emissions and low cation wet deposition also have relatively acidic precipitation due to the long range transport of S and N from the high emission areas to the south. Areas with high pH values (in the range of 5.3–6.7) occur where SO_2 and NO_x emissions are low and/or dust emissions are high, including the northern Mediterranean, central Africa and south Asia. H^+ wet deposition (Fig. 7.2a,b) are highest where both H^+ concentrations and precipitation depths are high or moderately high, most notably in eastern North America and areas of Europe and East Asia.

7.2. Temporal changes to pH and H^+ wet deposition

As discussed in Sections 2 and 3, changes in SO_2 and NO_x emissions from 2000–2002 to 2005–2007 resulted in measurable changes in SO_4^{2-} and NO_3^- wet deposition in many regions of the world (see Fig. 3.1 and 4.1). These changes, in turn, produced changes in pH and H^+ wet deposition. Shown in Fig. 7.3a are the between-period differences in pH and, in Fig. 7.3b, the % changes in H^+ wet deposition. Consistent with the major reductions in SO_2 and NO_x emissions in Europe and North America, 75% of the European and 85% of the North American sites had higher pH levels in 2005–2007 than in 2000–2002, with median (and 90th percentile) differences of +0.06 (and +0.30) pH units in Europe and +0.08 pH units (and +0.18) in North America, respectively. On both continents, the increases in pH were due predominantly to decreases in SO_4^{2-} and NO_3^- wet deposition as opposed to increases in the deposition of base cations. In Africa, all three monitoring sites had higher pHs in 2005–2007, with a median increase of +0.16 pH units. These increases were due mainly to increases in the deposition of base cations. In Asia, the between-period pH differences were inconsistent across the continent, with approximately half the sites having higher pHs and half having lower pHs (median = −0.03 pH units). Most of the Asian sites with lower pHs in 2005–2007 were located along the Pacific rim where SO_2 and NO_x emissions were highest. The decrease in pH at these sites was due mainly to increases in SO_4^{2-} and NO_3^- wet deposition.

The changes in H^+ wet deposition from 2000–2002 to 2005–2007 (Fig. 7.3c) were consistent with the changes in pH – with the exception of eight sites in western North America, one site in Asia and one site in Europe where they were instead consistent with major changes in precipitation depth. The wet deposition changes are plotted in Fig. 7.3c as the Median % Difference (M%D) = 100 [(2005–2007) − (2000–2002)]/[(2000–2002)]. The results are summarized as follows:

- Africa: M%D = −24.7% with 100% of the sites having lower H^+ deposition;
- Asia: M%D = +10.9% with 63% of the sites having higher H^+ deposition;
- Europe: M%D = −19.8% with 74% of the sites having lower H^+ deposition; and
- North America: M%D = −12.4% with 75% of the sites having lower H^+ deposition.

Thus, H^+ wet deposition decreased at most monitoring sites in North America, Europe and Africa, but increased at most sites in Asia. On all continents, the changes in H^+ wet deposition were related to changes in concentrations rather than changes in precipitation depth (Fig. 7.3c). Unfortunately, there were too few monitoring stations in the areas of Asia that had experienced the most rapid growth of SO_2 and NO_x emissions, especially China. This points to the need for additional stations in those areas to thoroughly resolve the regional deposition pattern and its changes with time.

7.3. Estimating global H^+ concentrations

The 2005–2007 measurement data collected for this assessment provide a unique opportunity to assess the ability of a number of ion charge balance equations to predict global concentrations of

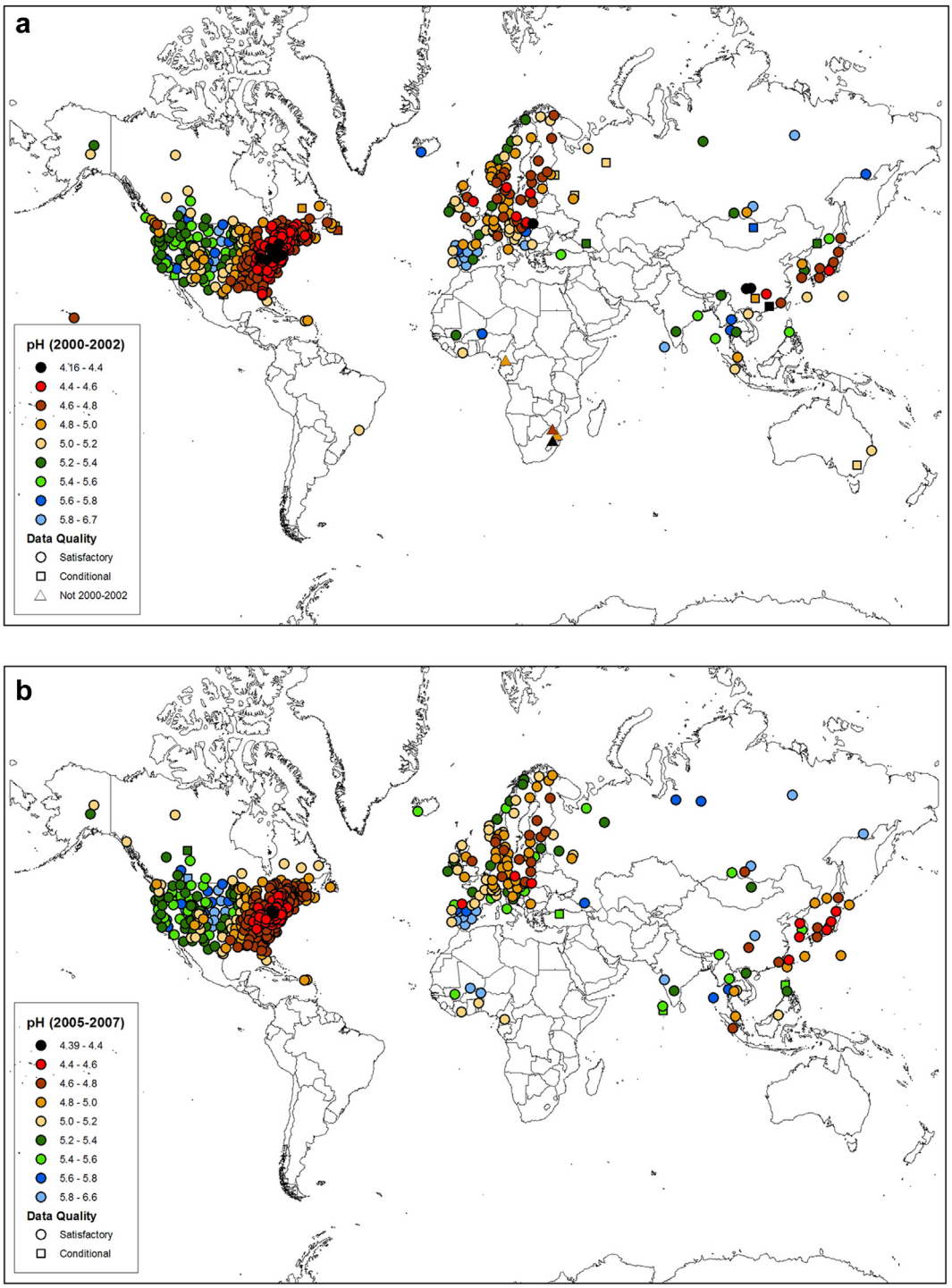

Fig. 7.1. Three-year-average pH values for (a) 2000–2002 and (b) 2005–2007.

H^+ in precipitation. This is analogous to the work of Rodhe et al. (2002) who used a chemical transport model instead of measurement data to estimate the global patterns of H^+ and bicarbonate in precipitation. Here, we used the measured 3-year average anion and cation concentrations in the data set to estimate H^+ concentrations which were, in turn, compared to the measured H^+ concentrations (hereafter referred to as $H^+_{measured}$). Four charge balance equations were assessed:

$$[H^+]_1 = 2[SO_4^{2-}] + [NO_3^-] \quad (7.1)$$

$$[H^+]_2 = 2[SO_4^{2-}] + [NO_3^-] - [NH_4^+] \quad (7.2)$$

$$[H^+]_3 = 2[SO_4^{2-}] + [NO_3^-] - [NH_4^+] - 2[Ca^{2+}] \quad (7.3)$$

$$[H^+]_4 = 2[SO_4^{2-}] + [NO_3^-] + [Cl^-] - [NH_4^+] - 2[Ca^{2+}] - 2[Mg^{2+}] - [Na^+] - [K^+] + 5.1/[H^+] \text{ (for pH} > 5.0) \quad (7.4)$$

where square brackets denote ion concentrations in μeq L^{-1}, SO_4^{2-} represents $nssSO_4^{2-}$ + $ssSO_4^{2-}$, and the term $5.1/[H^+]$ for pH > 5.0 represents the concentration of bicarbonate in equilibrium with

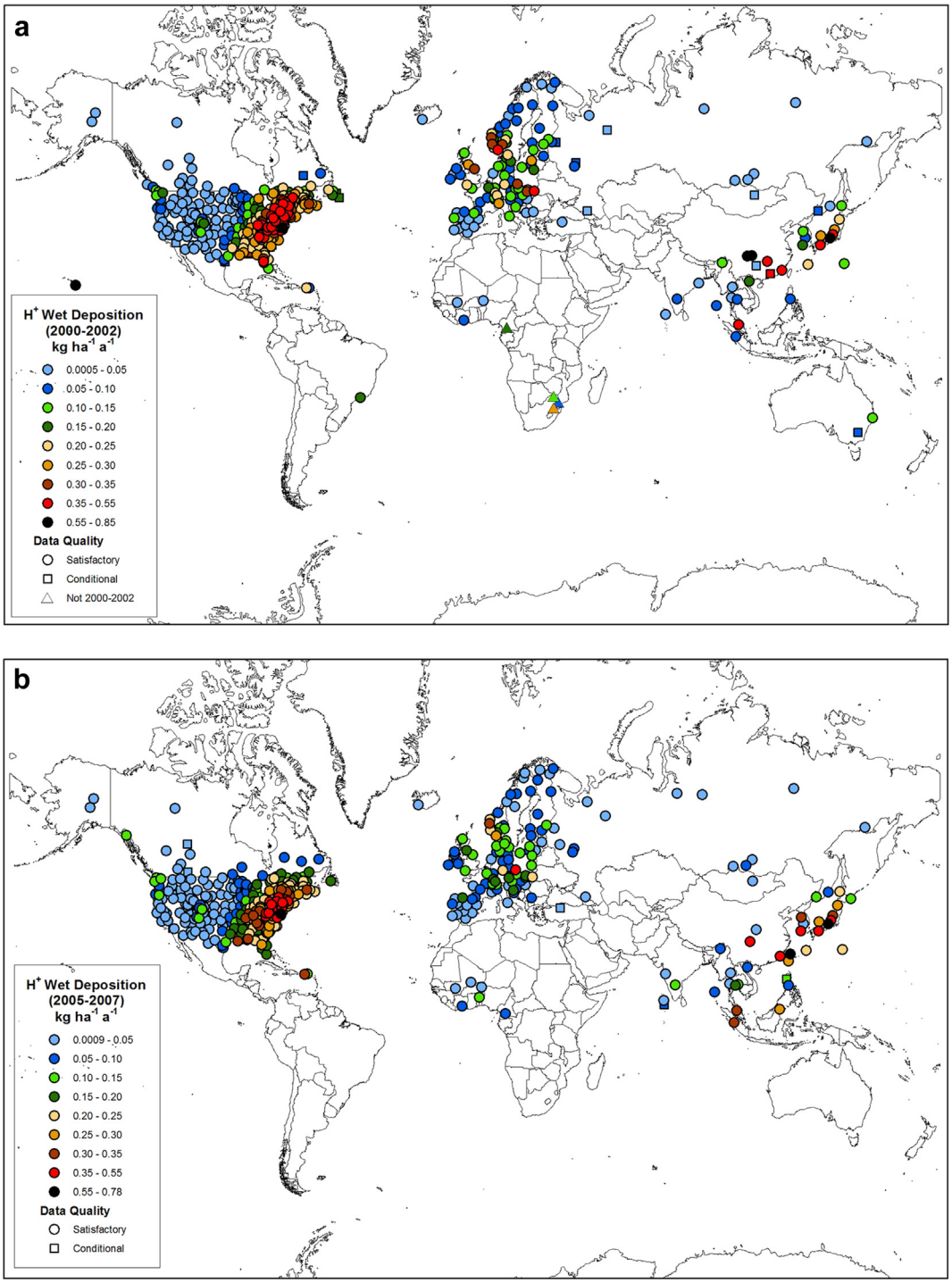

Fig. 7.2. Three-year-average H^+ wet deposition (kg ha^{-1} a^{-1}) for (a) 2000–2002 and (b) 2005–2007.

atmospheric CO_2 (WMO/GAW, 2004). The results of the four equations are shown in scatterplots of estimated $[H^+]_i$ versus $H^+_{measured}$ in Fig. 7.4.

Equation 7.1, the simplest equation, assumes that all H^+ in precipitation is from H_2SO_4 and HNO_3 with no contribution from neutral SO_4^{2-} and NO_3^- salts or from aqueous phase neutralization. As such, $[H^+]_1$ is equivalent to the non-logarithmic form of pA_i published by EANET (2011). Fig. 7.4a shows that the $[H^+]_1$ values from Eq. (7.1) overpredict and correlate poorly with ($r = 0.291$) the $H^+_{measured}$ values at almost all sites. At only a small number of sites in Asia and North America do the $[H^+]_1$ values come close to the $H^+_{measured}$ values.

Equation 7.2 includes an NH_4^+ term to account for the presence of neutral $(NH_4)_2SO_4$ and NH_4NO_3 and absorbed NH_3. The addition of NH_4^+ increases the correlation to $r = 0.431$ and reduces the overprediction of $H^+_{measured}$ at sites in Europe, Africa and North America (Fig. 7.4b). However, as with $[H^+]_1$, the $[H^+]_2$ values are biased high relative to the $H^+_{measured}$ values at almost all sites.

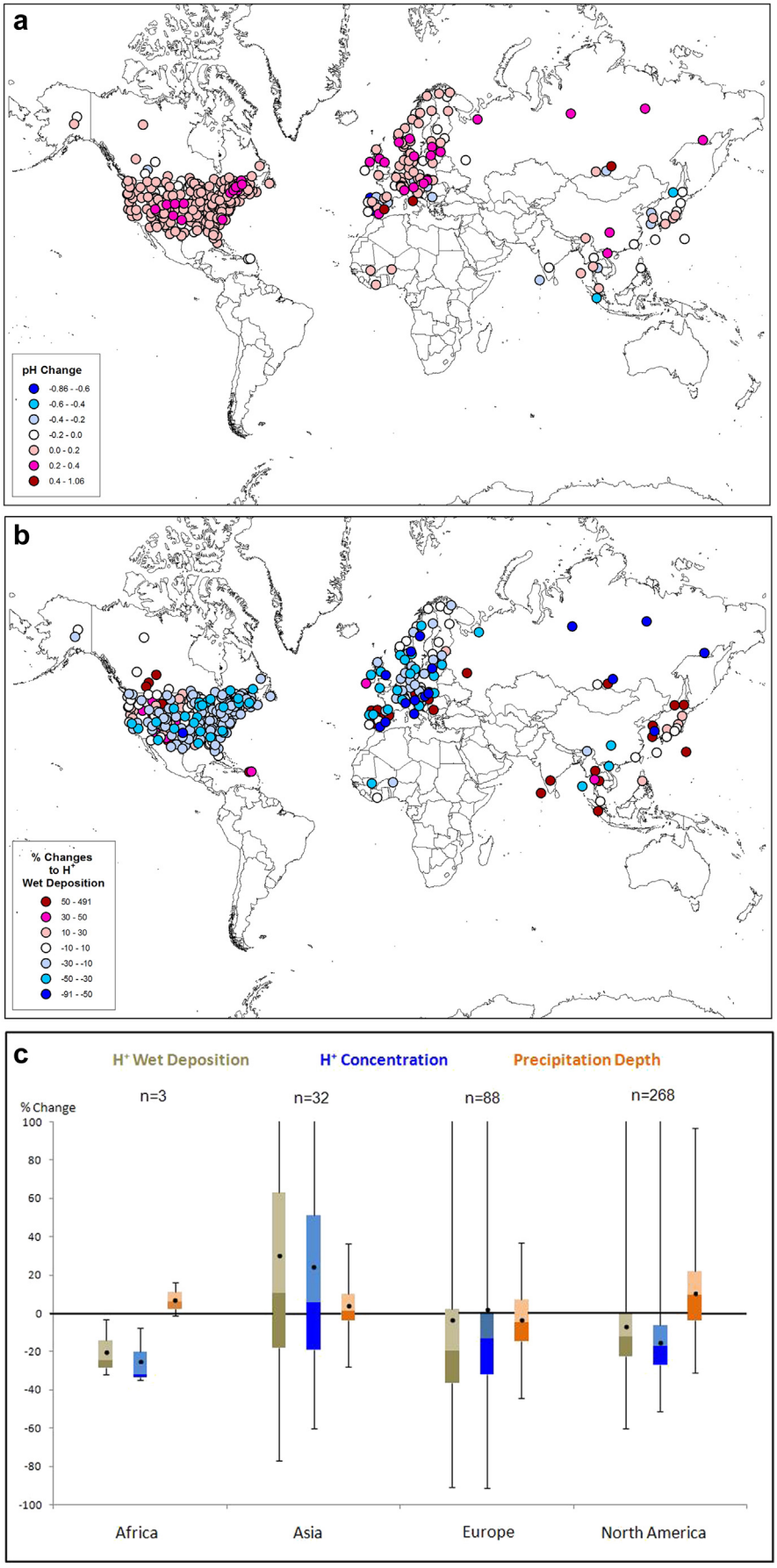

Fig. 7.3. Between-period (a) pH changes (in pH units) and (b) % changes in H^+ wet deposition from 2000–2002 to 2005–2007 (%) and (c) box-and-whisker plots of the % changes in H^+ wet deposition, concentrations and precipitation depths by continent (per Fig. 3.5).

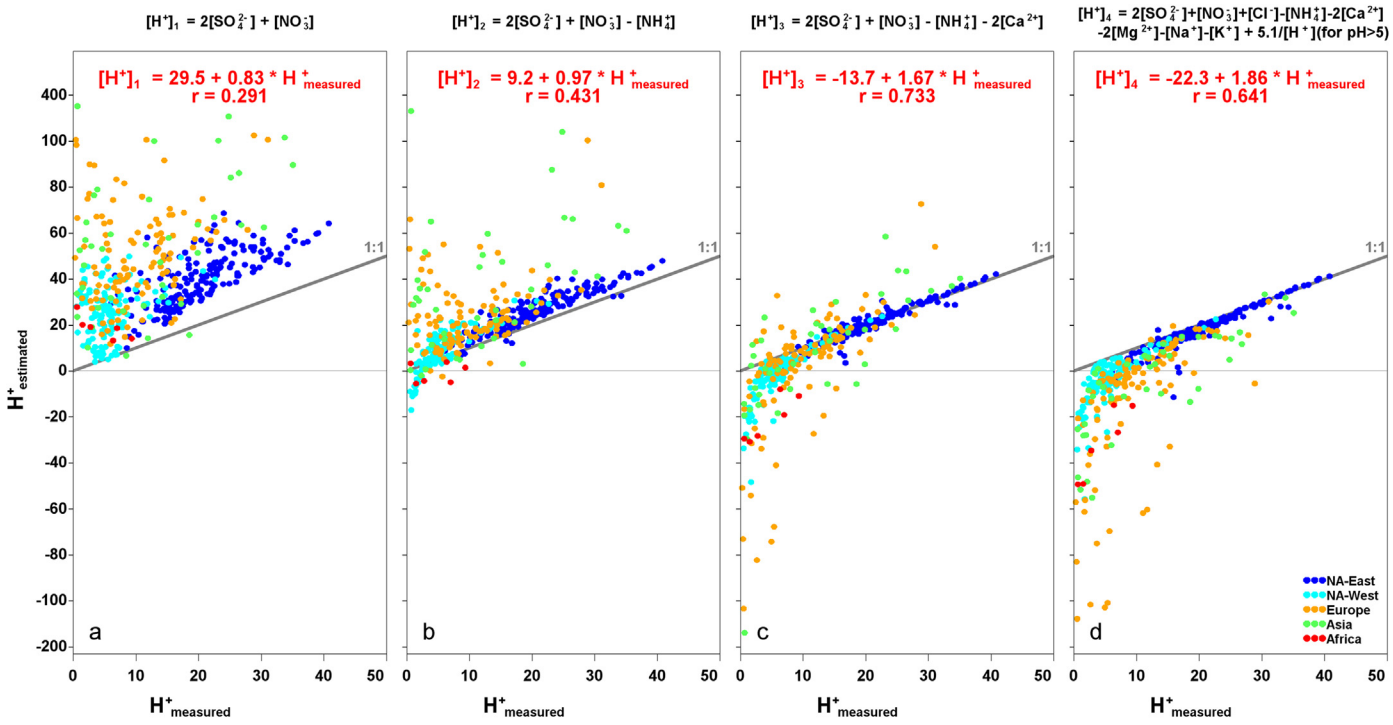

Fig. 7.4. Scatterplots of $[H^+]_i$ versus $H^+_{measured}$ based on (a) Equation 7.1, (b) Equation 7.2, (c) Equation 7.3, and (d) Equation 7.4.

Equation 7.3 includes a term for Ca^{2+} contributed by major natural and anthropogenic sources including windblown soil, agriculturally-derived soil, sea salt, fly ash and other industrial emissions. Fig. 7.4c shows that the addition of Ca^{2+} markedly improves the correlation to $r = 0.733$ and improves the predictions of $H^+_{measured}$ at almost all sites where $H^+_{measured} > 5$ μeq L^{-1}, i.e., in eastern North America, central Europe and Scandinavia. This suggests that neutral Ca^{2+} salts such as $CaSO_4$ and $Ca(NO_3)_2$ are important constituents of precipitation in those areas. In regions where $H^+_{measured} < 5$ μeq L^{-1}, the negative values of $[H^+]_3$ are assumed to represent unmeasured HCO_3^- associated mainly with soil-based $CaCO_3$ and/or organic acids.

Equation 7.4 represents the full charge balance equation for all anions and cations measured in the global data set. The values of $[H^+]_4$ can be thought of in two ways:

- as representing the best possible predictions of H^+ in the hypothetical case that all species in Equation (7.4) could be modeled perfectly;
- as identifying the areas of the globe where one or more key anions is not measured,

Regarding the latter, if one assumes that the last term in Equation (7.4) is a reasonable estimator of HCO_3^- in equilibrium with atmospheric CO_2, then the negative values of $[H^+]_4$ in Fig. 7.4d represent missing anions that should be measured and/or modeled but are not (see discussion below).

Fig. 7.4d shows that the $[H^+]_4$ values have a lower correlation coefficient ($r = 0.641$) than the $[H^+]_3$ values and are systematically lower than the $H^+_{measured}$ values – with the exception of a few high H^+ concentration sites in eastern North America. As was the case with Equation 7.3, Equation 7.4 produces a large number of negative values in Asia, southern Europe and Africa presumably due to missing soil-derived HCO_3^- and/or organic acids.

Fig. 7.5 illustrates the global predictability of $[H^+]_4$ by plotting the measured-modeled differences ($[H^+]_4 - H^+_{measured}$) on a global map. The figure shows that Equation 7.4 predicts $H^+_{measured}$ to within ±5 μeq L^{-1} in eastern North America, western North America and parts of northern Europe but is systematically biased low (from −5 to −20 μeq L^{-1}) in west-central North America, east-central North America, central Europe, northern Europe, and parts of East Asia, and extremely low (from −20 to −300 μeq L^{-1}) in central North America, southern Europe along the Mediterranean, the Russian Federation, central Africa and parts of Southeast Asia. This suggests that HCO_3^- and organic acids (especially in the tropics) should be measured on a routine basis in those regions, particularly where $H^+_{measured} < 5$ μeq L^{-1}. Unfortunately, only the IDAF sites in Africa make these measurements routinely. Rodhe et al. (2002), who estimated the global distribution of H^+ concentrations based on a modified version of Eq. 7.3 that used modeled non-sea-salt SO_4^{2-} and modeled windblown soil-derived Ca^{2+}, also found poor model-measurement comparability in those regions. Based on Fig. 7.5, it is likely that the modeled H^+ concentrations of Rodhe et al. (2002) were poor in those regions for the same reasons that our measurement results were poor, namely, the omission of soil-derived HCO_3^- and/or organic acids.

The key messages from Fig. 7.4 and 7.5 are as follows:

- Equation 7.3 is a very good model for estimating H^+ concentrations everywhere in the world where $H^+ > 5$ μeq L^{-1}. Equation 7.4 is not quite as good.
- In areas where $H^+ < 5$ μeq L^{-1}, Equations 7.3 and 7.4 are not good at estimating H^+. In fact, no matter how well one can measure or model the chemical constituents in Equations 7.3 and 7.4, if one does not measure or model weak acids and bases in areas where $H^+ < 5$ μeq L^{-1}, then the results shown in Fig. 7.4c and d are the best that one can achieve.

Thus, monitoring networks around the world are well advised to measure weak acids and bases including carbonates, organics, phosphates and iron in areas where $H^+_{measured} < 5$ μeq L^{-1}.

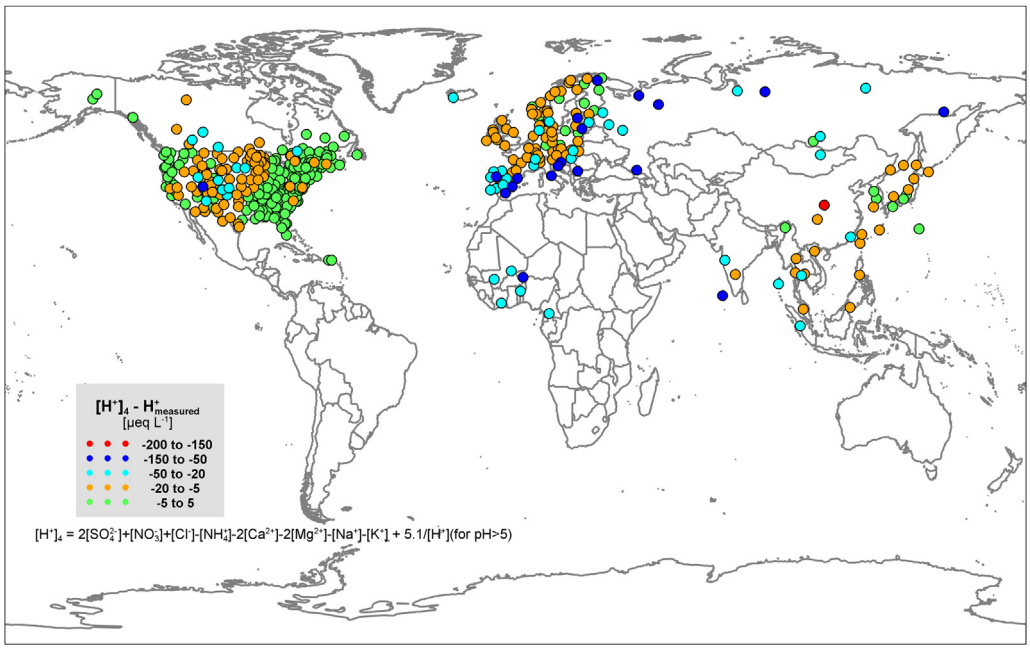

Fig. 7.5. Global pattern of $[H^+]_4 - H^+_{measured}$ for 2005–2007.

8. Phosphorus

Phosphorus (P) is an essential nutrient for terrestrial and aquatic life and its supply can promote or constrain biotic growth and production in soils, lakes and streams and in the ocean. Of particular interest is the role of phosphorus in the production of marine microorganisms due to their capacity for rapid growth and potential for affecting the concentration of atmospheric carbon dioxide (Arrigo, 2005). The links between phosphorus availability and the carbon dioxide cycle and its relationship with global climate change have renewed scientific interest in studying the biogeochemical cycling of phosphorus.

Unlike oxidized and reduced forms of nitrogen, which form stable gaseous compounds in the atmosphere, phosphorus has not been considered to be present in any stable gaseous elemental or molecular form in the atmosphere. However, phosphine (PH_3), a gas formed biogenically in decaying organic matter (Roels and Verstraete, 2001), has been reported recently at ng m^{-3} concentrations in marine and terrestrial atmospheres (Zhu et al., 2007; Han et al., 2011). It is unclear to what extent PH_3 might contribute to the overall atmospheric cycle of phosphorus and we do not consider it further in this section. In addition, volcanic emissions may contain volatilized inorganic phosphorus compounds, but these compounds condense rapidly onto particles under ambient atmospheric conditions (Mambo et al., 19991). Thus, in this section the emissions, transport, and deposition of atmospheric phosphorus is limited to aerosols.

Recently, Mahowald et al. (2008) conducted a comprehensive assessment of the global atmospheric cycling of phosphorus. Since phosphorus is not among the constituents routinely reported by aerosol monitoring programs, measurements are not widespread nor generally of long duration. Drawing on observations from the limited land-based measurements and oceanic cruises, they produced a map showing the global distribution of airborne phosphorus concentrations. Complementing these observations was a map produced from a chemical transport and deposition model that simulated the global phosphorus distribution in the year 2000. As input for this model, atmospheric phosphorus emissions were derived from ancillary models and from estimates of phosphorus from surficial dust, combustion, sea salt, volcanoes, and primary biogenic sources. Very little data are available on how phosphorus varies with aerosol size, adding to the uncertainty of the estimated deposition.

In this chapter, we draw extensively on the work of Mahowald et al. (2008) and include, where possible, data reported since that work. Because of the relatively small amount of observational data on atmospheric phosphorus and uncertainties in atmospheric phosphorus sources and deposition rates, our understanding of phosphorus deposition is poorer than for many of the other substances (N, S) addressed in this assessment. For this reason and unlike other chapters, we also present airborne concentrations in order to improve our understanding of the distribution of atmospheric phosphorus.

8.1. Global/regional perspective on sources of phosphorus

Mahowald et al. (2008) offer estimates of phosphorus emissions based on their global atmospheric phosphorus assessment. By far the largest source of total atmospheric phosphorus is mineral dust resulting from the wind erosion of soils. They suggest that this source accounts for 82% of the total global aerosol phosphorus. Numerous factors affect the rate of wind-driven soil erosion and the fraction of phosphorus in soils, so the importance of atmospheric phosphorus from mineral dust varies widely by region. The desert regions of northern Africa, the Middle East and central Asia are vast sources of mineral dust and atmospheric phosphorus. Ridame and Guieu (2002) studied the phosphorus content of Saharan dust to evaluate its importance in affecting the nutrient cycle of the western Mediterranean Sea. They found that water will dissolve up to 21% of the phosphorus in Saharan dust. Globally, windborne soils are a dominant source of atmospheric phosphorus.

Spores, pollen, and other small bits of plant matter constitute primary biogenic sources of atmospheric phosphorus. Doskey and

Ugoagwu (1989) investigated the macronutrient content of pollen in a temperate pine forest and reported that 60% of the total phosphorus in pine pollen was soluble reactive phosphorus (i.e., orthophosphate). Pollen and other biogenic sources can dominate atmospheric phosphorus in and near forests or other densely vegetated areas, though with a deposition velocity between 1.3 and 30 cm s^{-1} the importance of biogenic aerosols can be characterized as local and regional but not global in extent (Doskey and Ugoagwu, 1989). As a global average, Mahowald et al. (2008) estimate that 12% of atmospheric phosphorus is from primary biogenic sources.

Another important local and regional source of atmospheric phosphorus results from combustion, whether from fossil fuels combusted in utility and industrial boilers, incinerators, or biomass burning. Phosphorus occurs naturally in living and fossil matter and is emitted in fine and coarse particles during combustion of these materials. As a global average, estimates are that these sources generate 5% of the atmospheric phosphorus (Mahowald et al., 2008). On average, sea salt and volcanic aerosols account for approximately 1% of atmospheric P, and can be important in areas distant from other sources.

Orthophosphate (PO_4^{3-}) is readily soluble and available as a nutrient and can play an important role in affecting phytoplankton growth, especially in phosphorus-limited marine environments (Okin et al., 2011). Mineral dust is the dominant global source of PO_4^{3-}, though the PO_4^{3-} fraction of combustion-generated phosphorus is higher than in mineral dust (Mahowald et al., 2008). The fraction of total phosphorus that is soluble PO_4^{3-} varies widely. In common with other aspects of the atmospheric phosphorus cycle, the factors that control phosphorus solubility in mineral dust, biogenic particles and combustion aerosols are not well understood at present.

8.2. Simulated global patterns of phosphorus concentrations and deposition

As stated above, Mahowald et al. (2008) made the first attempt to model the global atmospheric cycle of P. They simulated the atmospheric transport of phosphorus associated with mineral dust, combustion products, primary biogenic particles, marine (sea salt) aerosols and volcanic emissions. Using the best available estimates of the soluble fraction of phosphorus in these materials they also simulated the atmospheric cycle of soluble phosphate. Their simulated global maps of aerosol total phosphorus and phosphate concentrations and deposition are shown in Fig. 8.1. The total phosphorus concentration and deposition maps show distributions consistent with mineral dust as the dominant source of atmospheric P. Dust was also an important source of phosphate, but other sources contributed greater proportions due to their higher soluble phosphorus fractions. Mahowald et al. (2008) assumed fractional phosphorus solubilities of 10% for dust, 100% for volcanic material and 50% for all other sources, but noted that these estimates were rather uncertain.

Mahowald et al. (2008) estimated atmospheric total phosphorus deposition to the globe to be 558 Gg yr^{-1}, with ~17% of this being soluble phosphate. Overall they estimated that ~5% of total phosphorus and ~14% of soluble phosphorus was from anthropogenic sources. Two subsequent modeling studies, both of which were based on the Mahowald et al. (2008) study, estimated total phosphorus deposition to the Earth to be 540 Gg yr^{-1}

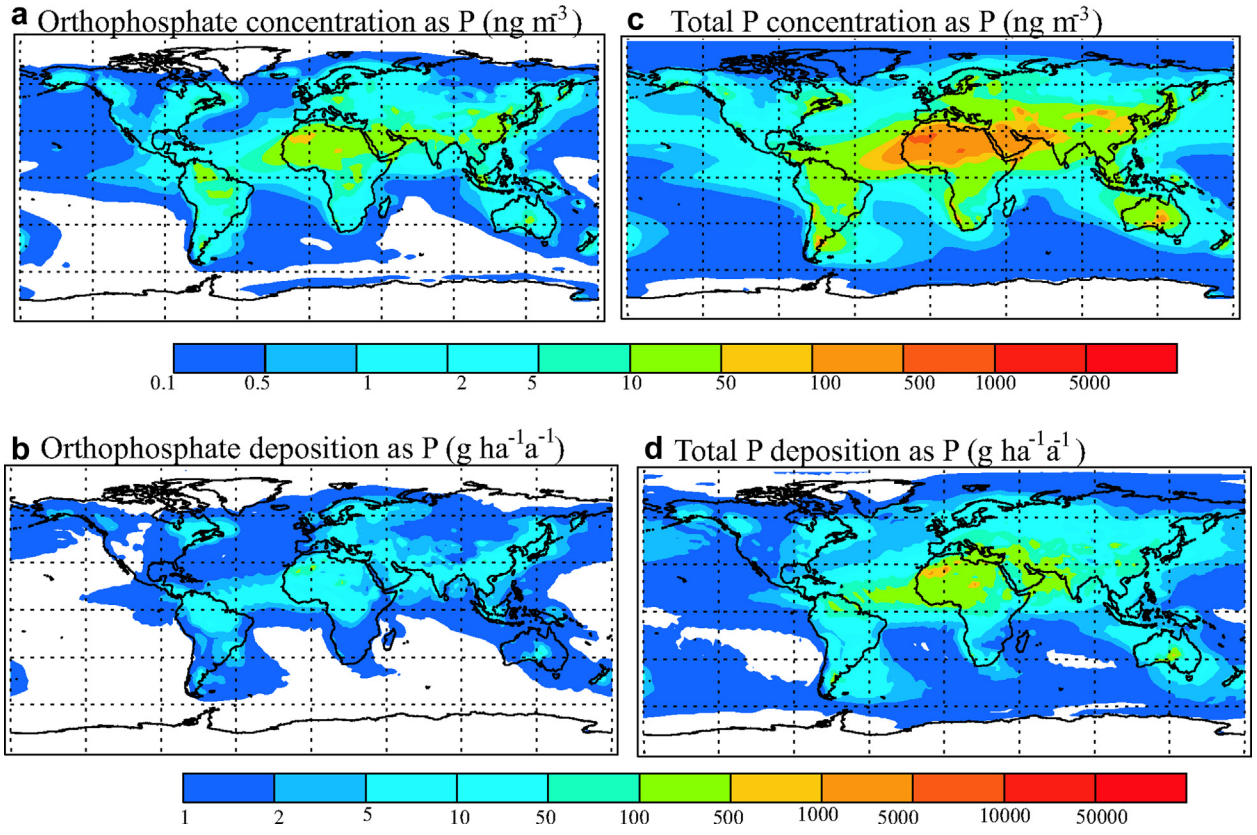

Fig. 8.1. Simulated global maps of aerosol soluble phosphorus (as P in PO_4^{3-}) as (a) concentrations and (b) deposition and aerosol total phosphorus as (c) concentrations and (d) deposition. Reproduced with permission from Mahowald et al. (2008) Global Biogeochemical Cycles, 22, GB4026, doi:1029/2008GB003240, 2008, copyright American Geophysical Union.

(Krishnamurthy et al., 2010) and total phosphorus deposition to the global ocean to be 320 Gg yr^{-1} (Okin et al., 2011).

8.3. Measured global patterns of the wet deposition of phosphorus

Precipitation scavenges phosphorus-containing aerosols in and below clouds. Aerosols contain inorganic and organic phosphorus compounds of varying solubility and stability. When precipitation is collected following wet-only deposition measurement protocols, the sample is exposed during precipitation and contains dissolved, partially dissolved, and insoluble particles, some of which contain phosphorus. When precipitation is collected following bulk deposition measurement protocols, the sample contains particles deposited in the sampler during precipitation as well as during dry weather. Unlike gaseous pollutants such as ammonia or sulfur dioxide, which during dry weather are virtually excluded by funnel-and-bottle bulk samplers (Vet, 1991), particles are not excluded by bulk samplers of any design during dry weather. Further, the fraction of dry-deposited phosphorus captured by bulk samplers is not well-defined. Particle size and density affects dry deposition velocities (Wesley and Hicks, 2000; Mahowald et al., 2008), so wind speed and turbulence affect the capture efficiency of particles on the receptor surfaces of bulk deposition collectors. Ibrahim et al. (1983) demonstrated that buckets overcollect supermicrometer particles and undercollect submicrometer particles relative to natural surfaces. Dolske and Gatz (1985) showed that dry deposition of sulfate varied by as much as an order of magnitude, depending on the sampler size, shape, and method of deployment. As a consequence, bulk-sampled phosphorus and wet-only-sampled phosphorus would be equivalent only if dry deposition contained virtually no phosphorus.

Given that mineral dust and pollen are two important sources of dry-deposited phosphorus, we elected not to present bulk deposition in the global deposition maps of Figs. 8.2 and 8.3 – in light of the fact that bulk deposition includes wet deposition plus an unknown fraction of dry deposition. In addition, we present filtered and unfiltered measurements differently. Filtration of precipitation through a 0.45 micron-pore-size filter is the most common practice for removal of non-dissolved particles. While this practice is effective, no claim is made that it results in a filtrate that is completely free of particles. Notwithstanding this caveat, the phosphorus measured in the filtrate was defined operationally as dissolved phosphorus.

As previously mentioned, PO_4^{3-} is a nutrient and the soluble form of inorganic phosphorus. The fraction of phosphorus that is PO_4^{3-} varies widely, depending on the atmospheric phosphorus source. Provided other nutrient requirements are met, living organisms readily assimilate PO_4^{3-}; it is the preferred phosphorus nutrient and can be consumed by organisms in a precipitation sample and converted to organic and other inorganic forms of P. Although PO_4^{3-} is preferred, organisms also assimilate other phosphorus forms (Migon and Sandroni, 1999), though presumably to a lesser degree and at a slower rate. As a consequence, PO_4^{3-} can be lost from a precipitation sample, while the total phosphorus content of the sample is preserved (Ayers et al., 2003). Given this instability, samples must either be analyzed promptly or preserved in some way. For this assessment, PO_4^{3-} measured in daily samples that were preserved between collection and analysis (e.g., by

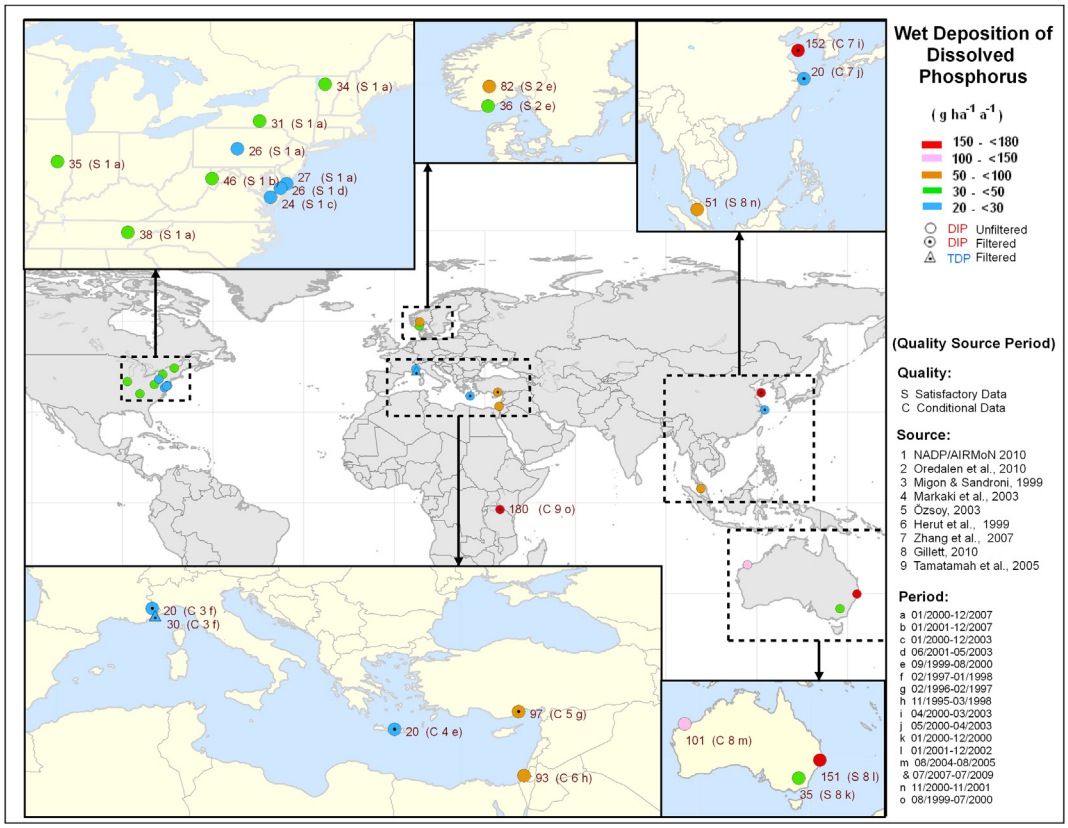

Fig. 8.2. Summary of available data for annual average wet deposition of soluble or dissolved phosphorus (g P ha^{-1} a^{-1}). As shown in the figure legend, symbol shapes identify the soluble phosphorus filtration method for each study and codes identify the data quality, data source and sampling period at each site. Symbols are color-coded according to their wet deposition levels; the annual average flux at each site appears next to the symbol.

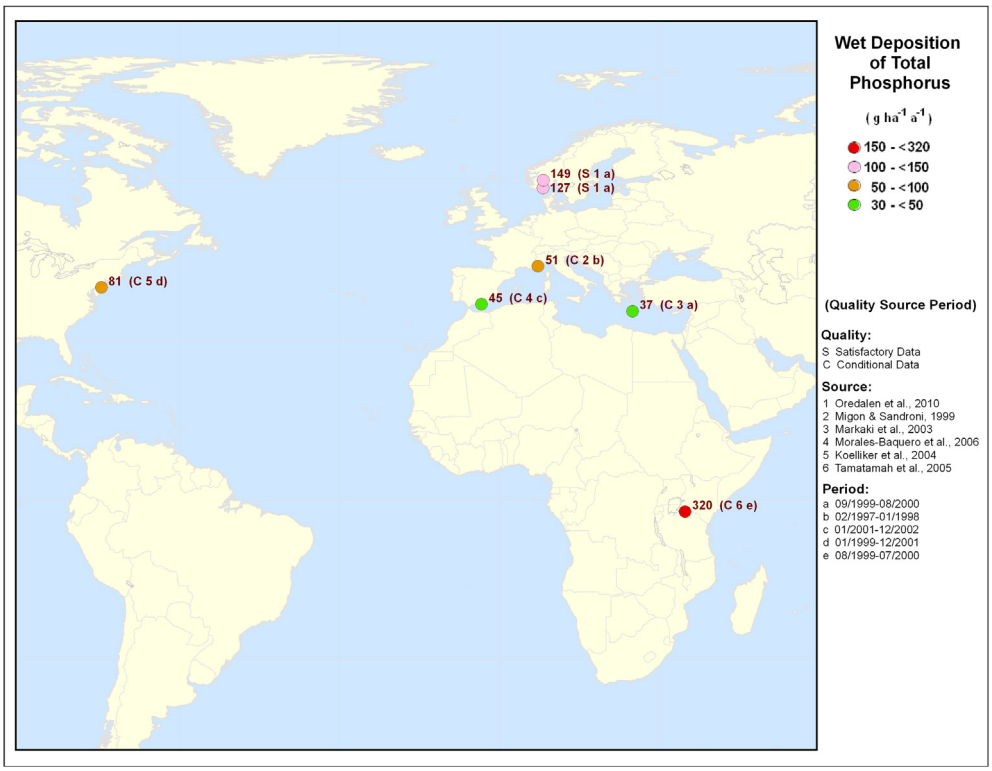

Fig. 8.3. Summary of available data for annual average wet deposition of total phosphorus (g P ha^{-1} a^{-1}). The codes beside each symbol identify the data quality, data source and sampling period at each site. Symbols are color-coded according to their wet deposition levels and the annual average flux at each site appears next to the symbol.

refrigeration) were deemed to be of *satisfactory* quality, as were longer-duration samples if preserved in situ in the sampler.

Measuring phosphorus in precipitation samples is challenging not only because of the instability of PO_4^{3-} but also because concentrations can be very low, e.g., 0.01 mg L^{-1} or less. Total phosphorus exists as PO_4^{3-} and other inorganic and organic phosphorus compounds. Although generally soluble, PO_4^{3-} can be bound by the mineral matter in soil particles of limited solubility (Bergametti et al., 1992). The solubility of other inorganic phosphorus compounds, e.g., phosphate chains or ring compounds known as condensed phosphates, depends on the molecular form, solution acidity, temperature, etc.

The most common method for analyzing phosphorus is a colorimetric test, termed the "ascorbic acid method" (Murphy and Riley, 1962). Without preliminary hydrolysis or oxidative digestion this test responds to PO_4^{3-} in the sample and to a small fraction of condensed phosphates, if present (APHA, AWWA, and WEF, 1999). Despite the possible small contribution from condensed phosphates, analysis results are typically defined operationally as measurements of PO_4^{3-} and are here termed as dissolved inorganic phosphorus (labeled DIP in Fig. 8.2) or, in other publications, as dissolved reactive phosphorus. In order to measure all forms of phosphorus in precipitation, samples must be digested before analysis by heating and acidifying in order to convert the condensed and organic phosphorus to PO_4^{3-}. There are several methods for digesting phosphorus, each having a different efficiency for converting condensed or organic phosphorus to PO_4^{3-}. Further research is needed to evaluate the efficacy of the various digestion procedures in precipitation samples although that work is beyond the scope of this assessment. For this assessment, results of the ascorbic acid analysis following sample digestion using any of these methods were defined operationally as total phosphorus. For filtered samples, the measurements were reported as total dissolved phosphorus (labeled TDP in Fig. 8.2) and for unfiltered samples they were reported as total phosphorus (as in Fig. 8.3).

8.3.1. Dissolved phosphorus

Fig. 8.2 displays measurements of the annual wet deposition of dissolved phosphorus at 23 sites around the world, based on data from studies conducted in the mid to late 1990s through 2007. Fluxes range from 20 to 180 g per hectare per annum (g ha^{-1} a^{-1}). Symbols in the Figure indicate how the samples were handled (filtered or unfiltered) and analyzed (orthophosphate with no digestion as DIP, or orthophosphate following digestion as TDP). Results of studies never previously published are presented for three sites in Australia (R. Gillett, personal communication, November, 2010), a site in Malaysia (R. Gillett, personal communication, November, 2010), two sites in southern Norway (Oredalen et al., personal communication, March, 2010), and nine sites in the eastern United States (NADP/AIRMoN, 2010). Access to individual sample measurements at these 15 sites made it possible to evaluate the data quality as either *satisfactory* or *conditional* and to calculate fluxes from annual precipitation-weighted-mean concentrations and precipitation amounts in the same manner as for other measurements in this assessment (e.g., using half the detection limit in calculations when a detection limit was reported). Data for the 8 other sites were taken from published studies and were rated as *conditional*, since we were unable to evaluate the methods used for the individual sample measurements. Citations for all of the studies are listed in the legend, as are the month and year of the beginning and ending of the reported measurements.

Virtually all of the studies reported substantial intra-annual variability in the wet deposition of dissolved phosphorus. Reasons included variations in precipitation amount and frequency (e.g., G. Zhang et al., 2007), dust storms (e.g., Özsoy, 2003) and incinerators and biomass burning (e.g., Migon and Sandroni, 1999).

Because of intra-annual variability, studies lasting less than one year were not included in the global map. For seven of the studies, the annual flux shown on the map was based on a single year of data, so there was no way to account for inter-annual variability. For the remaining studies, the sampling period ranged from 2 to 8 years in duration and an average annual flux was reported. Instead of adding estimates of variability to the values in Fig. 8.2, annual fluxes were placed in one of five deposition classes, depicted by color. The spatial distribution of the colored symbols shows the locations of heavy and light phosphorus deposition.

From January 2000 through December 2007, the U.S. Atmospheric Integrated Research Monitoring Network (NADP/AIRMoN, 2010) had the longest consistent set of wet-only PO_4^{3-} measurements among the data available for this assessment. AIRMoN samples were collected daily within 24 h of the onset of precipitation. In order to retard microbial degradation of nutrients including PO_4^{3-}, samples were refrigerated after collection, during storage and shipment, until analysis. The unfiltered samples were analyzed without digestion for dissolved PO_4^{3-}. Measurements affected by extrinsic contamination such as vegetation, insects, or other organic debris observed in the samples, were excluded. Six of the nine AIRMoN sites had eight *satisfactory* years of data. These are shown in the upper left inset as the sites with Quality/Source/Period = S 6 g. Average annual PO_4^{3-}–P fluxes ranged from 27 to 38 g ha^{-1} a^{-1} at these six sites and reflect the distribution of mineral, combustion, and biological particulate PO_4^{3-} sources in the eastern United States. Inter-annual variability at these six sites, as expressed by the coefficient of variation, ranged from 15 to 22 percent. With this relatively small amount of variation, only the southernmost site (average annual flux: 38 g ha^{-1} a^{-1}) was significantly different (t-test, $p < 0.05$) than any of the other sites.

Straightforward comparisons within and among regions are made difficult by differences in the sample types, sampling period lengths, and sample handling procedures. Least problematic are comparisons where the protocols and the Quality/Source/Period designations are identical. Examples include: coastal and inland DIP fluxes in southern Norway (Oredalen et al., personal communication, March, 2010) and DIP fluxes at sites around the Mediterranean Sea (Markaki et al., 2010). Readers are encouraged to examine these and other cited publications to gain insights into the relationships between the reported deposition and the local and regional sources affecting these fluxes. In one of these studies (Migon and Sandroni, 1999), investigators collected wet-only rain-event samples at Cap Ferrat, a coastal French site, in order to examine the partitioning between soluble and insoluble phosphorus and between TP and PO_4^{3-}–P. Results of this 1-year study showed that the TP flux of 51 g ha^{-1} a^{-1} comprised a TDP flux of 30 g ha^{-1} a^{-1} (or ~60 percent of TP), while the total suspended particle phosphorus flux, measured by digesting the residue on the filter, was 22 g ha^{-1} a^{-1}. Further, the PO_4^{3-}–P flux was 20 g ha^{-1} a^{-1}, or two-thirds of the TDP. While only one year in duration, studies of this type are useful for sorting out the various phosphorus types, forms, and sources, as well as informing investigations of the effects of phosphorus on marine, aquatic, and terrestrial ecosystems.

One other study of special note examined the DIP concentrations in unfiltered wet-only samples collected when air trajectories were incoming from the remote southern ocean at Cape Grim, a background site in northwestern Tasmania (R. Gillett, personal communication, November, 2010). The average DIP concentration under these conditions for each of five years was 0.003 mg per liter, suggesting that sea spray is a weak contributor to atmospheric P.

8.3.2. Total phosphorus

Fig. 8.3 displays measurements of annual TP wet deposition at 7 sites, based on data from studies conducted in the late 1990s and early 2000s. Fluxes range from 37 to 320 g ha^{-1} a^{-1}. Results of studies never previously published are presented for two sites in southern Norway (Oredalen et al., personal communication, March, 2010). These data are from a 1-year study in which TP (Fig. 8.3) and DIP (Fig. 8.2) were measured in wet-only samples at a coastal and an inland site. The DIP:TP at the coastal site was 0.28, which is somewhat lower than the 0.39 found at Cap Ferrat (Migon and Sandroni, 1999). The DIP:TP at the inland site was 0.55. One might infer from these differences that PO_4^{3-} is a larger fraction of TP at inland sites because of the effects of combustion, biomass burning, and phosphate fertilizers on airborne phosphorus concentrations. Deforestation and related biomass burning and cultivation practices were cited as likely causes of the high DIP:TP of ~0.6 in wet-only samples from a Serengeti National Park site in Tanzania, as well (Tamatamah et al., 2005). Scientists there are trying to better understand the causes of the increasingly eutrophic conditions in Lake Victoria, where phosphorus levels have more than doubled since the 1960s (Tamatamah et al., 2005). Based on all of these studies the ratio of dissolved to total phosphorus ranges from approximately 0.3–0.9. It is clear that isolating the effects of various phosphorus sources on TP, TDP, and DIP requires careful studies in which wet-only samples are analyzed for all phosphorus types and the results are coupled with trajectory analyses and airborne phosphorus measurements. TP wet deposition at three measurement sites in the Mediterranean Basin ranged from 37 to 51 g ha^{-1} a^{-1}.

Citations for all of the TP measurements are listed in the legend of Fig. 8.3, as are the month and year of the beginning and end of the reported measurements. Readers are encouraged to examine these publications for additional information about these studies.

8.4. Airborne concentrations of phosphorus

Due to the relative lack of dry deposition data for phosphorus, we examine here aerosol-phase phosphorus concentration data in an attempt to improve our understanding of the distribution and behavior of atmospheric P. As was the case with wet deposition, a variety of sampling (filter materials and sampler flow rates) and analytical techniques have been used to study aerosol phosphorus. Analysis methods include direct determination of total phosphorus on aerosol filters (e.g. by particle-induced X-ray emission (PIXE) analysis), total phosphorus analysis following complete filter digestion and aqueous extraction followed by diverse methods for determination of soluble inorganic, soluble organic and total dissolved phosphorus. As for wet deposition, we describe measurements of soluble phosphate based on the ascorbic acid method as dissolved inorganic phosphorus (DIP).

Measurements of aerosol phosphorus, as for phosphorus in wet deposition, are challenging because phosphorus concentrations in aerosol form are rather low, although aerosol collection procedures can be optimized (e.g., by increasing sampler flow rates or collection times) to compensate for this to some extent. Again, in contrast to the other substances included in this assessment, we have chosen to expand the few data available to us by including the results of studies carried out during short-term missions aboard ships on the open ocean (see Figs. 8.4 and 8.5). These studies give further insight into the distribution of atmospheric P, but it should be noted that these results only reflect the conditions prevalent at the time of each mission and are not necessarily representative of the long-term averages described elsewhere in this work.

8.4.1. Soluble aerosol phosphorus

Fig. 8.4 shows concentrations of aerosol dissolved inorganic phosphorus around the globe. There are rather few long-term measurements in this record, with a site in Taiwan (Chen and

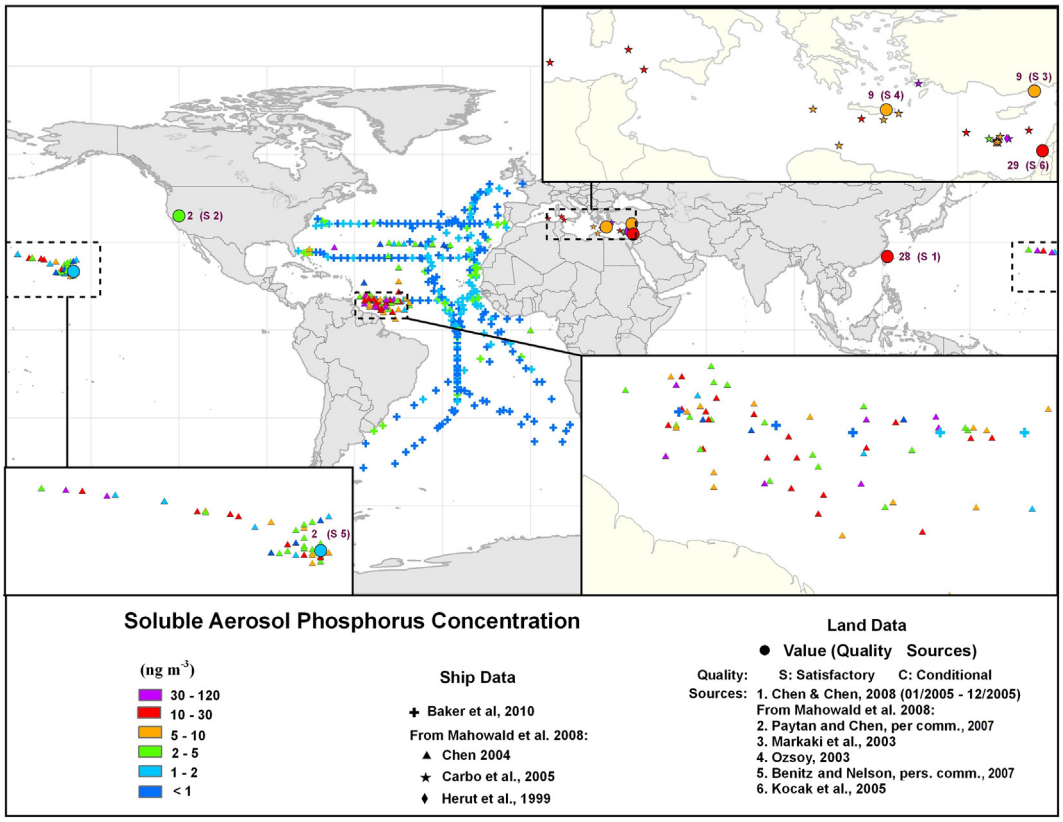

Fig. 8.4. Summary of available data for aerosol DIP concentrations (ng P m^{-3}). Large circular symbols denote long-term measurement sites for which annual average concentrations are shown. For these sites, symbols are color-coded according to their annual average concentrations which are given next to each symbol. Codes next to these symbols identify the data status and data origin shown in the legend. Smaller symbols show concentrations obtained from aerosol sampling aboard ships, color-coded according to their instantaneous measured concentrations. Symbol shapes identify the origin of the data.

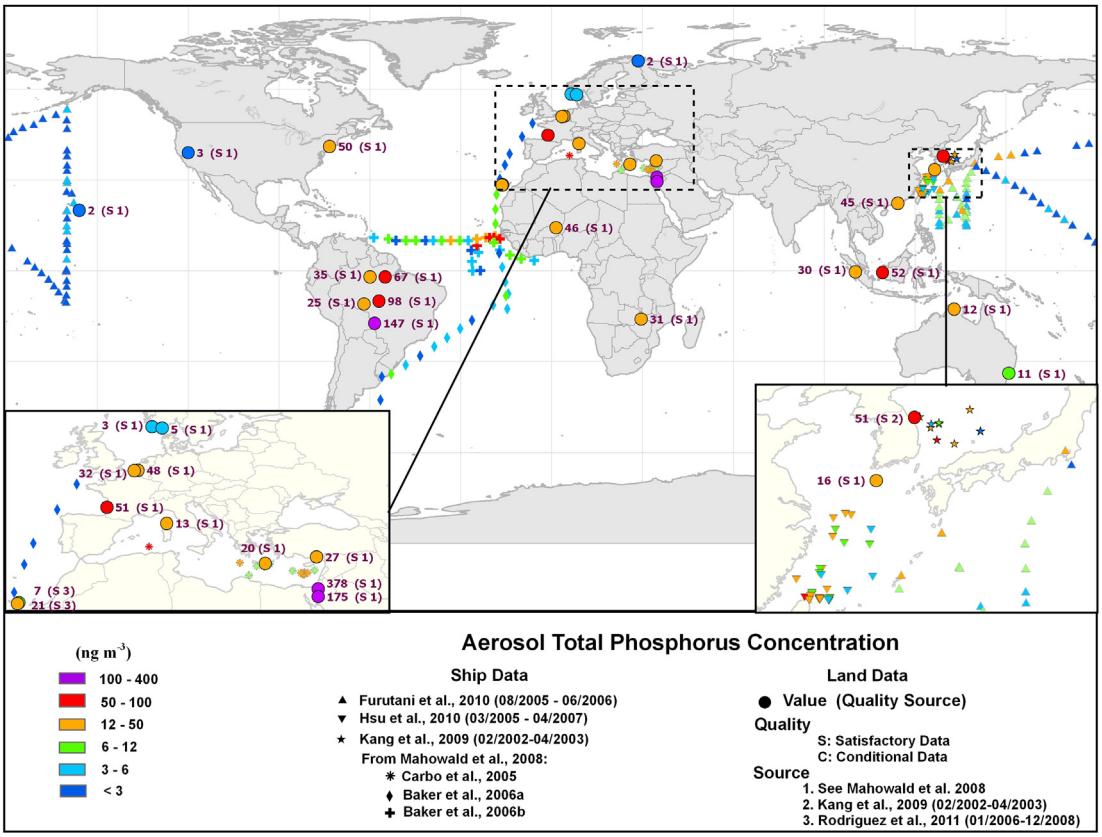

Fig. 8.5. Summary of available data for aerosol total phosphorus concentrations (ng P m^{-3}) per caption of Fig. 8.4.

Chen, 2008) and a few sites included in the Mahowald et al. (2008) compilation (Tel Shikmona, Israel; Finokalia, Crete; Erdemli, Turkey; Lake Tahoe and Hawaii, U.S.). Average DIP concentrations at these sites varied between 80 ng m^{-3} near major deserts (Herut et al., 1999 as cited in Mahowald et al., 2008) and 2.2 ng m^{-3} at Lake Tahoe (Paytan and Chen, personal communication, 2007 as cited in Mahowald et al., 2008).

Short-term measurements are available from cruises in the central North Pacific and Atlantic Oceans and the Mediterranean Sea. These data illustrate the difficulties in the use of short-term measurements for our assessment. For instance, in the western tropical North Atlantic (~5–12 °N) significant differences appear between the datasets of Chen (2004, as given in Mahowald et al., 2008) and Baker et al. (2010), while these two datasets are in much better agreement further to the north off North Africa (~25–35 °N). The differences between the datasets in the western Atlantic likely reflect the strong seasonality in Saharan dust transport. Much of the Chen (2004) dataset was acquired during boreal winter and summer periods of high dust transport (e.g. Basart et al., 2009), while the Baker et al. (2010) data in this region were obtained under autumn low dust transport conditions. As a whole, the Baker et al. (2010) dataset gives the impression of rather uniform DIP concentrations across the Atlantic basin, but as a long-term representation this is probably misleading. All of these data were obtained during periods of weak mineral dust transport, so that it does not show the strong spatial heterogeneity associated with dust-derived phosphorus transport. Where cruise data were acquired during different seasons in a given region (e.g., the western tropical North Atlantic and central Pacific) strong variations in aerosol DIP concentrations were observed.

Baker et al. (2010) classified their aerosol samples by source region. Median DIP concentrations varied from ~0.4 ng m^{-3} for samples that had spent at least 5 days over the South Atlantic Ocean to ~1.6 ng m^{-3} for samples that contained Saharan dust. They also reported that DIP concentrations of samples originating in southern Africa were slightly higher in samples influenced by biomass burning (median 1.1 ng m^{-3}) than in those that were not (median 0.9 ng m^{-3}).

8.4.2. Aerosol total phosphorus

For aerosol total phosphorus concentrations (Fig. 8.5) there were rather more long-term measurement sites and fewer ship campaigns than was the case for DIP. Coverage of long-term sites was best in western Europe and the Mediterranean, Southeast Asia and the Amazon region of South America. Sites were sparse elsewhere, with none available for eastern Europe and central and southern Asia.

Total phosphorus concentrations were highest adjacent to deserts (175–378 ng m^{-3} (Andreae et al., 2002; Chen et al., 2008)) and in the Brazilian savanna (147 ng m^{-3} (Maenhaut et al., 1999)), the former associated with high mineral dust loadings and anthropogenic emissions and the latter with biomass burning. Lowest concentrations were observed in Hawaii (2 ng m^{-3}: see Mahowald et al., 2008), at Lake Tahoe in western North America (3 ng m^{-3}: see Mahowald et al., 2008), and at sites in Scandinavia (2–3 ng m^{-3} (Virkkula et al., 1999)).

While there is little total phosphorus data available over the oceans, the studies of Baker et al. (2006a and b) show concentration maxima associated with Saharan dust plumes over the Atlantic Ocean. The results of Furutani et al. (2010) show relatively high concentrations of total phosphorus near the east coast of Asia and much lower concentrations in the central North Pacific. Furutani et al. (2010) estimated that a significant fraction (~20–40%) of total phosphorus was of anthropogenic origin, while a much smaller proportion came from mineral dust from Asia.

8.5. Calculated dry deposition of phosphorus

We use the data presented in Figs. 8.4 and 8.5 to estimate annual dry deposition of DIP and total P. In order to do this we calculated inferential values of dry deposition (F_d) from aerosol concentrations (C_a) according to Equation (8.1) in which v_d represents the dry deposition velocity of phosphorus-containing aerosols.

$$F_d = v_d C_a \tag{8.1}$$

Dry deposition velocities are poorly constrained and vary non-linearly with particle size, wind speed and deposition surface. They are particularly poorly understood over the ocean where direct measurements are very challenging and the size range of phosphorus-bearing aerosols is largely unknown. Because of this uncertainty and in order to provide a degree of comparability with the fluxes shown in Fig. 8.1, we used modeled gridded annual average deposition velocities from Mahowald et al. (2008) to calculate the fluxes shown in Figs. 8.6 and 8.7. The size distribution of the phosphorus aerosols was assumed to be the same as that of mineral dust. This assumption may not be valid over tropical forests where the concentrations of large primary biogenic particles are likely to be high and where dust concentrations are relatively low. We emphasize that the uncertainty in deposition velocities and the resultant dry deposition is considerable.

In order to maximize the information derived from the dataset available, we represent the calculated dry deposition of phosphorus in units of mg P ha^{-1} day^{-1} in Fig. 8.6 and 8.7. This recognizes that the daily aerosol sampling conducted during ship-based studies is unlikely to be representative of annual average conditions. For the long-term monitoring sites we also discuss annual average dry deposition below.

Daily calculated DIP dry deposition in the Atlantic, Mediterranean and North Pacific basins ranged from 0.1 to 250, 31 to 345 and 1.2 to 191 mg ha^{-1} day^{-1} respectively. As indicated in Section 8.4.1, there is considerable seasonality in different DIP sources. In Fig. 8.6 (where possible) we have plotted individual dry deposition estimates as a function of collection date in order to show how representative the observations are of the annual cycle. Only in two cases (the western tropical Atlantic and tropical North Pacific – see boxes in Fig. 8.6) do we consider that the available data can be combined to give a rough approximation of an annual average cycle. For these two areas we use the median daily fluxes to calculate tentative estimates of the annual average dry deposition of DIP of 3.0 (western tropical Atlantic) and 3.6 g ha^{-1} a^{-1} (tropical North Pacific). Based on an analysis of aerosol source frequency and characteristic DIP concentrations for those sources, Baker et al. (2010) estimated a lower limit for dry DIP deposition in a similar area of the western tropical Atlantic of 2.2 mg ha^{-1} day^{-1} (0.8 g ha^{-1} a^{-1}). Overall, these authors estimated the lower limit for dry DIP deposition to the Atlantic Ocean between 50°N and 50°S to be ~6 Gg a^{-1}.

For TP, daily dry deposition to the ocean (Fig. 8.7) varied from <0.5–106, 31–750 and <0.1–723 mg ha^{-1} day^{-1} for the Atlantic, Mediterranean and North Pacific Oceans respectively. Again, it should be remembered that these daily fluxes are not necessarily representative of the annual average. For the western North Pacific (see box in Fig. 8.7) we used the median of the available daily fluxes to estimate an annual average dry deposition of TP of 9.4 g ha^{-1} a^{-1}. This estimate should also be regarded as tentative due to the poor temporal coverage of the data.

Calculated annual dry deposition at the land stations for DIP is in the range <3–130 g ha^{-1} a^{-1} and for TP in the range <10–617 g ha^{-1} a^{-1}. These compare to the measured wet deposition (Fig. 8.2 and 8.3) ranges of 20–180 g ha^{-1} a^{-1} for DIP and 37–

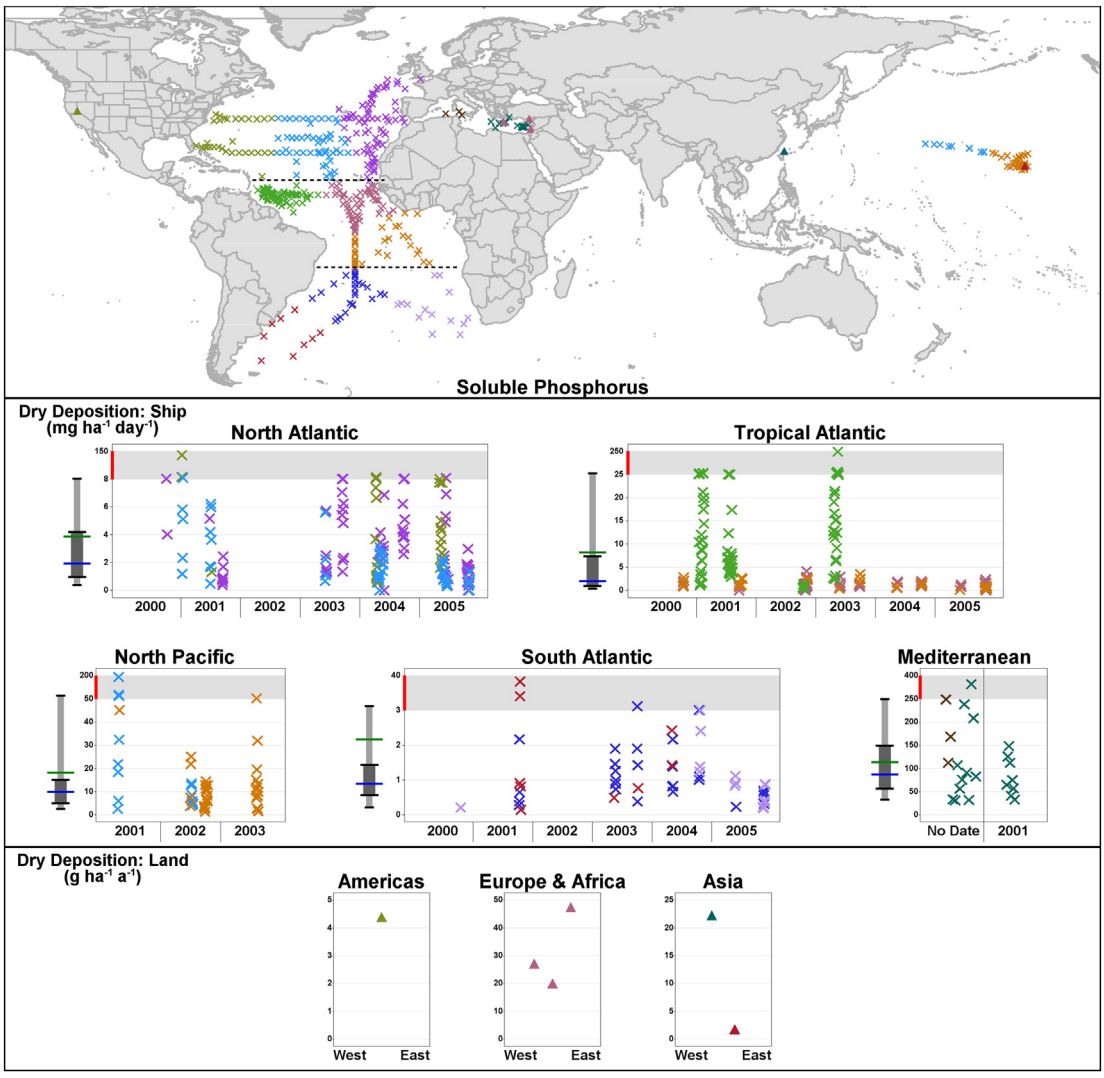

Fig. 8.6. Calculated dry deposition of DIP derived from the data presented in Fig. 8.4. Results from studies aboard ships are given in units of mg P ha^{-1} day^{-1}, while units from long-term measurements at land sites are in g P ha^{-1} a^{-1}. Where suitable, conversion from mg P ha^{-1} day^{-1} to g P ha^{-1} a^{-1} can be done by multiplying by 0.365. Methods used to calculate fluxes are given in Section 8.5. Samples are color-coded according to their location. Lower panels show individual flux values as a function of sampling date for various ocean regions (dashed lines in the Atlantic indicate the upper and lower boundaries of the Tropical Atlantic region), and annual average fluxes for the land sites plotted on an arbitrary scale indicating the longitudinal distribution of the sites through each region. Changes in *y*-axis scales on these panels are indicated by gray shading. Boxes on the map show ocean regions where individual values were averaged to produce annual dry deposition estimates (see text). The box-and-whisker plots identify the mean value (green) and the 5th, 25th, 50th (blue), 75th and 95th percentile values.

320 g ha^{-1} a^{-1} for TP. Direct comparisons between these dry and wet deposition estimates are inappropriate because there are no co-located (in time and space) wet deposition and aerosol concentration data. Notwithstanding the limited information available, it would appear that both wet and dry deposition make significant contributions to the global atmospheric phosphorus flux, but their relative contributions vary regionally depending on precipitation rates and proximity to sources.

8.6. *Summary, uncertainties and gaps*

In comparison to sulfur and nitrogen, few studies of atmospheric phosphorus deposition exist and several parts of its global cycle are poorly understood. There are very few long-term records of phosphorus deposition and many records are unevenly distributed in space and time. Sources of phosphorus to the atmosphere, and the processes that control the dissolution of phosphorus from those materials, are also relatively poorly understood. Condensed and organic phosphorus compounds have limited solubility and PO_4^{3-} can be readily adsorbed in soil mineral matter, limiting its solubility. Although mineral dust appears to be the dominant source of atmospheric phosphorus, the phosphorus content of this dust is not well characterized (see discussion in Mahowald et al., 2008). Phosphorus content is likely to be inherently variable due to the association of phosphorus with trace minerals (e.g., apatite) that are not uniformly distributed among different dust sources. In addition, Rodriguez et al. (2011) recently suggested that when high phosphorus concentrations occur with dust in the Saharan air layer they are augmented by emissions from phosphate mines and phosphate fertilizer industries. These sources were not included in the study of Mahowald et al. (2008), due to a lack of available information about their distribution and emission characteristics. As a whole, these uncertainties currently make parameterization of global phosphorus deposition even more difficult than the already complex problem of estimating global atmospheric mineral dust fluxes.

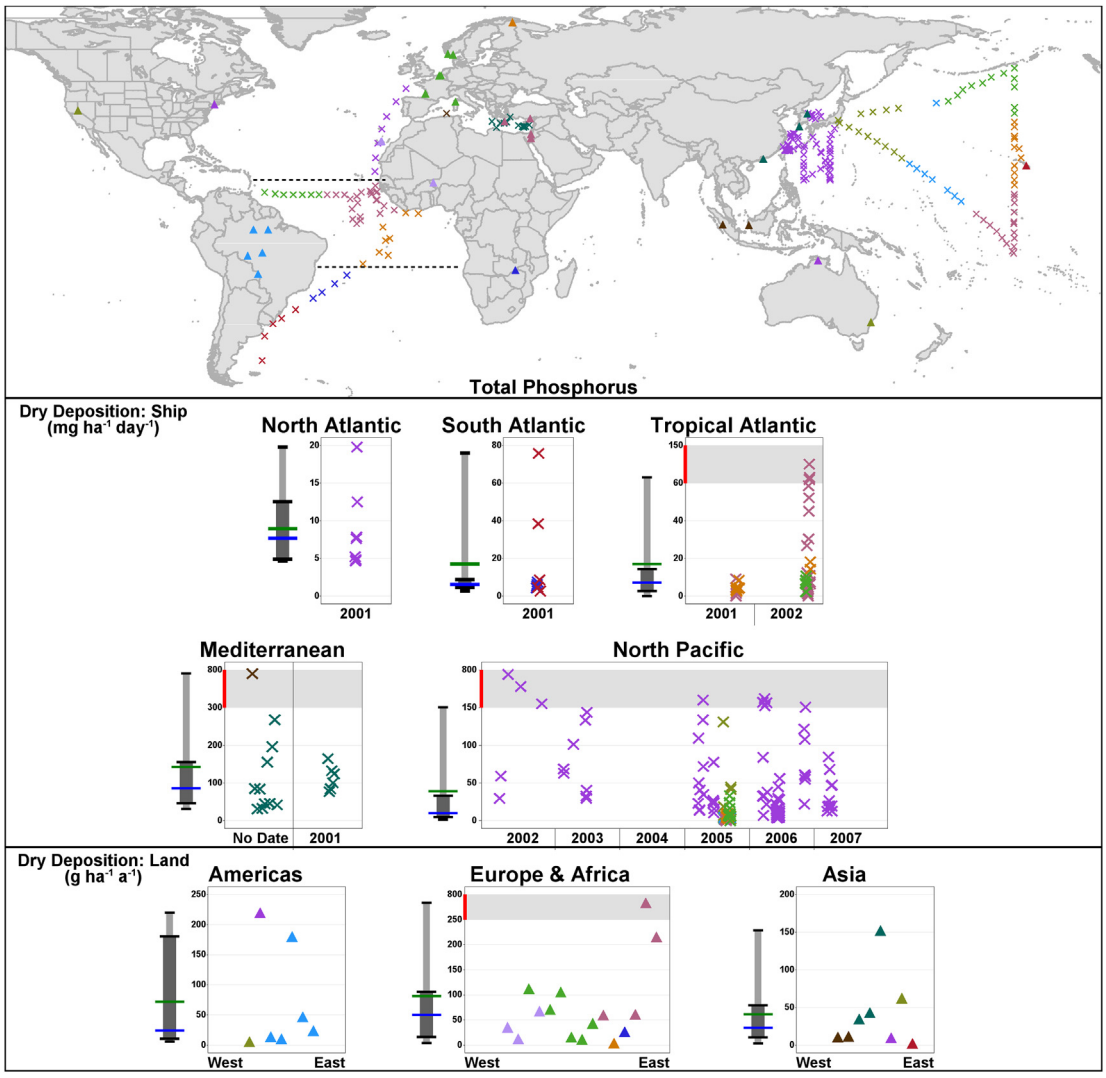

Fig. 8.7. Calculated dry deposition of total phosphorus derived from the data presented in Fig. 8.5 per caption of Fig. 8.6.

The fraction of atmospheric phosphorus that is bioavailable is also uncertain at present. DIP is generally assumed to be readily available to photosynthetic organisms, but soluble organic forms of phosphorus may also be available to organisms with alkaline phosphatase enzyme activity (Stihl et al., 2001). It also may be possible that some organisms are able to promote the dissolution of phosphorus from mineral particles, as appears to be the case for iron dissolution from dust particles for the marine diazotroph *Trichodesmium* (Rubin et al., 2011).

Atmospheric inputs of phosphorus are likely to be most important to ecosystems in which primary productivity is limited by low phosphorus availability. The eastern Mediterranean is probably the largest such marine ecosystem, prompting several workers to investigate atmospheric phosphorus in this region. Although P-limitation of primary productivity is probably rather uncommon in the present global ocean (Moore et al., 2002), trends towards increasing P-limitation in the Pacific Ocean near Hawaii (and perhaps elsewhere) may be related to anthropogenic influences on the atmospheric N and Fe cycles (Krishnamurthy et al., 2009). Phosphorus limitation (or co-limitation with Fe) may also be important for diazotrophic (nitrogen fixing) organisms in the tropical oceans (Mills et al., 2004). Over long times cales phosphorus may regulate the productivity of terrestrial ecosystems such as the western Hawaiian islands (Chadwick et al., 1999), the Amazon basin (Swap et al., 1992) and the semiarid steppes of Africa and Eurasia (Okin et al., 2004). The role of phosphorus as a limiting nutrient in freshwater lakes is also well established (Schindler, 1977). It is clear from the foregoing discussion that major gaps exist in our understanding of global wet and dry deposition of phosphorus and that further measurements and research are required to quantify the role of atmospheric deposition in the biogeochemical cycling of phosphorus.

Future measurements of phosphorus deposition will need to address wet deposition and size-resolved particle-phosphorus in air – the latter being used to estimate inferential dry deposition. In the past, a number of deposition studies have relied on bulk deposition measurements to estimate total deposition specifically at sites distant from phosphorus dust sources. These studies have assumed that, with proper chemical preservation and siting, bulk deposition measurements can reasonably represent the two main types of phosphorus deposition: wet deposition plus coarse particle dry deposition. In light of the uncertainties associated with bulk deposition measurements (Section 8.3; WMO/GAW, 2004), the atmospheric deposition community generally discourages bulk

measurements. For completeness, however, a number of these studies are summarized in Table S4 of the Addendum including published studies from Japan, Israel and the Mediterranean Basin (Tsukuda et al., 2005; Herut et al., 1999; Guieu et al., 2010; Markaki et al., 2010) and unpublished studies at forested sites in eastern Canada (data sources: Semkin, 2010; Yao et al., 2010). Readers are left to evaluate whether or not the bulk deposition values in Table S4 fall within their tolerance limits for total deposition.

9. Conclusions

The major objective of this assessment was to provide the science and policy communities with the best available information on the composition of precipitation and atmospheric deposition of major compounds globally and regionally. This was accomplished by presenting quality assured measurement-based data from monitoring networks and long-term research studies around the world, complemented by model results generated by 21 Eulerian global models that participated in the Coordinated Model Studies Activities of the Task Force on Hemispheric Transport of Air Pollution (TF HTAP). This approach resulted in the generation of maps that are useful for understanding concentrations and deposition of wet- and dry-deposited substances. The authors assessed the key information necessary to understand the spatial and temporal characteristics of precipitation chemistry and wet and dry deposition. Recognizing that different research communities would want different products from the paper, the authors aimed to address the needs of many science communities and to provide the basic building blocks to assist other environmental experts in their future research programs.

A major product of this assessment is a quality assured, regionally-representative set of global deposition data that is available for downloading from the web page of the World Meteorological Organization World Data Centre for Precipitation Chemistry (WDCPC) at http://wdcpc.org/. This data set was used to create global wet deposition maps for two time periods, 2000–2002 and 2005–2007, and was complemented by maps of the TF HTAP ensemble-mean modeling results for the year 2001. A subset of the maps generated have been included in the main manuscript; many additional maps and tables appear in the Addendum in this Special Issue. The authors, most of whom have expertise in precipitation chemistry and deposition for their particular region of the world, believe that this assessment provides as complete a picture of global deposition as possible at the present time.

The Introduction raises three key science questions that were the basis of this assessment. In some cases, the answers are thorough and in others they are quite limited. A short summary of the results and conclusions is presented here for each of the three questions. More detailed summaries may be found at the end of each preceding section.

1. What do measurements and model estimates of precipitation chemistry and wet, dry and total deposition of sulfur, nitrogen, sea salt, dust, organic acids, acidity (pH), and phosphorus show globally and regionally?

Despite the scarcity of sulfur measurements in many areas of the world, sulfur concentrations in precipitation and wet deposition are reasonably well characterized globally. This is due to the availability of high-quality observations from robust monitoring networks and studies dedicated to understanding and tracking the impact of SO_2 emissions over the last several decades. Highest sulfur wet deposition occurs in the major established and emerging industrial areas, principally in the northeastern United States, western Europe, and East Asia. Dry deposition methods remain imprecise and measurement-based inferential estimates are available only in a few countries. However, ensemble-mean model global patterns of dry and total deposition closely mimic the wet deposition patterns. The TF HTAP ensemble-mean global model results significantly overestimated total deposition of sulfur in Europe as well as dry and total deposition in North America.

Nitrogen deposition is also reasonably well characterized globally for nitrates and ammonium in precipitation and dry deposited nitric acid and particle-nitrate. Wet deposition of nitrogen is highest in eastern North America, southern Europe, northeast India, southeast Asia, and northern Oceania. In industrialized regions, oxidized nitrogen is often a larger contributor to nitrogen wet deposition than reduced nitrogen. In regions of intensive agriculture and many low deposition areas over the oceans, reduced nitrogen is often greater. Globally, deposition of reduced nitrogen deposition continues to exceed oxidized nitrogen. As with sulfur, many areas of the world have few if any measurements and measurement-based inferential dry deposition estimates exist for only a few regions. Model-based dry and total deposition are highest in the eastern United States, western Europe, South Asia and eastern China.

The contribution of organic acids to precipitation acidity is important in many regions of the world and may be relevant to climate and ecosystem issues because of the carbon content of these compounds. Long term measurements of organic acids in precipitation exist at only a few sites worldwide, and aside from DEBITS (Deposition of Biogeochemically Important Trace Species) sites in Africa, there are no routine measurements of organic acids in any of the major precipitation chemistry monitoring programs. An integrated global view of previously published organic acid data suggest that the highest concentrations of formate and acetate in precipitation are generally observed in forested tropical areas near the equator, with a gradual decrease toward the poles. Total wet carbon deposition from these two compounds exceeds that of sulfur at most African sites and is comparable to the reported wet nitrogen deposition. Organic acids are unstable in precipitation samples due to biodegradation, requiring careful sample preservation beyond the methods employed for major ions. There are no known network estimates of air concentrations or dry deposition of these compounds.

Wet deposition of ortho-phosphorus (as PO_4^{3-}) is measured routinely by only one network worldwide – the Atmospheric Integrated Research Monitoring Network (AIRMON) in the eastern United States. Routine, long term, network measurements of both wet and dry phosphorus deposition are needed on all continents and oceans in order to quantify the role of atmospheric deposition in the biogeochemical cycling of phosphorus. Phosphorus exists in organic and inorganic (mineral dust) forms that have limited solubility and are not well characterized. Model-simulated total phosphorus concentrations and deposition around the globe are consistent with mineral dust, which is believed to be the dominant source of atmospheric phosphorus. Atmospheric phosphorus occurs primarily in the form of coarse particles so the primary dry deposition process is gravitational sedimentation, a process that is not handled with confidence using currently-available measurement methodologies. Atmospheric inputs of phosphorus are likely most important to ecosystems where primary productivity is limited by phosphorus availability or by anthropogenic influences of nitrogen or iron deposition. The ranges of estimated annual dry deposition and measured wet deposition of DIP and TP at land stations are roughly equivalent. Direct comparisons between the dry and wet ranges, however, cannot be done because collocated wet deposition and aerosol concentration measurement data are not available. Despite the limited data availability, the existing data

suggest that both wet and dry deposition make significant contributions to the global atmospheric phosphorus flux, although their relative contributions vary regionally depending on precipitation rates and proximity to sources.

Acidity and pH are dominated by strong mineral acids in locations near and downwind of major industrial regions of the world including eastern North America, Europe, and east Asia. In locations where H^+ concentrations in precipitation are less than 5 μeq L^{-1}, weak acids including carbonates and organics play a major role in determining acidity. Based on either measured or modeled concentrations of SO_4^{2-}, NO_3^-, NH_4^+ and Ca^{2+}, global H^+ concentrations in precipitation can be estimated well except in areas where H^+ concentrations are less than 5 μeq L^{-1}. In these regions, the bicarbonate, formate and acetate ions, in some combination, must be included in the measurement and/or modeling scheme. Measurement programs in those areas are encouraged to measure these ions on a routine basis.

Wet deposition of sea salt closely parallels the modeled emissions patterns, with deposition being highest over the regions of the oceans where mean wind speeds are highest, principally over mid- and high-latitude oceans. Both wet and dry sea salt deposition decrease rapidly with distance inland from the coast, although saline inland water bodies such as the Black and Caspian Seas also influence deposition to surrounding regions. Of key importance is that total deposition of sea salt to inland lakes and forests is of ecological significance, and values of 20–40 kg ha^{-1} a^{-1} may occur as far as 500 km inland.

Measurements of base cation wet deposition provided the basis for estimating the sum of Na^++Ca^{2+}+Mg^{2+}+K^+ in wet deposition. This sum is of interest to the critical loads science community because it must quantify the total deposition of these four base cations in orer to calculate critical loads and exceedances of aquatic and terrestrial ecosystems. Although wet deposition is only one part of the total deposition, it serves as an important source of information to the critical loads community. The global measurements of wet deposition of the base cation sum ranged from 0.01 to 11.7 keq ha^{-1} a^{-1} in 2000–2002 and 0.01–8.5 keq ha^{-1} a^{-1} in 2005–2007. Unfortunately, the measurement data were too sparse to characterize base cation deposition in and downwind of the regions of the world where aeolian dust deposition is expected to be high, e.g., the major deserts and arid regions of the world. Enhanced monitoring in these areas is needed.

2. How has wet and dry deposition of major ions changed since 2000 and, where information and data are available, since 1990 as a result of changing precursor anthropogenic emissions?

Information is available to describe global changes in wet and dry deposition of sulfur (since 1990) and reduced and oxidized nitrogen (since 2000). However, global changes remain impossible to estimate for sea salt, organic acids and total phosphorus. Temporal changes to precipitation-weighted mean non-sea-salt sulfur (nssS) concentrations, wet deposition and total deposition vary widely across the globe. In North America, the success of Canadian and U.S. SO_2 emission reduction programs have led to marked decreases of S wet deposition across the continent, beginning in the mid-1990s. In Europe, wet deposition levels in 2005–2007 were also markedly lower than in 2000–2002, attributable to large SO_2 emission reductions which began after 1990. Ship emissions are of growing concern in several regions, although it is expected that recently adopted regulations will lower these considerably. In Africa, changes in sulfur wet deposition are difficult to assess because of limitations in deposition and emissions data, although limited data suggest marked increases and decreases at the few stations where measurements have been collected. In Asia, the average percent change for measurement sites was an increase of 8.5%, but both major increases and decreases occurred in some areas. A longer period of observations at a larger number of regionally representative monitoring stations will be required to elucidate temporal trends for Asia and Africa.

Major changes in the anthropogenic emissions of NO_x and NH_3 have occurred from 2000 to 2007 and have been documented in various parts of the world. These include major NO_x emission reductions in Europe, eastern Canada, and the eastern U.S., and major NO_x and NH_3 emission increases in India and China. Consistent with, and of the same order of magnitude as, the aforementioned continental changes in emissions, median wet deposition of nitrogen decreased in North America and Europe and increased in Africa and Asia. Robust measurement programs in Europe and North America do not identify major changes in oxidized or reduced nitrogen measurements prior to about 1999. Trends elsewhere on the globe cannot be assessed prior to about 2000.

In the previous assessment (Whelpdale and Kaiser, 1996), predictions were made concerning deposition for the future (ca. 2020) of sulfur and nitrogen. For sulfur, it was predicted that there would be a large increase in total deposition in the less developed regions caused by increases in population and per capita fossil fuel use. Increases in deposition of 50% or more were calculated for major parts of Latin America, Africa, and southeastern Asia, with the largest increases (more than a factor of three) over southern Africa and India. Large increases in total nitrogen deposition were predicted over the northern oceans, with only small increases to most of the southern oceans. The greatest relative increases, up to 400%, were expected over South America and South Africa, up to 300%, over Central America and parts of Asia, and up to 200% over the southwestern United States due to large increases in emissions from Mexico. These projections represent lower limits as emissions from biomass burning and increased use of fertilizer were not considered and even modest increases would be of relevance to deposition due to the relatively pristine base conditions. Fortunately, our present deposition estimates from observations and/or the TF HTAP models generally do not support these projected increases with the exception of Southeast Asia. While another decade must pass before the projections from the previous assessment can be fully assessed, it is apparent that additional measurements are necessary, particularly in Africa, Central America and the Southern Hemisphere, if a comprehensive assessment of measurement-based trends is to be generated for the rapidly developing regions of the globe. It can also be concluded that while areas projected to receive increasing deposition were generally correct, the previous assessment did not anticipate the magnitude of reductions in sulfur and nitrogen deposition in Europe and North America associated with the success of various emissions reductions programs.

3. What are the major gaps and uncertainties in our knowledge?

Since the previous global assessment of precipitation chemistry (Whelpdale and Kaiser, 1996), there have been encouraging improvements in measurement programs. Measurements of major ions in precipitation are readily available in much of North America and Europe, and increasingly so in East Asia and Africa. The establishment of standardized sampling protocols and analytical methods for regionally representative measurements (WMO/GAW, 2004) as well as a global laboratory quality assurance program (Quality Assurance/Science Activity Centre – Americas, http://qasac-americas.org/) has reduced methodology uncertainties and permitted more objective evaluation of disparate data sets from laboratories around the world. Coupled with encouraging improvements in measurement programs, there is an improved

understanding of atmospheric processes. For instance, global chemical transport models have succeeded in assimilating much of what is known about major ion cycling in the atmosphere in order to provide coherent model estimates of many of the major ions globally.

In spite of the above successes, many significant gaps and uncertainties in our knowledge of precipitation type and chemistry, and wet and dry deposition from observations and models remain.

Wet deposition estimates are a function of ion concentrations as well as precipitation amount. With regard to effects on deposition, the type and rate of precipitation are rarely considered and have not been considered in this assessment. It would be folly to assume that fog, drizzle, and convective precipitation do not affect deposition in different ways. Further work needs to be done to investigate the effects of precipitation on chemical composition and deposition on a region by region basis.

Major regions of the world, including South America, large areas of North America, much of Asia, Africa, Oceania, the polar regions, and all of the oceans, remain very poorly sampled for all of the major ions in precipitation. In those regions where sampling is relatively frequent, little information exists on phosphorus, organic forms of nitrogen, and weak acids including carbonates and organic acids.

Measurement-based inferential dry deposition estimates remain very limited aside from Canada, U.S., Japan, Africa, and Australia, and even these are incomplete - only addressing sulfur, some nitrogen species, and limited cation species. Measurements of gaseous NH_3 (principally dry deposited) and of NO_2 (principally associated with dry deposition in urban areas) have been called for in acid rain programs for decades and are still not in place. Filter-based measurement methods used today suffer from volatilization and absorption artifacts and improved methods are needed. In some regions (Europe and parts of eastern Asia) little effort has been made to adapt inferential techniques to estimate dry deposition where high quality atmospheric concentration measurements are available. Finally, the estimation of dry deposition remains highly uncertain because dry deposition velocities are not validated by direct flux measurements.

Considerable uncertainty continues to exist concerning measurement methodologies associated with wet deposition of organic nitrogen compounds and reduced nitrogen (ammonia) fluxes. Estimates of these nitrogen compounds are fairly crude and are not a part of most routine monitoring programs.

Major gaps exist in our understanding of global wet and dry deposition of phosphorus, and the present state of global phosphorus measurement programs is inadequate. Ortho-phosphate is measured routinely at a few stations in the eastern United States. Wet and dry deposition of phosphorus has been measured at only few stations globally. Dry deposition over the oceans has been estimated here from concentration measurements taken on cruises but long term measurements are not available. Wet and dry deposition measurements/estimates are needed for phosphorus on every continent and ocean.

The use of the global TF HTAP ensemble-mean modeling results permitted an assessment of total deposition in unmonitored regions of the world. It must be acknowledged, however, that there is an inherent uncertainty between gridded model estimates and point concentration and deposition measurements. The interpretation of intra-grid variability, the influence of local emission sources, topography, and other local conditions may make comparison of model grid concentrations with point measurements highly uncertain. In this assessment, scrutiny of models used in the TF HTAP intercomparison (HTAP, 2010) has identified important gaps that restrict their application to under-sampled regions of the globe. Continued model development and evaluation for all of the chemical compounds discussed in this assessment is needed.

9.1. Recommendations

A strategic approach to monitoring is required for future improvements to global concentration and deposition estimates. This will require increased spatial coverage of long term wet and dry deposition measurements of acidifying species, base cations, sea salt, dust, organic acids and nutrients such as phosphorus in regions of the world that are data sparse, highly sensitive, and/or affected by changing regional emissions. There is a pressing need for the atmospheric community to provide large-scale values of wet and dry deposition of the sum of calcium, magnesium, potassium, and sodium for the calculation of critical loads, particularly in areas sensitive to acidity. This will require high quality measurements of wet deposition coupled with inferential dry deposition of coarse and fine particles worldwide.

The focus for increased monitoring should be directed towards regions of strong population growth and industrial development, areas of high ecosystem sensitivity and intensifying agricultural activity, and regions where biomass burning is common due to land clearing or increased wildfire activity. These additional measurements are required to inform combined monitoring/modeling studies and assess chemical fluxes in a meaningful way.

Long term regionally-representative measurements of all major ions are necessary to be able to comprehensively assess measurement-based trends around the globe. As we have seen in Europe and North America, decades-long high quality data have contributed to scientific understanding and provided a reality check on virtually all emission control programs associated with the management of common air pollutants. These data sets provide the long term building blocks necessary to address ongoing and emerging air quality and deposition issues and to determine the costs associated with mitigation programs.

Emerging and existing measurement programs need to adopt standardized methods as described in WMO/GAW (2004). This reference manual was developed based on accepted methodologies used by all of the major long-established regional monitoring programs around the globe and represents the collective expert assessment of acceptable methodologies. It must be noted, however, that adaptations to the measurement methods are required for regions without reliable electricity, wherever blowing snow is a problem, in remote tropical regions where heavy downpours are common, and in windy arid regions where large particles dominate.

Emphasis should be placed on understanding organic nitrogen compounds and ammonia in precipitation to assess their origins and importance to the global nitrogen budget. Many organic nitrogen compounds are unstable and disappear upon collection. This argues for short measurement periods (e.g., daily sample collection) coupled with sample preservation, and speciation of these compounds to determine which are important to ecosystem dynamics. Thorough quantification of nitrogen globally will require a focus on measuring the full suite of important species commonly found in precipitation, followed by technique development to collect and quantify these compounds in network precipitation samples.

Inferential dry deposition models, including the bidirectional surface exchange of NO_2 and NH_3, must be improved, evaluated and applied routinely with the ambient air measurements to estimate dry deposition fluxes of these species. Also, more accurate gas and particle measurements are required. In order to eliminate the biases in the TF HTAP ensemble-mean global estimates of dry and/or total deposition in Europe and North America, further model

development and careful evaluation against measured gas concentrations and dry deposition are needed. Similarly, there is a need to resolve the large differences between the inferential dry deposition models of Canada and the United States.

Phosphorus is an important nutrient species and its atmospheric cycling characteristics must be understood and quantified in regions where it is abundant and environmentally significant. Measurement programs and research studies must be devised to quantitatively separate wet and dry deposited phosphorus. Appropriate treatment of large particles is essential for quantifying the role of atmospheric deposition in the biogeochemical cycling of phosphorus.

Deposition of organic acids plays an important role in controlling atmospheric acidity in many regions of the world. Deposition may also be relevant to the understanding of climate, biogeochemical cycling, and ecosystem issues. In order to enhance our understanding of the impact of wet deposition as a global input of nutrients, including carbon, wet deposition monitoring networks must start including measurements of formic and acetic acids and must rely on established preservation methods to stabilize labile chemical species. Improved understanding of the role of organic compounds, principally formic and acetic acids, requires implementation of measurements worldwide, particularly in relatively clean regions of the world and areas of North America and Europe where concentrations of strong mineral acids are decreasing. It is recommended that monitoring networks around the world begin to measure bicarbonate and organic acids in areas where concentrations of $H+$ are less than 5 $\mu eq\ L^{-1}$, especially where increases in pH are observed.

In conclusion, it is apparent that many of the emerging scientific questions associated with the protection of human and ecosystem health and the practical considerations associated with pollution management will, out of necessity, rely on a process that incorporates long term monitoring information augmented by model information to address gaps. It will not be possible from either a financial or practical standpoint to measure everything everywhere. It is strongly recommended that these issues be managed through coordinated efforts within a comprehensive international framework based upon established methodologies.

Acknowledgments

The authors gratefully acknowledge the many networks, institutions, agencies and organizations from within and outside the World Meteorological Organization system that contributed precipitation chemistry and wet and dry deposition data to this assessment including: the World Meteorological Organization Global Atmosphere Watch network and its associated national and regional networks, IDAF (International Global Atmospheric Chemistry/Deposition of Biogeochemically Important Trace Species/Africa) supported by INSU/CNRS “Institut National des Sciences de l’Univers/Centre National de Recherche Scientifique” and African universities, the Acid Deposition Monitoring Network in East Asia (EANET), WMO/GAW Network of the India Meteorological Department, the Atmospheric Brown Cloud network, the Integrated Programme on Acidification of Chinese Terrestrial Systems (IMPACTS), the Russian Federation Precipitation Chemistry Composition Network, Composition of Asian Deposition network, Taiwan Acid Deposition Network, Australia Regional GAW Precipitation Chemistry Network, WMO/GAW Cape Grim Baseline Air Pollution Station, the UNECE Programmes and their associated partners: European Monitoring and Evaluation Programme (EMEP) and the International Co-operative Programme on Assessment and Monitoring of Air Pollution Effects on Forests (ICP Forests, special thanks to Oliver Granke), the Norwegian Climate and Pollution agency, the Swedish Environmental Research Institute, the U.S. National Atmospheric Deposition Program’s National Trends Network and Atmospheric Integrated Research Monitoring Network, the U.S. EPA Clean Air Status and Trends Network, the Canadian Air and Precipitation Monitoring Network, Reseau d’echantillonnage des precipitations du Quebec, New Brunswick Precipitation Monitoring Network, Alberta Precipitation Quality Monitoring Program, British Columbia Precipitation Chemistry and Sampling Network, Newfoundland Acid Precipitation Monitoring Network, Nova Scotia Precipitation Study Network, INPE’s (Instituto Nacional de Pesquisas Espaciais) Earth Science System Center in Brazil (FAPESP project No99/5204-4), R. Semkin of Environment Canada and H. Yao, C. McConnell and A. Patterson of the Ontario Ministry of the Environment for phosphorus deposition data, B. Sukloff of Environment Canada for his assistance preparing graphics, and N.-H. Lin for his assistance with data collection. We also gratefully acknowledge the UNECE Task Force on Hemispheric Transport of Air Pollution and the participants in the Coordinated Model Studies Activities that greatly contributed to this assessment. We are grateful to the World Meteorological Organization, the National Oceanic and Atmospheric Administration Air Resources Laboratory, North-West University (Patchefstroom, South Africa), and Environment Canada for their financial and logistical support. We are also grateful to L. Jalkanen for her careful review of the manuscript and valuable comments prior to journal submission. Last but not least, we thank L.A. Barrie for conceiving the idea of this global precipitation chemistry and deposition assessment and J. Galloway for his encouragement and advice.

Addendum

The Addendum contains supplementary material for the article. It can be viewed electronically at http://dx.doi.org/10.1016/j.atmosenv.2014.02.017 or in hardcopy in the article that follows.

References

Aas, W., Shao, M., Jin, L., Larssen, T., Zhao, D., Xiang, R., Zhang, J., Xiao, J., Duan, L., 2007. Air concentrations and wet deposition of major inorganic ions at five non-urban sites in China, 2001–2003. Atmos. Environ. 41 (8), 1706–1716.

Adon, M., Galy-Lacaux, C., Yoboué, V., Delon, C., Lacaux, J.P., Castera, P., Gardrat, E., Pienaar, J., Al Ourabi, H., Laouali, D., Diop, B., Sigha-Nkamdjou, L., Akpo, A., Tathy, J., Lavenu, F., Mougin, E., 2010. Long-term measurements of sulphur dioxide, nitrogen dioxide, ammonia, nitric acid and ozone in Africa using passive samplers. Atmos. Chem. Phys. Discuss. 10, 4407–4461.

Adon, M., Galy-Lacaux, C., Yoboué, V., Delon, C., Solmon, F., Kaptue Tchuente, A.T., 2013. Dry deposition of nitrogen compounds (NO_2, HNO_3, NH_3), sulfur dioxide and ozone estimated by the inferential method in West and Central African ecosystems. Atmos. Chem. Phys. Discuss. 13, 11689–11744. http://dx.doi.org/10.5194/acpd-13-11689-2013.

Aiuppa, A., Bonfanti, P., D'Alessandro, W., 2003. Rainwater chemistry at Mt. Etna (Italy): natural and anthropogenic sources of major ions. J. Atmos. Chem. 46 (1), 89–102.

Al-Khashman, O.A., 2005a. Study of chemical composition in wet atmospheric precipitation in Eshidiya area, Jordan. Atmos. Environ. 39 (33), 6175–6183.

Al-Khashman, O.A., 2005b. Ionic composition of wet precipitation in the Petra region, Jordan. Atmos. Res. 78 (1–2), 1–12.

Al-Khashman, O.A., 2009. Chemical characteristics of rainwater collected at a western site of Jordan. Atmos. Res. 91 (1), 53–61.

Al-Momani, I.F., 2003. Trace elements in atmospheric precipitation at Northern Jordan measured by ICP-MS: acidity and possible sources. Atmos. Environ. 37, 4507–4515.

Aleksic, N., Roy, K., Sistla, G., Dukett, J., Houck, N., Casson, P., 2009. Analysis of cloud and precipitation chemistry at Whiteface Mountain, NY. Atmos. Environ. 43 (17), 2709–2716.

Allen, A.G., Machado, C.M.D., Cardoso, A.A., 2011. Measurements and modeling of reactive nitrogen deposition in southeast Brazil. Environ. Pollut. 159 (5), 1190–1197.

AMAP, 2006. AMAP Assessment 2006: Acidifying Pollutants, Arctic Haze and Acidification in the Arctic. Arctic Monitoring and Assessment Programme (AMAP), Oslo, Norway.

Anderson, K.A., Downing, J.A., 2006. Dry and wet atmospheric deposition of nitrogen, phosphorus and silicon in an agricultural region. Water Air Soil Pollut. 176 (1–4), 351–374.

Anderson, J.B., Baumgardner, R.E., Mohnen, V.A., Bowser, J.J., 1999. Cloud chemistry in the eastern United States, as sampled from three high-elevation sites along the Appalachian Mountains. Atmos. Environ. 33, 5105–5114.

Anderson, J.B., Baumgardner Jr., R.E., Grenville, S.E., 2006. Trends in cloud water sulfate and nitrate as measured at two mountain sites in the Eastern United States: Regional contributions and temporal changes compared with regional changes in emissions, 1986–1999. Atmos. Environ. 40 (23), 4423–4437.

Andreacute, F., Jonard, M., Ponette, Q., 2007. Influence of meteorological factors and polluting environment on rain chemistry and wet deposition in a rural area near Chimay, Belgium. Atmos. Environ. 41 (7), 1426–1439.

Andreae, M.O., Talbot, R.W., Li, S.-M., 1987. Atmospheric measurements of pyruvic and formic acid. J. Geophys. Res. 92, 6635–6641.

Andreae, M.O., Talbot, R.W., Andreae, T.W., Harriss, R.C., 1988. Formic and acetic acid over the Central Amazon Region, Brazil 1. Dry Season. J. Geophys. Res. 93 (D2), 1616–1624.

Andreae, T.W., Andreae, M.O., Ichoku, C., Maenhaut, W., Cafmeyer, J., Karnieli, A., Orlovsky, L., 2002. Light scattering by dust and anthropogenic aerosol at a remote site in the Negev desert, Israel. J. Geophys. Res. 107 (D2) doi:4010.1029/2001JD900252.

APHA, AWWA, WEF, 1999. Ascorbic Acid Method (4500–P, Phosphorus). Standard Methods for the Examination of Water and Wastewater. American Public Health Association, American Water Works Association, and Water Environment Federation, p. 9.

Arndt, R., Carmichael, G.R., Streets, D.G., Bhatti, N., 1997. Sulfur dioxide emissions and sectorial contributions to sulfur deposition in Asia. Atmos. Environ. 31, 1553–1572.

Arrigo, K.R., 2005. Marine microorganisms and global nutrient cycles. Nature 437, 349–355.

Arsene, C., Olariu, R.I., Mihalopoulos, N., 2007. Chemical composition of rainwater in the northeastern Romania, Iasi region (2003–2006). Atmos. Environ. 41 (40), 9452–9467.

Atkinson, R., Tuazon, E.C., Aschmann, S.M., 1995. Products of the gas-phase reactions of O_3 with alkenes. Environ. Sci. Technol. 29, 1860–1866.

Avila, A., Rodà, F., 2002. Assessing decadal changes in rainwater alkalinity at a rural Mediterranean site in the Montseny Mountains (NE Spain). Atmos. Environ. 36 (17), 2881–2890.

Avila, A., Queralt-Mitjans, I., Alarcon, M., 1997. Minerological composition of Africa dust delivered by red rains over northeastern Spain. J. Geophys. Res. 102 (D18), 21977–21996.

Ayers, G.P., Gillett, R.W., 1988. Acidification in Australia. In: Rodhe, H., Herrera, R. (Eds.), Acidification in Tropical Countries, SCOPE 36. Wiley, Chichester, England, pp. 347–402.

Ayers, G.P., Keywood, M.D., Gillett, R.W., Manins, P.C., Malfroy, H., Bardsley, T., 1998. Validation of passive diffusion samplers for SO_2 and NO_2 under Australian conditions. Atmos. Environ. 32, 3587–3592.

Ayers, G.P., Peng, L.C., Gillett, R.W., Fook, L.S., 2002. Rainwater composition and acidity at five sites in Malaysia, in 1996. Water Air Soil Pollut. 133 (1–4), 15–30.

Ayers, G.P., Gillett, R.W., Selleck, P.W., 2003. A universal bias in inorganic rainwater chemical composition data. Geophys. Res. Lett. 30 (13), 1715–1718. http://dx.doi.org/10.1029/2003GL016892.

Baboukas, E., Sciare, J., Mihalopoulos, N., 2004. Spatial, temporal and interannual variability of methanesulfonate and non-sea-salt sulfate in rainwater in the southern Indian Ocean (Amsterdam, Crozet and Kerguelen islands). J. Atmos. Chem. 48 (1), 35–57.

Báez, A., Belmont, R., Garcia, R., Padilla, H., Torres, M.C., 2007. Chemical composition of rainwater collected at a southwest site of Mexico City, Mexico. Atmos. Res. 86, 61–75. http://dx.doi.org/10.1016/j.atmosres.2007.03.005.

Baker, A.R., Jickells, T.D., Witt, M., Linge, K.L., 2006a. Trends in the solubility of iron, aluminium, manganese and phosphorus in aerosol collected over the Atlantic Ocean. Mar. Chem. 98 (1), 43–58.

Baker, A.R., French, M., Linge, K.L., 2006b. Trends in aerosol nutrient solubility along a west – east transect of the Saharan dust plume. Geophys. Res. Lett. 33 (7), L07805 doi:07810.01029/02005GL024764.

Baker, A.R., Lesworth, T., Adams, C., Jickells, T.D., Ganzeveld, L., 2010. Estimation of atmospheric nutrient inputs to the Atlantic Ocean from 50°N to 50°S based on large-scale field sampling: fixed nitrogen and dry deposition of phosphorus. Global Biogeochem. Cycles 24, GB3006. http://dx.doi.org/10.1029/2009GB003634.

Balasubramanian, R., Victor, T., Chun, N., 2001. Chemical and statistical analysis of precipitation in Singapore. Water Air Soil Pollut. 130 (1–4 II), 451–456.

Basart, C., Perez, C., Cuevas, E., Baldasano, J.M., Gobbi, G.P., 2009. Aerosol characterization in northern Africa, northeastern Atlantic, mediterranean basin and middle east from direct-sun AERONET observations. Atmos. Chem. Phys. 9, 8265–8282.

Brooks Avery Jr., G.B., Willey, J.D., Kieber, R.J., 2001. Diurnal variations in major rainwater components at a coastal site in North Carolina. Atmos. Environ. 35 (23), 3927–3933.

Baumgardner Jr., R.E., Lavery, T.F., Rogers, C.M., Isil, S.S., 2002. Estimates of the atmospheric deposition of sulfur and nitrogen species: clean air status and trends network, 1990–2000. Environ. Sci. Technol. 36 (12), 2614–2629.

Beem, K.B., Raja, S., Schwandner, F.M., Taylor, C., Lee, T., Sullivan, A.P., Carrico, C.M., McMeeking, G.R., Day, D., Levin, E., Hand, J., Kreidenweis, S.M., Schichtel, B., Malm, W.C., Collett Jr., J.L., 2010. Deposition of reactive nitrogen during the Rocky Mountain Airborne Nitrogen and Sulfur (RoMANS) study. Environ. Pollut. 158 (3), 862–872.

Benedictow, A., Fagerli, H., Gauss, M., Jonson, J.E., Nyíri, Á., Simpson, D., Tsyro, S., Valdebenito, A., Valiyaveetil, S., Wind, P., Aas, W., Hjelbrekke, A.-G., Mareckova, K., Wankmüller, R., Harmens, H., Cooper, D., Norris, D., Schröder, W., Pesch, R., Holy, M., 2009. Transboundary Acidification, Eutrophication and Ground Level Ozone in Europe 2007. EMEP Status Report 1/2009, ISSN 1504–6109(print), ISSN 1504-6192(on-line). http://emep.int/publ/reports/2009/status_report_1_2009.pdf.

Bergametti, G.E., Remoudaki, E., Losno, R., Steiner, E., Chatenet, B., Buat-Menard, P., 1992. Source, transport and deposition of atmospheric phosphorus over the northwestern Mediterranean. J. Atmos. Chem. 14, 501–513.

Bobbink, R., Hicks, K., Galloway, J., Spranger, T., Alkemade, R., Ashmore, M., Bustamante, M., Cinderby, S., Davidson, E., Dentener, F., Emmett, B., Erisman, J.-W., Fenn, M., Gilliam, F., Nordin, A., Pardo, L., de Vries, W., 2010. Global assessment of nitrogen deposition effects on terrestrial plant diversity: a synthesis. Ecol. Appl. 20 (1), 30–59. http://dx.doi.org/10.1890/08-1140.1.

Boone, A., De Rosnay, P., Balsamo, G., Beljaars, A., Chopin, F., Decharme, B., Delire, C., Ducharne, A., Gascoin, S., Grippa, M., Guichard, F., Gusev, Y., Harris, P., Jarlan, L., Kergoat, L., Mougin, E., Nasonova, O., Norgaard, A., Orgeval, T., Ottl, C., Poccard-Leclerq, I., Polcher, J., Sandholt, I., Saux-Picart, S., Taylor, C., Xue, Y., 2009. The AMMA land surface model intercomparison project (ALMIP). Bull. Am. Meteor. Soc., 1865–1880. http://dx.doi.org/10.1175/2009BAMS2786.1.

Bouwman, A.F., Van Vuuren, D.P., Derwent, R.G., Posch, M., 2002. A global analysis of acidification and eutrophication of terrestrial ecosystems. Water Air Soil Pollut. 141, (1–4), 349–382.

Brahney, J., Ballantyne, A.P., Sievers, C., Neff, J.C., 2013. Increasing Ca^{2+} deposition in the western US: the role of mineral aerosols. Aeolian Res. http://dx.doi.org/10.1016/j.aeolia.2013.04.003.

Bravo, H.A., Saavedra, M.I.R., Saacute;nchez, P.A., Torres, R.J., Granada, L.M.M., 2000. Chemical composition of precipitation in a Mexican Maya region. Atmos. Environ. 34 (8), 1197–1204.

Brocard, D., Lacaux, C., Lacaux, J.P., Kouadio, G., Yoboué, V., 1996. Emissions from the combustion of biofuels in western Africa. In: Levine, J.S. (Ed.), Global Biomass Burning. MIT Press, Cambridge.

Brooks Avery Jr., G., Kieber, R.J., Witt, M., Willey, J.D., 2006. Rainwater monocarboxylic and dicarboxylic acid concentrations in southeastern North Carolina, USA, as a function of air-mass back-trajectory. Atmos. Environ. 40, 1683–1693.

Butler, T.J., Likens, G.E., Stunder, B.J.B., 2001. Regional-scale impacts of phase I of the clean air act amendments in the U.S.: the relation between emissions and concentrations, both wet and dry. Atmos. Environ. 35, 1015–1028.

Butler, T.J., Likens, G.E., Vermeylen, F.M., Stunder, B.J.B., 2003. The relation between NO_x emissions and precipitation NO_3- in the eastern U.S. Atmos. Environ. 37 (15), 2093–2104.

Butler, T.J., Likens, G.E., Vermeylen, F.M., Stunder, B.J.B., 2005. The impact of changing nitrogen oxide emissions on wet and dry nitrogen deposition in the northeastern U.S. Atmos. Environ. 39 (27), 4851–4862.

Butler, T.J., Vermeylen, F.M., Rury, M., Likens, G.E., Lee, B., Bowker, G.E., McCluney, L., 2011. Response of ozone and nitrate to stationary source NO_x emission reductions in the eastern U.S. Atmos. Environ. 45, 1084–1094 http://dx.doi.org/10.1016/j.atmosenv.2010.11.040.

Bytnerowitz, A., Badea, O., Popescu, F., Musselman, R., Tanase, M., Barbu, I., Fraczek, W., Gembasu, N., Surdu, A., Danescu, F., Postelnicu, D., Cenusa, R., Vasile, C., 2005. Air pollution, precipitation chemistry and forest health in the Retezat Mountains, southern Carpathians, Romania. Environ. Pollut. 137, 546–567.

Cainey, J.M., Derek, N., Krummel, P.D. (Eds.), 2004. Baseline Atmospheric Program Australia 2001–2002. Published for the Bureau of Meteorology and CSIRO Marine and Atmospheric Research, Melbourne.

Cainey, J.M., Derek, N., Krummel, P.D. (Eds.), 2006. Baseline Atmospheric Program Australia 2003–2004. Published for the Bureau of Meteorology and CSIRO Marine and Atmospheric Research, Melbourne.

Cainey, J.M., Derek, N., Krummel, P.D. (Eds.), 2007. Baseline Atmospheric Program Australia 2005–2006. Published for the Bureau of Meteorology and CSIRO Marine and Atmospheric Research, Melbourne.

Calvert, J.G., Stockwell, W.R., 1983. Acid generation in the troposphere by gas-phase chemistry. Environ. Sci. Technol. 17, 428A–442A,.

Campos, V.P., Costa, A.C.A., Tavares, T.M., 2007. Partial neutralization of rain by seaspray: the case of Reconcavo, Bahia—Brazil. J. Environ. Manag. 84, 204–212.

Canada. Environment Canada and Health Canada, 2011. Canadian Smog Science Assessment – Highlights and Key Messages. Government of Canada, Ottawa. http://ec.gc.ca/Air/default.asp?lang=En&n=72F82C27-1.

Cape, J.N., Cornell, S.E., Jickells, T.D., Nemitz, E., 2011. Organic nitrogen in the atmosphere – where does it come from? A review of sources and methods. Atmos. Res. 102, 30–48.

Carrillo, J.H., Hastings, M.G., Sigman, D.M., Huebert, B.J., 2002. Atmospheric deposition of inorganic and organic nitrogen and base cations in Hawaii. Global Biogeochem. Cycles 16, 1076–1091. http://dx.doi.org/10.1029/2002GB001892.

Casartelli, M.R., Mirlean, N., Peralba, M.C., Barrionuevo, S., Goacute;mez-Rey, M.X., Madeira., M., 2008. An assessment of the chemical composition of precipitation and throughfall in rural-industrial gradient in wet subtropics (southern Brazil). Environ. Monit. Assess. 144 (1–3), 105–116.

Chadwick, O.A., Derry, L.A., Vitousek, P.M., Huebert, B.J., Hedin, L.O., 1999. Changing sources of nutrients during four million years of ecosystem development. Nature 397, 491–497.
Chapman, E.G., Sklarew, D.S., Flickinger, J.S., 1986. Organic acids in springtime Wisconsin precipitation samples. Atmos. Environ. 20 (9), 1717–1725.
Chen, Y., 2004. Sources and Fate of Atmospheric Nutrients over the Remote Oceans and Their Role on Controlling Marine Diazotrophic Microorganisms. Ph.D. diss.. Univ. of Maryland, College Park.
Chen, H.Y., Chen, L.D., 2008. Importance of anthropogenic inputs and continental-derived dust for the distribution and flux of water-soluble nitrogen and phosphorus species in aerosol within the atmosphere over the East China Sea. J. Geophys. Res. 113 (D11303), 11310 doi:11029/12007jd009491.
Chen, Y., Paytan, A., Chase, Z., Measures, C., Beck, A.J., Sañudo-Wilhelmy, S.A., Post, A.F., 2008. Sources and fluxes of atmospheric trace elements to the Gulf of Aqaba, Red Sea. J. Geophys. Res. 113, D05306 doi:05310.01029/02007JD009110.
Chudaeva, V.A., Chudaev, O.V., Yurchenko, S.G., 2008. Chemical composition of precipitation in the southern part of the Russian Far East. Water Resour./Vodnye Resursy 35 (1), 58–70.
Clow, D.W., Ingersoll, G.P., Mast, M.A., Turk, J.T., Campbell, D.H., 2002. Comparison of snowpack and winter wet-deposition chemistry in the Rocky Mountains, U.S.: implications for winter dry deposition. Atmos. Environ. 36 (14), 2337–2348.
Coelho, C.H., Allen, A.G., Fornaro, A., Orlando, E.A., Grigoletto, T.L.B., Campos, M.L.A.M., 2011. Wet deposition of major ions in a rural area impacted by biomass burning emissions. Atmos. Environ. 45, 5260–5265.
Cofala, J., Amann, M., Heyes, C., Klimont, Z., Posch, M., Schöpp, W., Tarasson, L., Jonson, J., Whall, C., Stavrakaki, A., 2007. Final Report: Analysis of Policy Measures to Reduce Ship Emissions in the Context of the Revision of the National Emissions Ceilings Directive. International Institute for Applied Systems Analysis, Laxenburg, Austria, p. 74.
Collett Jr., J.L., Herckes, P., Youngster, S., Lee, T., 2008. Processing of atmospheric organic matter by California radiation fogs. Atmos. Res. 87 (3–4), 232–241.
Daum, P.H., Kelly, T.J., Schwartz, S.E., Newman, L., 1984. Measurements of the chemical composition of stratiform clouds. Atmos. Environ. 18, 2671–2684.
De Mello, W.Z., 2001. Precipitation chemistry in the coast of the metropolitan region of Rio de Janeiro, Brazil. Environ. Pollut. 114, 235–242.
De Mello, W.Z., De Almeida, M.D., 2004. Rainwater chemistry at the summit and southern flank of the Itatiaia massif, Southeastern Brazil. Environ. Pollut. 129 (1), 63–68.
Deboudt, K., Flament, P., Bertho, M.-L., 2004. Cd, Cu, Pb and Zn concentrations in atmospheric wet deposition at a coastal station in Western Europe. Water Air Soil Pollut. 151 (1–4), 335–359.
Delmas, R., Loudjani, P., Podaire, A., Menaut, J.C., 1991. Biomass burning in Africa: an assessment of annually burnt biomass. In: Levine, J.S. (Ed.), Global Biomass Burning: Atmospheric, Climatic and Biospheric Implications. MIT Press, Cambridge, MA, pp. 126–133.
Delon, C., Galy-Lacaux, C., Boone, A., Liousse, C., Serça, D., Adon, M., Diop, B., Akpo, A., Lavenu, F., Mougin, E., Timouk, F., 2010. Atmospheric nitrogen budget in Sahelian dry savannas. Atmos. Chem. Phys. 10, 2691–2708. http://dx.doi.org/10.5194/acp-10-2691-2010.
Delon, C., Galy-Lacaux, C., Adon, M., Liousse, C., Serça, D., Diop, B., Akpo, A., 2012. Nitrogen compounds emission and deposition in West African ecosystems: comparison between wet and dry savanna. Biogeosciences 9, 385–402. http://dx.doi.org/10.5194/bg-9-385-2012.
Delon, C., Galy-Lacaux, C., Adon, M., Liousse, C., Boone, A., Serça, D., Diop, B., Akpo, A., Mougin, E., 2012b. In: Sutton, M.A., Mason, K.E., Sheppard, L.J., Sverdrup, H., Haeuber, R., Hicks, W.K. (Eds.), Chapter 11: Interannual Variability of the Atmospheric Nitrogen Budget in West African Dry Savannas. Nitrogen Deposition, Critical Loads and Biodiversity, Springer 2014, ISBN 978-94-007-7938-9, p. 539.
Dentener, F., Drevet, J., Lamarque, J.F., Bey, I., Eickhout, B., Fiore, A.M., Hauglustaine, D., Horowitz, W.W., Krol, M., Kulshrestha, U.C., Lawrence, M., Galy-Lacaux, C., Rast, S., Shindell, D., Stevenson, D., Van Noije, T., Atherton, C., Bell, N., Bergman, D., Butler, T., Cofala, J., Collins, B., Doherty, R., Ellingsen, K., Galloway, J., Gausee, M., Montanaro, V., Müller, J.F., Pitari, G., Rodriguez, J., Sanderson, M., Solmon, F., Strahan, S., Schultz, M., Sudo, K., Szopa, S., Wild, O., 2006. Nitrogen and sulfur deposition on regional and global scales: a multimodel evaluation. Global Biogeochem. Cycles 20, 21. http://dx.doi.org/10.1029/2005GB002672. GB4003.
Derek, N., Krummel, P.D. (Eds.), 2011. Baseline Atmospheric Program Australia 2007–2008. Published for the Bureau of Meteorology and CSIRO Marine and Atmospheric Research, Melbourne.
Dolske, D.A., Gatz, D.F., 1985. A field intercomparison of methods for the measurement of particle and gas dry deposition. J. Geophys. Res. 90 (D1), 2076–2084.
Doney, S.C., 2010. The growing human footprint on coastal and open-ocean biogeochemistry. Science 328, 1512. http://dx.doi.org/10.1126/science.1185198.
Dore, A.J., Vieno, M., Tang, Y.S., Dragosits, U., Dosio, A., Weston, K.J., Sutton, M.A., 2007. Modelling the atmospheric transport and deposition of sulphur and nitrogen over the United Kingdom and assessment of the influence of SO_2 emissions from international shipping. Atmos. Environ. 41, 2355–2367.
Doskey, P.V., Ugoagwu, B.J., 1989. Atmospheric deposition of macronutrients by pollen at a semi-remote site in northern Wisconsin. Atmos. Environ. 23, 2761–2766.
Dukett, J.E., Aleksic, N., Houck, N., Snyder, P., Casson, P., Cantwell, M., 2011. Progress toward clean cloud water at Whiteface Mountain New York. Atmos. Environ. 45, 6669–6673. http://dx.doi.org/10.1016/j.atmosenv.2011.08.070.
Durana, N., Casado, H., Ezcurra, A., Garcia, C., Lacaux, J.P., Van Dinh, P., 1992. Experimental study of the scavenging process by means of a sequential precipitation collector, preliminary results. Atmos. Environ. 26 (13), 2437–2443.
EANET, 2006. Periodic Report on the State of Acid Deposition in East Asia, Part I: Regional Assessment. Acid Deposition Monitoring Network in East Asia. Available from: http://www.eanet.cc/product.html.
EANET, 2011. Second Periodic Report on the State of Acid Deposition in East Asia (Part I) (Regional Assessment). Acid Deposition Monitoring Network in East Asia: http://www.eanet.cc/product/PRSAD/2_PRSAD/2_PRSAD1.pdf.
EMEP, 2004. EMEP Assessment Part 1 European Perspective (Chapter 5). European Monitoring and Evaluation Programme, Oslo, Norway, ISBN 82-7144-032-2.
EMEP/CEIP, 2012. EMEP Emissions Data. European Monitoring and Evaluation Programme/Centre on Emission Inventories and Projections. Available from: http://webdab1.umweltbundesamt.at/.
Endo, T., Yagoh, H., Sato, K., Matsuda, K., Hayashi, K., Noguchi, I., Sawada, K., 2011. Regional characteristics of dry deposition of sulfur and nitrogen compounds at EANET sites in Japan from 2003 to 2008. Atmos. Environ. 45 (6), 1259–1267.
Environment Canada, 2005. 2004 Canadian Acid Deposition Science Assessment. Ottawa, Canada, p. 440.
EPA, 2004. National Emission Inventory – Ammonia Emissions from Animal Husbandry Operations Draft Report. United States Environmental Protection Agency. January 2004. Available at http://www.epa.gov/ttn/chief/ap42/ch09/related/nh3inventorydraft_jan20.
Erickson, D.J., Duce, R.A., 1988. On the global flux of atmospheric sea salt. J. Geophys. Res. 93 (C11), 14079–14088.
Erickson, D.J., Seuzaret, C., Keene, W.C., Gong, S.L., 1999. A general circulation model based calculation of HCl and $ClNO_2$ production from sea salt dechlorination: reactive chlorine emissions inventory. J. Geophys. Res. 104 (D7), 8347–8372.
Eshleman, K.N., Sabo, R.D., Kline, K.M., 2013. Surface water quality is improving due to declining atmospheric N deposition. Environ. Sci. Technol. http://dx.doi.org/10.1021/es4029748.
European Commission, 2011. Emission Database for Global Atmospheric Research (EDGAR), Release Version 4.2. Joint Research Centre (JRC)/Netherlands Environmental Assessment Agency (PBL). http://edgar.jrc.ec.europa.eu.
European Commission, 2012. European Union Emission Inventory Report 1990–2010 under the UNECE Convention on Long-range Transboundary Air Pollution (CLRTAP). Technical Report No 8/2012. European Environment Agency, Copenhagen, Denmark.
European Parliament, 2012. Shipping Fuels: On Course for Better Health and Environment Protection. Press release 16-02-2012 12:12, available from: http://www.europarl.europa.eu/news/en/pressroom/content/20120130IPR36511/html/Shipping-fuels-on-course-for-better-health-and-environment-protection.
Eyring, V., Isaksen, I., Berntsen, T., Collins, W.J., Corbett, J., Endresen, O., Grainger, R.G., Moldanova, J., Schlager, H., Stevenson, D.S., 2010. Transport impacts on atmosphere and climate: shipping. Atmos. Environ. 44 (37), 4735–4771. http://dx.doi.org/10.1016/j.atmosenv.2009.04.059.
Fagerli, H., Aas, W., 2008. Trends of nitrogen in air and precipitation: model results and observations at EMEP sites in Europe, 1980–2003. Environ. Pollut. 154 (3), 448–461.
Fagerli, H., Spranger, T., Posch, M., 2006. Chapter 3: acidification and eutrophication – progress towards the Gothenburg protocol target year 2010. In: Transboundary Acidification, Eutrophication and Ground Level Ozone in Europe since 1990 to 2004. Norwegian Meteorological Institute, Oslo. EMEP Status Report 1/06, available from: http://emep.int/publ/reports/2006/status_report_1_2006_ch.pdf.
Fairall, C.W., Davidson, K.L., Schacher, G.E., 1983. An analysis of the surface production of sea-salt aerosols. Tellus 35B (1), 31–39.
Falkovich, A.H., Schkolnik, G., Ganor, E., Rudich, Y., 2004. Adsorption of organic compounds pertinent to urban environments onto mineral dust particles. J. Geophys. Res. 109 (D02208), 19. http://dx.doi.org/10.1029/2003JD003919.
Ferm, M., 1991. A Sensitive Diffusional Sampler. Swedish Environmental Research Institue, IVL, Göteborg, Sweden, pp. L91–L172. Report.
Fillion, N., Probst, A., Probst, J.L., 1999. Dissolved organic matter contribution to rain water, throughfall and soil solution chemistry. Analusis 27 (5), 409–413.
Fischer, R., Lorenz, M. (Eds.), 2011. Forest Condition in Europe, 2011 Technical Report of ICP Forests and FutMon. Work Report of the Institute for World Forestry 2011/1. ICP Forests, Hamburg, p. 212.
Fisseha, R., Saurer, M., Jäggi, M., Siegwolf, R., Dommen, J., Szidat, S., Samburova, V., Baltensperge, U., 2009. Determination of primary and secondary sources of organic acids and carbonaceous aerosols using stable carbon isotopes. Atmos. Environ. 43 (2), 431–437.
Flechard, C.R., Nemitz, E., Smith, R.I., Fowler, D., Vermeulen, A.T., Bleeker, A., Erisman, J.W., Simpson, D., Zhang, L., Tang, Y.S., Sutton, M.A., 2011. Dry deposition of reactive nitrogen to European ecosystems: a comparison of inferential models across the NitroEurope network. Atmos. Chem. Phys. 11, 2703–2728.
Flues, M., Hama, P., Lemes, M.J.L., Dantas, E.S.K., Fornaro, A., 2002. Evaluation of the rainwater acidity of a rural region due to a coal-fired power plant in Brazil. Atmos. Environ. 36 (14), 2397–2404.
Fornaro, A., Gutz, I.G.R., 2003. Wet deposition and related atmospheric chemistry in the São Paulo metropolis, Brazil: part 2-Contribution of formic and acetic acids. Atmos. Environ. 37 (1), 117–128.

Fornaro, A., Gutz, I.G.R., 2006. Wet deposition and related atmospheric chemistry in the São Paulo metropolis, Brazil. Part 3: trends in precipitation chemistry during 1983–2003. Atmos. Environ. 40 (30), 5893–5901.
Forti, M.C., personal communication, April 29, 2010. Ministério Ciência e Tecnologia.
Forti, M.C., Melfi, A.J., Astolfo, R., Fostier, A.H., 2000. Rainfall chemistry composition in two ecosystems in the northeastern Brazilian Amazon (Amapa State). J. Geophys. Res. Atmos. 105, 28895–28905.
Forti, M.C., Carvalho, A., Melfi, A.J., Montes, C.R., 2001. Deposition patterns of SO_4^{2-}, NO_3^- and H^+ in the Brazilian territory. Water Air Soil Pollut. 130, 1121–1126.
Forti, M.C., Bicudo, D.C., Cicco, V., Arcova, F.C.S., 2005. Rainfall and throughfall chemistry in the Atlantic Forest: a comparison between urban and natural areas (São Paulo State, Brazil). Hydrol. Earth Syst. Sci. 9, 570–585.
Fowler, D., Gallagher, M.W., Lovett, G.M., 1993. Fog, cloudwater, and wet deposition. In: Lovblad, G., Erisman, J.-W., Fowler, D. (Eds.), Models and Methods for the Quantification of Atmospheric Inputs to Ecosystems, Nordiske Seminar-og Arbejdsrapporter, pp. 51–74.
Fowler, D., Smith, R.I., Muller, J.B.A., Hayman, G., Vincent, K.J., 2005. Changes in the atmospheric deposition of acidifying compounds in the UK between 1986 and 2001. Environ. Pollut. 137, 15–25.
Fowler, D., Pilegaard, K., Sutton, M.A., Ambus, P., Raivonen, M., Duyzer, J., Simpson, D., Fagerli, H., Fuzzi, S., Schjoerring, J.K., Granier, C., Neftel, A., Isaksen, I.S.A., Laj, P., Maione, M., Monks, P.S., Burkhardt, J., Daemmgen, U., Neirynck, J., Personne, E., Wichink-Kruit, R., Butterbach-Bahl, K., Flechard, C., Tuovinen, J.P., Coyle, M., Gerosa, G., Loubet, B., Altimir, N., Gruenhage, L., Ammann, C., Cieslik, S., Paoletti, E., Mikkelsen, T.N., Ro-Poulsen, H., Cellier, P., Cape, J.N., Horvath, L., Loreto, F., Niinemets, U., Palmer, P.I., Rinne, J., Misztal, P., Nemitz, E., Nilsson, D., Pryor, S., Gallagher, M.W., Vesala, T., Skiba, U., Brueggemann, N., Zechmeister-Boltenstern, S., Williams, J., O'Dowd, C., Facchini, M.C., de Leeuw, G., Flossman, A., Chaumerliac, N., Erisman, J.W., 2009. Atmospheric composition change: ecosystems-Atmosphere interactions. Atmos. Environ. 43, 5193–5267.
Furutani, H., Meguro, A., Iguchi, H., Uematsu, M., 2010. Geographical distribution and sources of phosphorus in atmospheric aerosol over the North Pacific Ocean. Geophys. Res. Lett. 37, L03805. http://dx.doi.org/10.1029/2009GL041367.
Galloway, J.N., Likens, G.E., Keene, W.C., Miller, J., 1982. The composition of precipitation in remote areas of the world. J. Geophys. Res. 87 (11), 8771–8786.
Galloway, J.N., Keene, W.C., Artz, R.S., Miller, J.M., 1989. Processes controlling the concentrations of SO_4^-, NO_3^-, NH_4^+, HCOOT and CH3COOT in precipitation on Bermuda. Tellus 41B, 427–443.
Galloway, J.N., Keene, W.C., Likens, G.E., 1996. Processes controlling the composition of precipitation at a remote southern hemispheric location: Torres del Paine National Park, Chile. J. Geophys. Res. 101 (D3), 6883–6897.
Galloway, J.N., Dentener, F.J., Capone, D.G., Boyer, E.W., Howarth, R.W., Seitzinger, S.P., Asner, G.P., Cleveland, C.C., Green, P.A., Holland, E.A., Karl, D.M., Michales, A.F., Porter, J.H., Townsend, A.R., Vorosmarty, C.J., 2004. Global and regional nitrogen cycles: past, present and future. Biogeochemistry 70, 153–226.
Galloway, J.N., Townsend, A.R., Erisman, J.W., Bekunda, M., Cai, Z., Freney, J.R., Martinelli, L.A., Seitzinger, S.P., Sutton, M.A., 2008. Transformation of the nitrogen cycle: recent trends, questions, and potential solutions. Science 320, 889–892.
Galy-Lacaux, C., Modi, A.I., 1998. Precipitation chemistry in the Sahelian Savanna of Niger, Africa. J. Atmos. Chem. 30, 319–334.
Galy-Lacaux, C., personal communication, March 14–20, 2010. Laboratoire d'Aérologie, Observatoire Midi Pyrénées, Toulouse, France.
Galy-Lacaux, C., Carmichael, G.R., Song, C.H., Lacaux, J.P., Modi, I., 2001. Heterogenous processes involving nitrogenous compounds and Saharan dust inferred from measurements and model calculations Region. J. Geophys. Res. 106, 12559–12578.
Galy-Lacaux, C., Al Ourabi, H., Lacaux, J.P., Gardrat, E., Mphepya, J., Pienaar, K., 2003. Dry and wet atmospheric nitrogen deposition in Africa. Geophys. Res. Abstr. 5, 09644.
Galy-Lacaux, C., Laouali, D., Descroix, L., Gobron, N., Liousse, C., 2009. Long term precipitation chemistry and wet deposition in a remote dry savanna site in Africa (Niger). Atmos. Chem. Phys. 9, 1579–1595.
Galy-Lacaux, C., Delon, C., Solmon, F., Adon, M., Yoboué, V., Mphepya, J., Pienaar, J.J., Diop, B., Sigha, L., Dungall, L., Akpo, A., Mougin, E., Gardrat, E., Castera, P., 2014. Chapter 10: dry and wet atmospheric nitrogen deposition in West Central Africa. In: Sutton, M.A., Mason, K.E., Sheppard, L.J., Sverdrup, H., Haeuber, R., Hicks, W.K. (Eds.), Nitrogen Deposition, Critical Loads and Biodiversity. Springer, ISBN 978-94-007-7938-9, p. 539.
Garcia, R., del Torres Ma, C., Padilla, H., Belmont, R., Azpra, E., Arcega-Cabrera, F., Báez, A., 2006. Measurement of chemical elements in rain from Rancho Viejo, a rural wooded area in the State of Mexico, Mexico. Atmos. Environ. 40, 6088–6100. http://dx.doi.org/10.1016/j.atmosenv.2006.05.048.
Garg, A., Shukla, P.R., Kapshe, M., 2006. The sectoral trends of multigas emissions inventory of India. Atmos. Environ. 40, 4608–4620.
Ge, B.Z., Wang, Z.F., Xu, X.B., Tang, J., He, Y.J., Uno, I., Ohara, T., 2011. Impact of the East Asian summer monsoon on long-term variations in the acidity of summer precipitation in Central China. Atmos. Chem. Phys. 11 (4), 1671.
Germer, S., Neill, C., Krusche, A.V., Neto, S.G.N., Elsenbeer, H., 2007. Seasonal and within-event dynamics of rainfall and throughfall chemistry in an open tropical rainforest in Rondonia, Brazil. Biogeochemistry 86, 155–174.
Gillett, R., personal communication, November, 2010. Data from the CAAP (Composition and Acidity of Asian Precipitation) Programme and Commonwealth Scientific and Industrial Research Organization (CSIRO), Australia. http://www.csiro.au/.
Gillett, R.W., Ayers, G.P., Noller, B.N., 1990. Rainwater acidity at Jabiru, Australia in the wet season 1983/84. Sci. Total Environ. 92, 129–144.
Gillett, R.W., Ayers, G.P., Mhwe, T., Selleck, P.W., Harjanto, H., 2000. Concentrations of nitrogen and sulfur species in gas and rainwater from several sites in Indonesia. Water Air Soil Pollut. 120 (3–4), 205–215.
Glasius, M., Wessel, S., Christensen, C.S., Jacobsen, J.K., Jorgensen, H.E., Klitgaard, K.C., Petersen, L., Rasmussen, J.K., Hansen, T.S., Lohse, C., Boaretto, E., Heinemeier, J., 2000. Sources to formic acid studied by carbon isotopic analysis and air mass characterization. Atmos. Environ. 34 (15), 2471–2479.
Golden, H.E., Boyer, E.W., 2009. Contemporary estimates of atmospheric nitrogen deposition to the watersheds of New York state, U.S. Environ. Monit. Assess. 155 (1–4), 319–339 http://dx.doi.org/10.1007/s10661-008-0438-8.
Goldstein, A.H., Galbally, I.E., 2007. Known and unexplored organic constituents in the Earth's atmosphere. Environ. Sci. Technol. 41, 1514–1521.
Goldstein, A.H., Koven, C.D., Heald, C.L., Fung, I.Y., 2009. Biogenic carbon and anthropogenic pollutants combine to form a cooling haze over the southeastern U.S. Proc. Natl. Acad. Sci. 106, 8835–8840.
Golobočanin, D., Žujić, A., Milenković, A., Miljević, N., 2008. Precipitation composition and wet deposition temporal pattern in Central Serbia for the period from 1998 to 2004. Environ. Monit. Assess. 142 (1–3), 185–198.
Goncalves, F.L.T., Andrade, M.F., Forti, M.C., Astolfo, R., Ramos, M.A., Massambani, O., Melfi, J., 2003. Preliminary estimation of the rainfall chemical composition evaluated through the scavenging modeling for north-eastern Amazonian region (Amapaacute; State, Brazil). Environ. Pollut. 121 (1), 63–73.
Gonzalez, C.M., Aristizabal, B.H., 2012. Acid rain and particulate matter dynamics in a mid-sized Andean city: the effect of rain intensity on ion scavenging. Atmos. Environ. 60, 164–171.
Graedel, T.E., Weschler, C.J., 1981. Chemistry within aqueous atmospheric aerosols and raindrops. Rev. Geophys. Space Phys. 19, 505–539.
Grigholm, B., Mayewski, P.A., Kurbatov, A.V., Casassa, G., Staeding, A.C., Handley, M., Sneed, S.B., Introne, D.S., 2009. Chemical composition of fresh snow from Glaciar Marinellu, Tierra del Fuego, Chile. J. Glaciol. 55 (193), 769–776.
Grimshaw, H.J., Dolske, D.A., 2002. Rainfall concentrations and wet atmospheric deposition of phosphorus and other constituents in Florida, U.S.A. Water Air Soil Pollut. 137, 117–140.
Gu, B., Ge, Y., Ren, Y., Xu, B., Luo, W., Jiang, H., Gu, B., Chang, J., 2012. Atmospheric reactive nitrogen in China: sources, recent trends, and damage costs. Environ. Sci. Technol. 46 (17), 9420–9427. http://dx.doi.org/10.1021/es301446g.
Guenther, A., 2002. The contribution of reactive carbon emissions from vegetation to the carbon balance of terrestrial ecosystems. Chemosphere 49, 837–844.
Guenther, A., Hewitt, N.C., Erickson, D., Fall, R., Geron, C., Graedel, T., Harley, P., Klinger, L., Lerdau, M., McKay, W.A., Pierce, T., Scholes, B., Steinbrecher, R., Taalamraju, R., Taylor, J., Zimmermann, P., 1995. A global model of natural volatile organic compound emissions. J. Geophys. Res. 100 (D5), 8873–8892.
Guieu, C., Loÿe-Pilot, M.-D., Benyahya, L., Dufour, A., 2010. Spatial variability of atmospheric fluxes of metals (Al, Fe, Cd, Zn and Pb) and phosphorus over the whole Mediterranean from a one-year monitoring experiment: biogeochemical implications. Mar. Chem. 120, 164–178.
Guttikunda, S.K., Thongboonchoo, N., Arndt, R.L., Calori, G., Carmichael, G.R., Streets, D.G., 2001. Sulfur deposition in Asia: seasonal behavior and contributions from various energy sectors. Water Air Soil Pollut. 131 (1–4), 383–406.
Han, Z., Ueda, H., Sakurai, T., 2006. Model study on acidifying wet deposition in East Asia during wintertime. Atmos. Environ. 40 (13), 2360–2373.
Han, C., Geng, J.J., Hong, Y.N., Zhang, R., Gu, X.Y., Wang, X.R., Gao, S.X., Glindemann, D., 2011. Free atmospheric phosphine concentrations and fluxes in different wetland ecosystems, China. Environ. Pollut. 159 (2), 630–635.
Helas, G., Bingemer, H., Andreae, M., 1992. Organic acids over equatorial Africa: results from DECAFE 88. J. Geophys. Res. 97 (D6), 6187–6193.
Hellsten, S., van Loon, M., Tarrason, L., Vestreng, V., Tørseth, K., Kindbom, K., Aas, W., 2007. Base Cations Deposition in Europe. Swedish Environmental Research Institute, Stockholm, IVL (IVL Report B1722).
Herut, B., Krom, M.D., Pan, G., Motimer, R., 1999. Atmospheric input of nitrogen and phosphorus to the southeast Mediterranean: sources, fluxes, and possible impact. Limnol. Oceanogr. 44 (7), 1683–1692.
Herut, B., Starinsky, A., Katz, A., Rosenfeld, D., 2000. Relationship between the acidity and chemical composition of rainwater and climatological conditions along a transition zone between large deserts and mediterranean climate, Israel. Atmos. Environ. 34 (8), 1281–1292.
Hettelingh, J.-P., Posch, M., Slootweg, J., 2008. Critical Load, Dynamic Modelling and Impact Assessments in Europe. Tech. Rep. Status Report 2008. Coordination Center for Effects, Bilthoven, Netherlands.
Hicks, W.K., Kuylenstierna, J.C.I., Owen, A., Dentener, F., Seip, H.-M., Rodhe, H., 2008. Soil sensitivity to acidification in Asia: status and prospects. Ambio 37 (4), 295–303.
Hidy, G.M., 2003. Snowpack and precipitation chemistry at high altitudes. Atmos. Environ. 37 (9–10), 1231–1242.
Hjellbrekke, A.-G., 2003. Acidifying and Eutrophying Compounds. Annual report for 2001. Norwegian Institute for Air Research, Kjeller Norway. EMEP/CCC-Report 3/2003.
Hjellbrekke, A.-G., Fjæraa, A.M., 2009. Data Report 2007 Acidifying and Eutrophying Compounds and Particulate Matter. Annual report for 2008. Norwegian Institute for Air Research, Kjeller Norway. EMEP/CCC-Report 1/2009.

Hobbs, P.V., 1995. Basic Physical Chemistry for the Atmospheric Sciences. Cambridge University Press, Cambridge, UK.
Hole, L.R., Christensen, J.H., Ruoho-Airola, T., Tørseth, K., Ginzburg, V., Glowacki, P., 2009. Past and future trends in concentrations of sulphur and nitrogen compounds in the Arctic. Atmos. Environ. 43 (4), 928–939.
Holland, D.M., Principe, P.P., Sickles II, J.E., 1999. Trends in atmospheric sulfur and nitrogen species in the eastern United States for 1989–1995. Atmos. Environ. 33, 37–49.
Howarth, R.W., 2008. Review: coastal nitrogen pollution: a review of sources and trends globally and regionally. Harmful Algae 8, 14–20.
HTAP, 2010. Hemispheric transport of air pollution. Part A: ozone and particulate matter. In: Dentener, F., Keating, T., Akimoto, H. (Eds.), Air Pollution Studies No. 17. United Nations, New York and Geneva, p. 304 available at: http://www.htap.org.
Hutchings, J.W., Robinson, M.S., McIlwraith, H., Triplett Kingston, J., Herckes, P., 2009. The chemistry of intercepted clouds in northern Arizona during the North American monsoon season. Water Air Soil Pollut. 199, 191–202.
ICP, 2004. In: Posch, M. (Ed.), International Cooperative Programme on Modelling and Mapping Critical Loads & Levels and Air Pollution Effects, Risks and Trends: Chapter 5.3. Laxenburg, Austria. Available at: icpmapping.org/cms/zeigeBereich/11/manual-english.html.
IJC, 2010. Canada-United States Air Quality Agreement Progress Report 2010. Report, ISBN 978-1-100-17179-1. available from: http://www.epa.gov/airmarkets/progsregs/usca/docs/2010report.pdf.
IJC, 2012. Canada-United States Air Quality Agreement Progress Report 2012 available from: http://www.epa.gov/airmarkets/progsregs/usca/docs/2012report.pdf.
IJC (International Joint Commission), 2008. Canada –United States Air Quality Agreement Progress Report 2008. Report, ISBN 978-1-100-10516-1. available from: http://www.epa.gov/airmarkets/progsregs/usca/docs/2008report.pdf.
Im, U., 2013. Impact of sea-salt emissions on the model performance and aerosol chemical composition and deposition in the East Mediterranean coastal regions. Atmos. Environ. 75, 329–340.
Ingersoll, G.P., Mast, M.A., Campbell, D.H., Clow, D.W., Nanus, L., Turk, J.T., 2008. Trends in snowpack chemistry and comparison to National Atmospheric Deposition Program results for the Rocky Mountains, U.S., 1993–2004. Atmos. Environ. 42 (24), 6098–6113.
IPCC, 2007. Climate change 2007: impacts, adaptation and vulnerability. In: Parry, M.L., Canziani, O.F., Palutikof, J.P., van der Linden, P.J., Hanson, C.E. (Eds.), Contribution of Working Group II to the Fourth Assessment Report of the Intergovernmental Panel on Climate Change. Cambridge University Press, Cambridge, UK, p. 976.
Jickells, T.D., An, Z.S., Andersen, K.K., Baker, A.R., Bergametti, G., Brooks, N., Cao, J.J., Boyd, P.W., Duce, R.A., Hunter, K.A., Kawahata, H., Kubilay, N., laRoche, J., Liss, P.S., Mahowald, N., Prospero, J.M., Ridgwell, A.J., Tegen, I., Torres, R., 2005. Global iron connections between desert dust, ocean biogeochemistry, and climate. Science 308, 67–71. http://dx.doi.org/10.1126/science.1105959.
Johnson, B.J., Dawson, G.A., 1993. A preliminary study of the carbon-isotopic content of ambient formic acid and two selected sources: automobile exhaust and formicine ants. J. Atmos. Chem. 17, 123–140.
Kaufman, Y.J., Koren, I., Remer, L.A., Tanre, D., Ginoux, P., Fan, S., 2005. Dust transport and deposition observed from the Terra-Moderate Resolution Imaging Spectroradiometer (MODIS) spacecraft over the Atlantic Ocean. J. Geophys. Res. 110 (D24202) doi:10.1029.
Kawamura, K., Kaplan, I.R., 1983. Organic compounds in the rainwater of Los Angeles. Environ. Sci. Technol. 17, 497–501.
Kawamura, K., Steinberg, S., Ng, L., Kaplan, I.R., 2001. Wet deposition of low molecular weight mono- and di-carboxylic acids, aldehydes and inorganic species in Los Angeles. Atmos. Environ. 35 (23), 3917–3926.
Keene, W.C., Galloway, J.N., 1986. Considerations regarding sources for formic and acetic acids in the troposphere. J. Geophys. Res. 91 (D13), 14466–14474.
Keene, W.C., Galloway, J.N., Holden Jr., J.R., 1983. Measurement of weak organic acidity from remote areas of the world. J. Geophys. Res. 88 (C9), 5122–5130.
Keene, W.C., Pszenny, A.A.P., Galloway, J.N., Hawley, M.E., 1986. Sea-salt corrections and interpretation of constituent ratios in marine precipitation. J. Geophys. Res. 91 (D6), 6647–6658.
Kelly, V.R., Lovett, G.M., Weathers, K.C., Likens, G.E., 2002. Trends in atmospheric concentration and deposition compared to regional and local pollutant emissions at a rural site in southeastern New York, U.S. Atmos. Environ. 36 (10), 1569–1575.
Kesselmeier, J., Schäfer, L., Bliefernicht, M., Andreae, M.O., Helas, G., 1991. Exchange of Organic Acids between Plants and Atmosphere. EUROTRAC Annual Report 1990, Part 4 BIATEX. Garmisch-Partenkirchen, pp. 214–219.
Kesselmeier, J., Bode, K., Gerlach, C., Jork, E.-M., 1998. Exchange of atmospheric formic and acetic acid with trees and crop plants under controlled chamber and purified air conditions. Atmos. Environ. 32 (10), 1765–1775.
Khare, P., Kumar, N., Kumari, K.M., Srivastava, S.S., 1999. Atmospheric formic and acetic acids: an overview. Rev. Geophys. 37, 227–248.
Kieber, R.J., Peake, B., Willey, J.D., Brooks Avery, G., 2002. Dissolved organic carbon and organic acids in coastal New Zealand rainwater. Atmos. Environ. 36, 3557–3563.
Kim, J.Y., Ghim, Y.S., Lee, S.B., Moon, K.-C., Shim, S.-G., Bae, G., Yoon, S.-C., 2010. Atmospheric deposition of nitrogen and sulfur in the Yellow Sea region: significance of long-range transport in east Asia. Water Air Soil Pollut. 205 (1–4), 259–272.
Kleynhans, E.H., Martins, J.J., Pienaar, J.J., Galy-Lacaux, C., van Zyl, P.G., Beukes, J.P., 2008. Spatial and temporal distribution of aerosols at southern African Debits sites. In: The Joint NACA (National Association for Clean Air) and Regional IUAPPA (International Union of Air Pollution Prevention and Environmental Protection Association) Conference, where Did All the Clean Air Go?, Nelspruit, 1–3 October 2008.
Klimont, Z., Smith, S.J., Cofala, J., 2013. The last decade of global anthropogenic sulfur dioxide: 2000–2011 emissions. Environ. Res. Lett. 8 (1), 014003. http://dx.doi.org/10.1088/1748-9326/8/1/014003.
Kominami, T., Matsuda, K., Ohizumi, T., Hara, H., 2005. Estimation of annual deposition of sulfur oxides during the year 2001 at EANET monitoring sites. Jpn. J. Atmos. Environ. 40, 104–111 (in Japanese).
Krishnamurthy, A., Moore, J.K., Mahowald, N., Luo, C., Doney, S.C., Lindsay, K., Zender, C.S., 2009. Impacts of increasing anthropogenic soluble iron and nitrogen deposition on ocean biogeochemistry. Global Biogeochem. Cycles 23 (GB3016). http://dx.doi.org/10.1029/2008gb003440.
Krishnamurthy, A., Moore, J.K., Mahowald, N., Luo, C., Zender, C.S., 2010. Impacts of atmospheric nutrient inputs on marine biogeochemistry. J. Geophys. Res. 115 (G01006). http://dx.doi.org/10.1029/2009jg001115.
Kulshrestha, U.C., Granat, L., Engardt, M., Rodhe, H., 2005. Review of precipitation monitoring studies in India—a search for regional patterns. Atmos. Environ. 39 (38), 7403–7419.
Kvale, K.F., Pryor, S.C., 2006. Precipitation composition in the Ohio River valley: spatial variability and temporal trends. Water Air Soil Pollut. 170 (1–4), 143–160.
Lacaux, J.P., Delmas, R., Kouadio, G., Cros, B., Andreae, M.O., 1992. Precipitation chemistry in the Mayombe forest of equatorial Africa. J. Geophys. Res. 97 (D6), 6195–6206.
Lacaux, J.P., Tathy, J.P., Sigha, L., 2003. Acid wet deposition in the tropics: two case studies using DEBITS measurements. DEBITS Special Issue No. 27. In: IGACtivities Newsletter of the International Global Atmospheric Chemistry Project, pp. 17–19.
Lafreniere, M., Sinclair, K.E., 2011. Snowpack and precipitation chemistry at a high altitude site in the Canadian Rocky Mountains. J. Hydrol. 409, 737–748.
Laj, P., Klausen, J., Bilde, M., Plaß-Duelmer, C., Pappalardo, G., Clerbaux, C., Baltensperger, U., Hjorth, J., Simpson, D., Reimann, S., Coheur, P.-F., Richter, A., De Mazie` re, M., Rudich, Y., McFiggans, G., Torseth, K., Wiedensohler, A., Morin, S., Schulz, M., Allan, J.D., Attié, J.-L., Barnes, I., Birmili, W., Cammas, J.P., Dommen, J., Dorn, H.-P., Fowler, D., Fuzzi, S., Glasius, M., Granier, C., Hermann, M., Isaksen, I.S.A., Kinne, S., Koren, I., Madonna, F., Maione, M., Massling, A., Moehler, O., Mona, L., Monks, P.S., Müller, D., Müller, T., Orphal, J., Peuch, V.-H., Stratmann, F., Tanré, D., Tyndall, G., Abo Riziqmm, A., Van Roozendael, M., Villani, P., Wehner, B., Wex, H., Zardini, A.A., 2009. Measuring atmospheric composition change. Atmos. Environ. 43, 5351–5414.
Lamarque, J.-F., Kiehl, J., Brasseur, G., Butler, T., Cameron-Smith, P., Collins, W.D., Collins, W.J., Granier, C., Hauglustaine, D., Hess, P., Holland, E., Horowitz, L., Lawrence, M., McKenna, D., Merilees, P., Prather, M., Rasch, P., Rotman, D., Shindell, D., Thornton, P., 2005. Assessing future nitrogen deposition and carbon cycle feedback using a multi-model approach. Analysis of nitrogen deposition. J. Geophys. Res. 110 (D19303).
Lamarque, J.F., Kyle, G.P., Meinshausen, M., Riahi, K., Smith, S.J., van Vuuren, D.P., Conley, A.J., Vitt, F., 2011. Global and regional evolution of short-lived radiatively-active gases and aerosols in the representative concentration pathways. Clim. Change 109 (1–2), 191–212.
Laouali, D., Galy-Lacaux, C., Diop, B., Delon, C., Orange, D., Lacaux, J.P., Akpo, A., Lavenu, F., Hiernaux, P., Gardrat, E., Castera, P., 2012. Long term monitoring of precipitation chemical composition and wet deposition over three Sahelian savannas. Atmos. Environ. 50, 314–327. http://dx.doi.org/10.1016/j.atmosenv.2011.12.004.
Lara, L., Artaxo, P., Martinelli, L.A., Victoria, R.L., Camargo, P.B., Krusche, A., Ayers, G.P., Ferraz, E.S.B., Ballester, M.V., 2001. Chemical composition of rainwater and anthropogenic influences in the Piracicaba River Basin, Southeast Brazil. Atmos. Environ. 35 (29), 4937–4945.
Larssen, T., Lydersen, E., Tang, D., He, Y., Gao, J., Liu, H., Duan, L., Seip, H.M., Vogt, R.D., Mulder, J., Shao, M., Wang, Y., Shang, H., Zhang, X., Solberg, S., Aas, W., Okland, T., Eilertsen, O., Angell, V., Li, Q., Zhao, D., Xiang, R., Xiao, J., Luo, J., 2006. Acid rain in China. Environ. Sci. Technol. 40, 418–425.
Lawrence, G.B., Goolsby, D.A., Battaglin, W.A., Stensland, G.J., 2000. Atmospheric nitrogen in the Mississippi River basin – emissions, deposition and transport. Sci. Total Environ. 248 (2–3), 87–100.
Lee, D.S., Kingdon, R.D., Pacyna, J.M., Bouwman, A.F., Tegens, I., 1999. Modelling base cations in Europe – sources, transport and deposition of calcium. Atmos. Environ. 33, 2241–2256.
Legrand, M., Preunkert, S., Wagenbach, D., Cachier, H., Puxbaum, H., 2003. A historical record of formate and acetate from a high-elevation Alpine glacier: implications for their natural versus anthropogenic budgets at the European scale. J. Geophys. Res. 108 (D24), 4788–4802. http://dx.doi.org/10.1029/2003JD003594.
Lehmann, C.M.B., Bowersox, V.C., Larson, S.M., 2005. Spatial and temporal trends of precipitation chemistry in the United States, 1985–2002. Environ. Pollut. 135 (3), 347–361. http://dx.doi.org/10.1016/j.envpol.2004.11.016.
Lehmann, C.M.B., Bowersox, V.C., Larson, R.S., Larson, S.M., 2007. Monitoring long-term trends in sulfate and ammonium in U.S. precipitation: results from the national atmospheric deposition program/national trends network. Water Air Soil Pollut. Focus 7 (1), 59–66. http://dx.doi.org/10.1007/s11267-006-9100-z.
Lelieveld, J., Berresheim, H., Borrmann, S., Crutzen, P.J., Dentener, F.J., Fischer, H., Feichter, J., Flatau, P.J., Heland, J., Holzinger, R., Korrmann, R., Lawrence, M.G., Levin, Z., Markowicz, K.M., Mihalopoulos, N., Minikin, A., Ramanathan, V., de

Reus, M., Roelofs, G.J., Scheeren, H.A., Sciare, J., Schlager, H., Schultz, M., Seigmund, P., Steil, B., Stephanou, E.G., Stier, P., Traub, M., Warneke, C., Williams, J., Ziereis, H., 2002. Global air pollution crossroads over the mediterranean. Science 298, 794. http://dx.doi.org/10.1126/science.1075457.

Lelieveld, J., Butler, T.M., Crowley, J.N., Dillon, T.J., Fischer, H., Ganzeveld, L., Harder, H., Lawrence, M.G., Martinez, M., Taraborrelli, D., Williams, J., 2008. Atmospheric oxidation capacity sustained by a tropical forest. Nature 452, 737–740.

Lesack, L.F.W., Melack, J.M., 1991. The deposition, composition, and potential sources of major ionic solutes in rain of the Central Amazon Basin. Water Resour. Res. 27 (11), 2953–2977.

Li, C., Kang, S., Zhang, Q., Kaspari, S., 2007. Major ionic composition of precipitation in the Nam Co region, Central Tibetan plateau. Atmos. Res. 85 (3–4), 351–360.

Likens, G.E., 1983. The composition and deposition of organic carbon in precipitation. Tellus 35B, 16–24.

Likens, G.E., Keene, W.C., Miller, J.M., Galloway, J.N., 1987. Chemistry of precipitation from a remote, terrestrial site in Australia. J. Geophys. Res. 92 (D11), 13299–13314. http://dx.doi.org/10.1029/JD092iD11p13299.

Likens, G.E., Buso, D.C., Butler, T.J., 2005. Long-term relationships between SO_2 and NO_x emissions and SO_4^{2-} and NO_3^- concentrations in bulk deposition at the Hubbard Brook Experimental Forest, New Hampshire. J. Environ. Monitor. 7, 964–968.

Liousse, C., Assamoi, E., Criqui, P., Granier, C., Rosset, R., 2013. African Combustion Emission Explosive Growth from 2005 to 2030 (submitted to ERL).

Lorenz, M., Granke, O., 2009. Deposition measurements and critical loads calculations: monitoring data, results and perspective. iForest 2, 11–14. http://dx.doi.org/10.3832/ifor0478-002 (online 2009-01-21). http://www.sisef.it/iforest/contents/?ifor0478-002 iForest.

Lorenz, M., Fischer, R., Becher, G., Granke, O., Roskams, P., Nagel, H.-D., Kraft, Ph, 2007. Forest Condition in Europe, 2007. Technical Report of ICP Forests. Federal Research Centre for Forestry and Forest Products, Hamburg, Germany.

Lövblad, G., Tarrason, L., Tørseth, K., Dutchak, S., 2004. EMEP Assessment, Part I, European Perspective. Norwegian Meteorological Institute, Oslo. Available from: http://emep.int/publ/reports/2004/assessment_2004.html.

Lowman, G., Scholes, M., 2002. Nitrogen deposition impacts on natural and forested ecosystems in Mpumulanga, South Africa. In: 7th Scientific Conference of the IGAC Project, Heraklion, Crête, Greece, September 2002.

Lu, C., Tian, H., 2007. Spatial and temporal patterns of nitrogen deposition in China: synthesis of observational data. J. Geophys. Res. 112 (D22S05). http://dx.doi.org/10.1029/2006JD007990.

Lu, Z., Streets, D.G., Zhang, Q., Wang, S., Carmichael, G.R., Cheng, Y.F., Wei, C., Chin, M., Diehl, T., Tan, Q., 2010. Sulfur dioxide emissions in China and sulfur trends in East Asia since 2000. Atmos. Chem. Phys. 10, 6311–6331. http://dx.doi.org/10.5194/acp-10-6311-2010.

Luo, Y., Yang, X., Carley, R.J., Perkins, C., 2002. Atmospheric deposition of nitrogen along the Connecticut coastline of Long Island Sound: a decade of measurements. Atmos. Environ. 36 (28), 4517–4528.

Lynch, J.A., Bowersox, V.C., Grimm, J.W., 2000. Changes in sulfate deposition in eastern U.S. following implementation of phase I of title IV of the clean air act amendments of 1990. Atmos. Environ. 34, 1665–1680.

Macdonald, B.C.T., Denmeadb, O.T., Whitea, I., Michael, D., Melvillec, M.D., 2004. Natural sulfur dioxide emissions from sulfuric soils. Atmos. Environ. 38, 1473–1480.

Madhavan, B.L., Niranjan, K., Skreekanth, V., Sarin, M.M., Sudheer, A.K., 2008. Aerosol characterization during the sumMer monsson period over a tropical coastal Indian station. J. Geophys. Res. 113 (D21208). http://dx.doi.org/10.1029/2008JD010272.

Maenhaut, W., Fernandez-Jimenez, M.T., Artaxo, P., 1999. Long-term study of atmospheric aerosols in Cuiabá, Brazil: Multielemental composition, sources and source apportionment. J. Aerosol Sci. 30 (Suppl. 1), S259–S260.

Mahowald, N., Jickells, T.D., Baker, A.R., Artaxo, P., Benitez-Nelson, C.R., Bergametti, G., Bond, T.C., Chen, Y., Cohen, D.D., Herut, B., Kubilay, N., Losno, R., Luo, C., Maenhaut, W., McGee, K.A., Okin, G.S., Siefert, R.L., Tsukuda, S., 2008. Global distribution of atmospheric phosphorus sources, concentrations, and deposition rates, and anthropogenic impacts. Global Biogeochem. Cycles 22 (4), GB4026 doi:1029/2008GB003240.

Mambo, V.S., Yoshida, M., Matsuo, S., 1991. Partition of arsenic and phosphorus between volcanic gases and rock. Part 1: analytical data and magmatic conditions of Mt. Usu, Japan. J. Volcanol. Geotherm. Res. 46, 37–47.

Manins, P.C., 1994. Modelling dry deposition in the Klang Valley. In: Workshop on Acid Rain Network in South, East and Southeast Asia (ARNSESEA), 17 – 19 May 1994, Federal Hotel, Kuala Lumpur, Malaysia. Malaysian Scientific Association and Others.

Markaki, Z., Loye-Pilot, M.D., Violaki, K., Benyahya, L., Mihalopoulos, N., 2010. Variability of atmospheric deposition of dissolved nitrogen and phosphorus in the Mediterranean and possible link to the anomalous seawater N/P ratio. Mar. Chem. 120, 187–194.

Martin, C.W., Likens, G.E., Buso, D.C., 2000. Comparison of long-term precipitation chemistry measurements at the Hubbard Brook experimental forest, New Hampshire. Water Air Soil Pollut. 120 (3/4), 359–379.

Martin, R.V., Chance, K., Jacob, D.J., Kurosu, T.P., Spurr, R.J.D., Bucsela, E., Gleason, J.F., Palmer, P.I., Bey, I., Fiore, A.M., Li, Q., Yantosca, R.M., Koelemeijer, R.B.A., 2002. An improved retrieval of tropospheric nitrogen dioxide from GOME. J. Geophys. Res. Atmos. 107, 4437,. http://dx.doi.org/10.1029/2001JD0010127.

Martinelli, L.A., Howarthe, R.W., Cuevas, E., Filoso, S., Austin, A.T., Donoso, L., Huszar, V., Keeney, D., Lara, L.L., Llerena, C., Mcissac, G., Medina, E., Ortiz-Zayas, J., Scavia, D., Schindler, D.W., Soto, D., Townsend, A., 2006. Sources of reactive nitrogen affecting ecosystems in Latin America and the Caribbean: current trends and future perspectives. Biogeochemistry 79, 3–24. http://dx.doi.org/10.1007/s10533-006-9000-3.

Martins, J.J., Dhammapala, R.S., Lachmann, G., Galy-Lacaux, C., Pienaar, J.J., 2007. Long-term measurements of sulphur dioxide, nitrogen dioxide, ammonia, nitric acid and ozone in southern Africa using passive samplers. S. Afr. J. Sci. 103 (7–8), 336–342.

Matsuda, K., 2008. Estimation of dry deposition of sulfur and nitrogen compunds in the atmosphere: updated parameterization of deposition velocity. J. Jpn. Soc. Atmos. Environ. 43, 332–339.

Mayaux, P., Bartholomé, E., Massart, M., Van Cutsem, C., Cabral, A., Nonguierma, A., Diallo, O., Pretorius, C., Thompson, M., Cherlet, M., Pekel, J.-F., Defourny, P., Vasoncelos, M., Di Gregorio, A., Fritz, S., De Grandi, G., Elvidge, C., Vogt, P., Belward, A., 2003. A Land-cover Map of Africa. European Commission Joint Research Centre Report EUR 20665 EN. Office for Official Publications of the European Communities, Luxembourg. ISBN 92-894-5370-2.

McCormick, J., 1997. Acid Earth – the Politics of Acid Pollution, third ed. Earthscan Publications, London.

Meyers, T.P., Hicks, B.B., Hosker, R.P., Womack, J.D., Satterfield, L.C., 1991. Dry deposition inferential techniques. II. Seasonal and annual deposition rates of sulfur and nitrate. Atmos. Environ. 25, 2361–2370.

Migliavacca, D., Teixeira, E.C., Pires, M., Fachel, J., 2004. Study of chemical elements in atmospheric precipitation in south Brazil. Atmos. Environ. 38 (11), 1641–1656.

Migliavacca, D., Teixeira, E.C., Wiegand, F., Sanchez, J.D., Fachel, J., Ribeiro, M., 2005. Evaluation of the atmospheric deposition in an urban region in south Brazil. Water Air Soil Pollut. 167 (1–4), 91–110.

Migon, C., Sandroni, V., 1999. Phosphorus in rainwater: partitioning inputs and impact on the surface coastal ocean. Limnol. Oceanogr. 44 (4), 1160–1165.

Mihaljevič, M., Ettler, V., Šebek, O., Sracek, O., Kříbek, B., Kyncl, T., Majer, V., Veselovský, F., 2011. Lead isotopic and metallic pollution record in tree rings from the copperbelt mining–smelting area, Zambia. Water Air Soil Pollut. 216, 657–668. DOI 10.1007/s11270-010-0560-4.

Mills, M.M., Ridame, C., Davey, M., La Roche, J., Geider, R.J., 2004. Iron and phosphorus co-limit nitrogen fixation in the eastern tropical North Atlantic. Nature 429, 292–294.

Ministry of Environment and Forests, Government of India, 2009. State of the Environment Report (New Delhi, India).

Mitchell, M.J., Lovett, G., Bailey, S., Beall, F., Burns, D., Buso, D., Clair, T.A., Courchesne, F., Duchesne, L., Eimers, C., Jeffries, D., Kahl, S., Likens, G., Moran, M.D., Rogers, C., Schwede, D., Shanley, J., Weathers, K., Vet, R., 2011. Comparisons of watershed sulfur budgets in southeast Canada and northeast US: new approaches and implications. Biogeochemistry 103, 181–207.

Monks, P.S., Granier, C., Fuzzi, S., Stohl, A., Williams, M.L., Akimoto, H., Amann, M., Baklanov, A., Baltensperger, U., Bey, I., Blake, N., Blake, R.S., Carslaw, K., Cooper, O.R., Dentener, F., Fowler, D., Fragkou, E., Frost, G.J., Generoso, S., Ginoux, P., Grewe, V., Guenther, A., Hansson, H.C., Henne, S., Hjorth, J., Hofzumahaus, A., Huntrieser, H., Isaksen, I.S.A., Jenkin, M.E., Kaiser, J., Kanakidou, M., Klimont, Z., Kulmala, M., Laj, P., Lawrence, M.G., Lee, J.D., Liousse, C., Maione, M., McFiggans, G., Metzger, A., Mieville, A., Moussiopoulos, N., Orlando, J.J., O'Dowd, C.D., Palmer, P.I., Parrish, D.D., Petzold, A., Platt, U., Pöschl, U., Prévôt, A.S.H., Reeves, C.E., Reimann, S., Rudich, Y., Sellegri, K., Steinbrecher, R., Simpson, D., ten Brink, H., Theloke, J., van der Werf, G.R., Vautard, R., Vestreng, V., Vlachokostas, Ch., von Glasow, R., 2009. Atmospheric composition change – global and regional air quality. Atmos. Environ. 43 (33), 5268–5350.

Moody, J.L., Pszenny, A.A.P., Gaudry, A., Keene, W.C., Galloway, J.N., Polian, G., 1991. Precipitation composition and its variability in the southern Indian Ocean: Amsterdam Island, 1980–1987. J. Geophys. Res. 96 (11), 20769–20786.

Moore, J.K., Doney, S.C., Glover, D.M., Fung, I.Y., 2002. Iron cycling and nutrient-limitation patterns in surface waters of the world ocean. Deep Sea Res. II 49 (1–3), 463–507.

Morales, J.A., Sanchez, L., Velasquez, H., De Borrego, B., De Nava, M., Portillo, D., Cano, Y., Morillo, A., Albornoz, A., Socorro, E., 2001a. Nutrient loading by precipitation in the Maracaibo Lake basin, Venezuela. Water Air Soil Pollut. 130 (1–4 II), 511–516.

Moschonas, N., Glavas, S., 2002. Weak organic acidity in a wet-only precipitation study at a Mediterranean coastal site, Patras, Greece. Atmos. Res. 63 (1–2), 147–157.

Mphepya, J.N., Pienaar, J.J., Galy-Lacaux, C., Held, G., Turner, C.R., 2004. Precipitation chemistry in semi-arid areas of Southern Africa: a case study of a rural and an industrial site. J. Atmos. Chem. 47 (1), 1–24.

Mphepya, J.N., Galy-Lacaux, C., Lacaux, J.P., Held, G., Pienaar, J.J., 2006. Precipitation chemistry and wet deposition in Kruger National Park, South Africa. J. Atmos. Chem. 53 (2), 169–183.

Muller, J.F., 1992. Geographical-distribution and seasonal-variation of surface emissions and deposition velocities of atmospheric trace gases. J. Geophys. Res. 97, 3787–3804.

Murphy, J., Riley, J.P., 1962. A modified single solution method for determination of phosphate in natural waters. Anal. Chim. Acta 27, 134–139.

NADP (National Atmospheric Deposition Program), 2013. NADP Maps and Data (accessed in February 2013). http://nadp.sws.uiuc.edu/data/.

NADP/AIRMoN (Atmospheric Integrated Research Monitoring Network), 2010. National Atmospheric Deposition Program (NADP) Office, Illinois State Water Survey, 2204 Griffith Dr., Champaign, IL, U.S.. Website: http://nadp.sws.uiuc.edu/AIRMoN/.

Nakayama, S., Personal Communication, 9–11 May 2009. EANET Data. http://www.eanet.cc.

NAPAP, 2005. National Acid Precipitation Assessment Program Report to Congress: an Integrated Assessment. National Acid Precipitation Assessment Program Office of the Director, Washington, DC, p. 85.
NAPAP, 2011. National Acid Precipitation Assessment Program Report to Congress: an Integrated Assessment. National Acid Precipitation Assessment Program Office of the Director, Washington, DC, p. 114.
NAPAP (National Acid Precipitation Assessment Program (U.S.)), Irving, P.M, 1990. Acidic Deposition: State of Science and Technology: Summary Compendium Document: Summaries of NAPAP State-of-science/technology Reports 1–28. Washington, D.C. (722 Jackson Place, NW, Washington 20503): The Program.
Nastos, P.T., Alexakis, D., Kanellopoulou, H.A., Kelepertsis, A.E., 2007. Chemical composition of wet deposition in a mediterranean site Athens, Greece related to the origin of air masses. J. Atmos. Chem. 58 (2), 167–179.
Ncube, E., Banda, C., Mundike, J., 2012. Air pollution on the copperbelt province of Zambia: effects of sulphur dioxide on vegetation and humans. Nat. Env. Sci. 3 (1), 34–41.
Nilles, M.A., Conley, B.E., 2001. Changes in the chemistry of precipitation in the United States, 1981–1998. Water Air Soil Pollut. 130 (1–4 II), 409–414.
Noguchi, I., Hara, H., 2004. Ionic balance due to hydrogen carbonate from Asian dust. Atmos. Environ. 38, 6969–6976.
Noguchi, I., Kato, T., Akiyama, M., Otsuka, H., Matsumoto, Y., 1995. Water Air Soil Pollut. 85, 2357–2362.
Noihan, J., Mahfouf, J.F., 1996. The ISBA land surface parameterisation scheme. Global Planet. Change 13 (1), 145–159.
Okin, G.S., Mahowald, N., Chadwick, O.A., Artaxo, P., 2004. Impact of desert dust on the biogeochemistry of phosphorus in terrestrial ecosystems. Global Biogeochem. Cycles 18, GB2005 doi:2010.1029/2003GB002145.
Okin, G., Baker, A.R., Tegen, I., Mahowald, N.M., Dentener, F.J., Duce, R.A., Galloway, J.N., Hunter, K., Kanakidou, M., Kubilay, N., Prospero, J.M., Sarin, M., Surapipith, V., Uematsu, M., Zhu, T., 2011. Impacts of atmospheric nutrient deposition on marine productivity: roles of nitrogen, phosphorus, and iron. Global Biogeochem. Cycles 25, GB2022. http://dx.doi.org/10.1029/2010GB003858.
Oredalen, T., Aas, W., Maenhaut, W., 2010. Atmospheric dry and wet deposition of phosphorus in southern Norway. In: Data obtained from the World Meteorological Organization Scientific Advisory Group of Precipitation Chemistry Workshop, Berg-en-Dal, South Africa, 15–20 March 2010.
Otter, L., Scholes, M., 2005. Biogenic fluxes of carbon and nitrogen in arid and semi-arid ecosystems. Geophys. Res. Abstr. 7, 09593. SRedf-ID: 1607–7962/gra/EGU-A-09593.
Otter, L.B., Marufu, L., Scholes, M.C., 2001. Biogenic, biomass and biofuel sources of trace gases in southern Africa. S. Afr. J. Sci. 97, 131–138.
Ouimet, R., Arp, P.A., Watmough, S.A., Aherne, J., Demerchant, I., 2006. Determining and mapping critical loads of acidity and exceedances for upland forest soils in eastern Canada. Water Air Soil Pollut. 172, 57–66.
Oulehle, F., Hleb, R., Houška, J., Šamonil, P., Hofmeister, J., Hruška, J., 2010. Anthropogenic acidification effects in primeval forests in the Transcarpathian Mts., western Ukraine. Sci. Total Environ. 408 (4), 856–864.
Özsoy, T., 2003. Atmospheric wet deposition of soluble macro-nutrients in the Cilician Basin, northeastern Mediterranean Sea. J. Environ. Monitor. 5, 971–976.
O'Dowd, C.D., De Leeuw, G., 2007. Marine aerosol production: a review of the current knowledge. Philosophical Transactions of the Royal Society A: mathematical. Phys. Eng. Sci. 365, 1753–1774.
Pauliquevis, T., Lara, L.L., Antunes, M.L., Artaxo, P., 2012. Aerosol and precipitation chemistry measurements in a remote site in Central Amazonia: the role of biogenic contribution. Atmos. Chem. Phys. 12, 4987–5015.
Paulot, F., Wunch, D., Crounse, J.D., Toon, G.C., Millet, D.B., DeCarlo, P.F., Vigouroux, C., Deutscher, N.M., González Abad, G., Notholt, J., Warneke, T., Hannigan, J.W., Warneke, C., de Gouw, J.A., Dunlea, E.J., De Mazière, M., Griffith, D.W.T., Bernath, P., Jimenez, J.L., Wennberg, P.O., 2011. Importance of secondary sources in the atmospheric budgets of formic and acetic acids. Atmos. Chem. Phys. 11, 1989–2013.
Pelicho, A.F., Martins, L.D., Nomi, S.N., Solci, M.C., 2006. Integrated and sequential bulk and wet-only samplings of atmospheric precipitation in Londrina, South Brazil (1998–2002). Atmos. Environ. 40 (35), 6827–6835.
Pena, R.M., Garciacute;a, S., Herrero, C., Losada, M., Vaacute;zquez, A., Lucas, T., 2002. Organic acids and aldehydes in rainwater in a northwest region of Spain. Atmos. Environ. 36 (34), 5277–5288.
Peters, N.E., Meyers, T.P., Aulenbach, B.T., 2002. Status and trends in atmospheric deposition and emissions near Atlanta, Georgia, 1986–99. Atmos. Environ. 36 (10), 1577–1588.
Phoenix, G.K., Hicks, W.K., Cinderby, S., Kuylenstierna, J.C.I., Stock, W.D., Dentener, F.J., Giller, K.E., Austin, A.T., Lefroy, R.D.B., Gimeno, B.S., Ashmore, M.R., Ineson, P., 2006. Atmospheric nitrogen deposition in world biodiversity hotspots: the need for a greater global perspective in assessing N deposition impacts. Global Change Biol. 12, 470–476.
Piccot, S.D., Watson, J.J., Jones, J.W., 1992. A global inventory of volatile organic-compound emissions from anthropogenic sources. J. Geophys. Res. 97, 9897–9912.
Pilson, M.E.Q., 1998. Introduction to Chemistry of the Sea. Prentice Hall, Upper Saddle River, NJ, U.S.A.
Pineda Rojas, A.L., Venegas, L.E., 2008. Dry and wet deposition of nitrogen emitted in Buenos Aires city to waters of de la Plata River. Water Air Soil Pollut. 193 (1–4), 175–188.
Pineda Rojas, A.L., Venegas, L.E., 2009. Atmospheric deposition of nitrogen emitted in the metropolitan area of Buenos Aires to coastal waters of de la Plata River. Atmos. Environ. 43 (6), 1339–1348.
Poor, N., Pribble, R., Greening, H., 2001. Direct wet and dry deposition of ammonia, nitric acid, ammonium and nitrate to the Tampa Bay estuary, FL, U.S. Atmos. Environ. 35 (23), 3947–3955.
Pöschl, U., Martin, S.T., Sinha, B., Chen, Q., Gunthe, S.S., Huffman, J.A., Borrmann, S., Farmer, D.K., Garland, R.M., Helas, G., Jimenez, J.L., King, S.M., Mikhailov, E., Pauliquevis, T., Petters, M.D., Prenni, A.J., Roldin, P., Rose, J., Schneider, J., Su, H., Zorn, S.R., Artaxo, P., Andreae, M.O., 2010. Rainforest aerosols as biogenic nuclei of clouds and precipitation in the Amazon. Science 329, 1513–1516.
Powledge, F., 2006. The millennium assessment. BioScience 56 (11), 880–886.
Puxbaum, H., Gregori, M., 1998. Seasonal and annual deposition rates of sulfur, nitrogen and chloride species to an oak forest in north-eastern Austria (Wolkersdorf, 240 m A.S.L.). Atmos. Environ. 32, 3557–3558.
Querol, X., Pey, J., Pandolfi, M., Alastuey, A., Cusack, M., Pérez, N., Moreno, T., Viana, M., Mihalopoulos, N., Kallos, G., Kleanthous, S., 2009. African dust contributions to mean ambient PM10 mass-levels across the Mediterranean Basin. Atmos. Environ. 43, 4266–4277.
Rahman, A.F.M.D.A., Hiura, H., Shino, K., 2006. Trends of bulk precipitation and streamwater chemistry in a small mountainous watershed on the Shikoku Island of Japan. Water Air Soil Pollut. 175 (1–4), 257–273.
Ridame, C., Guieu, C., 2002. Saharan input of phosphate to the oligotrophic water of the open western Mediterranean Sea. Limnol. Oceanogr. 47 (3), 856–869.
Rocha, F.R., Fracassi da Silva, J.A., Lago, C.L., Fornaro, A., Gutz, I.G.R., 2003. Wet deposition and related atmospheric chemistry in the São Paulo metropolis, Brazil: Part 1. Major inorganic ions in rainwater as evaluated by capillary electrophoresis with contactless conductivity detection. Atmos. Environ. 37 (1), 105–115.
Rodhe, H., Dentener, F., Schulz, M., 2002. The global distribution of acidifying wet deposition. Environ. Sci. Technol. 36 (20), 4382–4388.
Rodríguez, S., Alastuey, A., Alonso-Pérez, S., Querol, X., Cuevas, E., Abreu-Afonso, J., Viana, M., Pérez, N., Pandolfi, M., de la Rosa, J., 2011. Transport of desert dust mixed with North African industrial pollutants in the subtropical Saharan air layer. Atmos. Chem. Phys. 11, 6663–6685.
Roels, J., Verstraete, W., 2001. Biological formation of volatile phosphorus compounds, a review. Bioresour. Technol. 79, 243–250.
Rubin, M., Berman-Frank, I., Shaked, Y., 2011. Dust- and mineral-iron utilization by the marine dinitrogen-fixer Trichodesmium. Nat. Geosci. 4, 529–534.
Ryaboshapko, A.G., Bryukhanov, P.A., Bruskina, I.M., 2010. Atmospheric transport and wet depositions of acidifying substances in northwestern Russia. Rus. Meteorol. Hydrol. 35 (6), 394–400.
Sanets, E.V., Chuduk, V.N., 2005. Sulphur atmospheric deposition in areas with different anthropogenic loads in Belarus. Atmos. Res.. ISSN: 0169-8095 77 (1–4), 88–99. http://dx.doi.org/10.1016/j.atmosres.2004.10.019.
Sanhueza, E., Andreae, M.O., 1991. Emission of formic and acetic acids from tropical savanna soils. Geophys. Res. Lett. 18, 1707–1710.
Sanhueza, E., Figueroa, L., Santana, M., 1996. Atmospheric formic and acetic acids in Venezuela. Atmos. Environ. 30 (10), 1861–1873.
Schäfer, L., Kesselmeier, J., Helas, G., 1992. Formic and acetic acid emission from conifers measured with a 'cuvette' technique. In: Beilke, S., et al. (Eds.), Field Measurements and Interpretation of Species Related to Photooxidants and Acid Deposition, CEC Air Pollution Research 39, E. Guyot SA, Brussels, ISBN 2-87263-070-8, pp. 319–323.
Schindler, D.W., 1977. Evolution of phosphorus limitation in lakes. Science 195, 260–262.
Schlesinger, W.H., Hartley, A.E., 1992. A global budget for NH_3. Biogeochemistry 15, 191–211.
Schroth, G., Elias, M.E.A., Uguen, K., Seixas, R., Zech, W., 2001. Nutrient fluxes in rainfall, throughfall and stemflow in tree-based land use systems and spontaneous tree vegetation of central Amazonia. Agric. Ecosyst. Environ. 87, 37–49.
Schwede, D., Zhang, L., Vet, R., Lear, G., 2011. An intercomparison of the deposition models used in the CASTNET and CAPMoN networks. Atmos. Environ. 45 (6), 1337–1346.
Scudlark, J.R., Jennings, J.A., Roadman, M.J., Savidge, K.B., Ullman, W.J., 2005. Atmospheric nitrogen inputs to the Delaware inland bays: the role of ammonia. Environ. Pollut. 135 (3), 433–443.
Semkin, R., April, 2010. Personal Communication. Environment Canada, National Water Research Institute, Burlington, Ontario, Canada website: http://www.ec.gc.ca/inre-nwri/default.asp?lang=En&n=7CE9E3AC-1.
Sequeira, R., 1982. Acid Rain: an assessment based on acid-base concentration. J. Air Pollut. Control Assoc. 32, 241–245.
Serça, D., Delmas, R., Le Roux, X., Parsons, D.A.B., Scholes, M.C., Abbadie, L., Lensi, R., Ronce, O., Labroue, L., 1998. Comparison of nitrogen monoxide emissions from several African tropical ecosystems and influence of season and fire. Global Biogeochem. Cycles 12 (4), 637–651.
Seto, S., Hara, H., 2006. Precipitation chemistry in western Japan: its relationship to meteorological parameters. Atmos. Environ. 40 (8), 1538–1549.
Shen, J.L., Tang, A.H., Liu, X.J., Fangmeier, A., Goulding, K.T.W., Zhang, F.S., 2009. High concentrations and dry deposition of reactive nitrogen species at two sites in the North China Plain. Environ. Pollut. 157 (11), 3106–3113.
Sickles II, J.E., Grimm, J.W., 2003. Wet deposition from clouds and precipitation in three high-elevation regions of the eastern United States. Atmos. Environ. 37 (2), 277–288.

Sickles II, J.E., Shadwick, D.S., 2007. Changes in air quality and atmospheric deposition in the eastern United States: 1990–2004. J. Geophys. Res. 112 (d17301). http://dx.doi.org/10.1029/2006JD007843.
Sickles II, J.E., Hodson, L.L., Vorburger, L.M., 1999. Evaluation of the filter pack for long-duration sampling of ambient air. Atmos. Environ. 33, 2187–2202.
Sigha-Nkamdjou, L., Galy-Lacaux, C., Pont, V., Richard, S., Sighomnou, D., Lacaux, J.P., 2003. Rainwater chemistry and wet deposition over the equatorial forested ecosystem of Zoeacute;teacute;leacute; (Cameroon). J. Atmos. Chem. 46 (2), 173–198.
Simpson, D., Fagerli, H., Hellsten, S., Knulst, J.C., Westling, O., 2006. Comparison of modelled and monitored deposition fluxes of sulphur and nitrogen to ICP-forest sites in Europe. Biogeosciences 3, 337–355.
Singh, S.P., Khare, P., Kumari, K.M., Srivastava, S.S., 2006. Chemical characterization of dew at a regional representative site of north-central India. Atmos. Res. 80 (4), 239–249.
Siva Soumya, B., Sekhar, M., Riotte, J., Braun, J.-J., 2009. Non-linear regression model for spatial variation in precipitation chemistry for South India. Atmos. Environ. 43 (5), 1147–1152.
Skiba, U., Drewer, J., Tang, Y.S., van Dijk, N., Helfter, C., Nemitz, E., Famulari, D., Cape, J.N., Jones, S.K., Twigg, M., Pihlatie, M., Vesala, T., Larsen, K.S., Carter, M.S., Ambus, P., Ibrom, A., Beier, C., Hensen, A., Frumau, A., Erisman, J.W., Brüggemann, N., Gasche, R., Butterbach-Bahl, K., Neftel, A., Spirig, C., Horvath, L., Freibauer, A., Cellier, P., Laville, P., Loubet, B., Magliulo, E., Bertolini, T., Seufert, G., Andersson, M., Manca, G., Laurila, T., Aurela, M., Lohila, A., Zechmeister-Boltenstern, S., Kitzler, B., Schaufler, G., Siemens, J., Kindler, R., Flechard, C., Sutton, M.A., 2009. Biosphere–atmosphere exchange of reactive nitrogen and greenhouse gases at the NitroEurope core flux measurement sites: measurement strategy and first data sets. Agric. Ecosyst. Environ.. ISSN: 0167-8809 133 (3–4), 139–149. http://dx.doi.org/10.1016/j.agee.2009.05.018.
Smith, S.J., van Aardenne, J., Klimont, Z., Andres, R.J., Volke, A., Delgado Arias, S., 2011. Anthropogenic sulfur dioxide emissions: 1850–2005. Atmos. Chem. Phys. 11, 1101–1116. http://dx.doi.org/10.5194/acp-11-1101-2011.
Sofiev, M., Soares, J., Prank, M., de Leeuw, G., Kukkonen, J., 2011. A regional-to-global model of emission and transport of sea salt particles in the atmosphere. J. Geophys. Res. 116 (D21302). http://dx.doi.org/10.1029/2010JD014713.
Stephen, K., Aneja, V.P., 2008. Trends in agricultural ammonia emissions and ammonium concentrations in precipitation over the Southeast and Midwest United States. Atmos. Environ. 42 (14), 3238–3252.
Stevenson, D.S., Dentener, F.J., Schultz, M.G., Ellingsen, K., Van Noije, T.P.C., Wild, O., Zeng, G., Amann, M., Atherton, C.S., Bell, N., Bergmann, D.J., Bey, I., Butler, T., Cofala, J., Collins, W.J., Derwent, R.G., Doherty, R.M., Drevet, J., Eskes, H.J., Fiore, A., Gauss, M.A., Hauglustaine, D.A., Horowitz, L.W., Isaksen, I.S.A., Krol, M.C., Lamarque, J.F., Lawrence, M.G., Montanero, V., Müller, J.F., Pitari, G., Prather, M.J., Pyle, J.A., Rast, S., Rodriguez, J.M., Sanderson, M.G., Savage, N.H., Shindell, D.T., Strahan, S.E., Sudo, K., Szopa, S., 2006. Multi-model ensemble simulations of present-day and near-future tropospheric ozone. D08301 J. Geophys. Res. 111 (D8). http://dx.doi.org/10.1029/2005JD006338.
Stihl, A., Sommer, U., Post, A.F., 2001. Alkaline phosphatase activities among populations of the colony-forming diazotrophic cyanobacterium Trichodesmium spp. (cyanobacteria) in the Red Sea. J. Phycol. 37, 310–317.
Strayer, H., Smith, R., Mizak, C., Poor, N., 2007. Influence of air mass origin on the wet deposition of nitrogen to Tampa Bay, Florida-an eight-year study. Atmos. Environ. 41 (20), 4310–4322.
Stuut, J.-B., Smalley, I., O'Hara-Dhand, K., 2009. Aeolian dust in Europe: African sources and European deposits. Quat. Int. 198 (1–2), 234–245. http://dx.doi.org/10.1016/j.quaint.2008.10.007.
Swap, R., Garstang, M., Greco, S., Talbot, R., Kallberg, P., 1992. Saharan dust in the Amazon Basin. Tellus Ser. B Chem. Phys. Meteorol. 44, 133–149.
Talbot, R.W., Beecher, K., Harriss, R.C., Cofer III, W.R., 1988. Atmospheric geochemistry of formic and acetic acid at a mid-latitude temperate site. J. Geophys. Res. 93, 1638–1652.
Talbot, R.W., Andreae, M.O., Berresheim, H., Jacob, D.J., Beecher, K.M., 1990. Sources and sinks of formic, acetic and pyruvic acids over Central Amazonia. 2. Wet season. J. Geophys. Res. 95, 16,799–16,811.
Talbot, R.W., Vijgen, A.S., Harriss, R.C., 1992. Soluble species in the Arctic summer troposphere: acidic gases, aerosols, and precipitation. J. Geophys. Res. 97 (D15), 16531–16543.
Tamatamah, R.A., Hecky, R.E., Duthie, H.C., 2005. The atmospheric deposition of phosphorus in Lake Victoria (East Africa). Biogeochemistry 73, 325–344.
Tanner, P.A., Law, P.T., 2003. Organic acids in the atmosphere and bulk deposition of Hong Kong. Water Air Soil Pollut. 142 (1–4), 279–297.
Tessier, J.T., Masters, R.D., Raynal, D.J., 2002. Changes in base cation deposition across New York State and adjacent New England following implementation of the 1990 Clean Air Act amendments. Atmos. Environ. 36 (10), 1645–1648.
Thöni, L., Seitler, E., Meier, M., Zücher, F., Hertz, J., 2008. The development of loads of cations, anions, Cd and Pb in precipitation and of atmospheric concentrations of N-components, in Switzerland from 1988 to 2003. Environ. Monit. Assess. 138 (1–3), 207–218.
Tindale, N.W., Derek, N., Fraser, P.J. (Eds.), 2003. Baseline Atmospheric Program Australia 1999–2000. Published for the Bureau of Meteorology and CSIRO Marine and Atmospheric Research, Melbourne.
Toom-Sauntry, D., Barrie, L.A., 2002. Chemical composition of snowfall in the high Arctic: 1990–1994. Atmos. Environ. 36 (15–16), 2683–2693.
Topcu, S., Incecik, S., Atimtay, A.T., 2002. Chemical composition of rainwater at EMEP station in Ankara, Turkey. Atmos. Res. 65 (1–2), 77–92.
Trebs, I., Lara, L.L., Zeri, L.M.M., Gatti, L.V., Artaxo, P., Dlugi, R., Slanina, J., Andreae, M.O., Meixner, F.X., 2006. Dry and wet deposition of inorganic nitrogen compounds to a tropical pasture site (Rondonia, Brazil). Atmos. Chem. Phys. 6 (2), 447–469.
Tsukuda, S., Sugiyama, M., Harita, Y., Nishimura, K., 2005. Atmospheric bulk deposition of soluble phosphorus in Ashiu Experimental Forest, Central Japan: source apportionment and sample contamination problem. Atmos. Environ. 39, 823–836.
Tsyro, S., Aas, W., Soares, J., Sofiev, M., Berge, H., Spindler, G., 2011. Modelling of sea salt concentrations over Europe: key uncertainties and comparison with observations. Atmos. Chem. Phys. 11, 10367–10388. http://dx.doi.org/10.5194/acp-11-10367-2011.
Tuncer, B., Bayar, B., Yeşilyurt, C., Tuncel, G., 2001. Ionic composition of precipitation at the central Anatolia (Turkey). Atmos. Environ. 35 (34), 5989–6002.
Turk, J.T., Taylor, H.E., Ingersoll, G.P., Tonnessen, K.A., Clow, D.W., Mast, M.A., Campbell, D.H., Melack, J.M., 2001. Major-ion chemistry of the Rocky Mountain snowpack, U.S. Atmos. Environ. 35, 3957–3966.
Tørseth, K., Aas, W., Breivik, K., Fjæraa, A.M., Fiebig, M., Hjellbrekke, A.G., Lund Myhre, C., Solberg, S., Yttri, K.E., 2012. Introduction to the European Monitoring and Evaluation Programme (EMEP) and observed atmospheric composition change during 1972–2009. Atmos. Chem. Phys. 12, 5447–5481. http://dx.doi.org/10.5194/acp-12-5447-2012.
UNECE, 2004. Mapping Manual 2004. UNECE Convention on Long-range Transboundary Air Pollution, ICP Modelling and Mapping available from: http://wge-cce.org/Publications/Mapping_Manual.
UNEP, 2000. Global Environment Outlook – 2. United Nations Environmental Programme, Global State of the Environment Report 2000. Oxford University Press, New York.
Van Loon, M., Tarrasón, L., Posch, M., 2005. Modelling Base Cations in Europe. EMEP/MSC-W & CCE Note 2/2005. ISSN: 0804-2446. Norwegian Meteorological Institute. URL: http://emep.int/publ/reports/2005/emep_technical_2_2005.pdf.
Vestreng, V., Myhre, G., Fagerli, H., Reis, S., Tarrasón, L., 2007. Twenty-five years of continuous sulphur dioxide emission reduction in Europe. Atmos. Chem. Phys. 7, 3663–3681.
Vestreng, V., Ntziachristos, L., Semb, A., Reis, S., Isaksen, I.S.A., Tarrasón, L., 2009. Evolution of NO_x emissions in Europe with focus on road transport control measures. Atmos. Chem. Phys. 9, 1503–1520. http://dx.doi.org/10.5194/acp-9-1503-2009.
Vet, R.J., 1991. Wet deposition measurement techniques, volume 2, Part F, reactions and processes. In: Hutzinger, O. (Ed.), The Handbook of Environmental Chemistry. Springer-Verlag, Heidelberg, p. 77.
Vet, R., Ro, C.-U., 2008. Contribution of Canada-United States transboundary transport to wet deposition of sulfur and nitrogen oxides – a mass balance approach. Atmos. Environ. 42, 2518–2529. http://dx.doi.org/10.1016/j.atmosenv.2007.12.034.
Vet, R., Brook, J., Ro, C., Shaw, M., Narayan, J., Zhang, L., Moran, M., Lusis, M., 2005. Chapter 3: atmospheric response to past emission control programs. In: 2004 Canadian Acid Deposition Science Assessment. Environment Canada, Toronto, Canada. Cat. No. En4–46/2004.
Virkkula, A., Aurela, M., Hillamo, R., Mäkelä, T., Pakkanen, T., Kerminen, V.M., Maenhaut, W., François, F., Cafmeyer, J., 1999. Chemical composition of atmospheric aerosol in the European subarctic: contribution of the Kola Peninsula smelter areas, central Europe, and the Arctic Ocean. J. Geophys. Res. 104 (D19), 23681–23696.
Walker, J.T., Aneja, V.P., Dickey, D.A., 2000. Atmospheric transport and wet deposition of ammonium in North Carolina. Atmos. Environ. 34 (20), 3407–3418.
Wang, Y., McElroy, M.B., Martin, R.V., Streets, D.G., Zhang, Q., Fu, T.-M., 2007. Seasonal variability of NO_x emissions over China constrained by satellite observations: implications for combustion and microbial sources. J. Geophys. Res. 112 (D06301). http://dx.doi.org/10.1029/2006JD007538.
Wang, Z., Xie, F., Sakurai, T., Ueda, H., Han, Z., Carmichael, G.R., Streets, D., Engardt, M., Holloway, T., Hayami, H., Kajino, M., Thongboonchoo, N., Bennet, C., Park, S.U., Fung, C., Chang, A., Sartelet, K., Amann, M., 2008. MICS-Asia II: model inter-comparison and evaluation of acid deposition. Atmos. Environ. 42 (15), 3528–3542.
Wang, S.W., Zhang, Q., Streets, D.G., He, K.B., Martin, R.V., Lamsal, L.N., Chen, D., Lei, Y., Lu, Z., 2012. Growth in NO_x emissions from power plants in China: bottom-up estimates and satellite observations. Atmos. Chem. Phys. 12, 4429–4447. http://dx.doi.org/10.5194/acp-12-4429-2012.
Wesely, M.L., Hicks, B.B., 2000. A review of the current status of knowledge on dry deposition. Atmos. Environ. 34 (12–14), 2261–2282.
WGE, 2011. 30 years of Effects Research, Monitoring and Modelling under the Convention on Long-range Transboundary Air Pollution. Working Group on Effects (WGE), Federal Environment Agency (UBA), Dessau, Germany, p. 17.
Whelpdale, D.M., Kaiser, M.S. (Eds.), 1996. Global Acid Deposition Assessment. World Meteorological Organization/Global Atmosphere Watch, No. 106.
Whitfield, C.J., Aherne, J., Watmough, S.A., McDonald, M., 2010. Estimating the sensitivity of forest soils to acid deposition in the Athabasca Oil Sands Region, Alberta. J. Limnol. 69 (Suppl. 1), 201–208. http://dx.doi.org/10.3274/JL10-69-S1-20.
Willey, J.D., Kieber, R.J., Avery Jr., G.B., 2006. Changing chemical composition of precipitation in Wilmington, North Carolina, U.S.A.: implications for the continental U.S.A. Environ. Sci. Technol. 40 (18), 5675–5680.
Williams, M.R., Fisher, T.R., Melack, J.M., 1997. Chemical composition and deposition of rain in the central Amazon, Brazil. Atmos. Environ. 31, 207–217.

WMO/GAW, 2004. Manual for the GAW Precipitation Chemistry Programme: Guidelines, Data Quality Objectives and Standard Operating Procedures. No. 160. World Meteorological Organization/Global Atmosphere Watch, Geneva, Switzerland.

WMO/GAW, 2007. World Meteorological Organization (WMO) Global Atmosphere Watch (GAW) Strategic Plan: 2008–2015. In: A Contribution to the Implementation of the WMO Strategic Plan: 2008–2011. World Meteorological Organization, Geneva, Switzerland. GAW Report No. 172, available from: http://www.wmo.int/pages/prog/arep/gaw/gaw_home_en.html.

Yang, Y., Yu, W., Pan, Y., Wu, D., 2012. Acid neutralization of precipitation in Northern China. J. Air Waste Manag. Assoc. 62, 204–211.

Yao, H., McConnell, C., Paterson, A., 2010. Personal Communication. Ontario Ministry of the Environment, Dorset Experimental Science Centre, Dorset, Ontario, Canada website: http://www.ene.gov.on.ca/en/index.php.

Yoboué, V., Galy-Lacaux, C., Lacaux, J.P., Silué, S., 2005. Rainwater chemistry and wet deposition over the wet savanna ecosystem of Lamto (Côte d'Ivoire). J. Atmos. Chem. 52 (2), 117–141.

Zbieranowski, A.L., Aherne, J., 2011. Long-term trends in atmospheric reactive nitrogen across Canada: 1988–2007. Atmos. Environ. 45 (32), 5853–5862.

Zhang, L., Brook, J., Vet, R., Shaw, M., Finkelstein, P., 2001. Evaluation and improvement of a dry deposition model using SO_2 and O_3 measurements over a mixed forest. Water Air Soil Pollut. Focus 1, 67–78.

Zhang, D.D., Peart, M., Jim, C.Y., He, Y.Q., Li, B.S., Chen, J.A., 2003. Precipitation chemistry of Lhasa and other remote towns, Tibet. Atmos. Environ. 37 (2), 231–240.

Zhang, L., Brook, J.R., Vet, R., Wiebe, A., Mihele, C., Shaw, M., O'Brien, J.M., Iqbal, S., 2005. Estimation of the contributions of NO_2 and PAN to total atmospheric deposition of oxidized nitrogen across eastern Canada. Atmos. Environ. 39, 7030–7043.

Zhang, G., Zhang, J., Liu, S., 2007. Characterization of nutrients in the atmospheric wet and dry deposition observed at the two monitoring sites over the Yellow Sea and East China Sea. J. Atmos. Chem. 57, 41–57.

Zhang, Q., Streets, D.G., He, K., Wang, Y., Richter, A., Burrows, J.P., Uno, I., Jang, C.J., Chen, D., Yao, Z., Lei, Y., 2007. NO_x emission trends for China, 1995–2004: the view from the ground and the view from space. J. Geophys. Res. 112 (D22306). http://dx.doi.org/10.1029/2007JD008684.

Zhang, L., Vet, R., O'Brien, J.M., Mihele, C., Liang, Z., Wiebe, A., 2009. Dry deposition of individual nitrogen species at eight Canadian rural sites. J. Geophys. Res. 114 (D02301). http://dx.doi.org/10.1029/2008JD010640.

Zhang, N., He, Y., Cao, J., Ho, K., Shen, Z., 2012. Long-term trends in chemical composition of precipitation at Lijiang, southeast Tibetan Plateau, southwestern China. Atmos. Res.. ISSN: 0169-8095 106, 50–60. http://dx.doi.org/10.1016/j.atmosres.2011.11.006.

Zhao, Y., Duan, L., Xing, J., Larssen, T., Nielsen, C.P., Hao, J., 2009. Soil acidification in China: is controlling SO_2 emissions enough? Environ. Sci. Technol. 43 (21), 8021–8026.

Zhong, Z.C., Victor, T., Balasubramanian, R., 2001. Measurement of major organic acids in rainwater in Southeast Asia during burning and non-burning periods. Water Air Soil Pollut. 130 (1–4 II), 457–462.

Zhu, R., Glindemann, B.D., Kong, D.M., Sun, L.G., Geng, J.J., Wang, X.R., 2007. Phosphine in the marine atmosphere along a hemispheric course from China to Antarctica. Atmos. Environ. 41 (7), 1567–1573.

Zimmermann, F., Plessow, K., Queck, R., Bernhofer, C., Matschullat, J., 2006. Atmospheric N- and S-fluxes to a spruce forest – comparison of inferential modelling and the throughfall method. Atmos. Environ.. ISSN: 1352-2310 40 (25), 4782–4796. http://dx.doi.org/10.1016/j.atmosenv.2006.03.056.

Zunckel, M., Saizarb, C., Zarauz, J., 2003. Rainwater composition in northeast Uruguay. Atmos. Environ. 37, 1601–1611. http://dx.doi.org/10.1016/S1352-2310(03)00007-4.

Further reading

Gillett, R.W., Keywood, M.D., Selleck, P.W., Boast, K.M., 2007. Precipitation chemistry. In: Cainey, J.M., Derek, N., Krummel, P.B. (Eds.). Baseline Atmospheric Program (Australia) 2005–2006, Australian Bureau of Meteorology and CSIRO Marine and Atmospheric Research, Melbourne, pp. 95–96.

Gillett, R.W., Selleck, P.W., Powell, J.C., 2012. An acid deposition study in a remote area of north Western Australia. Air Qual. Clim. Chang. 46, 28–34.

Ryaboshapko, A.G., Gromov, S.A. (Eds.), 1999. Expert Meeting on Chemistry of Aerosols, Clouds and Atmospheric Precipitation in the Former USSR, Saint Petersburg, Russian Federation, 13–15 November, 1995. World Meteorological Organization /GAW Report 116, Geneva, Switzerland.